NATIONAL INSTITUTE FOR HIGHER EDUCATION DUBLIN

SCHOOL OF ELECTRONIC ENGINEERING

CONTROL TECHNOLOGY RESEARCH UNIT

THESIS SUBMITTED FOR THE DEGREE OF MASTER OF ENGINEERING

Digital Current Loop Control of a Brushless DC motor

by

Noel Patrick Cox BE

SUBMITTED TO

Dr Frank Devitt BE PhD

September 1987

I declare that the research herein was completed by the undersigned

Signed Noel Cox Date 25/9/87

TABLE OF CONTENTS

ACKNOWLEDGEMENTS

Thank you to Dr Frank Devitt, my project supervisor, for his invaluable technical support and guidance especially in the areas of machines and power electronics. Thank you also to the staff of Moog Ireland Ltd, especially Aidan O'Dwyer. I thank Dr Charles McCorkell and Mr Jim Dowling for their advice during the writing of this thesis, and the technicians of the School of Electronic Engineering, NIHE Dublin, especially Peter McGorman, for their invaluable assistance. Thanks to the members of the Control Technology Research Unit, Ciaran Allen, George Anderson, and Seamus O'Driscoll, for their help and encouragement. Also thank you to Breda McManus who typed this thesis.

ABSTRACT

Servo control of motors has important applications in such areas as robotics, numerically controlled machines and 'fly by wire' aircraft systems. The development of high power high coercivity magnetic alloys, such as samarium cobalt, has led to the advent of the brushless dc machine, which offers a more advantageous alternative to the brush machine. The brushless DC machine eliminates the need for brush contacts, through the use of electronic commutation. It has better thermal characteristics, as the rotor does not carry any current, and the rotor moment of inertia tends to be smaller than an equivalent brush machine. To achieve servo performance with a brushless dc machine requires the control of the motors torque angle. This thesis proposes digital control schemes for torque angle control, presents a simulation of the motor system with the schemes implemented, and concludes that digital schemes are more advantageous than analog control schemes, in the context of torque angle control of a brushless DC system.

Summary

The objective of the research undertaken was to develop a digital current control system for a brushless dc motor. The project was sponsored by Moog Ireland, and the test motor and controller used was the Moog 304-8 brushless dc motor and control system.

The introductory chapter to this thesis provides some general background information to motors. The information is presented in the form of a historical perspective, which traces motor development to the present age, and a theoretical overview which presents a summary of the basics of machine theory.

In chapter two, machine theory is developed along 2 parallel paths, resulting in 2 separate models, ie the 3 phase model and the DQ model representing the same system. The superior model is indicated and its advantages highlighted. Both models, however are used in subsequent chapters.

Power conversion methods used in machine propulsion are discussed in chapter 3. The advantages of PWM over the six step sine wave approximation are indicated. The harmonic spectrum of a PWM wave is developed mathematically and the results compared to the experimentally obtained spectrum. A substantial harmonic distortion effect discovered in the course of experimental work is quantified using a defined ratio called the "harmonic distortion ratio". Possible causes of the harmonic distortion are proposed and the actual effects of the distortion are highlighted. Although an apparently major effect no documentation in the form of papers or text books has been found it.

The parameters for the equations presented in chapter two are experimentally derived in chapter four, for the test motor. The parameters are derived for the cases of both model representations. The condition of a 90^0 torque angle is chosen as a special case and the simplification of the DQ model resulting from such a condition is stressed. The transfer function pertaining to this model is evaluated and presented.

Chapter five uses the models developed in chapter four to enable the design of suitable current control schemes. The design of a 3 phase controller uses a bode plot based procedure while a DQ controller is designed using the method of root locus. More than one control structure is proposed in both the case of 3 phase control and DQ control and the associated merits and demerits of each scheme are discussed.

A simulation of both motor and controller is performed in chapter six. This enables the controllers proposed in chapter five be tested and fully evaluated without the necessity of physical implementation.

In chapter seven a digital control system is designed using a selected microprocessor. The basis for choosing the microprocessor type is outlined and the effect of the sampling rate on the choice of PWM generation method is stressed.

1. Introduction

1.1 Historical Perspective

1.1.1 The principle of electromechanical power conversion was first demonstrated by Michael Faraday in 1821. Using a simple rig comprising a current carrying conductor and magnet he demonstrated that interaction between the magnetic fluxes of the magnet and conductor produced a torque, which resulted in rotation. [E1,E2]

1.1.2 The first simple DC machine was demonstrated by the American, Joseph Henry, using a battery, an electromagnet and a simple commutation device. This was not a commercially viable machine and it was not until the 1870s with the invention of the DC generator that the first practical DC motors appeared. In the 1880s work done by the English inventors Crompton and Hopkinson produced the first commercial DC motors. [E1,E2]

1.1.3 Pioneering work carried out by the Italian Ferraris produced the first induction machine. Ferraris produced a rotating flux wave using a split single phase. He did not realise the commercial viability of the motor, and the invention of the induction motor is generally accredited to Nikola Tesla. Tesla independently discovered the principle of the rotating flux wave, but with foresight he patented the idea, along with the induction motor, and sold the rights to the Westinghouse Corporation. [E1,E2]

1.1.4 The invention of the Synchronous machine was a logical progression from the induction machine using, as it does, the principle of the rotating flux wave. The motor was developed by Westinghouse based on Tesla's ideas and it was seen as an improvement on the induction motor.

1.1.5 The second member is that part of the motor that interacts with the rotating flux wave to produce motion. This member has to have a flux associated with it. In the induction machine this flux is produced by the rotating flux wave itself. In the DC machine and synchronous machine it is produced independently. There are 2 methods to generate this flux. The use of an electromagnet, or the use of permanent magnets. In the case of the synchronous machine, using permanent magnets eliminates the need for brush contacts.

In a servo context such a machine is commonly referred to as a brushless DC machine, by analogy with a permanent magnet DC machine with inverted (or inside out) topology, ie magnets on the rotor. Position sensing and current switching are then done electronically, rather than by brush/commutator arrangement.

1.2. Theoretical overview of synchronous motors and controllers

1.2.1 The synchronous machine

The operation of the synchronous machine depends on the principle of a rotating magnetomotive force (mmf) wave. Synchronous machines are polyphase in operation, and the correct generation of the mmf depends on two factors:

1. The stator coils are distributed in space with the correct spacial phase angle separating adjacent coils. The expression governing the spacial distribution is:

$$\theta = 2\pi/n \text{ mechanical radians}$$

where n is the number of phases, and θ is the phase angle [B1,B2,B3].

2. The voltages driving the coils are balanced, in that their magnitudes are equal and the phase difference in time between adjacent coils is represented by:

$$\theta' = 2\pi/n \text{ electrical radians}$$

where n is as defined above. The relationship between spacial angle and electrical angle is

$$\theta' = P\theta \text{ radians}$$

where P is the number of magnetic pole pairs on the rotor [B1,B2,B3]

The production of a rotating mmf alone is not sufficient to produce rotation. This mmf interacts with the flux on the rotor to produce torque and hence motion. In the case of a permanent magnet machine, the rotor flux is generated by distributed magnets, even in number, with alternate north and south poles pointing radially outwards. The mmf waves of the stator and rotor must be complementary in shape in order to produce a smooth interacting torque during rotation. Some machines are designed for trapezoidal mmf profiles although much more commonly sinusoidal profiles are used. The spacial flux (mmf) waves produced by the windings and magnets in this case may not be exactly sinusoidal; however, to a good approximation, the first fourier harmonic can be used to represent them. During machine operation a phase angle exists between the rotating mmf and the first harmonic of the rotor flux distribution. This angle is known as the torque angle, and it determines the amount of torque the machine can generate. Torque is also dependant on the magnitudes of both the stator (rotating) mmf and the magnitude of the rotor mmf first harmonic. The exact expression for torque is,

$$T = k.Fs.Fr.\mathrm{Sin}\epsilon \ \mathrm{Nm}$$

where F represents mmf, and ϵ is the torque angle [B1,B2,B3]

The speed of a synchronous machine is determined solely by the frequency of the rotating mmf wave. In particular

$$W_m = W_E/P$$

where W_E is the electrical frequency and W_m is the mechanical frequency. [B1,B2,B3,B4]

1.2.2 Variable speed production

Variable speed can be achieved on a synchronous machine by varying the excitation frequency on the stator windings. To achieve servo performance in a synchronous machine, or in other words to produce a brushless DC machine, a control structure like that of Figure (1.1) is used. In general, the voltage applied to the machine windings is not sinusoidal, but contains a first harmonic of the desired frequency and magnitude of excitation. There are two main methods of generating such a harmonic:

1. Six step sine wave approximation
2. Pulse width modulation

The two methods are described below.

1. Six step sine wave approximation

This can be implemented using a power converter [P1,B4,B5,B6] in conjunction with digital hardware [B6]. The power converter generally consists of an n phase inverter-bridge feeding the n phases of the motor. In the case of a 3 phase motor the switching sequence generates, in a single phase, a sine wave approximated in six steps. The higher harmonics of this wave tend to be large in magnitude and at lower machine speeds when the machine impedance is small these serve only to generate losses in the motor.

2. Pulse width modulation

This technique uses a high frequency carrier, modulated by a sine wave of desired frequency and magnitude, in

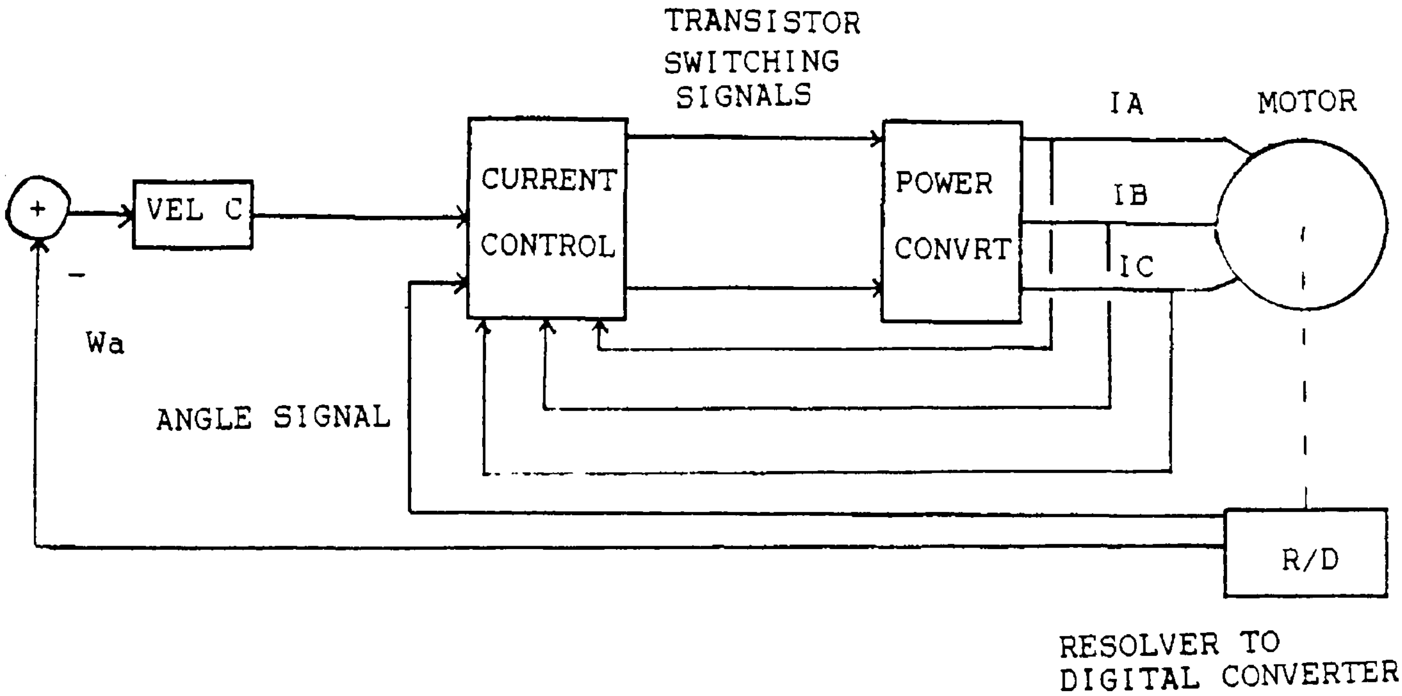

FIGURE(1 1)
BLOCK DIAGRAM OF A BRUSHLESS DC MOTOR CONTROL SYSTEM

conjunction with a power converter bridge [P1,P2,P4,P5,P7,B4,B5,B6]. Unlike the six step approximation this technique does not produce any significant harmonics, except at multiples of the carrier frequency. Because of this, pulse width modulation is generally the preferred method of variable speed production, where technically feasible.

1.2.3 Power Conversion

There are 2 main types of power converter used in variable speed production. These are:

1. The current source Inverter (CSI)
2. The voltage source Inverter (VSI)

Their principles of operation are described below.

1. The Current Source Inverter

The CSI provides a constant source of current in the motor phases. It is generally used conjointly with the six step sine wave approximation to provide a measure of open loop current control [B6]. The CSI dynamics dominate the motor winding electrical dynamics by circumventing the voltage to current stage. Because of this the CSI dynamics dictate the system dynamics, which is disadvantageous, as the CSI tends to be sluggish dynamically. The advantages of the CSI are that it is simple in structure, easy to control in that it can easily be operated in the open loop current mode.

2. The Voltage Source Inverter

The VSI comprises a voltage source applied to the terminals of the inverter bridge [B6]. The method of variable frequency and magnitude signal generation with VSI can be the six step approximation or PWM. Different hardware configurations are necessary for each method, however [B4,B6]. The six step approximation requires a variable voltage source, whereas PWM requires a fixed voltage source. Because of this, PWM is the preferred variable frequency generation method with voltage source inverters.

1.2.4 Current Control

Power converters provide a means of varying voltage and hence current in a synchronous motor's windings. Alone they do not provide control, so it is necessary to incorporate within the system, separate control hardware. The CSI inherently provides current control but the VSI does not. To achieve good dynamic performance in the motor the current loop needs to be closed around the synchronous motors windings. This leaves two parameters to control. The phase angle of the current (with respect to the back emf), and the magnitude of the current [B1,B2,B3].

The current in the stator windings of a synchronous machine is proportional to the magnitude of the rotating stator mmf wave. This makes it proportional to the torque generated, for a permanent magnet machine Under fixed torque angle conditions, torque control is achieved with current magnitude control. Good wideband current control is necessary for high speed servo motor performance.

Controlling the phase angle of the current allows the extension of the motors speed range. When current and back emf are in phase this means a torque angle of 90^0 exists between the 2 mmf's. The back emf is proportional to speed, but by decreasing the torque angle below 90^0 (or increasing the angle between the current and back emf) the constant of proportionality decreases. This means that for a certain speed, less driving voltage is required with increased angle than with 90^0 torque angle. So the maximum magnitude of excitation voltage available is capable of driving the machine at higher speed. The technique of torque angle decrease is known as field weakening.

A torque angle of 90^0 is of special significance in current control. Under this condition motor dynamic analysis can be greatly simplified, using an axis transformation [B2,B3,P8,P9,P10], and the resultant equations turn out linear in form. These equations directly parallel the equations of the DC brush motor. This circumstance justifies the permanent magnet synchronous machine to be called a brushless DC motor.

1.2.5 Approaches to Current Control Hardware

Current control can be implemented in either analog or digital form. The test motor and controller uses analog current control in its present form. It was decided to replace this with digital control using an 80186 microprocessor system, to benefit from all the flexibility advantages that ensue The 80186 processor itself is 16 bit and runs at a clock frequency of 8 MHz. It also contains some inbuilt peripheral devices, useful in a system implementation. Digital control allows the easy tuning and changing of control algorithms, and also the implementation of advanced control structures such as adaptive control. In the context of this thesis the most applicable advantage was the ease of tuning and changing, as it was envisaged to implement and test a variety of controllers in the current loop.

1.2.6 The test motor, described in appendix (6), is a current driven brushless DC machine used in servo applications. This being the case the weight of the theory presented in this thesis is particular to the brushless DC machine.

2. The general theory of AC synchronous machines

2.1 The AC synchronous machine: a physical description

2.1.1 The AC sychronous machine can generally be subdivided into two major elements, the rotating member or rotor, and the stationary member or stator. In servo applications for the purpose of low inertia, and hence low mechanical time constant, the phase coils are usually situated on the stator. This also allows the elimination of brush contacts, and produces a machine with better thermal conductivity. The rotor, which is situated inside the stator contains the other flux producing element, either permanent magnets or a distributed field coil. Since in the course of experimental work, the motor used was a MOOG 304-8 permanent magnet synchronous machine, all theory presented will be for a permanent magnet machine [B1].

2.1.2 Figure (2 1) shows a cross section of the machine, with the stator and rotor sections clearly indicated. The stator, marked S, comprises the conductors for the 3 phases, spacially distributed around the periphery. The rotor, marked R, consists of a shaft on which are mounted the magnet pole pairs. Figure (2.2) shows the diagrammatical representation of the stator, each coil shown as its equivalent inductance and the spacial displacement between adjacent coils shown as an angle in radians. The coil direction indicated is called the coil axis. Figure (2.3) shows a motor with two magnet arrangement possibilities. Arrangement A is generally used with weaker magnets such as alnico. Because the magnets are embedded into iron, and as iron has a higher

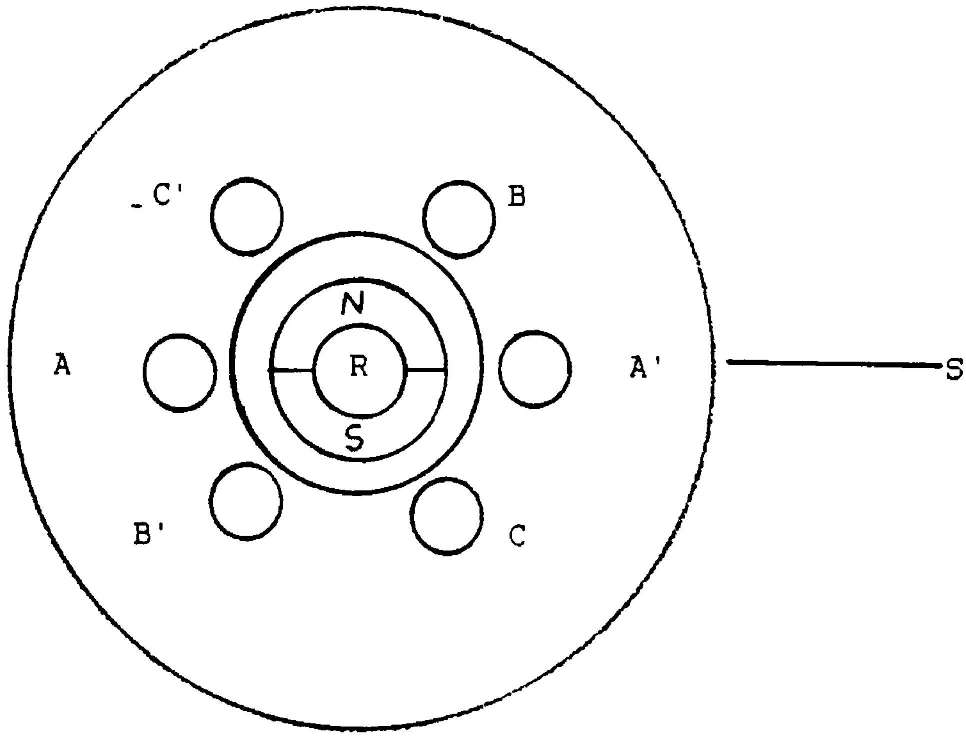

FIGURE(2 1)
A CROSS SECTIONAL VIEW OF THE AC MACHINE

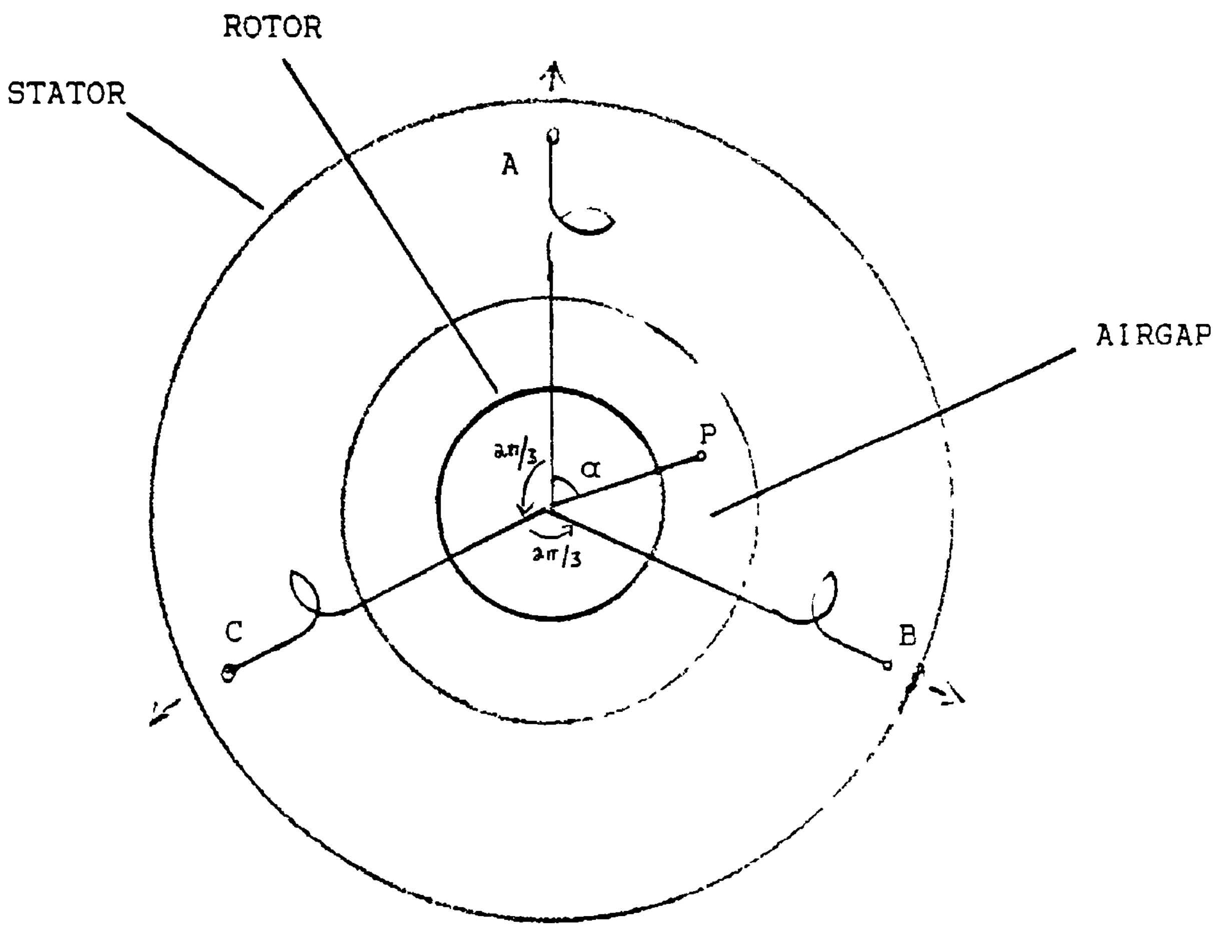

FIGURE(2 2)
THE STATOR EQUIVALENT COILS AND ASSOCIATED DIRECTIONS

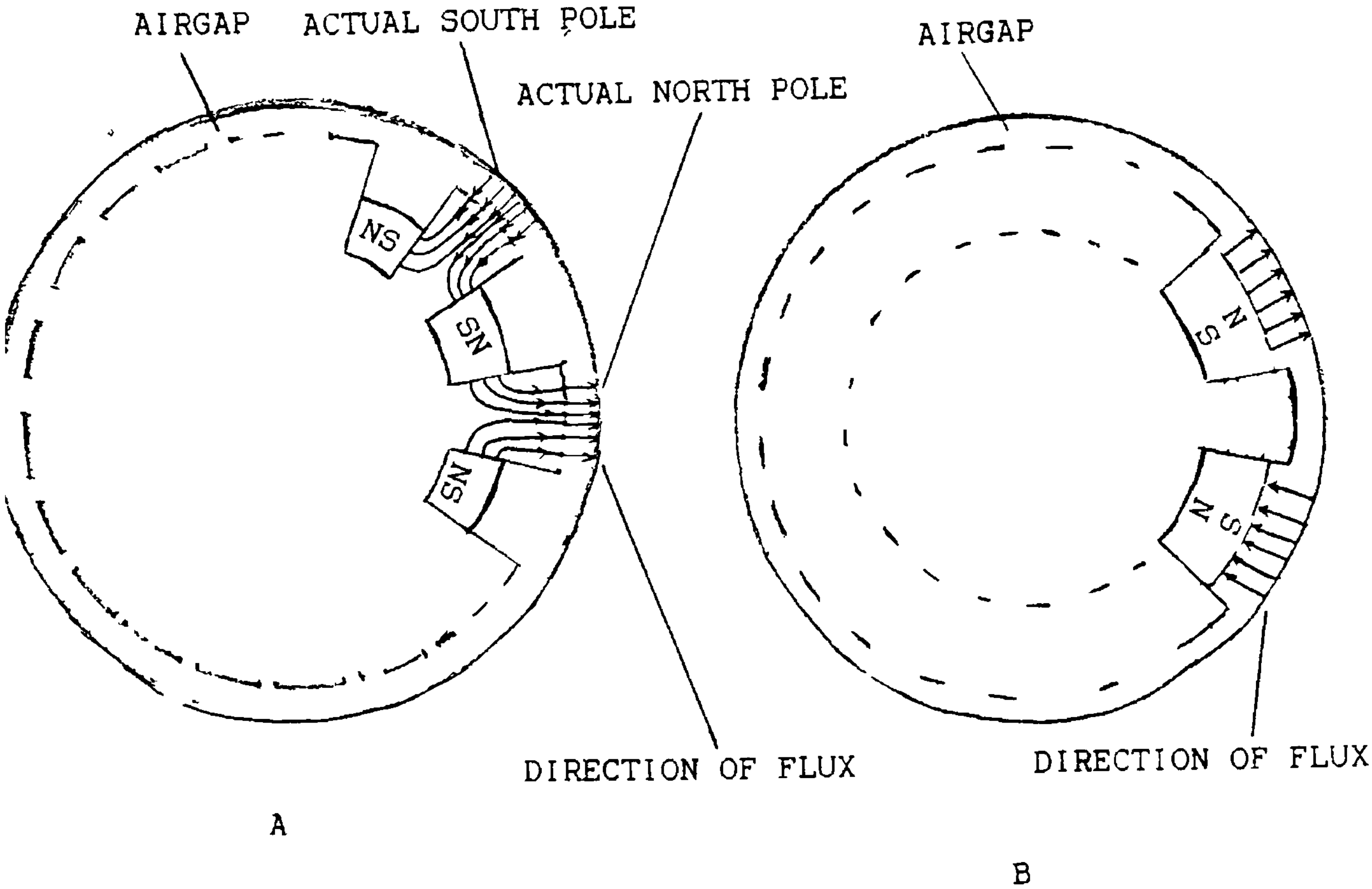

FIGURE(2 3)

MOUNTING PERMANENT MAGNETS

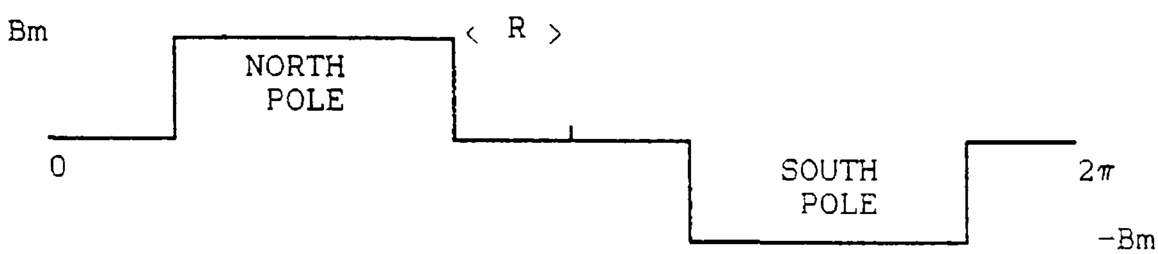

FIGURE(2 4)

THE MAGNET FLUX DISTRIBUTION

permeability than air, arrangement A has high saliency. Arrangement B which is used with more powerful magnets such as samarium cobalt exhibits almost zero saliency. This is the arrangement used in the test motor.

2.1.3 The currents impressed in the phase coils are sinusoidal in nature, and these produce in turn sinusoidal fluxes. In particular

$$I_A = |I| \text{ Cos } (We.t) \quad \ldots\ldots (2.1)$$
$$I_B = |I| \text{ Cos } (We.t-2\pi/3) \quad (2\ 2)$$
$$I_C = |I|. \text{ Cos } (We.t-4\pi/3) \quad (2\ 3)$$

and

$$B_A = |B| \text{ Cos } (We.t) \quad \ldots\ldots (2.4)$$
$$B_B = |B|. \text{ Cos } (We.t-2\pi/3) \quad (2\ 5)$$
$$B_C = |B|. \text{ Cos } (We.t-4\pi/3) \quad (2\ 6)$$

where B_A, B_B, B_C are the air gap flux densities generated by the A, B and C phases respectively.

2.1.4 Referring to figure (2.2), the fluxes produced radiate outwards across the airgap in the direction indicated. Since the stator is fixed in relation to the airgap, any point on the airgap will experience a time varying flux whose magnitude is the summation of the flux contributions of each coil at that point. Consider point P in the airgap, displaced an angle α from the A phase. The total flux at point P is:

$$B_p = |B|.\text{CosWetCos}\alpha + |B|\text{Cos}(\theta-2\pi/3)\text{Cos}(2\pi/3-\alpha) + |B| \text{ Cos}(\theta-4\pi/3) \text{ Cos}(4\pi/3-\alpha) \quad \ldots\ \ldots (2.7)$$

Using the laws of trigonometry, equation (2.7) can be reduced to

$$B_p = \frac{3|B|}{2} \mathrm{Cos}(\mathrm{We}t-\alpha)$$

which is a time varying function.

As the flux magnitude at point P is time variant, and in particular sinusoidal it can be concluded that sinusoidal currents of the nature of (2.1, 2.2, 2.3) produce a rotating flux wave in the air-gap.

2.1.5 Figure (2.4) illustrates the flux distribution produced by the magnets on the rotor. Only one pole pair is shown, and it will be assumed that the period is 2π. Fringing between the magnets is neglected. Using Fourier series theory the magnitude of the first harmonic is:

$$|B_{R1}| = 2Bm/\pi \quad (\mathrm{Cos}\ R - \mathrm{Cos}\ (\pi-R)] \ldots\ldots\ldots\ldots(2.8)$$

Neglecting upper harmonics, the fundamental is used to represent the flux produced by the rotor magnets. With the rotor stationary, reference to figure (2.3) shows that the magnets in effect produce a standing wave of flux, whose period in space is 2π mechanical radians.

2.2 The AC synchronous machine: a mathematical description

2.2.1 To derive the electrical equations of the synchronous machine it is necessary, only, to derive the equations for a single phase coil, and using the assumption that the phase coils are balanced in their distribution around the stator, the equations for the remaining coils can be obtained [B2]. The electrical characteristics of a coil can be subdivided into 3 areas:

1) self effects
2) mutual effects between phase coils
3) mutual effects between phase coils and rotor magnets.

To simplify analysis it is assumed that the rotor magnet distribution can be represented by an equivalent two pole distribution. This assumption is validated since the number of magnet pole pairs affects only the relationship between electrical and mechanical speed, and the machine torque equation [B3].

2.2.2 The self inductance of a phase coil depends on the distance across the air gap. If this distance is constant around the stator periphery, then the coil self inductance remains constant irrespective of coil position. If however, the machine is salient pole, then the self inductance varies. Figure (2.5) shows the situation in a two pole salient machine. The gaps between the magnet poles vary the air gap distance, which affects the self inductance. It is assumed that the inductance is a periodic function of θ, the angle between the axis of coil A and a selected reference axis. This being the case, the self inductance of coil A can be written as a fourier series. In particular

$$L_A = A_0 + A_2 . \operatorname{Cos} 2\theta + A_4 . \operatorname{Cos} 4\theta + \ldots \qquad \ldots\ldots(2\ 9)$$

The total distance of rotation is 2π, and the period of L_A is π. Using the same reasoning for B and C coils, and substituting $\theta - 2\pi/3$ and $\theta - 4\pi/3$ for θ in equation (2.9), expressions for L_B and L_C are obtained. [B2].

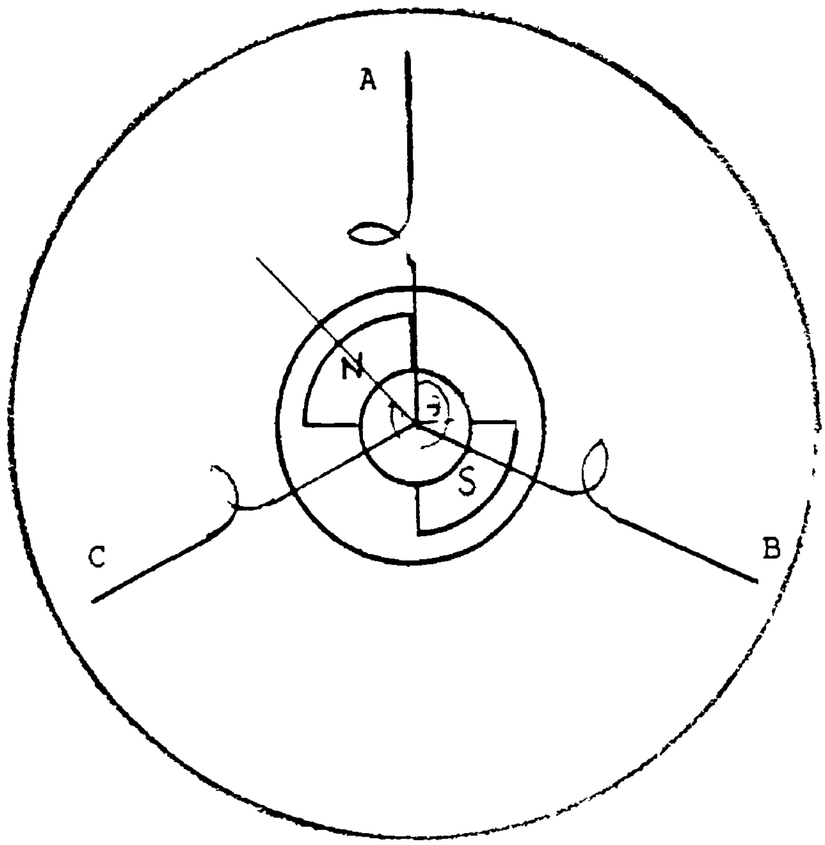

FIGURE(2 5)
THE TWO POLE SALIENT MACHINE

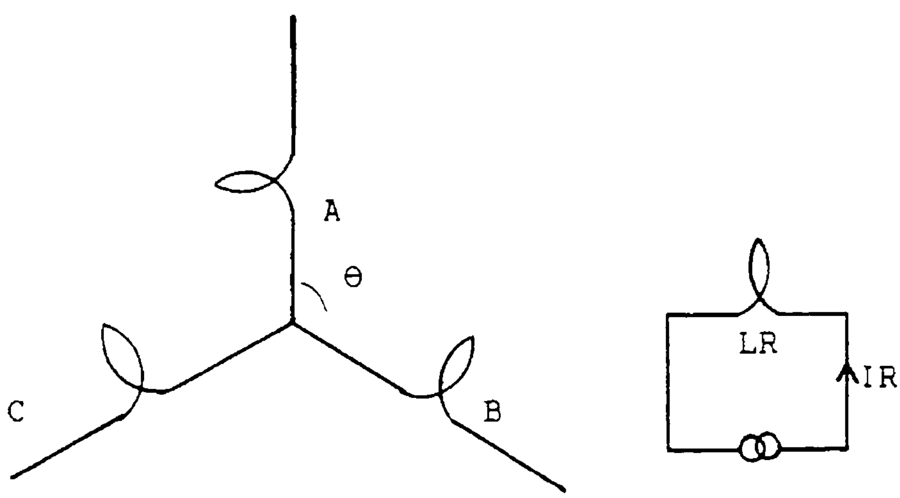

FIGURE(2 6)
THE EQUIVALENT MAGNET ELECTRICAL CIRCUIT

2.2.3 The mutual inductance between phase coils varies periodically with θ also. The mutual inductance between coils A and B, L_{AB}, can also be written as a fourier series.

$$L_{AB} = -B_0+B_2.\cos 2\theta+B_4\cos 4\theta \qquad (2.10)$$

Substitution of $\theta-2\pi/3$ and $\theta-4\pi/3$ for θ in (2.10) yields expressions for L_{AC} and L_{BC}.

2.2.4 The pole pair of figure (2.5) can be represented as an equivalent coil with a constant current source. Coil and current source should yield the same flux in the air gap as the pole pair. This enables an analysis to be made on the effects between magnet poles and stator coils in terms of mutual inductances. Figure (2.6) illustrates this situation. The phase coil does not affect the magnet coil, as the magnet equivalent coil is current driven. The magnet coil however does induce voltage in the phase coil. In particular

$$L_{PA} = C_1.\cos\theta+C_3.\cos 3\theta+ \quad ....(2.11)$$

where L_{PA} is the inductance between the magnet coil and the A phase. Using the angle substitution of sections 2.2.3 and 2.2.4 expressions for L_{PB} and L_{PC} are obtained.

2.2.5 If terms of order 3 and higher are neglected in the inductances, an impedance equation for the machine can be written in matrix form: $U = \bar{Z}\bar{I}$ [B2,B3] where

$$Z = \begin{bmatrix} (R_A+\frac{d}{dt}L_A) & \frac{d}{dt}L_{AB} & \frac{d}{dt}L_{AC} & \frac{d}{dt}L_{pa} \\ \frac{d}{dt}L_{BA} & (R_B+\frac{d}{dt}L_B) & \frac{d}{dt}L_{BC} & \frac{d}{dt}L_{pb} \\ \frac{d}{dt}L_{CA} & \frac{d}{dt}L_{CB} & R_C+\frac{d}{dt}L_C & \frac{d}{dt}L_{pc} \end{bmatrix} \qquad \text{..........(2.12)}$$

$$I = \begin{bmatrix} I_A \\ I_B \\ I_C \\ I_f \end{bmatrix} \qquad \text{..........(2.13)}$$

$$U = \begin{bmatrix} U_A \\ U_B \\ U_C \end{bmatrix} \qquad \text{..........(2.14)}$$

and
$$\begin{aligned}
L_A &= A_0 + A_2\mathrm{Cos}2\theta \\
L_B &= A_0 + A_2\mathrm{Cos}(2\theta-4\pi/3) \\
L_C &= A_0 + A_2\mathrm{Cos}(2\theta-4\pi/3) \\
L_{AB} &= -B_0 + B_2\mathrm{Cos}(2\theta-2\pi/3) \\
L_{AC} &= -B_0 + B_2\mathrm{Cos}(2\theta-4\pi/3) \\
L_{PA} &= C_1\mathrm{Cos}\theta \\
L_{BA} &= L_{AB} \\
L_{BC} &= -B_0 + B_2\mathrm{Cos}2\theta \\
L_{PB} &= C_1\mathrm{Cos}(\theta-2\pi/3) \\
L_{CA} &= L_{AC} \\
L_{CB} &= L_{BC} \\
L_{PC} &= C_1\mathrm{Cos}(\theta-4\pi/3)
\end{aligned}$$

2.3 The machine equations : a simplification

2.3.1 The nature of the equations presented above is that of a nonlinear system whose parameters vary with angle θ. This makes analysis, whether dynamic or steady state very complex. It is necessary, therefore, to simplify the equations to produce a workable set.

2.3.1 To simplify the equations, two assumptions are made.

1. The degree of machine saliency is low or negligible.

2. All mutual effects between coils can be lumped together to form a single phase inductance term.

The first assumption can reasonably be made in the case of the Test motor, as the magnet mounting arrangement is that of Figure (2.3) B. The second assumption follows indirectly from the first, as zero saliency means non varying inductances. This ensures that all mutual voltages are of the same frequency, and hence can be combined as phasors. [B2].

2.3.2 The electrical equation for a single phase coil can now be written

$$V_A = L_A \frac{dI_A}{dt} + R_A IA + E_A \qquad (2\ 15)$$

where $E_A = K_E W_m \mathrm{Cos}(W_E . t + \beta)$

K_E is a constant of proportionality called the back emf constant, and β is a phase angle with respect to an arbitrary reference. The equation in steady state is phasor in form.

$$V_A = R_A I_A + jW_E L_A I_A + E_A \quad \text{..........(2.16)}$$

Figure (2.7) shows the machine represented in its simplified form. Figure (2.8) illustrates equation (2.18) in phasor diagram form [B7].

2.3.3 The amount of torque produced by the machine depends on the amount of power crossing the air gap The power per phase is the dot product of the current and voltage. For the A phase

$$P_A = V_A . I_A . \quad \text{........................(2.17)}$$

A similar equation holds for the B and C phases. Substituting (2.16) for V_A in (2.15) results in:

$$P_A = R_A I_A^2 + L_A \frac{dI_A}{dt} . I_A + I_A E_A \quad (2\ 18)$$

The first 2 terms of this equation refer to the power dissipated in the coil resistance, and stored inductive energy respectively. The last term represents electromechanical power conversion and produces torque. Torque is defined as the ratio of the total mechanical power to the mechanical speed, Wm.

$$\Rightarrow \quad T = \frac{3 I_A E_A}{Wm} \quad (2\ 19)$$

From equation (2.17) $E_A = K_E W_m \exp(j\beta)$
If σ is defined as the angle between I_A and E_A, torque can be written as

$$T = K_T \ I_A \ \mathrm{Sin}(\pi/2-\sigma) \quad \text{.... .. ..(2.20)}$$

where the angle $\pi/2-\sigma$ is defined as the torque angle. [B1, B2, B4].

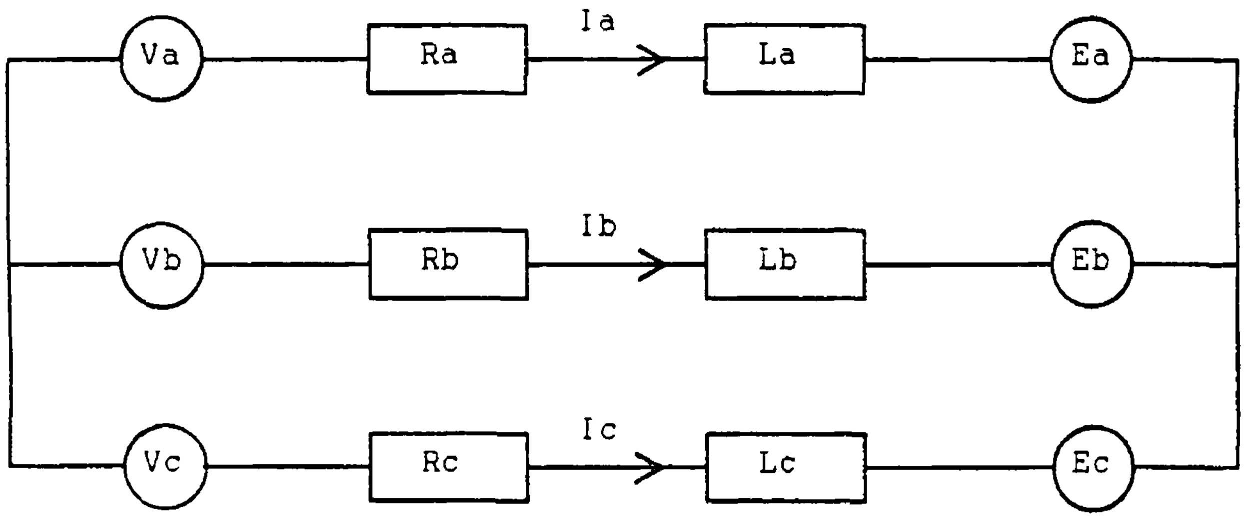

FIGURE(2 7)

THE ELECTRICAL CIRCUIT OF AN AC MACHINE

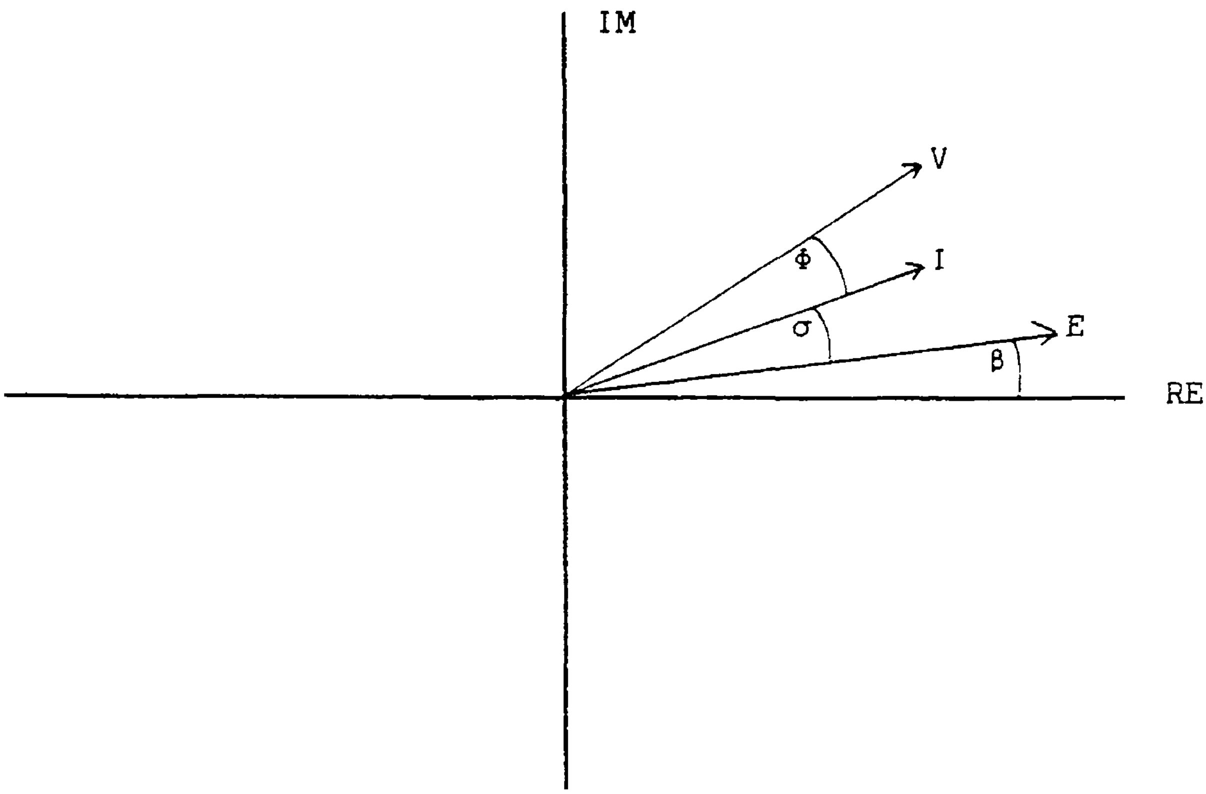

FIGURE(2 8)
THE PHASOR DIAGRAM OF AN AC MACHINE

2.4 The 3 phase to 2 axis transformation

2.4.1 Equations (2.15 .. 2.20) are suitable for steady state analysis, as all variables can be represented as phasors. Unfortunately they are not readily applicable to dynamic analysis. If the variables could be transformed to a reference frame, where they were represented by equivalent DC values, this would constitute a major advantage to analysis.

2.4.2 The transformation due to R.H. Park [B2, B3] performs such a task. Park used a reference frame transformation, where the new reference frame was rotating at machine synchronous speed, or in other words it was situated on the rotor rather than the stator. If reference is made back to paragraphs 2.1.4, 2.1.5, 2.1.6, it was proven that a point p moving through the airgap at machine electrical speed, W_E, witnesses no variation in flux. So a reference frame moving at machine electrical speed needs only coils carrying DC values to represent the flux in the air gap.

2.4.3 Park called the new axes produced by transformation the D and Q axes. The D or direct axis is defined to be along the axis of the rotor north pole. (The rotor here is considered to be the two pole equivalent). The Q or quadrature axis is situated in interpolar space between the north and south poles. If the angle θ is defined as the angle between the A phase coil and the direct axis, reference to figure (2.9) and simple phasor arithmetic produces the following matrix equations [B2, B3, B4].

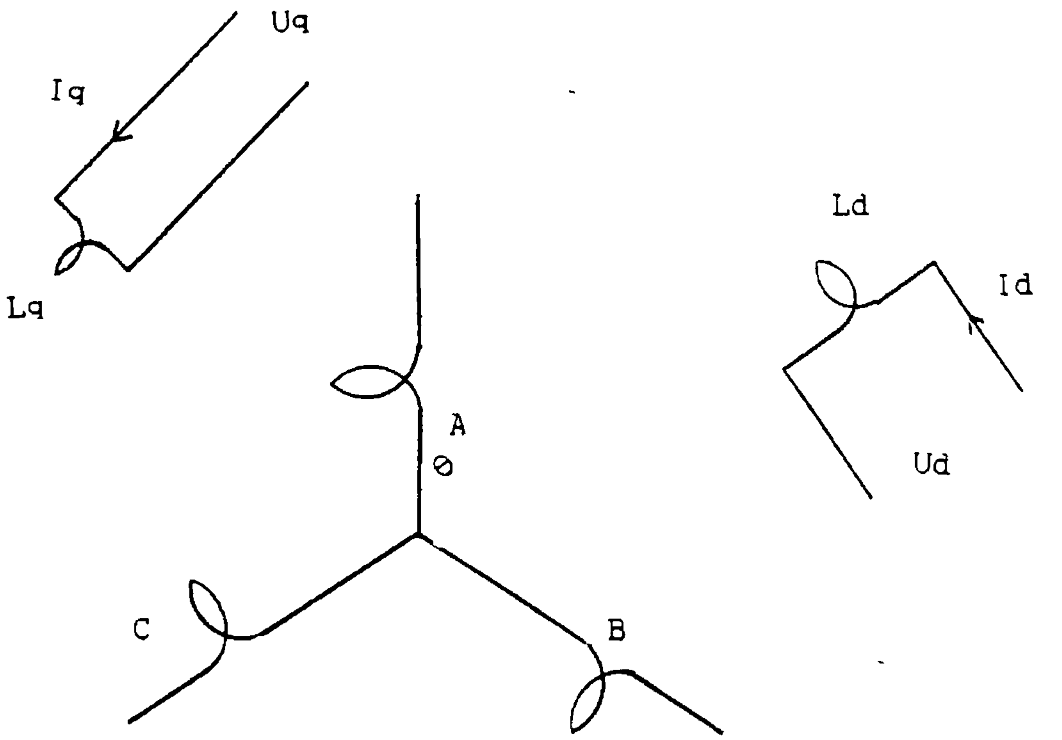

FIGURE(2 9)
THE 3 PHASE MACHINE AND ITS DQ REPRESENTATION

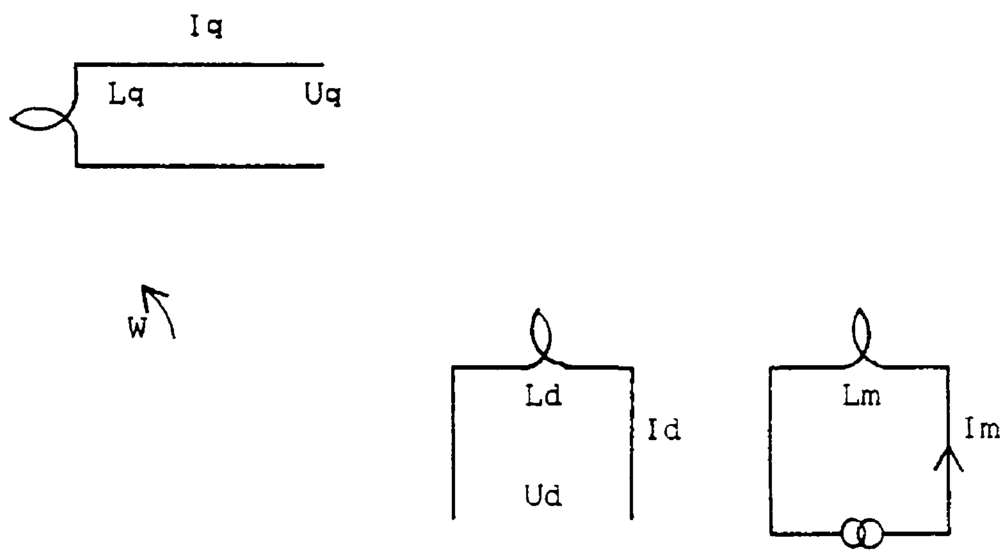

FIGURE(2 10)

THE TRANSFORMED MACHINE

$$\begin{bmatrix} Id \\ Iq \end{bmatrix} = \frac{2}{3} \begin{bmatrix} \cos(\theta) & \cos(\theta-2\pi/3) & \cos(\theta-4\pi/3 \\ \sin(\theta) & \sin(\theta-2\pi/3) & \sin(\theta-4\pi/3) \end{bmatrix} \begin{bmatrix} IA \\ IB \\ IC \end{bmatrix} \qquad (2\ 21)$$

$$\begin{bmatrix} IA \\ IB \\ IC \end{bmatrix} = \begin{bmatrix} \cos\theta & \sin\theta \\ \cos(\theta-2\pi/3) & \sin(\theta-2\pi/3) \\ \cos(\theta-4\pi/3) & \sin(\theta-4\pi/3) \end{bmatrix} \begin{bmatrix} Id \\ Iq \end{bmatrix} \qquad (2\ 22)$$

Similar equations hold for the voltages The transformation is made with the assumption that the D and Q coils have the same number of turns as the phase coils.

2.4.4 The D and Q coil dynamic equations can be derived from first principles by a consideration of the voltages across each coil, whether induced or applied. The following rules are used in the derivation.

1. Coils on the same axis are transformer coupled.

2. Coils 90 degrees apart where one coil is on the stator and the other is on the rotor are pseudo stationary. This means that the coil itself does not move, but voltages can be induced in the coil by virtue of the rotation of the element it is used to represent.

Figure (2.10) shows the transformed system for the test motor. The pseudo-stationary coils are defined to be the stator coils, although the stator does not move. This convention can be applied as the stator moves relative to the rotor. Using equations (2.23, 2.24) and basic flux theory the following coil equations can be derived.

$$U_d = \frac{d\lambda d}{dt} + R_d I_d - W_E \lambda_q \quad \ldots\ldots\ldots\ldots\ldots (2.23)$$

$$U_q = \frac{d\lambda q}{dt} + R_q I_q + W_E \lambda_d \quad \ldots\ldots\ldots\ldots\ldots (2.24)$$

where λ_d and λ_q are the D and Q axis flux linkages respectively. Also:

$$\lambda_d = L_d I_d + \lambda_m \quad \ldots\ldots\ldots\ldots\ldots\ldots (2.25)$$

$$\lambda_q = L_q I_q \quad \ldots\ldots\ldots\ldots\ldots\ldots (2.26)$$

$$R_d = R_q \quad \ldots\ldots\ldots\ldots\ldots\ldots (2.27)$$

where λ_m is the equivalent flux linkage of the magnet pole, L_d and L_q are the total self inductances of the D and Q axis coils respectively.

2.4.5 The torque equation can be determined by a consideration of the power crossing the air gap.

$$U_d I_d = L_d \frac{dI_d}{dt} \cdot I_d + R_d I_d^2 - W_E L_q I_q I_d \quad \ldots\ldots\ldots (2.28)$$

$$U_q I_q = L_q \frac{dI_q}{dt} \cdot I_q + R_q I_q^2 + W_E L_d I_d I_q + W_E \lambda_m I_q \quad \ldots (2.29)$$

The first 2 terms of each of the above equations relate to stored inductive energy and power dissipated as heating loss. The combination of the other terms comprises the power crossing the air gap. Torque is the ratio of this power to the mechanical speed.

$$T = k(W_E L_d I_d I_q + W_{E_\lambda} I_q - W_E L_q I_d)/W_m$$

$$T = K\ p/2\ (\lambda_d I_q - \lambda_q I_d) \quad \ldots\ldots\ldots\ldots (2.30)$$

where p is the number of pole pairs on the rotor. The factor k is a constant of proportionality used to compensate for a scaling factor introduced in the 3 phase to 2 axis transformation.

2.4.6 The equations presented in this chapter constitute a full set of representative equations for the 3 phase PM synchronous machine. They therefore are the basis of work presented in the following chapters.

3. Pulse width modulation in AC motor propulsion

3.1 The voltage source inverter and the six step approximation

3.1.1 For variable speed AC motor control, it is necessary to control the phase excitation frequency. The voltage source inverter allows not only variable frequency control but also variable voltage magnitude control, over the motor phase voltage.

3.1.2 Figure (3.1) illustrates the structure of the voltage source inverter. It comprises three distinct legs, one for each phase, each leg itself consisting of two power transistors. A flywheel diode is provided in antiparallel with each transistor to allow inductive regeneration current flow during transistor off times. The DC bus has low regulation, ie the voltage level does not vary with load current. This low dynamic regulation is provided by the capacitor, C.

3.1.3 The function of the VSI is to provide sinusoidal currents in the motor windings. One method of producing this current is the six step approximation [B5, P6, P7]. Figure (3.2) illustrates the transistor turn on sequence necessary to provide the six step approximation to current. The frequency of the approximation is W_E, which is variable.

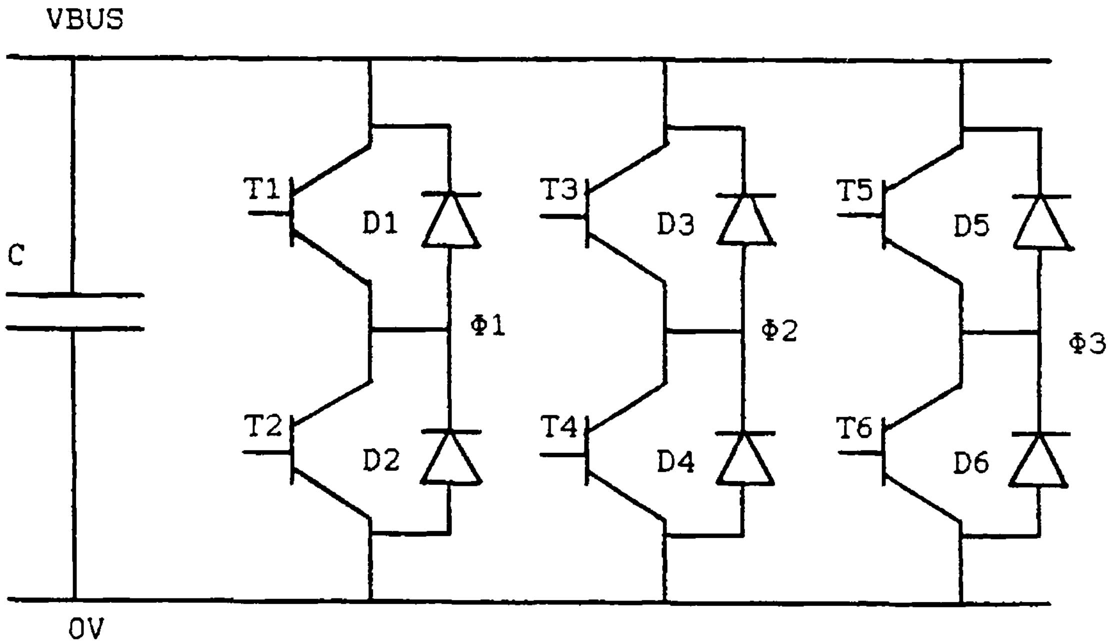

FIGURE(3 1)
THE VOLTAGE SOURCE INVERTER

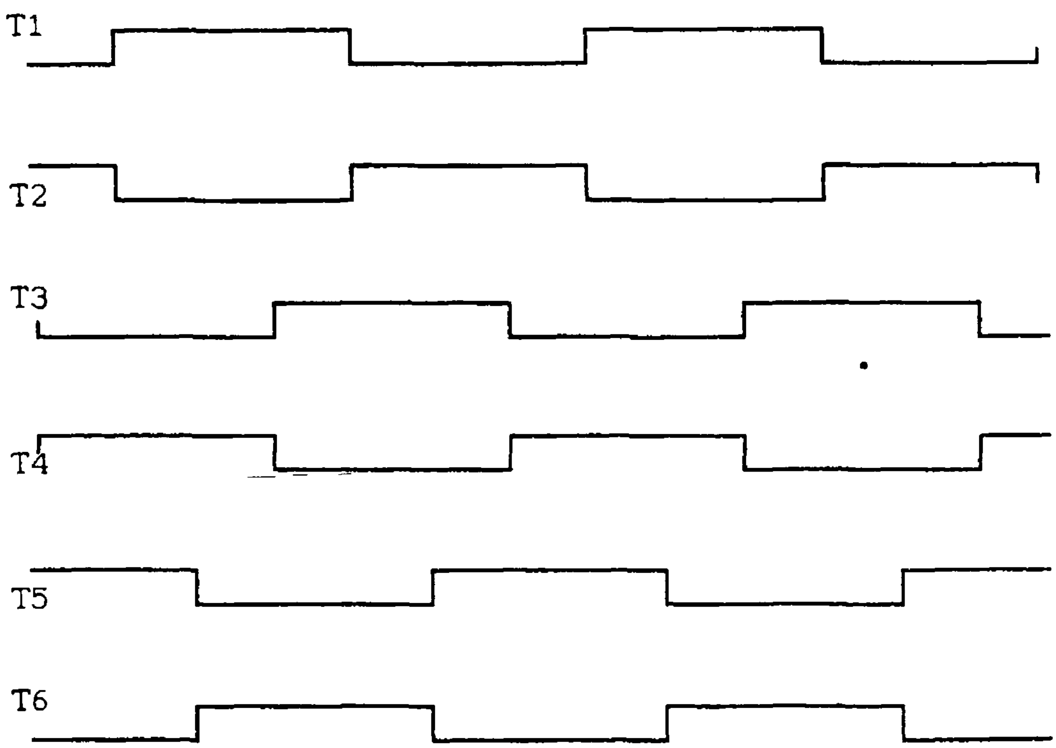

FIGURE(3 2)
THE SIX STEP SWITCHING SEQUENCE

3.1.4 Figure (3.3) shows a possible hardware configuration. The DC voltage feeding the VSI is variable, dependent on the magnitude of current demanded. The current demanded is itself dependent on the magnitude of the velocity error. The thyristor bridge rectifier is fed from a 3 phase voltage supply. This, combined with the filtering action of capacitor C, ensures a low ripple DC supply to the inverter.

3.1.5 The transistor turn on sequence of figure (3.2) generates a per phase voltage like that of figure (3.4). The harmonic content of this wave can be described by:

$$bn = \frac{2V_{BUS}}{3n\pi}\left[[1-(-1)^n] + \cos\frac{n\pi}{3} - \cos\frac{2n\pi}{3}\right] \quad \ldots.(3\ 1)$$

This equation is developed in appendix (1).

The harmonic spectrum, visually represented in plot (3.1) comprises the fundamental or driving voltage for the phase which produces the desired phase current and upper harmonics. The upper harmonics serve no useful purpose and cause heating losses and torque pulsations [P12]. This problem can be compounded at low speeds, when the only effective impedance to the upper voltage harmonics is the phase resistance. The fundamental voltage, only, is opposed by the back emf, (in trapezoidal back emf motors, all harmonics would in some way be opposed [B5, P12]) so the actual first harmonic phase current is generated by the voltage phasor sum of these two quantities.

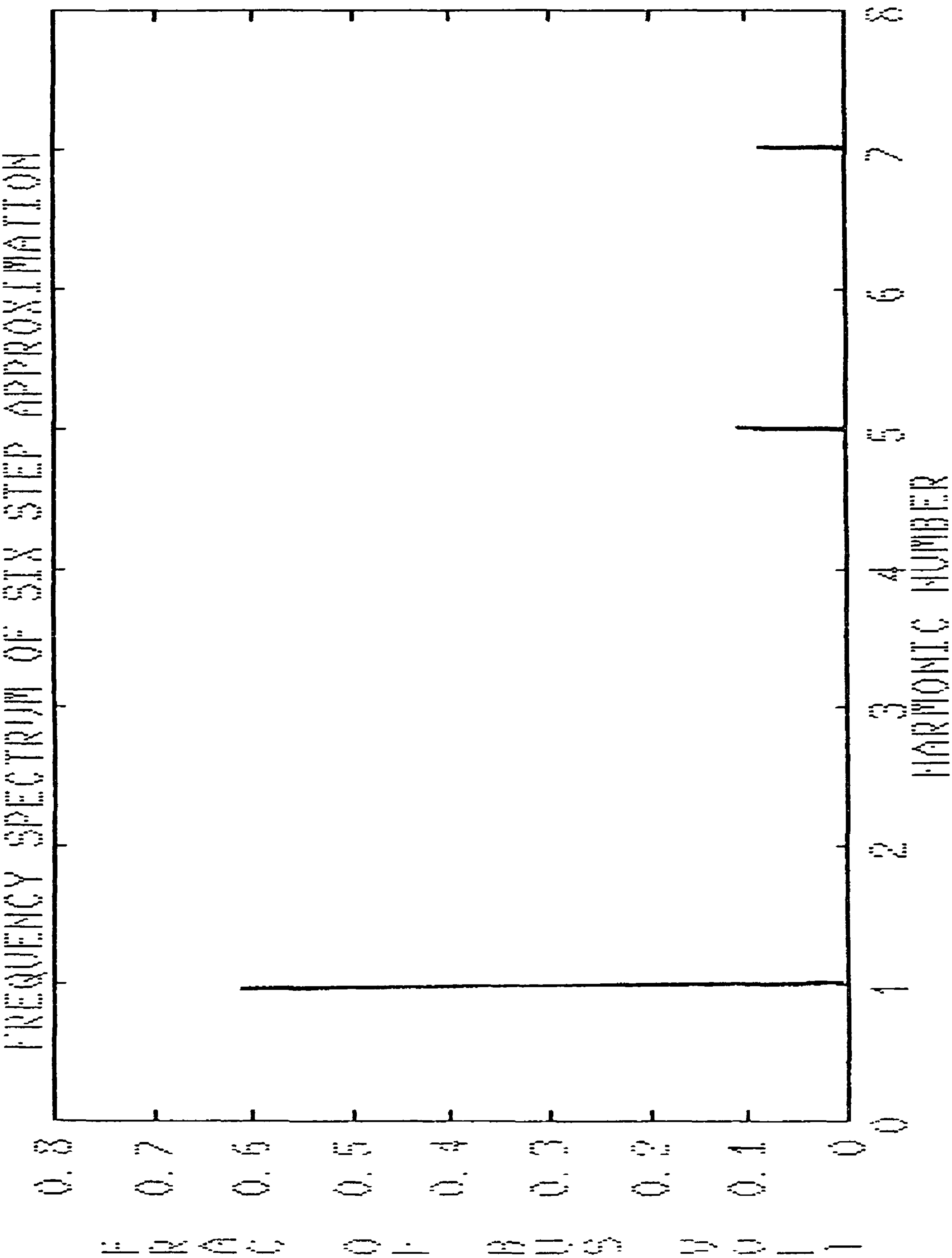
FREQUENCY SPECTRUM OF SIX STEP APPROXIMATION
HARMONIC NUMBER
0
1
2
3
4
5
6
7
8
0
0.1
0.2
0.3
0.4
0.5
0.6
0.7
0.8

PLOT(3 1)

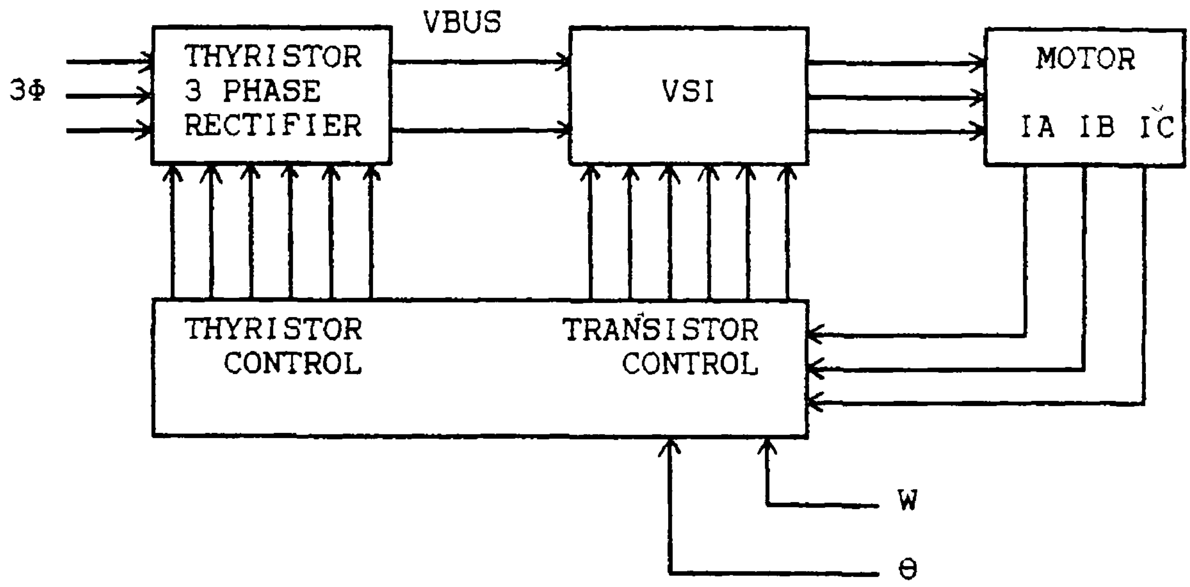

FIGURE(3 3)
THE SIX STEP CONTROL SCHEME

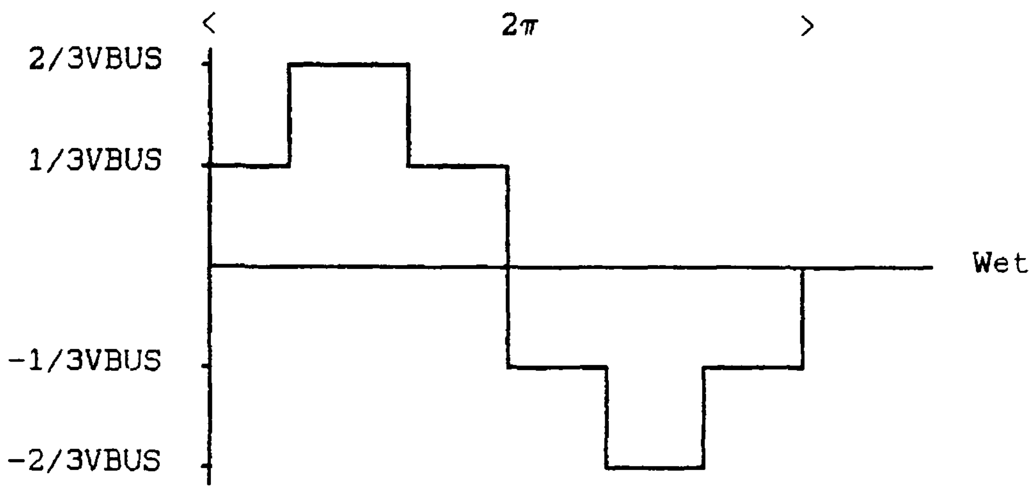

FIGURE(3 4)
THE SIX STEP SINE WAVE APPROXIMATION

3.2 The voltage source inverter and pulse width modulation

3.2.1 A more efficient drive method for a 3 phase synchronous machine would have to reduce or eliminate the harmonic problems of the six step approximation. Pulse width modulation achieves this aim. By using a carrier wave to carry the desired frequency and magnitude of sine wave, the harmonic spectrum of the resultant signal can be made to emulate the modulation spectrum of a typical communications system. This is where the information signal is of a significantly lower frequency than the carrier signal. This makes filtering out of the unwanted carrier much easier. [B9].

3.2.2 Figure (3.5) shows how a PWM wave is generated from a modulating wave and carrier. Where the modulating wave is larger than the carrier the PWM signal is high, and the signal is low when the magnitude of the carrier exceeds the modulating signal. Thus a PWM wave could be defined as a digital signal. Figure (3.6) illustrates in block diagram form, a PWM generator.

3.2.3 The structure of the voltage source inverter does not change whether the six step approximation, or PWM is used as the driving signal. The inverter of figure (3.1) is that used in a PWM driven machine. Figure (3.7) is a block diagram representation of a complete 3 phase synchronous motor control system, using PWM. The power stages indicated on the diagram comprise the separate legs of the inverter. The position/speed sensor, in conjunction with the resolver to digital, or R/D converter produces a velocity signal

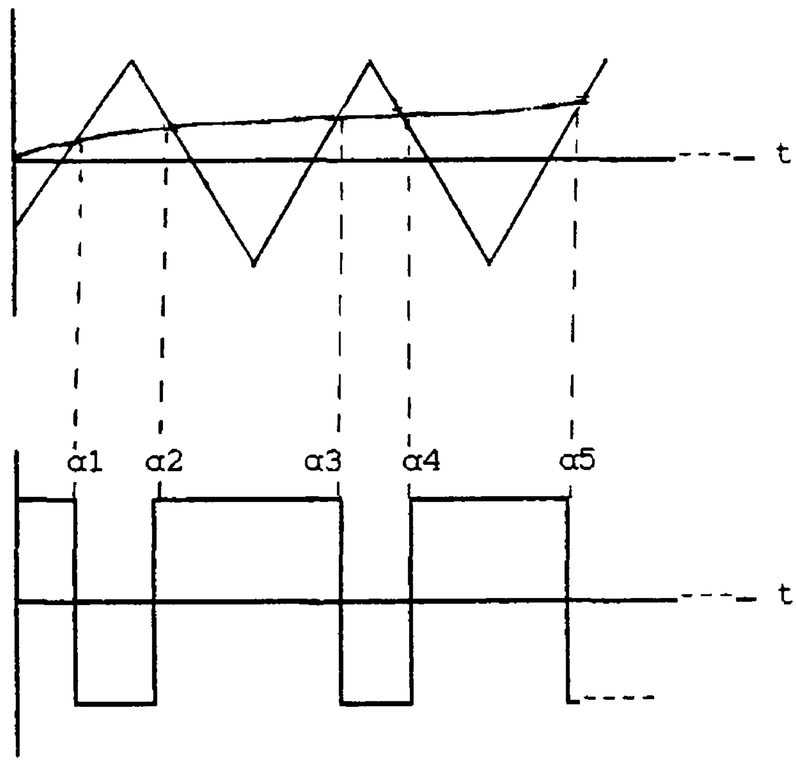

FIGURE(3 5)
GENERATION OF A PWM SIGNAL

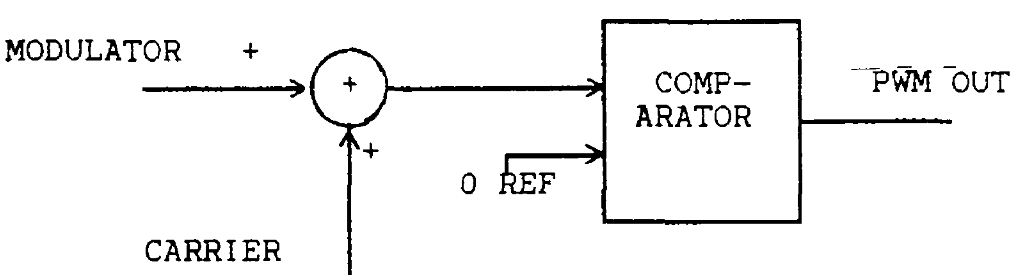

FIGURE(3 6)
BLOCK DIAGRAM OF A PWM GENERATOR

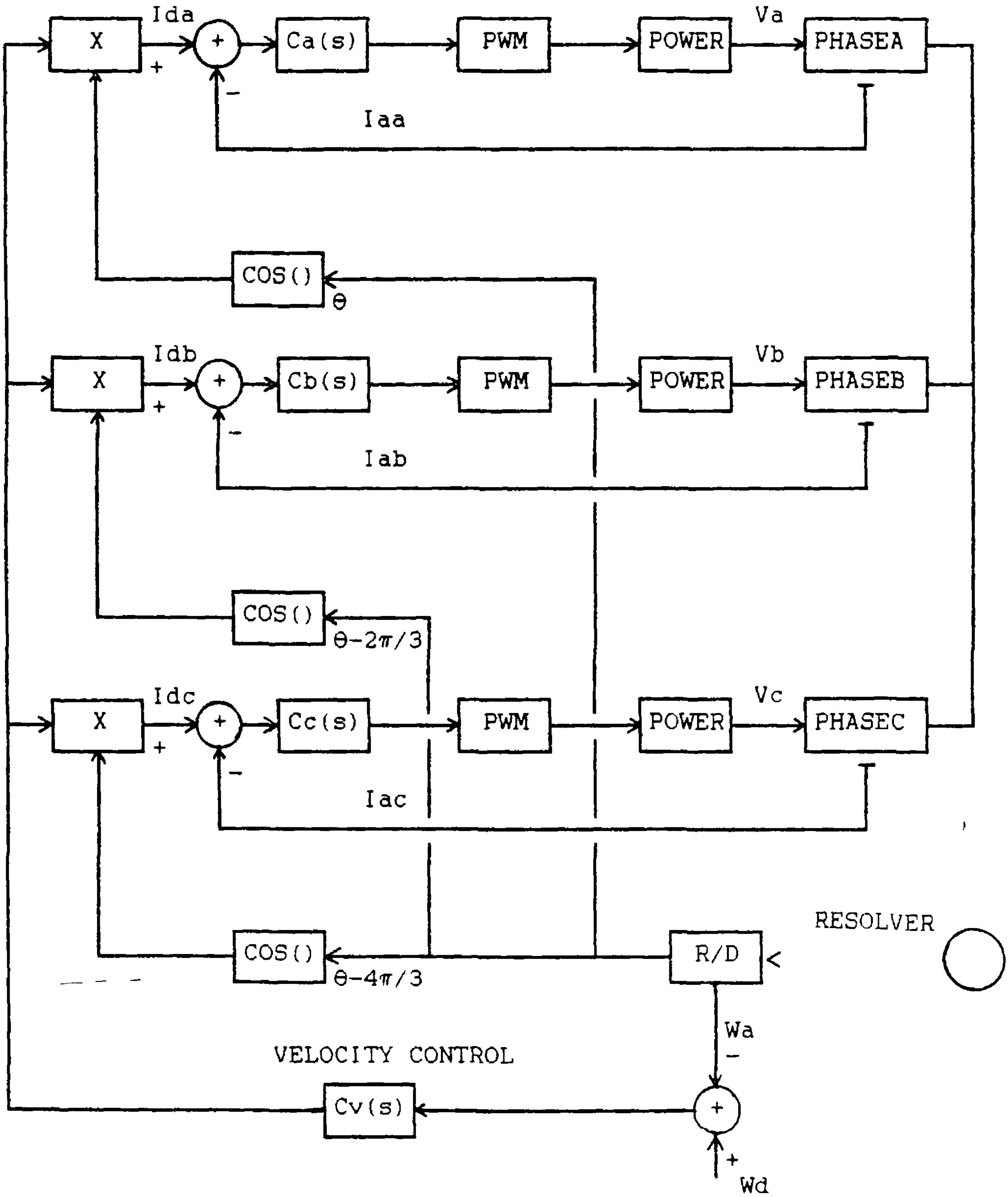

FIGURE(3 7)
A COMPLETE 3 PHASE CONTROL SYSTEM

and 3 angle signals. The Cosine of each angle signal is obtained and these in turn are scaled by the velocity controller output to generate 3 current demands, Ida, Idb, Idc. Reference back to equations (2.1, 2.2, 2.3) shows that these current demands are in the form required to produce machine rotation. The current control compensators Ca, Cb, Cc generate as their output signals the inputs to the 3 PWM stages.

3.2.4 The main function of the VSI is to act as a voltage amplifier. The signals produced by the PWM stages would generally be of a level constrained by analog or digital hardware, so amplification is necessary. The single signal generated by the circuit of figure (3.6) is not sufficient to drive a leg of the VSI. It is necessary in order to emulate the signal emanting from the PWM stage at the motor phase, to also produce the inverse of the signal. The signal is used to drive the top transistor of the inverter and its inverse drives the bottom (refer to figure (3.1)). Thus when the signal is high, the top transistor is turned on, and the bottom is turned off and the bus voltage is applied to the motor phase. When the signal is low the phase has 0V applied to it.

3.2.5 The signals to drive each leg of the VSI are mutually exclusive of each other in that when the upper transistor of the leg is turned on, the lower is turned off, and vice versa. The moment of transition is a crucial time, ie when T1 switches from on to off and when T2 switches from off to on. At this instant it is possible, due to a variation in on and off switching times of the power transistors that both transistors could be on at the same time. This would mean V_{BUS} shorted to 0V and subsequent breakdown of both transistors. To guard against this a hysteresis circuit is introduced into the system. Figure (3.8) illustrates such a circuit along with the outputs to drive both transistors that result. Figure (3.9) shows the voltage appearing at the motor phase. The shaded areas indicate the time when both transistors are off. During these intervals the voltage appearing at the phase is not directly controlled and is dependent on the state of conduction of either flywheel diode in that phase.

3.3 Spectral analysis of PWM

3.3.1 To completely define a PWM wave, two ratios are needed

1. modulation index. This describes the modulation depth of the signal. It is defined as,

$$\frac{\text{Peak magnitude of modulating signal}}{\text{Peak magnitude of carrier}}$$

2. Carrier ratio. This describes the ratio of the carrier frequency to the modulating wave frequency. It is defined as:

$$\frac{\text{Carrier frequency}}{\text{modulating frequency}}$$

Knowledge of both ratios and one frequency and magnitude will yield a complete description of the modulation system.

3 3.2 Although the PWM signal is relatively simple to generate, its spectrum is very complex in structure. A method of analysis called the "Wall method" as proposed by W R Bennett can be used to successfully analyse the

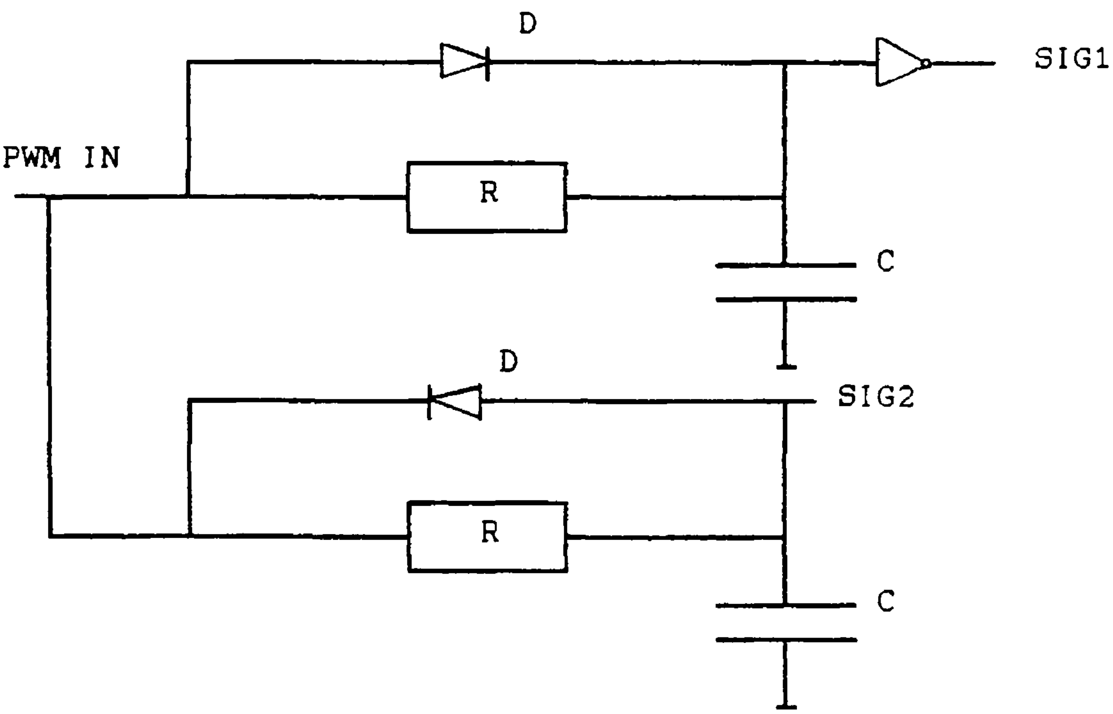

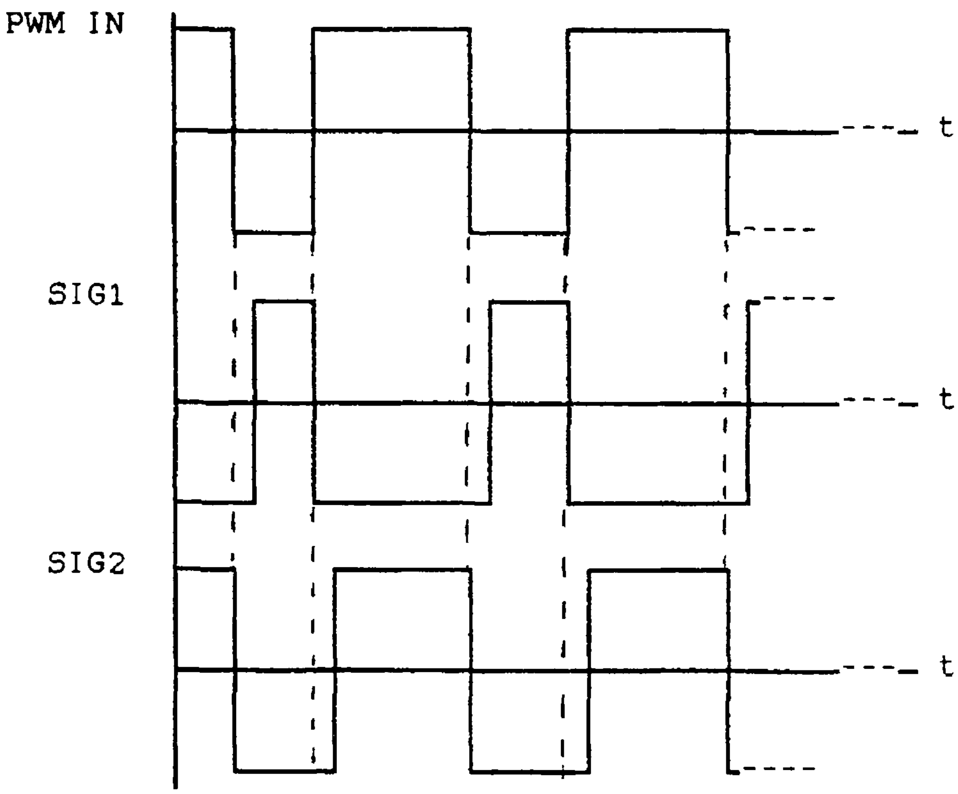

FIGURE(3 8)
THE HYSTERESIS CIRCUIT AND GENERATED OUTPUTS

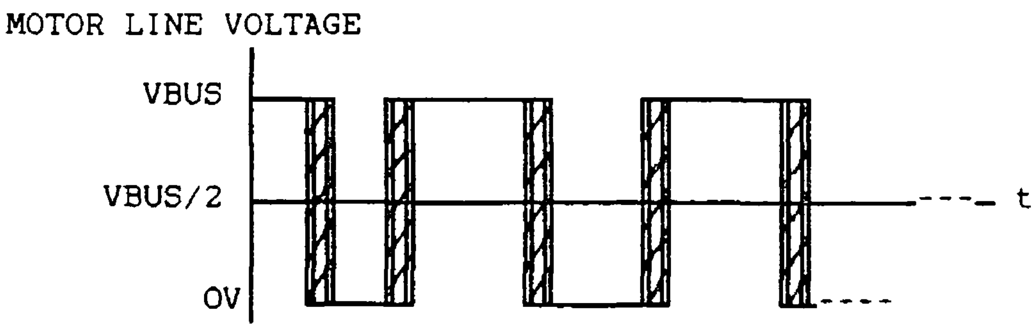

FIGURE(3 9)
THE MOTOR LINE VOLTAGE

signal [B9, P4, P5]. Normal fourier analysis assumes that the spectrum of the analysed signal comprises only harmonics falling on integer numbers of the fundamental. The fundamental is assumed to be at the modulating frequency. If the carrier ratio is an integer, then normal fourier series analysis will yield the correct signal spectrum. If however the ratio is non integer then evaluation will not indicate harmonics of multiples of the carrier or the sidebands centred around the carrier and its multiples, as the actual period of the PWM wave will not match the period of the modulating wave. The wall method overcomes these problems by using a two dimensional fourier series. So a PWM wave can be represented by, [B9]

$$F(x,y) = 1/2\ A_{oo} + \sum_{n=1}^{\infty} (A_{on}\operatorname{Cos} ny + B_{on}\operatorname{Sin} ny)$$

$$+ \sum_{m=1}^{\infty} (A_{mo}\operatorname{Cos} mx + B_{mo}\operatorname{Sin} mx)$$

$$+ \sum_{n=1}^{\infty} \sum_{m=\pm 1}^{\infty} [A_{mn}\operatorname{Cos}(mx+ny) + B_{mn}\operatorname{Sin}(mx+ny)] \qquad \ldots\ldots (3.1)$$

where

$$A_{mn} + jB_{mn} = 1/2\pi^2 \int_0^{2\pi} \int_0^{2\pi} F(x,y)\exp[j(mx+ny)]dxdy \qquad \ldots\ldots (3.2)$$

and

$$x = W_C t \qquad \ldots\ldots\ldots\ldots (3.3)$$

$$y = W_R t \qquad \ldots\ldots\ldots\ldots (3.4)$$

where W_C is the carrier frequency

W_R is the modulating frequency

3.3.3 Referring to equation (3.1) the first term is the DC component of the signal. The second term consists of the frequency components of the modulator and its harmonics. The third terms corresponds to the carrier wave and its harmonics, while the fourth terms frequency spectrum is given by the ensemble of all possible pairs formed by taking the sum and difference of integral multiples of each fundamental.

3.3.4 The "wall method" yields the exact spectrum of a PWM wave. However, evaluation of equations of the form (3.1 ...3.4) can be difficult and time consuming. The normal fourier series allows the evaluation of the lower harmonics almost exactly. Since the lower harmonics are of primary interest this is a workable alternative. The fourier coefficients of the signal of figure (3.5) can be computed as, [P2]

$$a_n = \frac{(1+\sum_{i=1}^{k} 2\ (-1)^{i}\ \mathrm{Cos}(n\alpha_i))\ V_{BUS}}{\pi n} \qquad \ldots\ldots\ (3.5)$$

$$b_n = \frac{(\sum_{i=1}^{k} 2.(-1)^{i-1}.\ \mathrm{Sin}(n\alpha_i)).V_{BUS}}{\pi n} \qquad \ldots\ldots\ (3.6)$$

where the α_is are the switching angles of the PWM wave over one period and k is the number of switching angles over one period.

The magnitude of the n^{th} harmonic can be expressed as:

$$An = \sqrt{a_n^2 + b_n^2} \qquad \ldots\ldots\ (3.7)$$

and its phase angle is defined to be

$$\beta = \mathrm{TAN}^{-1}\left[\frac{an}{bn}\right] \qquad (3.8)$$

These equations are developed in appendix (2).

3.3.5 The accuracy of equations (3.5 ... 3.7) can be evaluated by comparing a simulated spectrum to an actual spectrum. The test motor and controller was used in such an evaluation. Tests were carried out for modulation indices of 30%, 45% and 55%. The fundamental frequencies of the modulating signals were 20 Hz, 80 Hz and 120 Hz, the 20 Hz modulating signal referring to a modulating index of 30% and the 80 Hz, 120 Hz signals referring to indices of 45%, 55% respectively. In the following plots, the voltage harmonics peak to peak value are ratioed with line bus voltage. Plots (3.2 .. 3.4) illustrate the theoretical results compared to the experimental results. The experimentally derived spectra were measured at the PWM stage output before the hysteresis circuit, and scaled to the level of the bus voltage. The theoretical spectra compare favourably with the experimental. The lower harmonics, located at multiples of the modulating signal, are very small in magnitude, and as such most are not indicated in the plots. The upper harmonics, located at multiples of the carrier, are also not included. The reason for this is that the currents they produce are not sizeable in magnitude, and will not be considered in subsequent analysis. The first harmonic of the spectrum can be related to the modulation index by

$$V_1 = \frac{V_{BUS}\cdot(\mathrm{MOD\ INDEX})}{2} \qquad \ldots\ldots\ (3.9)$$

This relation holds in the region of under modulation. Thus it can be concluded that the first harmonic of a PWM signal is directly proportional to the modulation index.

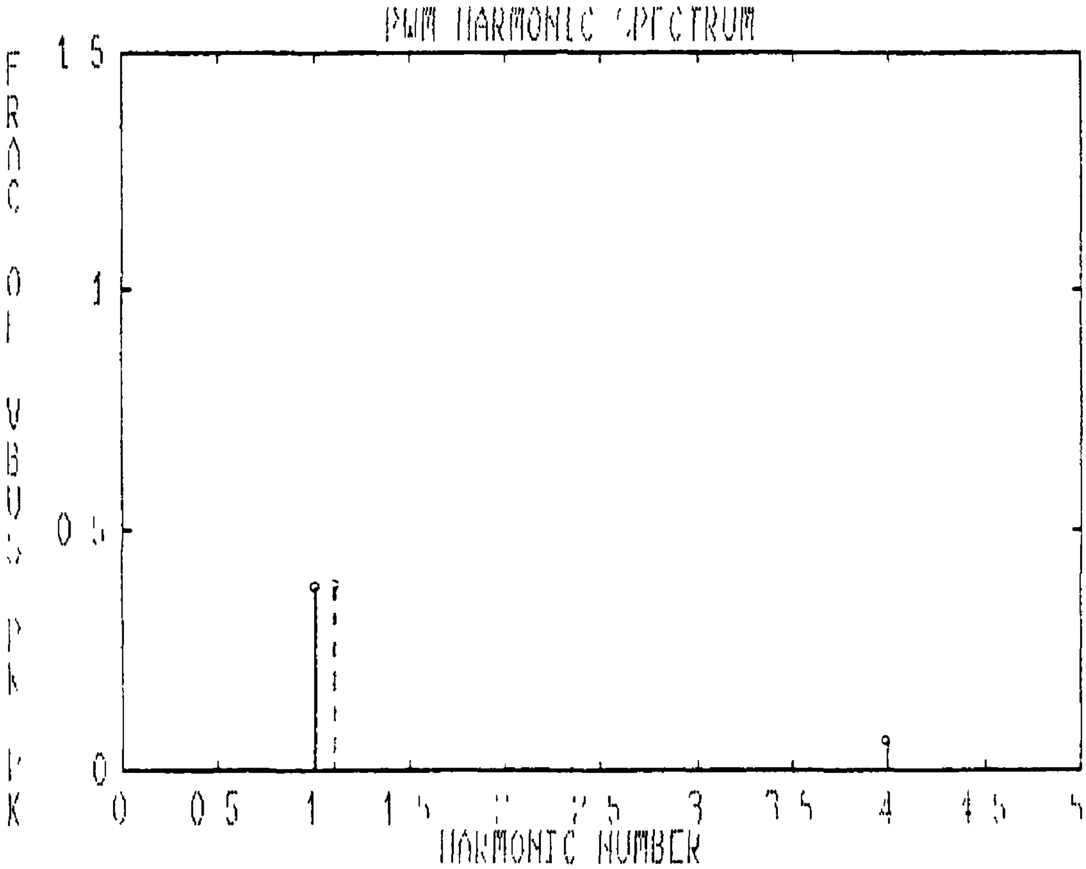

PLOT(3 2)

- - - - - EXPERIMENTAL ———— THEORETICAL

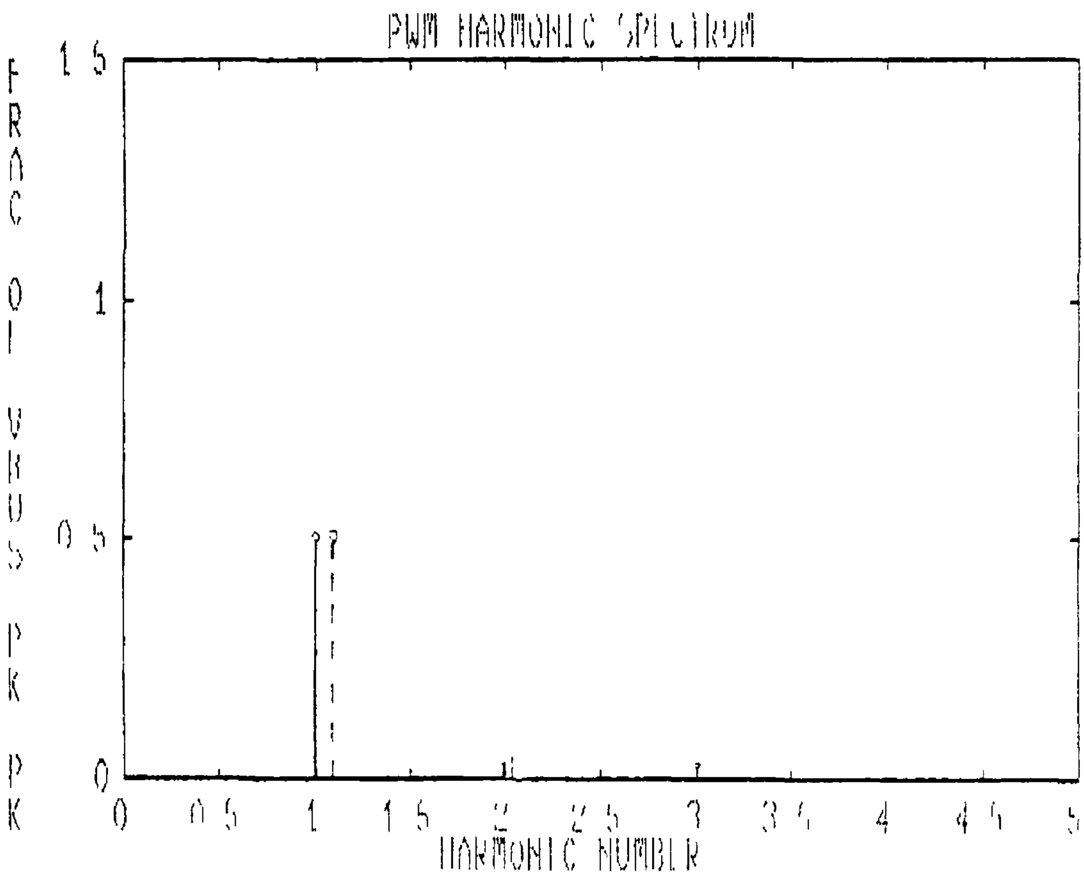

PLOT(3 3)

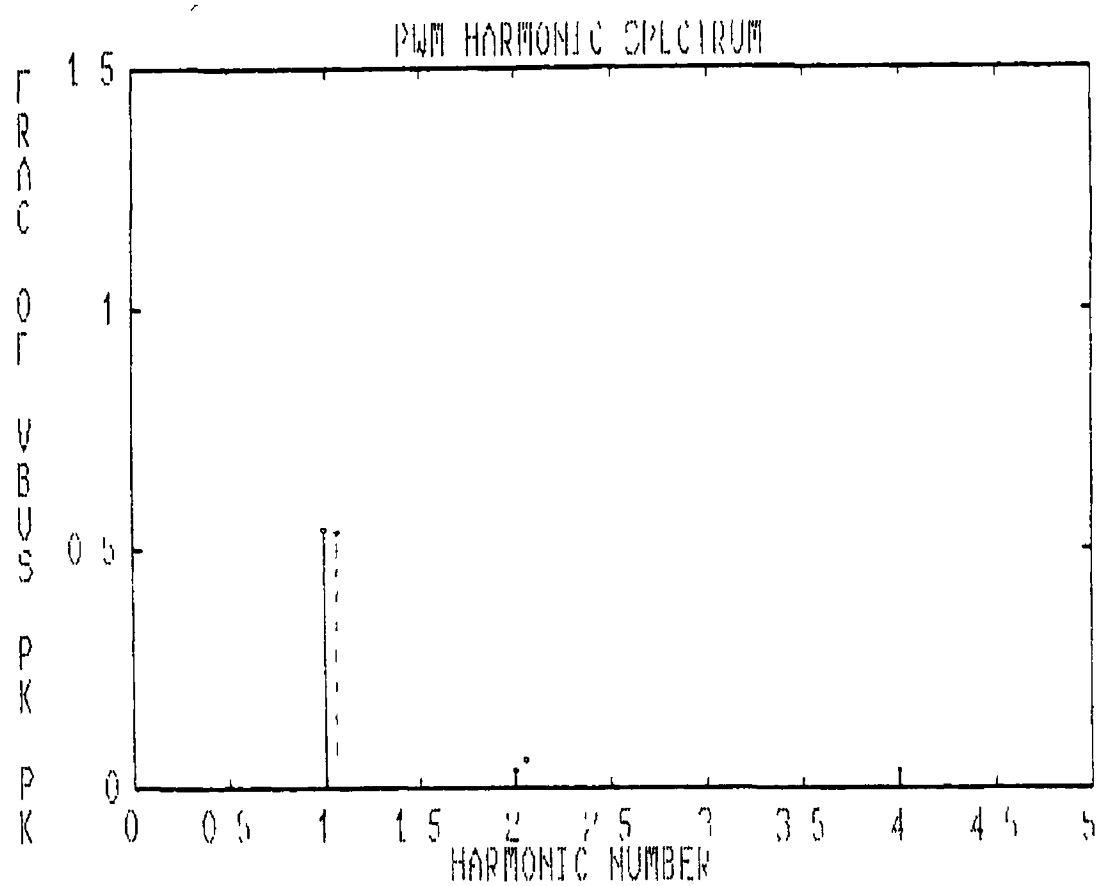

PLOT(3 4)

- - - - - EXPERIMENTAL ———— THEORETICAL

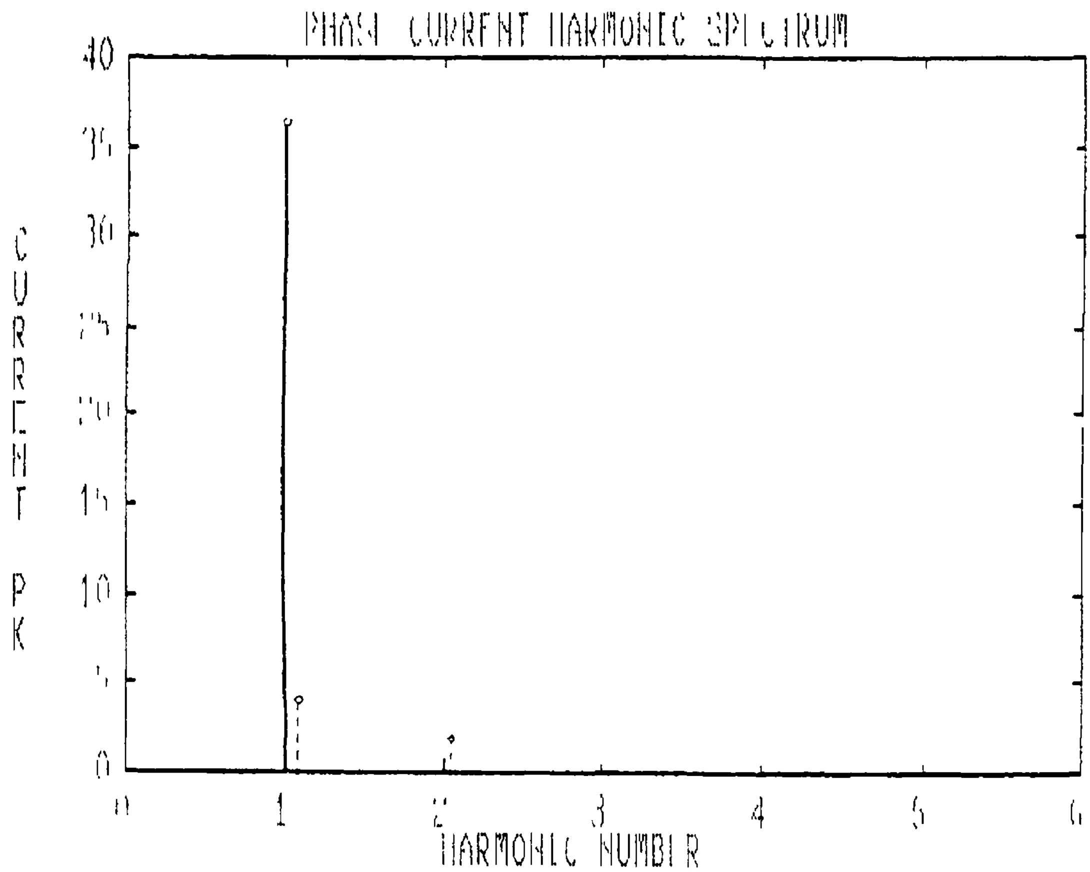

PLOT(3 5)

3.3.6 The procedure of harmonic evaluation can be extended to the evaluation of the phase current harmonics. In appendix (2) the theory is developed that allows the theoretical evaluation. The first current harmonic is a special case as it alone is affected by the back emf. The spectra both theoretical and experimental are evaluated for the same modulation conditions, as section 3.3.5. Plots (3.5 ... 3.7) show the spectra. There is a substantial difference in magnitude between the first harmonics, to such an extent that the theoretical harmonic is consistently of an order ten in magnitude greater than the experimental harmonic. This would seem to make no sense. When the PWM signal was measured, it was taken after the PWM stage, but before the hysteresis circuit. This is significant in light of the fact that the effect of the hysteresis circuit has not been considered. The voltage appearing at the motor pnase should ideally have the same pattern as that signal from the PWM generator. Plots (3.8 ... 3.10), showing the actual spectrum appearing at the motor phase as compared to the spectrum of the PWM stage, indicate that this is not the case. There is a substantial amount of harmonic distortion, which has been introduced between the PWM block and the inverter. An attempt will be made to quantify this distortion.

3.4 The Harmonic Distortion Ratio

3.4.1 To attempt to quantify the level of distortion of the harmonic spectra, various tests were performed. The tests can be separated into two categories:

1. Fixed motor speed (fixed modulating frequency) with a variable torque load.

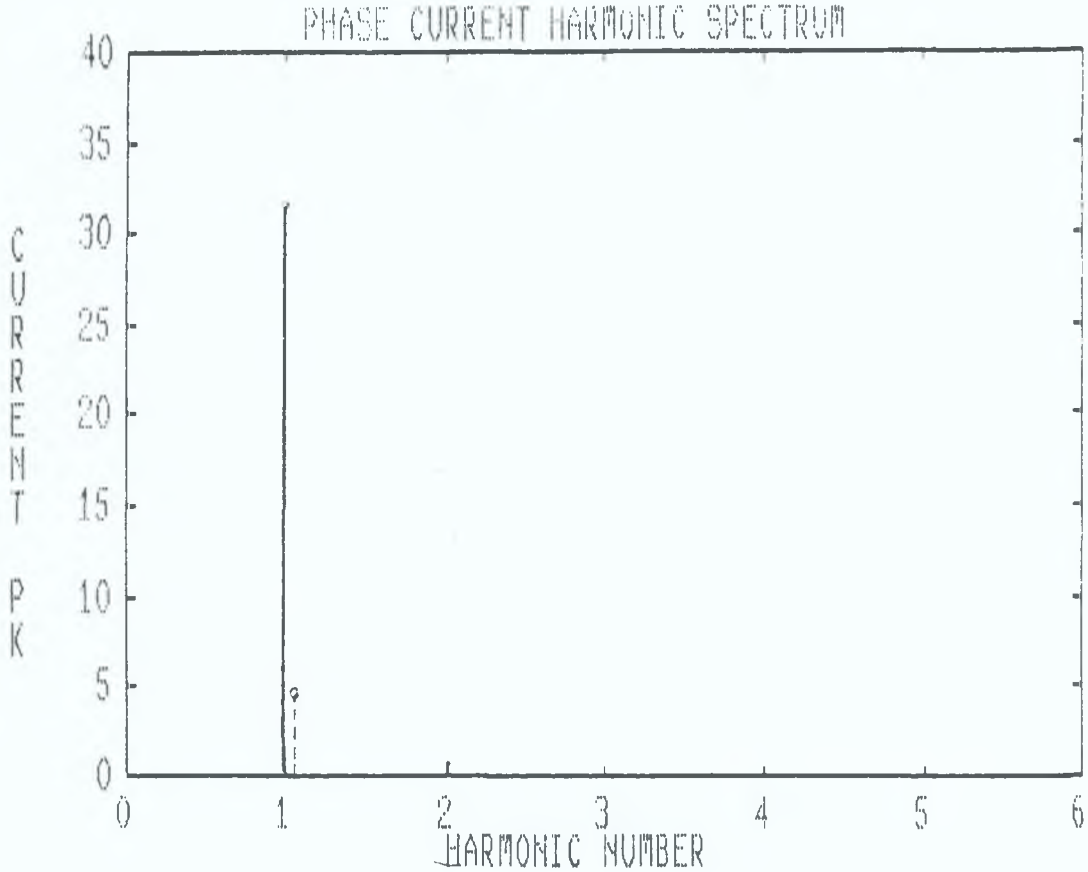

PLOT(3.6)

- - - - - EXPERIMENTAL ———— THEORETICAL

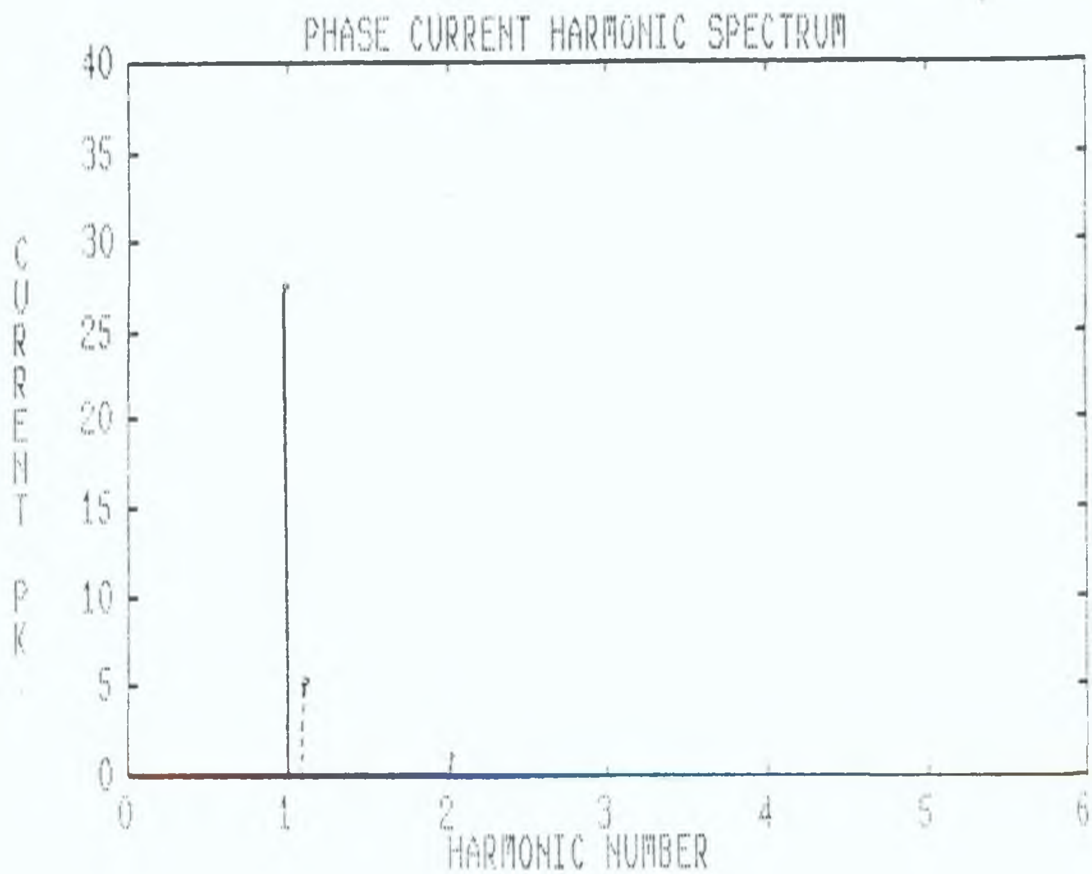

PLOT(3.7)

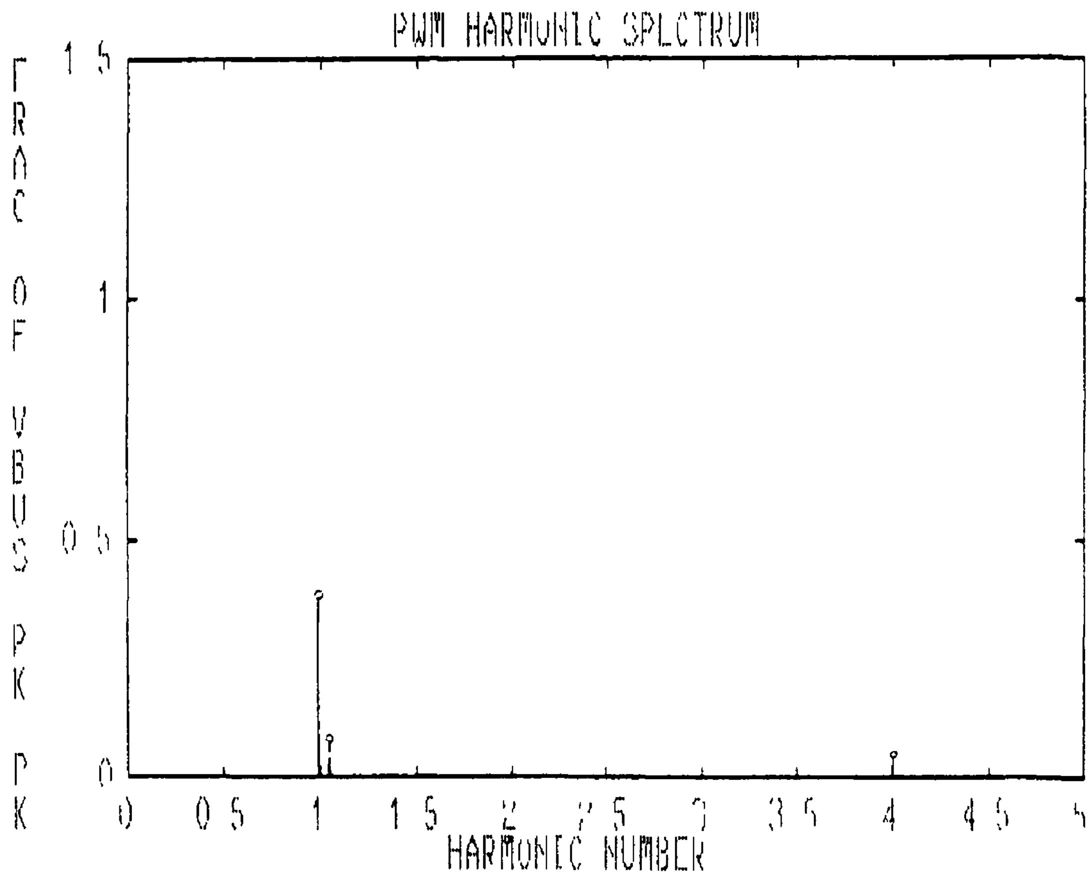

PLOT(3 8)

- - - - - EXPERIMENTAL ———— THEORETICAL

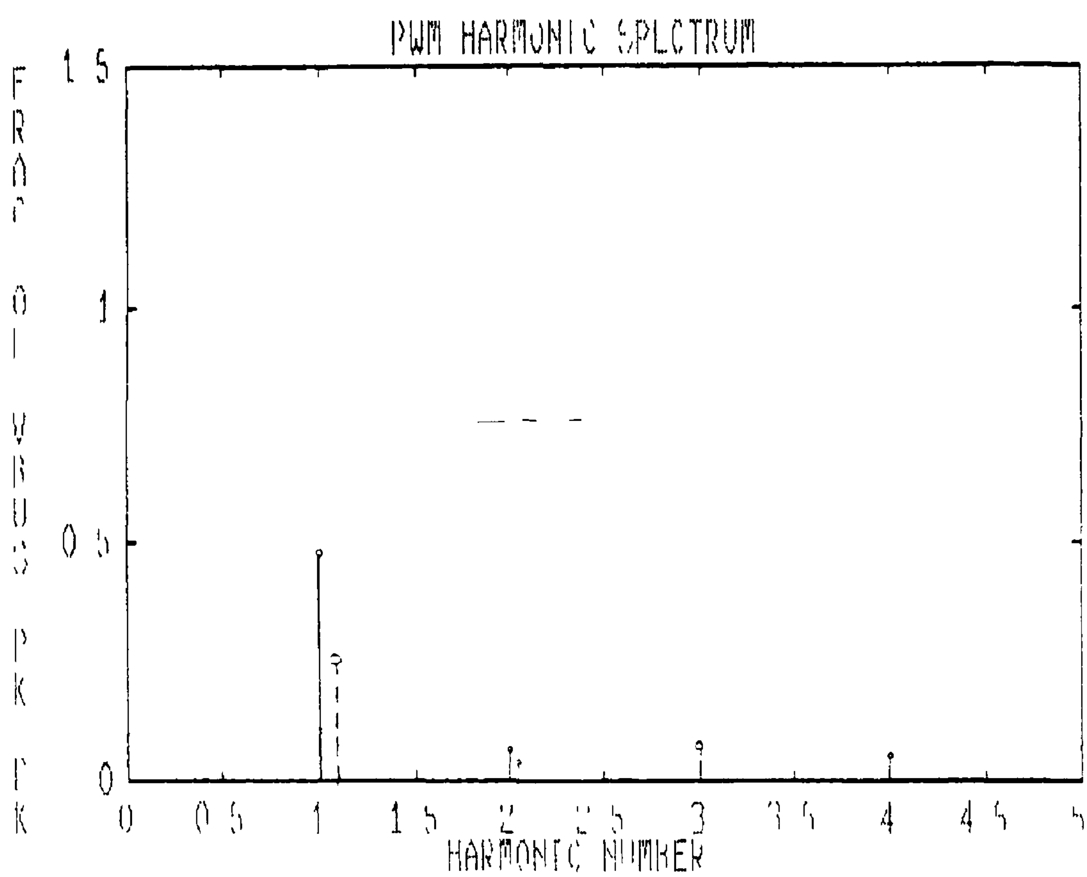

PLOT(3 9)

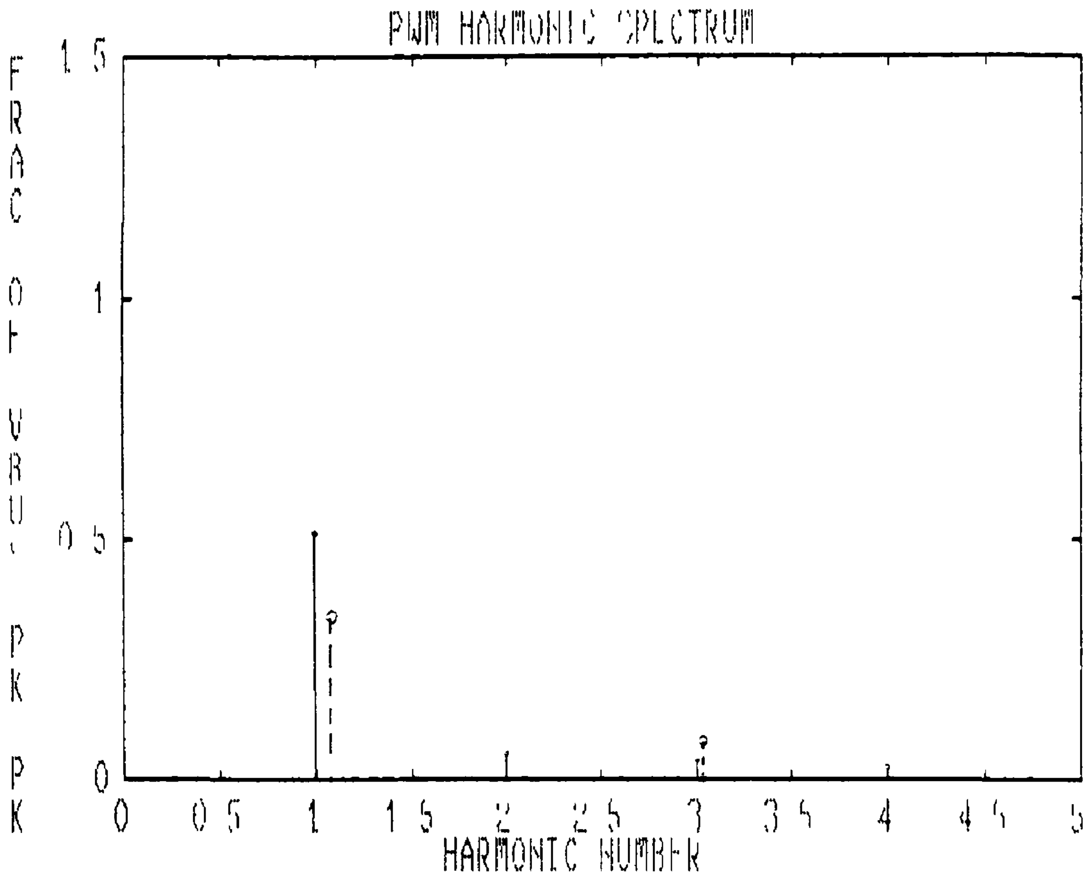

PLOT(3 10)

- - - - - EXPERIMENTAL ———— THEORETICAL

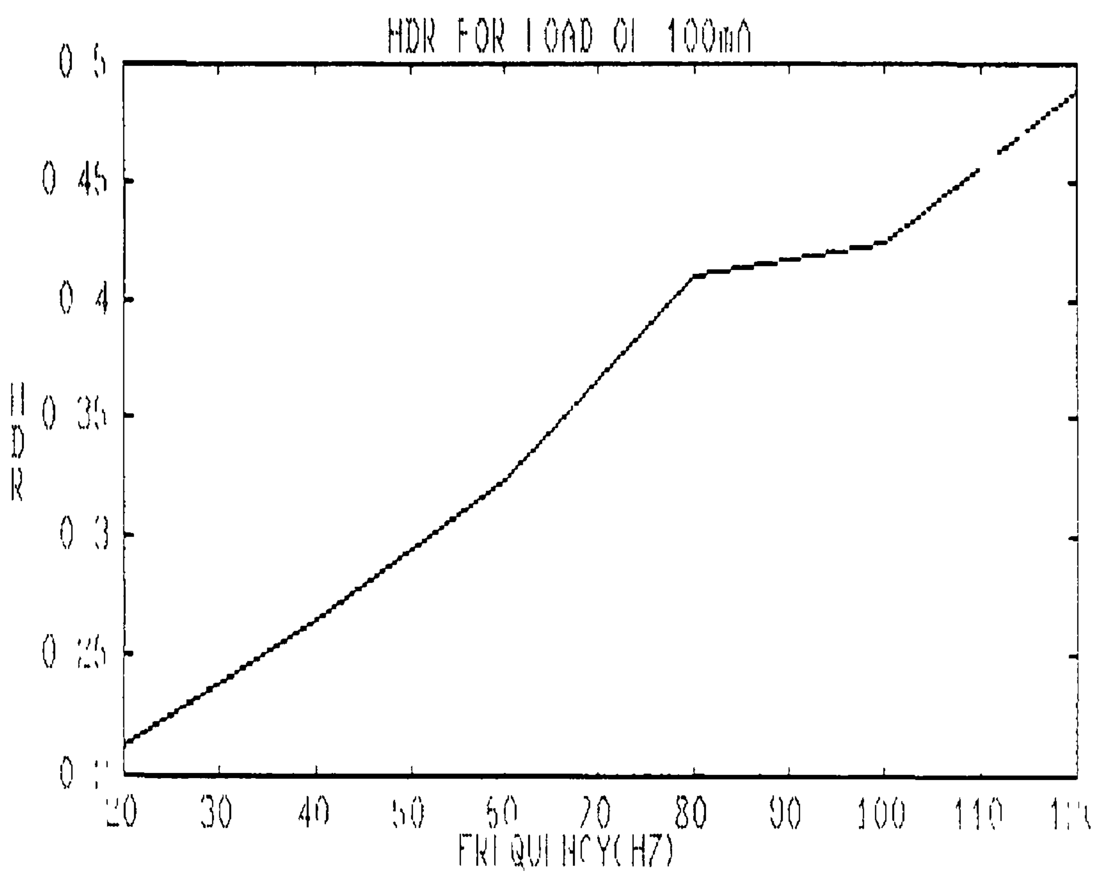

PLOT(3 11)

2. Fixed load torque, variable motor speed.

As is evident from plots (3.8, 3.10) the voltage appearing at the motor phase (ie the voltage at the output of the power stages of figure (3.7)) has a lower first harmonic than the output of the PWM section would indicate. The harmonic distortion ratio is defined to be:

$$\text{HDR} = \frac{\text{magnitude of 1st harmonic at motor phase}}{\text{magnitude of 1st harmonic at PWM stage}}$$

The upper harmonics are also distorted, but as the first harmonic produces machine rotation the level of its distortion is of primary importance.

3.4.2 Plots (3.11 ... 3.13) indicate the variation of HDR with motor speed. The load was kept constant for each plot, being 100 mA, 300 mA, 500 mA for Plots (3.11 ... 3.13) respectively. This load refers to the current flowing in the windings of an eddycurrent dynomometer, which acted as a constant torque source. Plots (3.14 ... 3.15) are dynomometer calibration curves for speeds of 200 RPM, 600 RPM, 1000 RPM (20 Hz, 60 Hz, 100 Hz). Plots (3.17 ... 3.19) illustrate how the ratio changes with torque for speeds of 200 RPM, 600 RPM, 1000 RPM respectively.

3.4.3 Plots (3.11 ... 3.13) clearly show a trend of harmonic distortion ratio increase with speed increase. Plots (3.17 ... 3.19) show an increase in the ratio with load increases. There is a common denominator between the two sets of plots. A speed increase means an increase in the back emf of the motor. In this situation a larger level of voltage is needed to drive the same level of current in the windings. This

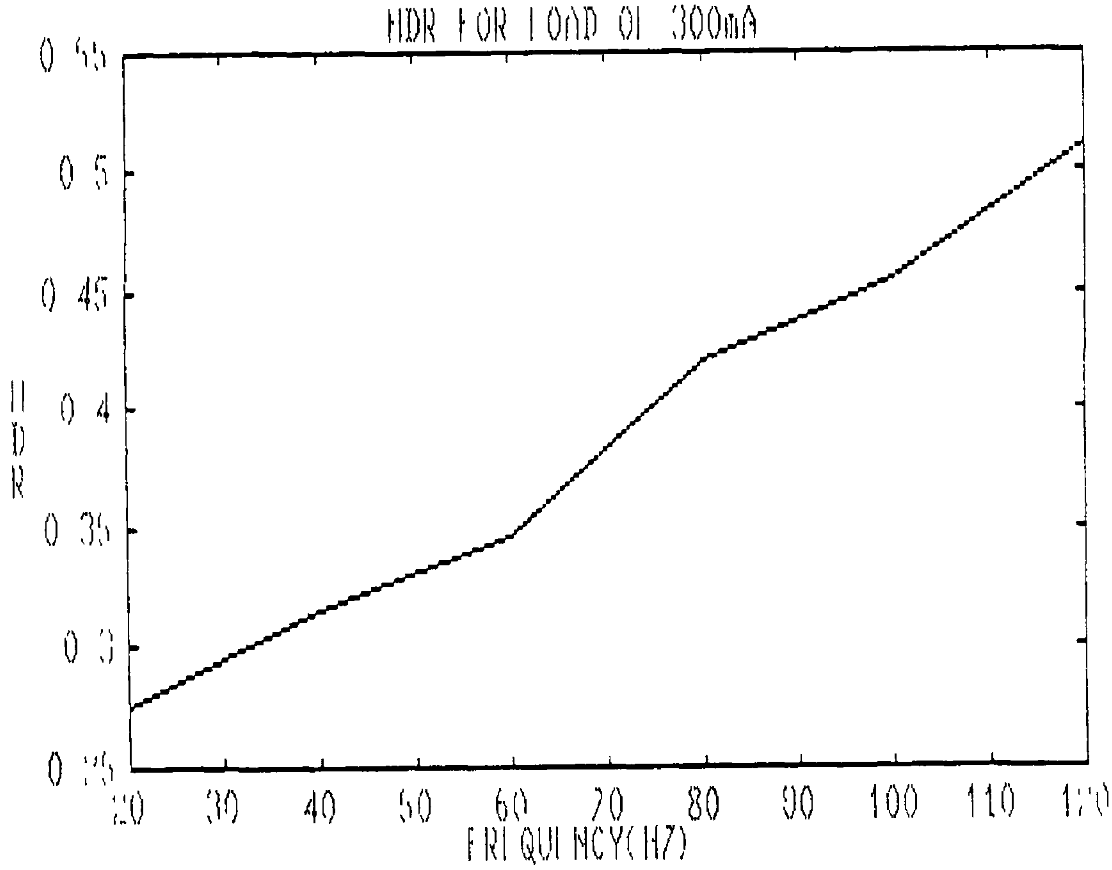

PLOT(3 12)

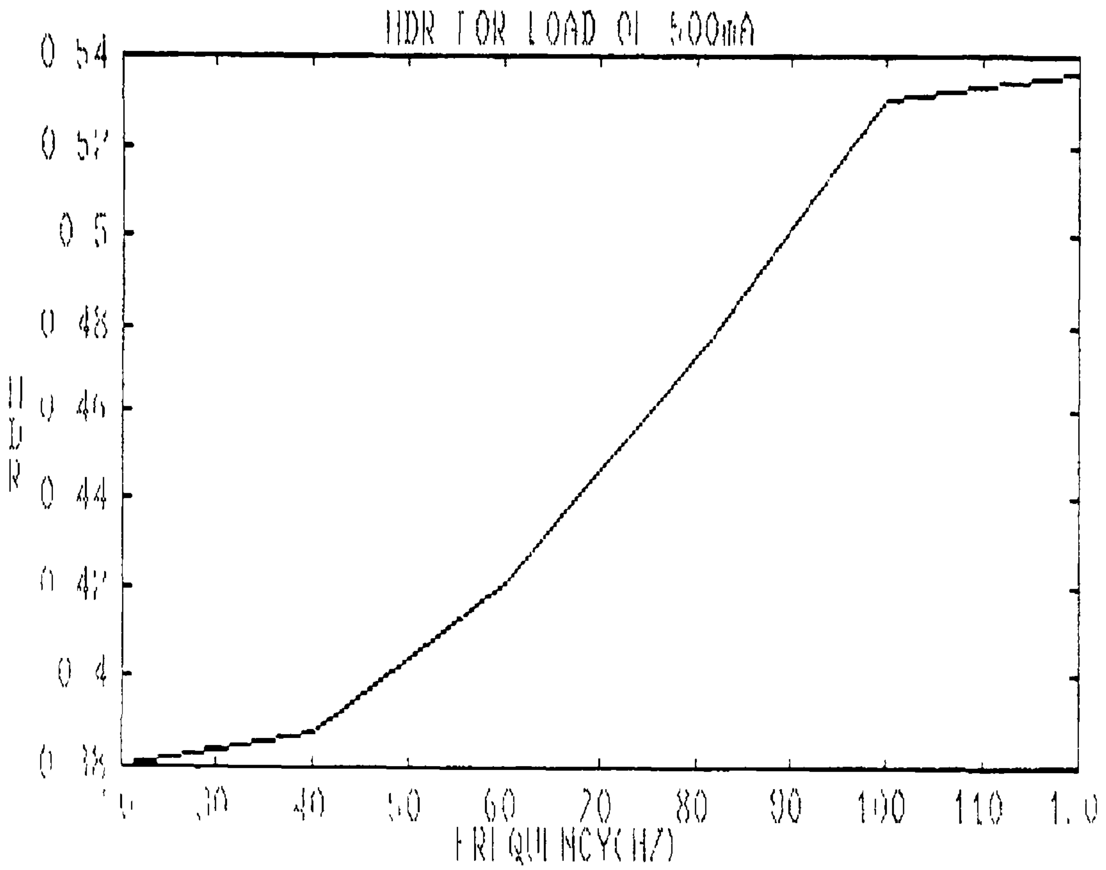

PLOT(3 13)

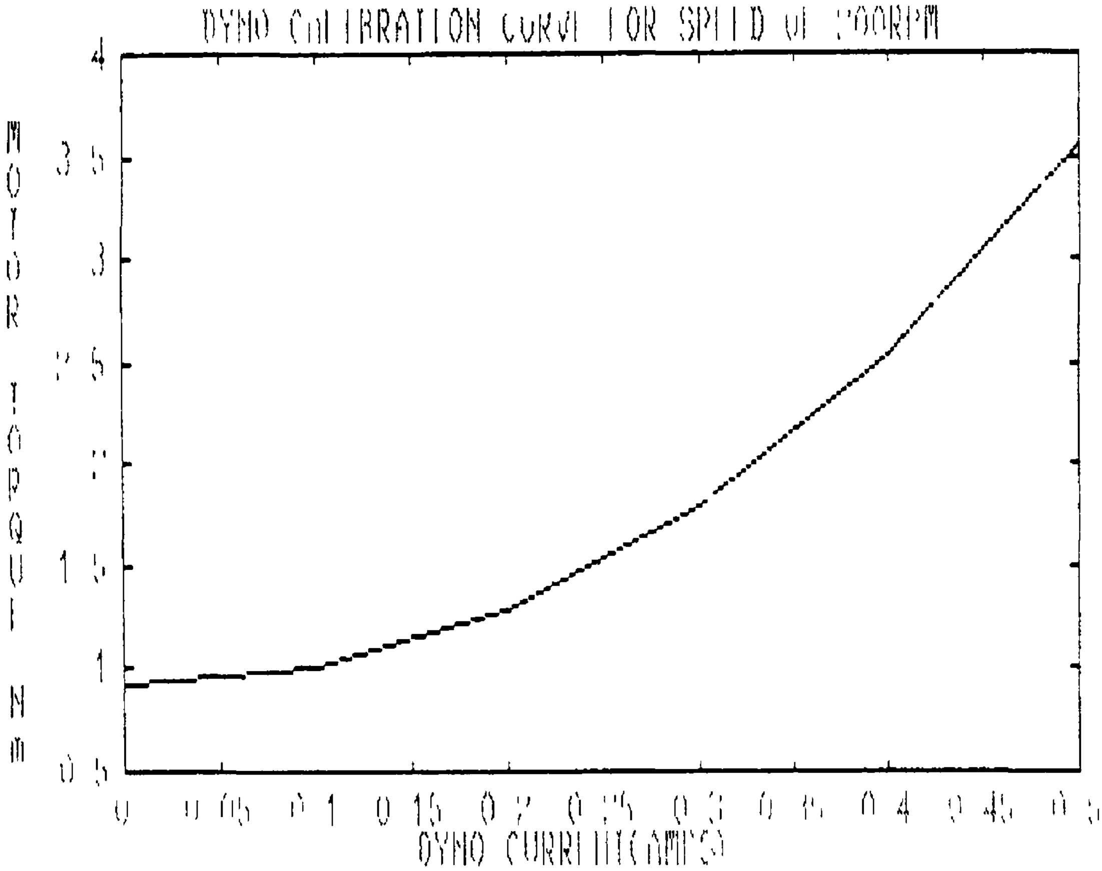

PLOT(3 14)

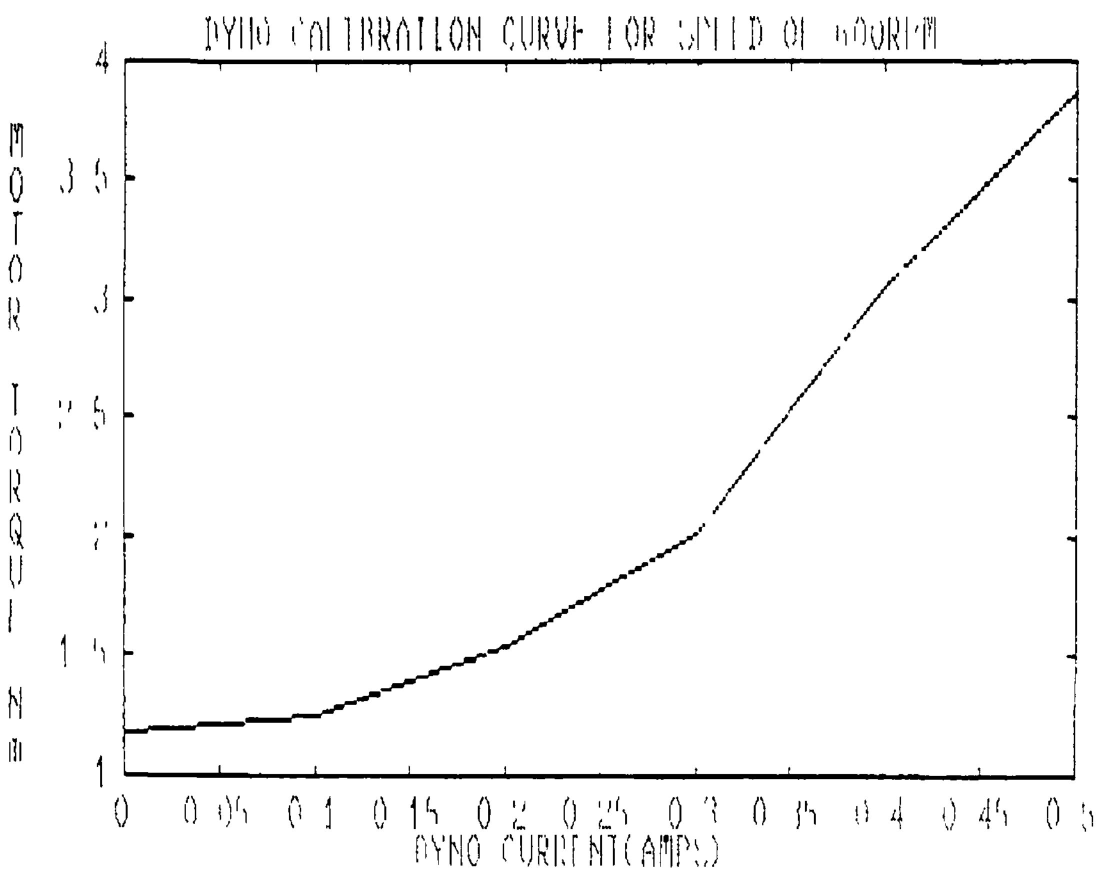

PLOT(3 15)

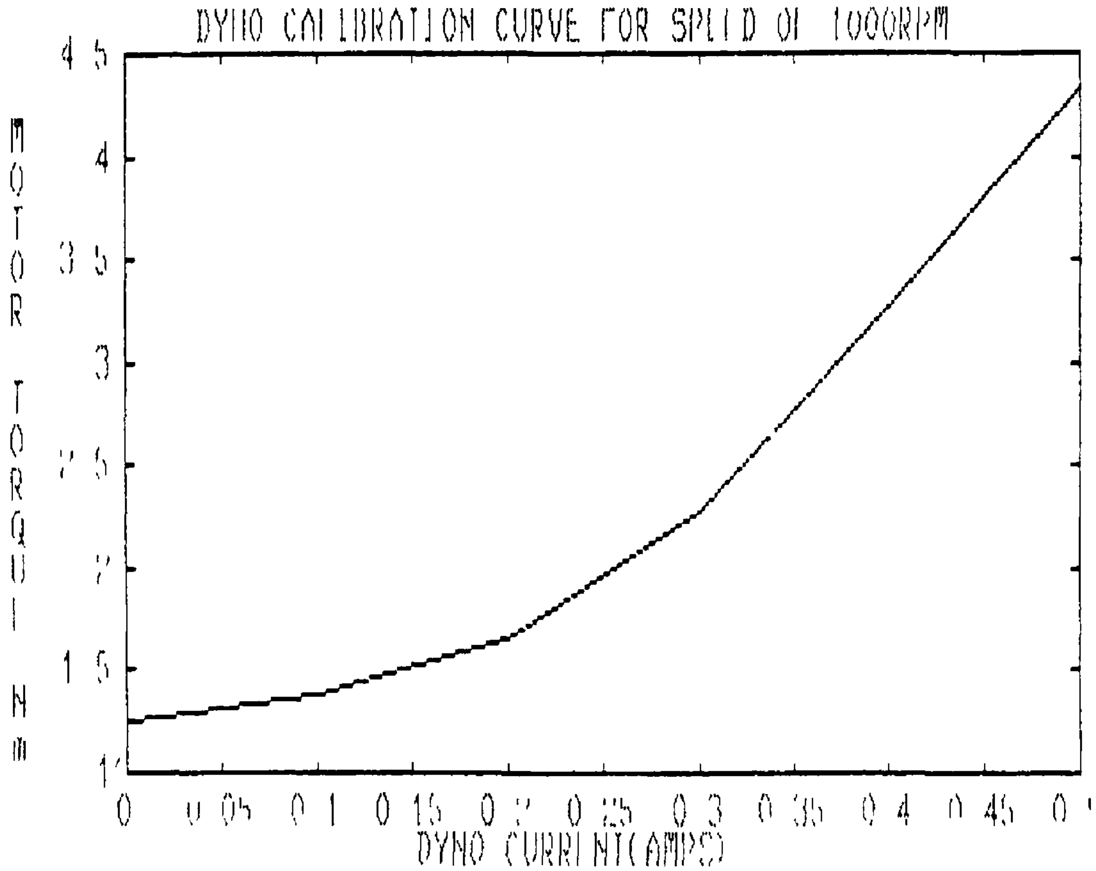

PLOT(3 16)

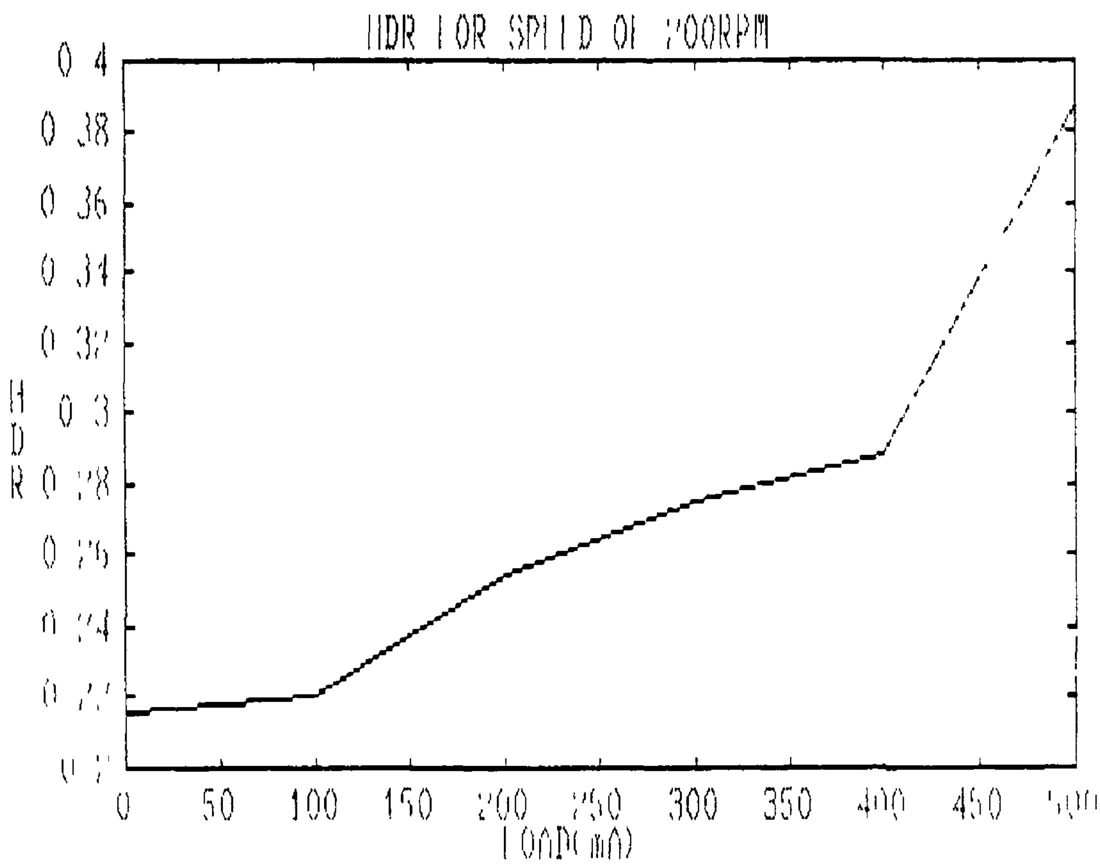

PLOT(3 17)

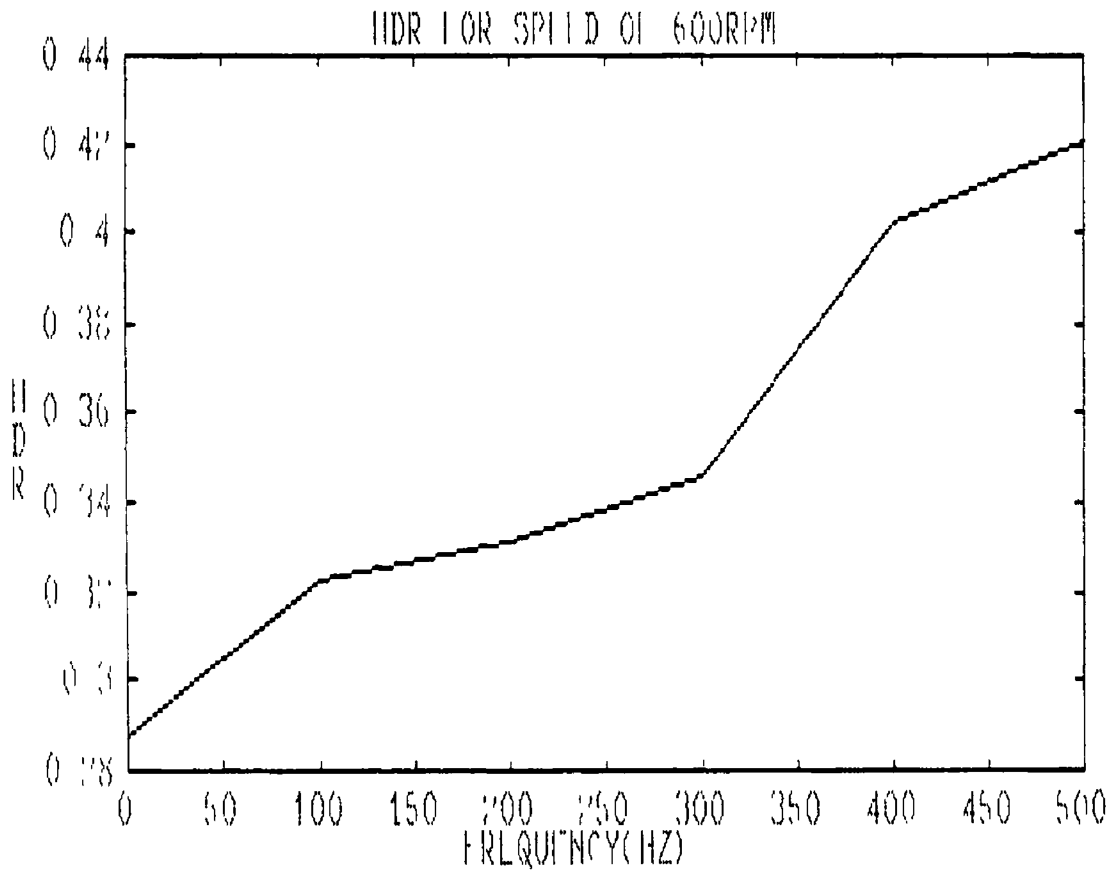

PLOT(3 18)

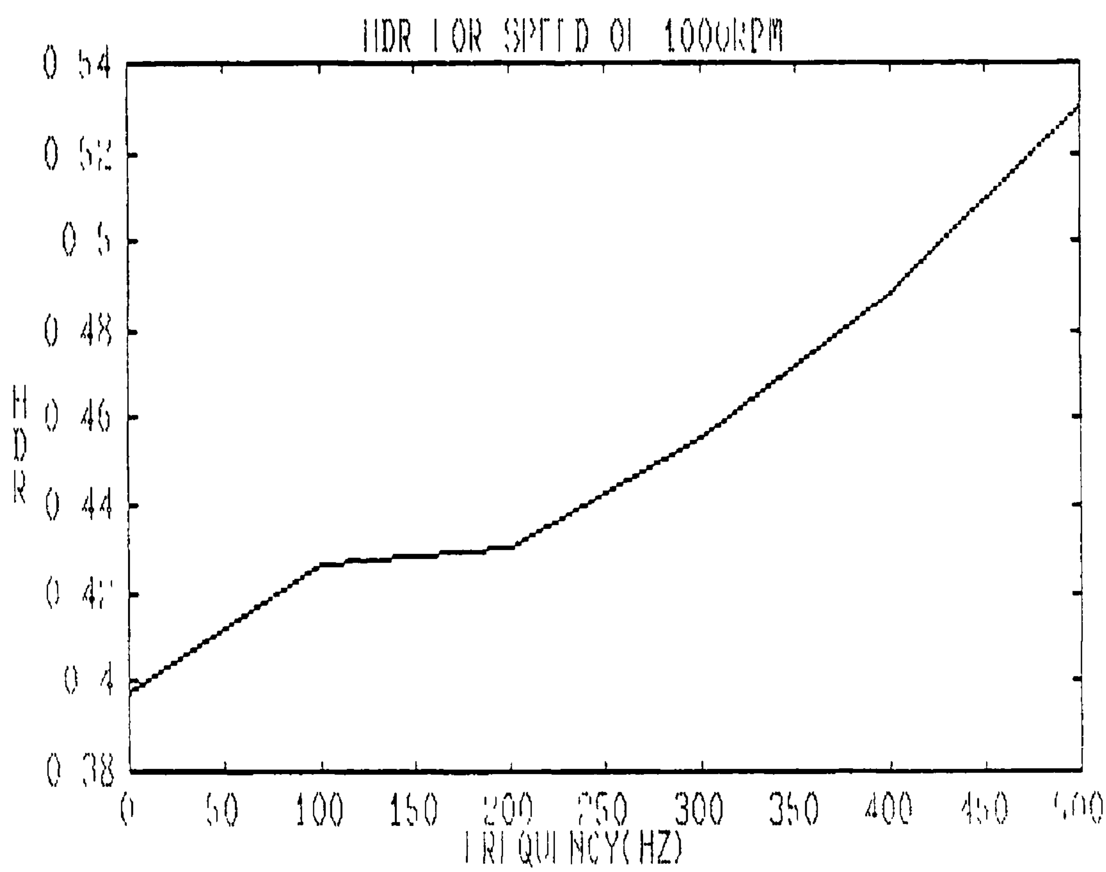

PLOT(3 19)

necessitates a larger modulation index. An increase in motor load requires a larger level of current in the windings to produce the extra torque. A larger modulation index is also needed under these circumstances. Thus it would seem that the harmonic distortion is a function of the modulation index. This is conclusively proven in plot (3.20). Here, the speed is kept constant at 800 RPM, and the load remains fixed at 200 mA (dynamometer current). The modulation index is varied by variations in the bus voltage. For a fixed set of operating conditions, ie fixed speed and load the bus voltage is inversely proportional to the modulation index. The trend displayed by the graph is obvious. The harmonic distortion ratio increases with increasing modulation index. The increase is sharp, initially, then at 100% modulation and beyond, it settles out at a value of one, which effectively means no distortion is experienced by the first harmonic.

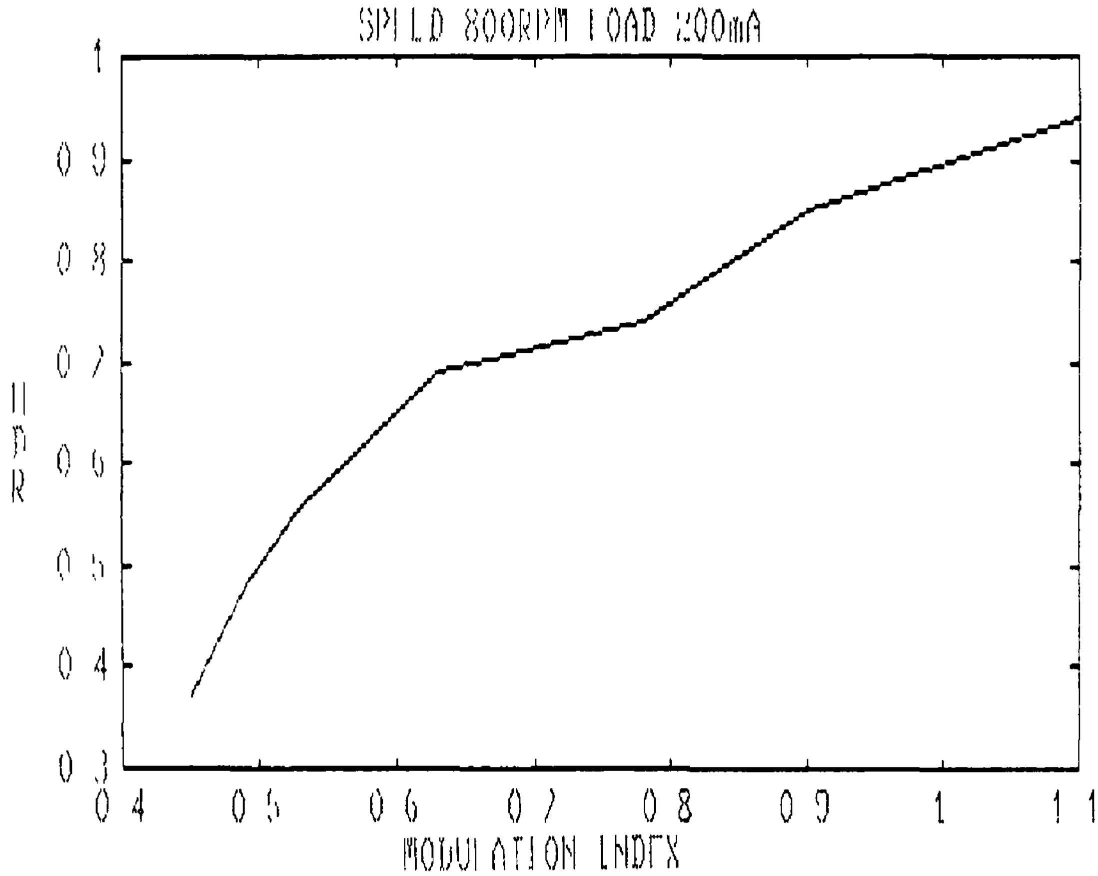

PLOT(3 20)

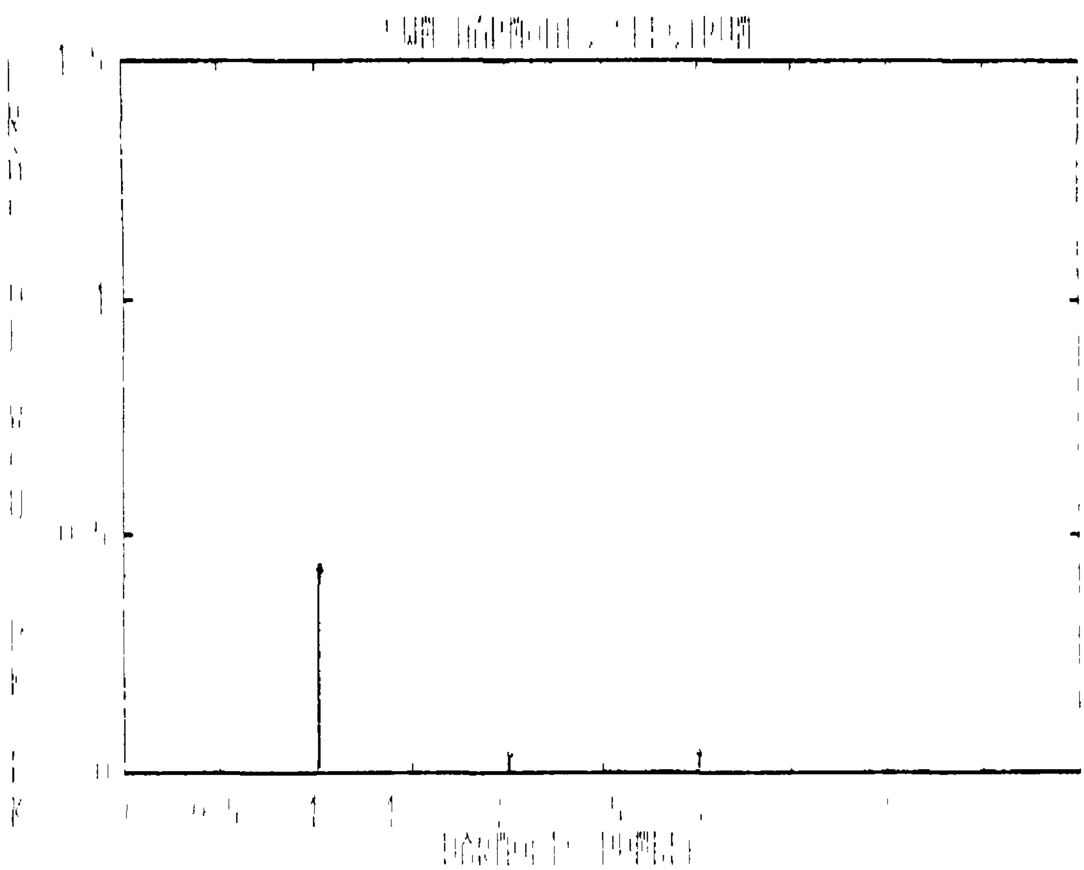

PLOT(3 21)

3.5 The causes of harmonic distortion

3.5.1 The results of 3.4.3 would seem to indicate that the distortion is introduced between the PWM and power stages. The only circuitry between these stages is the hysteresis generator of figure (3.8), which has a hysteresis value, Δt, of 0.02 mS.

3.5.2 The voltage appearing at the motor phase, as illustrated in figure (3.9), has areas (shaded in figure) where the signal is not directly controlled. This occurs because the hysteresis generator ensures that at each transition of voltage, ie when the pwm signal goes from high to low or from low to high, both transistors in the inverter leg are turned off. Referring to figure (3.1), if during this interval the current flowing in the motor phase is sufficient to bias either diode in the inverter leg, then the voltage at the phase assumes a level of either V_{BUS} or 0V. Specifically, if the voltage is initially high, then when both transistors are turned off positive current flows upwards through the lower diode of the leg and the voltage assumes a level of 0V. If the voltage is initially low then conduction occurs through the upper diode and the voltage for the duration of the shaded interval assumes a level of V_{BUS} [B5].

3.5.3 Assuming that this is the situation at all such intervals, a simulation of the signal spectrum with the appropriate voltage levels assumed in the transition intervals, ie V_{BUS} or 0V, should indicate if any distortion is present under such circumstances. A simulation was performed and the resultant spectrum did not differ from the measured spectrum by any considerable amount. The first harmonic in particular seemed not to be affected at all. Plot (3.21) shows the spectrum of a 50% modulated wave with a modulation frequency of 500 Hz assuming no hysteresis, while Plot (3.22) describes the spectrum with the hysteresis included.

3.5.4 Under most operating conditions, the level of current would not always be sufficient to bias the diodes of the inverter leg. If the other extreme to the situation of section 3.5.3 is considered, ie if at each transition interval the voltage at the phase goes to $V_{BUS}/2$, and the spectrum evaluated, the amount of distortion under such circumstances can be assessed. The spectrum of figure (3.10) is plotted in plot (3.23) assuming 50% modulation and modulating frequency of 500 Hz. The first harmonic does not differ from that of plot (3.21).

3.5.5 The actual voltage at the phase assumes a level during transition in between the two extremes described in the previous sections. Figure (3.11) illustrates the type of signal encountered based on tests. The voltage at transition interval $\alpha 1$ corresponds almost to $V_{BUS}/2$ while the voltage at interval $\alpha 2$ is close to that of 0V. Other transition intervals would have voltage level of differing degrees between V_{BUS} and 0V. If these voltage levels at the intervals are assumed to be in proportion to the current magnitude at that instant, ie where the current crosses the zero axis the voltage level assumes $V_{BUS}/2$ and when the current is at its positive or negative maximum, the voltage takes the level of V_{BUS} or 0V, then figure (3.12) describes the resultant PWM wave. Harmonic evaluation of this signal results in plot (3.24). The first harmonic has been reduced by about 20%. This

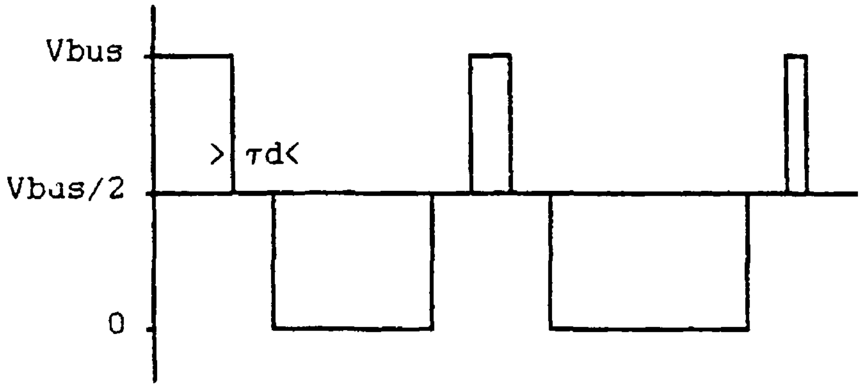

FIGURE(3 10)
THE MOTOR LINE VOLTAGE ASSUMING THE DIODES NOT CONDUCTING

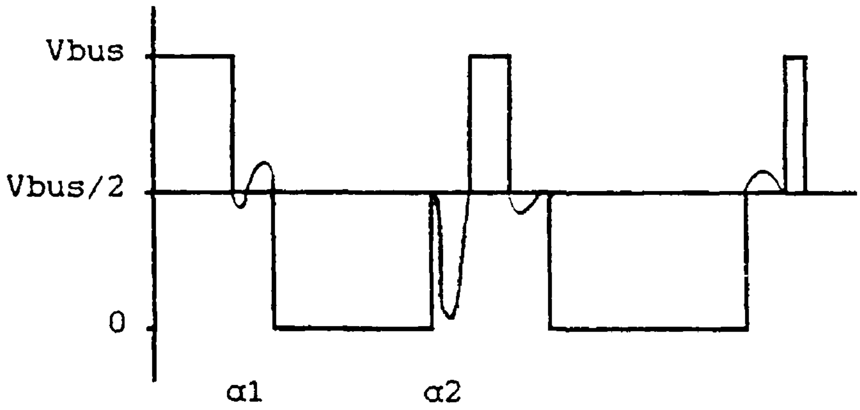

FIGURE(3 11)
THE ACTUAL LINE VOLTAGE

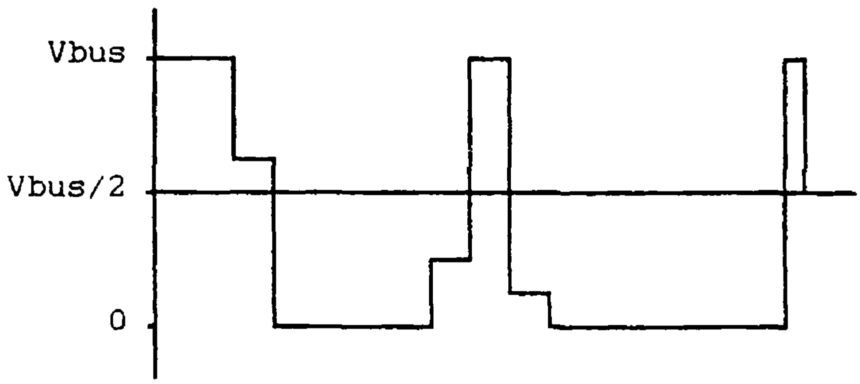

FIGURE(3 12)
APPROXIMATION TO MOTOR LINE VOLTAGE

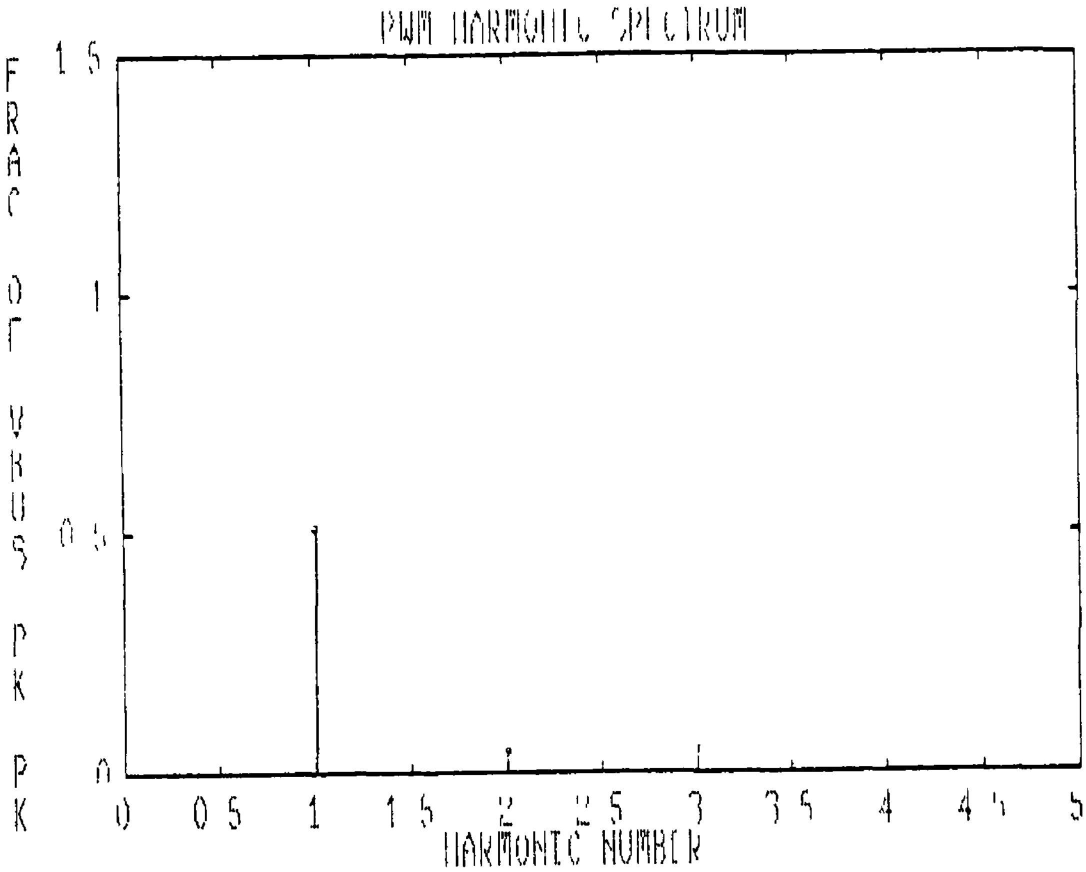

PLOT(3 22)

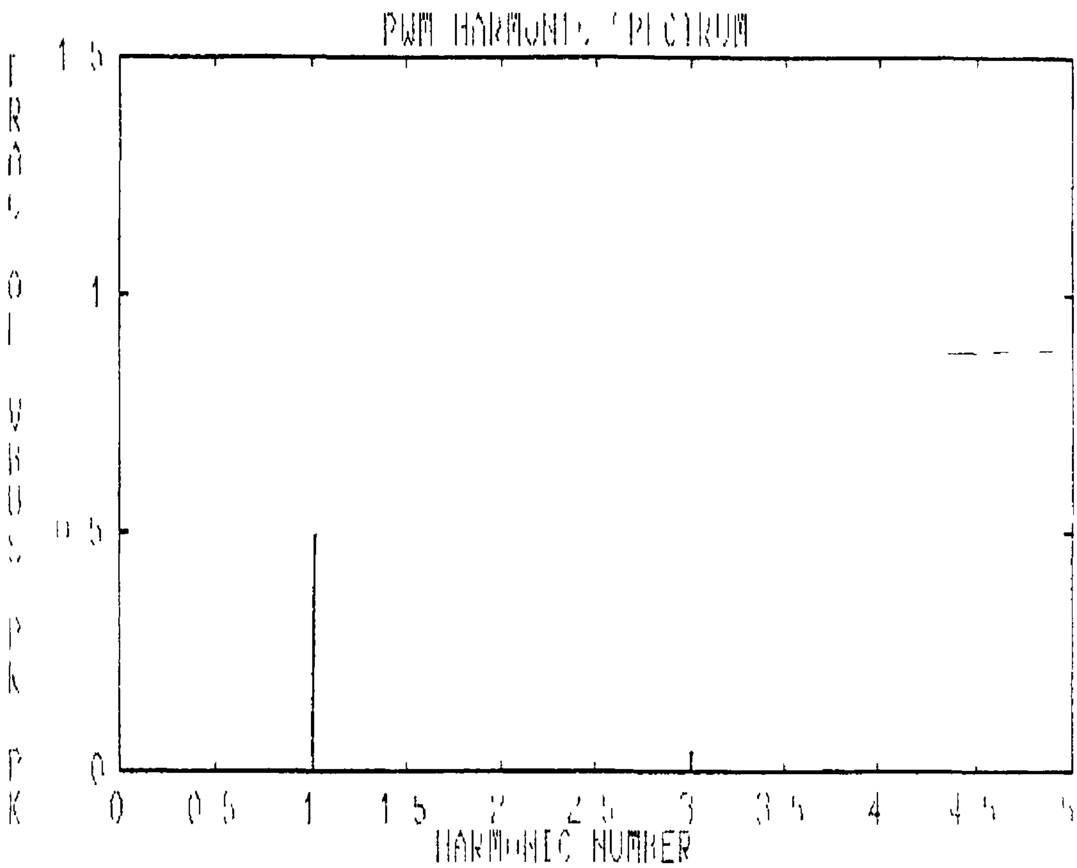

PLOT(3 23)

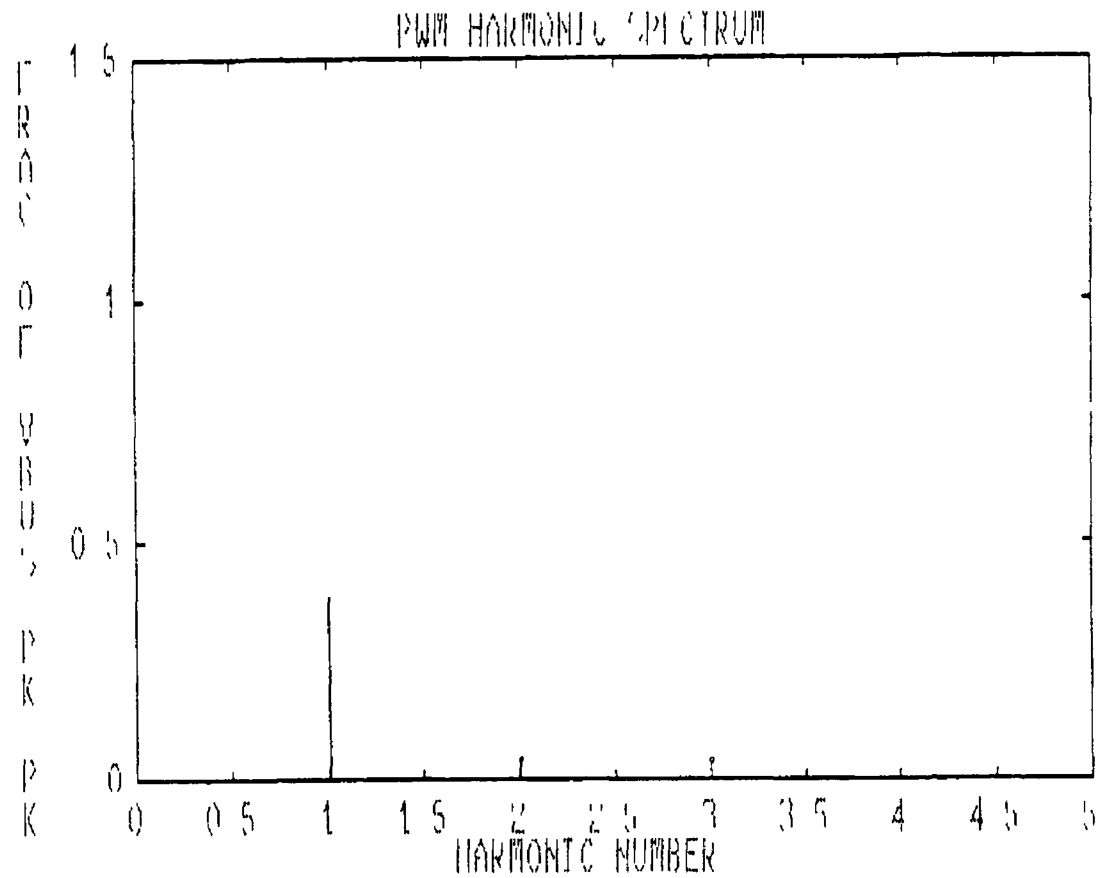

PLOT(3 24)

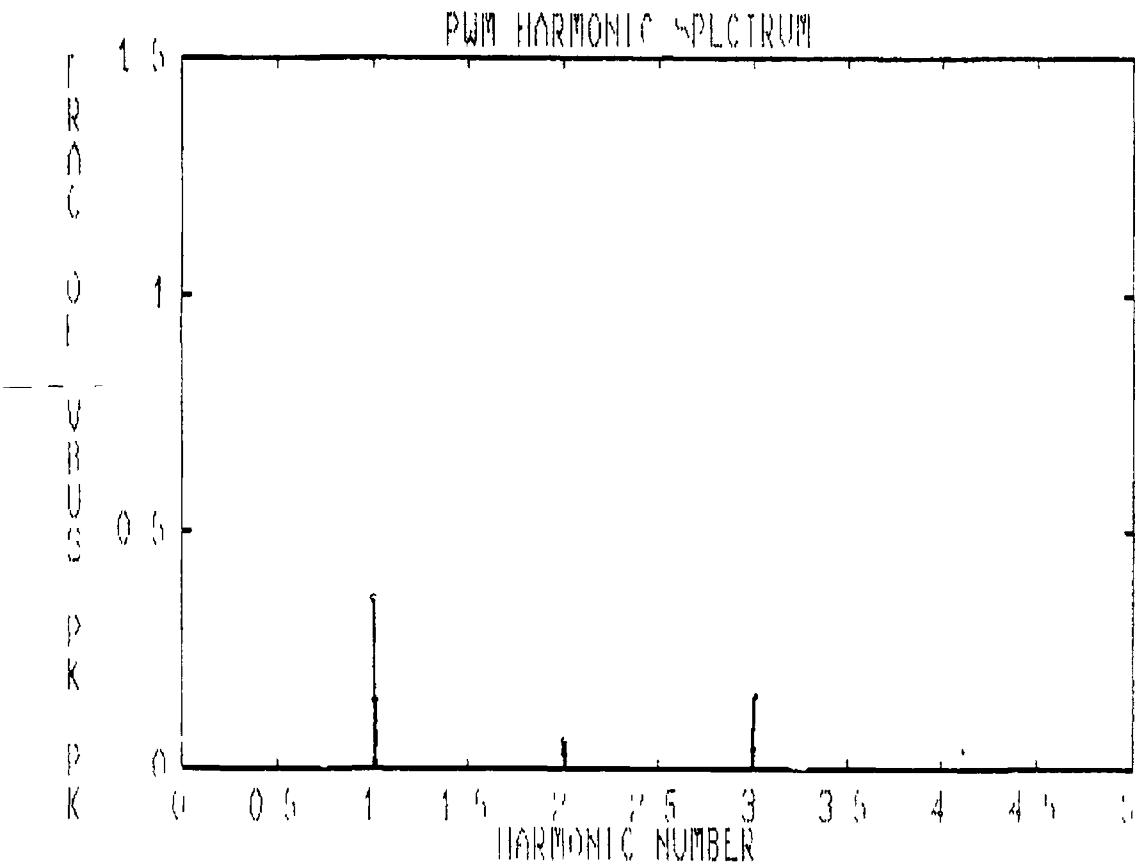

PLOT(3 25)

does not correspond to experimental results, although the first harmonic is reduced in magnitude. Further simulations indicated that the reduction in first harmonic is a nearly constant 20% irrespective of modulating index or carrier ratio.

3.5.6 It is clear that the course of harmonic distortion can be attributed to the hysteresis circuit of figure (3.8). The overall effect of harmonic distortion can be quantified in terms of the harmonic distortion ratio, which is defined in section 3.4.1. What has not been fully explained is the actual physical mechanism that generates the distortion. Section 3.5 attempts to explain, in terms of envisaged waveforms appearing at the motor phase, the distortion effect. Only the spectrum of the PWM waveform of figure (3.12) comes any way near to the measured spectrum. Figure (3.12) itself is an approximation to figure (3.11), the actual voltage appearing at the motor phase. It is necessary, in order to fully quantify the effect for all conceivable machine driving conditions, to quantify, in terms of a mathematical or statistical model, the voltage signals appearing during the hysteresis interval. If such a model were produced, then better understanding of the effect of distortion on system dynamics could be obtained.

3.6 The effects of harmonic distortion

3.6.1 Although the ideas presented in the preceding sections do not fully explain the causes of the distortion, the harmonic distortion ratio can be used to quantify it fully. The ratio itself, for any set of steady state operating conditions, indicates the level of variation of forward path gain in the closed loop control system of figure (3.7). This forward path gain variation is dynamic, varying with changes in modulation index. The full extent of its effect on system stability can not be gauged without a fuller understanding of harmonic distortion in terms of a mathematical model. However the existence of harmonic distortion necessitates its full consideration in brushless dc motor control.

3.6.2 Besides the dynamic effects of harmonic distortion, static effects also exist. During the course of experimental measurement it was discovered that the upper harmonics were also distorted. Plot (3.25) shows the situation with a 60 Hz modulator, and an eddycurrent dynamometer coil current of 400 mA. The third harmonic of the line voltage is over 40% of the fundamental. In this particular situation no voltage appears across the motor windings due to the 3 phase cancellation effect. The second harmonic, which has a magnitude of 10% of the fundamental, however does produce current and this current in turn generates heating losses in the winding. Although 10% of the fundamental does not seem to be substantial it must be noted that the second harmonic encounters an impedance of less than twice that encountered by the fundamental, and it does not have any back emf to overcome.

3.6.3 One method to overcome the effects of the harmonic distortion ratio would be to fix the modulation level at around 100% and vary the bus voltage in accordance with the amount of voltage required per phase. This would require an adaptation of the control system of figure (3.7) to include a controlled 3 phase thyristor rectifier. Figure (3.13) illustrates the adapted system.

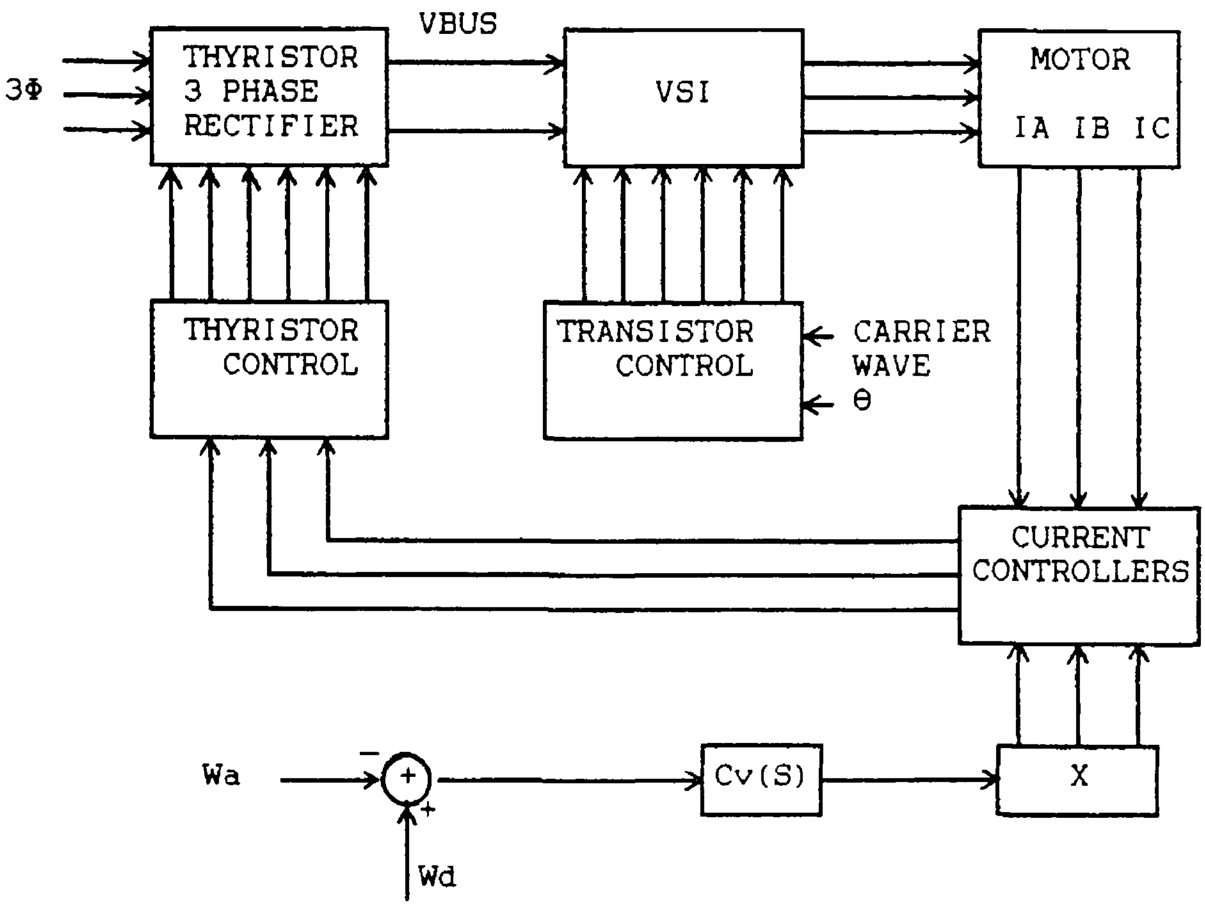

FIGURE(3 13)

PROPOSED CONTROL STRUCTURE TO OVERCOME DISTORTION EFFECT

Modelling of a 3 Phase Synchronous Machine

4.1 The 3 Phase Model

4.1.1 The theory presented in Chapter 2 constitutes the full descriptive set of electrical equations for the machine. In particular equations (2.15 . . 2.20) comprise the electrical characteristic of the synchronous machines 3 phase representation. The parameters of the equations can easily be derived from test. The mechanical characteristics of the machine can be described by:

$$T = T_L + J \frac{dW_m}{dt} + DW_m \quad \text{........(4.1)}$$

where T is the developed motor torque
T_L is the system load torque
J is the system moment of inertia
D is the system damping.

4.1.2 The parameters that require evaluation are:

1) Phase Resistance
2) Phase inductance
3) Back emf constant
4) Torque constant
5) Rotor moment of inertia
6) Rotor damping factor

Test procedures were developed in order to determine the parameters, and these procedures will be described in detail in the subsequent paragraphs.

4.1.3 The stator resistance can be determined by use of a resistance meter. The system is balanced so that R_A, R_B, R_C should be equal in magnitude. Phase resistances were measured as:

$R_A = 0.95\ \Omega$
$R_B = 0.94\ \Omega$
$R_C = 0.95\ \Omega$

4.1.4 The phase inductance is more difficult to measure. The stator is star connected and it is impossible to measure a single phase inductance, so it is necessary to determine this from the line to line measurement. Unfortunately because of coupling between phase coils it is impossible to separate self inductance, leakage inductance and mutual inductance between coils. The phase inductance has to be estimated as half the line to line measurement. This is in keeping with section 2.3.1. Plot (4.1) shows the line to line inductance plotted against θ. This variation can be attributed to changes in the air gap length, due to saliency. The offset level of the periodic wave is used as the approximation to the line to line inductance. Therefore the phase inductances can be determined.

$L_A = 2mH$
$L_B = 2mH$
$L_C = 2mH$

4.1.5 The back emf constant can be determined simply by driving the motor as an unloaded generator, and plotting the line to line voltage against speed. The slope of Plot (4.2) yields the back emf constant in volts per RPM Scaling the slope by C where C is defined as:

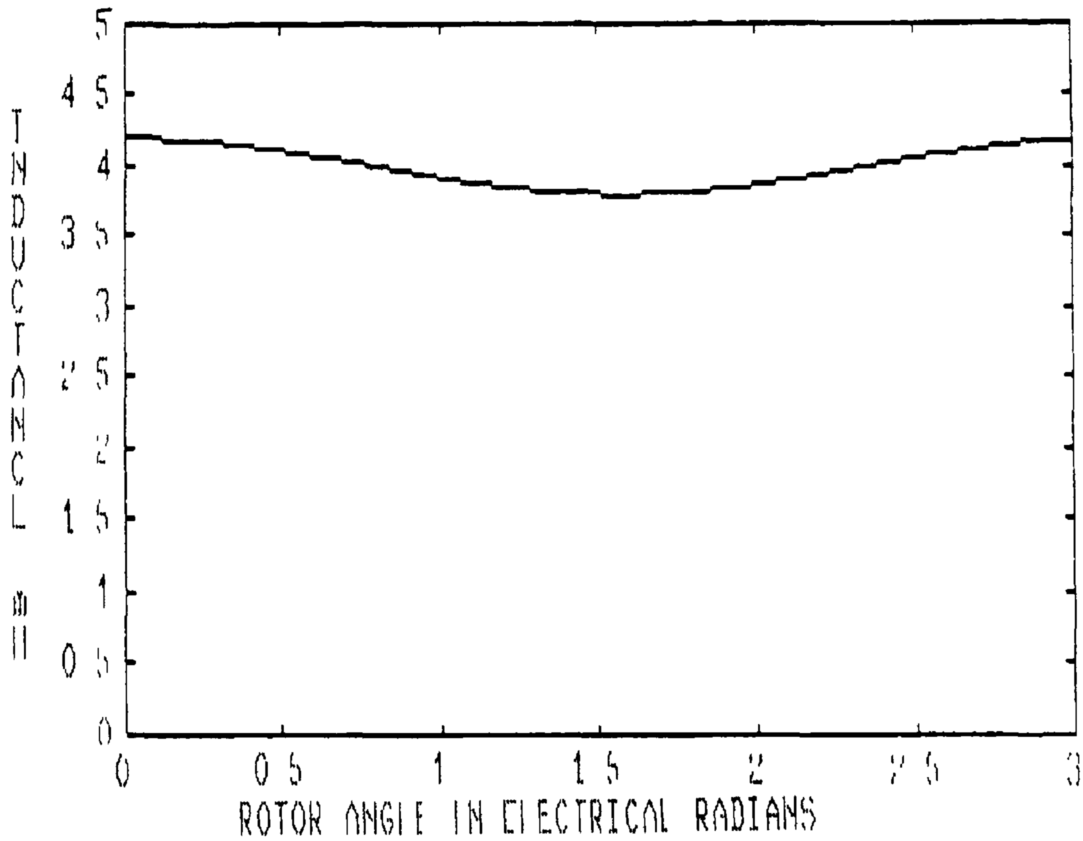

PLOT(4 1)

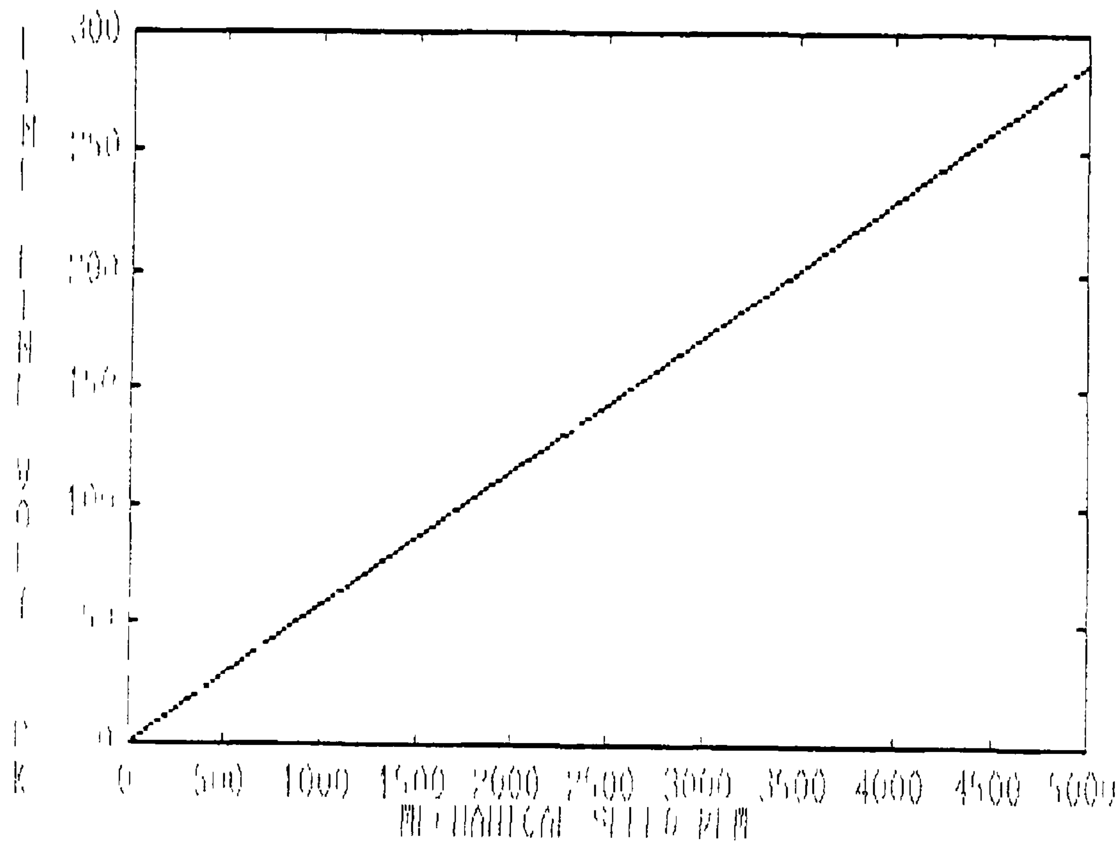

PLOT(4 2)

$$\frac{2\pi}{60\sqrt{3}} \qquad \ldots\ldots\ldots\ldots\ldots\ldots \quad (4.2)$$

gives the back emf constant per phase as,

K_E = .3175 Volts/Rad/S

4.1.6 The torque constant for the test motor is defined as the ratio of the torque output to the peak phase current, assuming a torque angle of 90^0. Tests using an eddycurrent dynamometer result in Plot (4.3). The slope of the graph is 0.47 N_m/A. This quantity is the torque constant. It can also be derived from equation (2.21). Power is defined in terms of rms current and voltage. The back emf constant defined in section 4.1.5 is in term of peak volts, so division by the square root of 2 rescales it in terms of rms. The current, I_A can be replaced in equation (2.19) by the equivalent peak current divided by root 2. Equation (2.19) becomes.

$$T = \frac{W_m \cdot 3(0.3175) I_A(\text{Peak})}{W_m\sqrt{2}\,\sqrt{2}} \qquad \ldots\ldots\ldots\ldots \quad (4\ 3)$$

or

$$T = \quad 0.476 I_A(\text{Peak}) \qquad \ldots\ldots\ldots\ldots \quad (4.4)$$

4.1.7 The rotor moment of inertia can either be calculated or derived from test. The equation for the moment of inertia of any body is:

$$J \;=\; \int_V r^2 dm \qquad \ldots\ldots\ldots\ldots \quad (4.5)$$

where dm is the differential mass element, and r is the distance from the axis of rotation to dm. The integration is performed over the entire volume.
The value of inertia of the test motor is

$$J \;=\; 2.8\text{x}10^{-4}\text{Nm S}^2$$

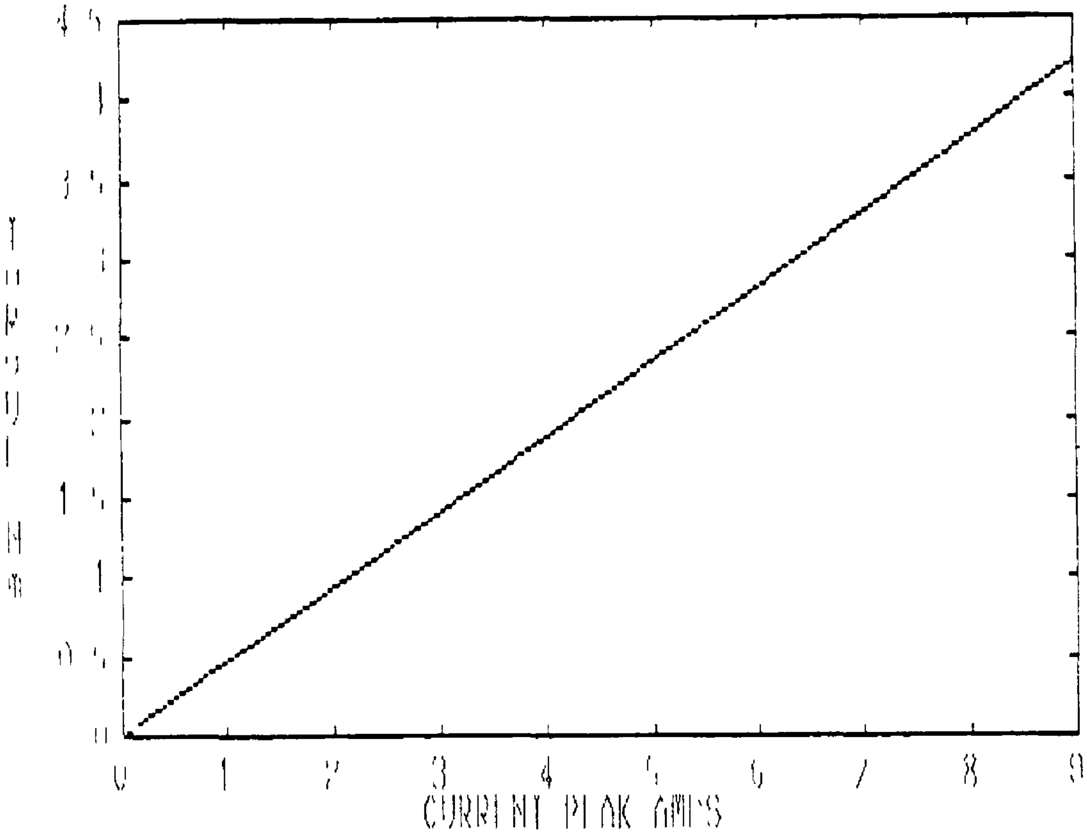

PLOT(4 3)

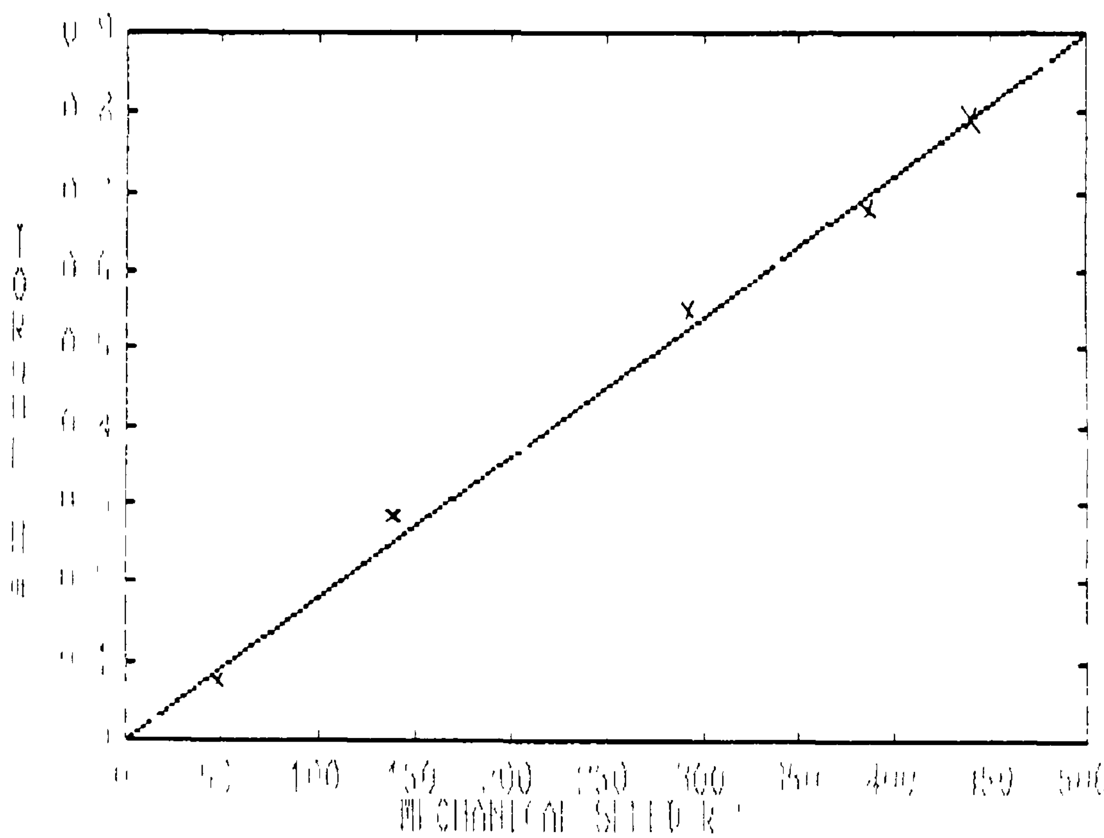

PLOT(4 4)

4.1.8 The rotor damping factor including a windage element, can be determined from motor no load tests at various speeds. Plot (4.4) shows torque against rotor speed in rad/s. The slope of the graph yields the damping factor.

$$D = 0.0018 \text{ Nms}$$

4.2 The DQ model

4.2.1 The mechanical equation of section 4.1.1 can equally be applied to the DQ electrical representation of the machine, so the parameters J and D derived in sections 4.1.7 and 4.1.8 respectively can be used in the DQ model. Referring to equations (2.23 ... 2.32) the parameters to be evaluated are:

1) R_d, R_q
2) L_d, L_q
3) λ_m
4) K

Figure (4.1) shows the motor in block diagram form.

4.2.2 One of the bases for the DQ transformation is that the resultant DQ coils have the same number of turns as the 3 phase coils they represent. This ensures that the coil resistance remains the same after the transformation [B2].

$$R_d = 0.95\Omega$$
$$R_q = 0.95\Omega$$

4.2.3 The Direct and Quadrature axes inductances can vary considerably with load depending on driving conditions [P16]. A closed current loop can minimise these variations. The axes inductances are experimentally derived with the current loop closed and also with the assumption that the torque angle is 90^0. Consider equation (2.25). Under steady state conditions the derivative goes to zero. If the torque angle is 90^0 then the direct axis current is also zero. Equation (2.25) becomes

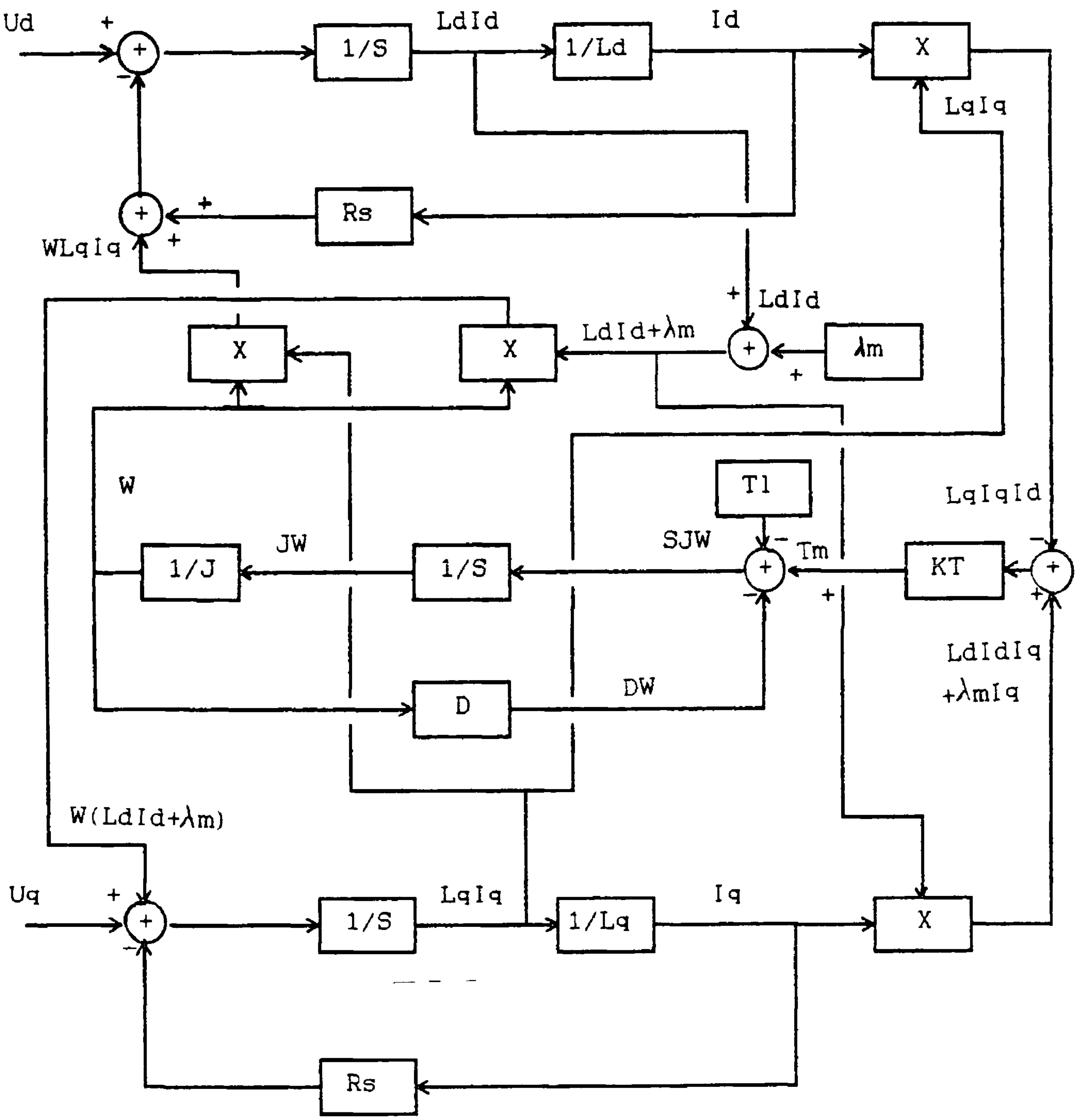

FIGURE(4 1)

MOTOR DQ MODEL

$$L_q = \frac{-Ud}{W_E I_q} \qquad (4\ 6)$$

Assuming low saliency, and neglecting saturation effects,the value of L_q can be used as the value of L_d

$$\Longrightarrow \quad L_d = \frac{-Ud}{W_E I_q} \qquad (4\ 7)$$

4.2.4 In order to evaluate L_d and L_q knowledge is needed of the driving 3 phase currents and voltages. If the driving 3 phase currents are assumed to be

$$\begin{bmatrix} I_A \\ I_B \\ I_C \end{bmatrix} = \begin{bmatrix} -|I|.\mathrm{Sin}(W_E t) \\ -|I|.\mathrm{Sin}(W_E t-2\pi/3) \\ -|I|.\mathrm{Sin}(W_E t-4\pi/3) \end{bmatrix} \ldots\ldots\ldots\ldots \quad (4.8)$$

Applying the transformation of equation (2.23) the D and Q currents are evaluated as:

$$\begin{bmatrix} I_d \\ I_q \end{bmatrix} = \begin{bmatrix} 0 \\ -|I| \end{bmatrix} \quad \ldots\ldots\ldots\ldots \quad (4.9)$$

So the set of driving currents of equation (4.8) result in a torque angle of 90^0. The 3 phase driving voltages should lead the currents by some phase angle Figure (4.2) illustrates the position of the 3 phase voltage vector with reference to the 3 phase current vector. The voltage vector can be split into D and Q components. U leads I_q by the angle k, so the driving voltages needed to generate the currents of equation (4.8) are,

$$\begin{bmatrix} U_A \\ U_B \\ U_C \end{bmatrix} = \begin{bmatrix} -|U|.\mathrm{Sin}(W_E t+k) \\ -|U|.\mathrm{Sin}(W_E t-2\pi/3+k) \\ -|U|.\mathrm{Sin}(W_E t-4\pi/3+k) \end{bmatrix} \quad \ldots\ldots \quad (4.10)$$

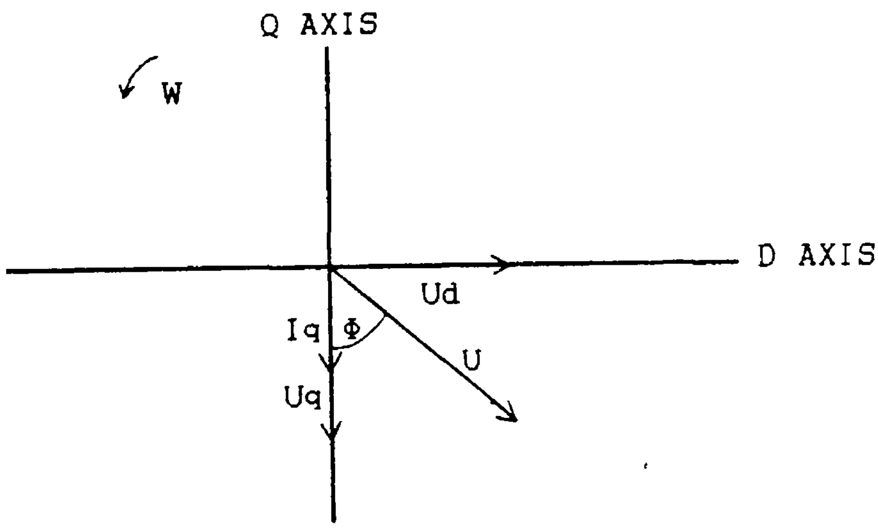

FIGURE(4 2)

SPA IAL VOLTAGE AND CURRENT VECTORS

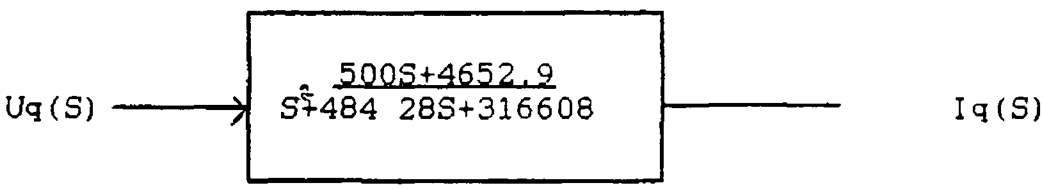

FIGURE(4 3)

THE LINEARISED MOTOR IN BLOCK DIAGRAM FORM

4.2.5 Tests were carried out at 600 RPM and 1200 RPM with the load varying, to quantify the variation in inductance with load. The results are plotted in Plots (4.5, 4.6). The voltage and current values measured at lower loads tended to be small, and the measurement equipment used, in this case a spectrum analyser, tended to give inaccurate results at these lower values. In the case of Plots (4.5, 4.6) the value of inductance tends towards 2 mH as the load increases. This corresponds to the theoretical value of inductance, so a value of 2 mH will be taken to represent L_d and L_q.

4.2.6 The magnet equivalent flux linkage can be determined from equation (2.29). Assuming steady state conditions, and a 90^0 torque angle, equation (2.29) becomes:

$$\lambda_m = \frac{U_q - R_q I_q}{W_E} \qquad (4.11)$$

Tests carried out at speeds of 600 RPM and 1200 RPM, with load varying yield plots (4.7, 4.8) respectively. The flux linkage is in mWb-turns. An average for λ_m was obtained from the measurements taken.

$$\lambda_m = -0.053 \text{ Wb-turns}$$

4 2.7 The value of the constant K, of equation (2.30) can be determined using the criterion that torque equations (2.19, 2.30) must yield identical torque values, under identical machine driving conditions. Equation (2.19) can be written as:

$$T = 3/2\ K_E I_A(\text{Peak}) \qquad \ldots\ldots\ldots\ldots \quad (4.12)$$

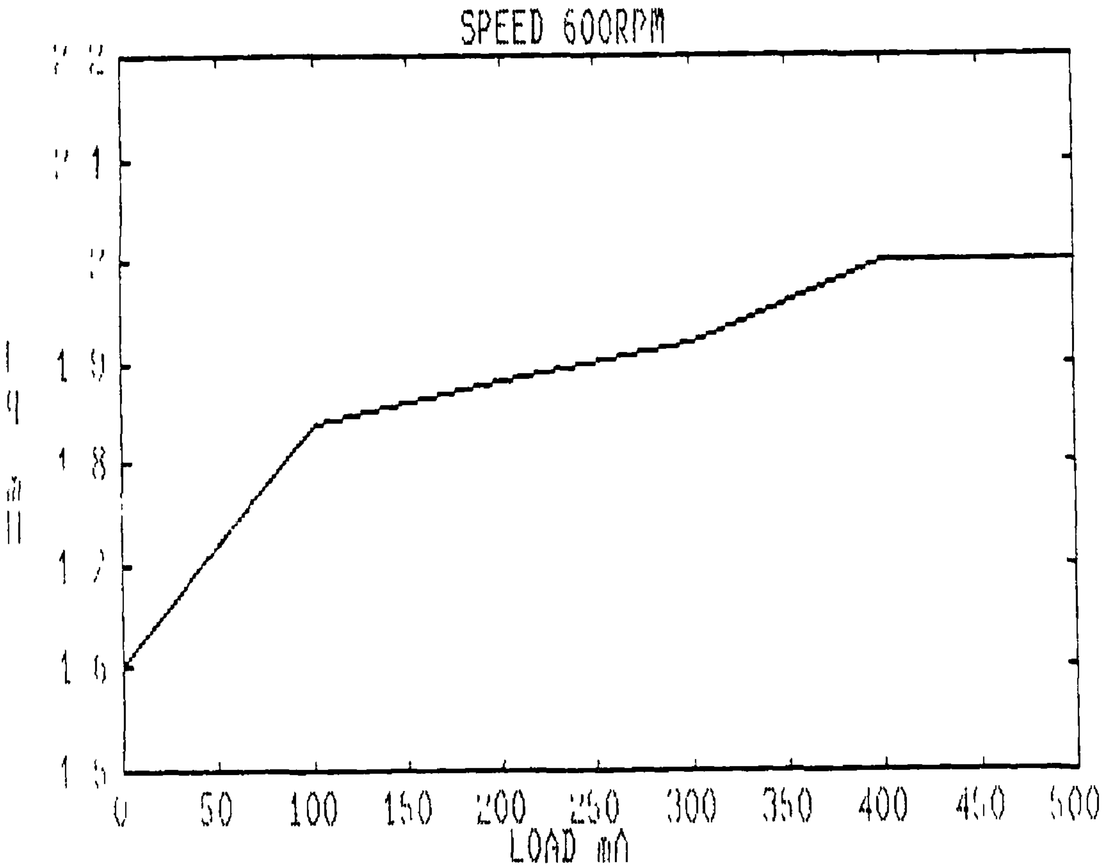

PLOT(4 5)

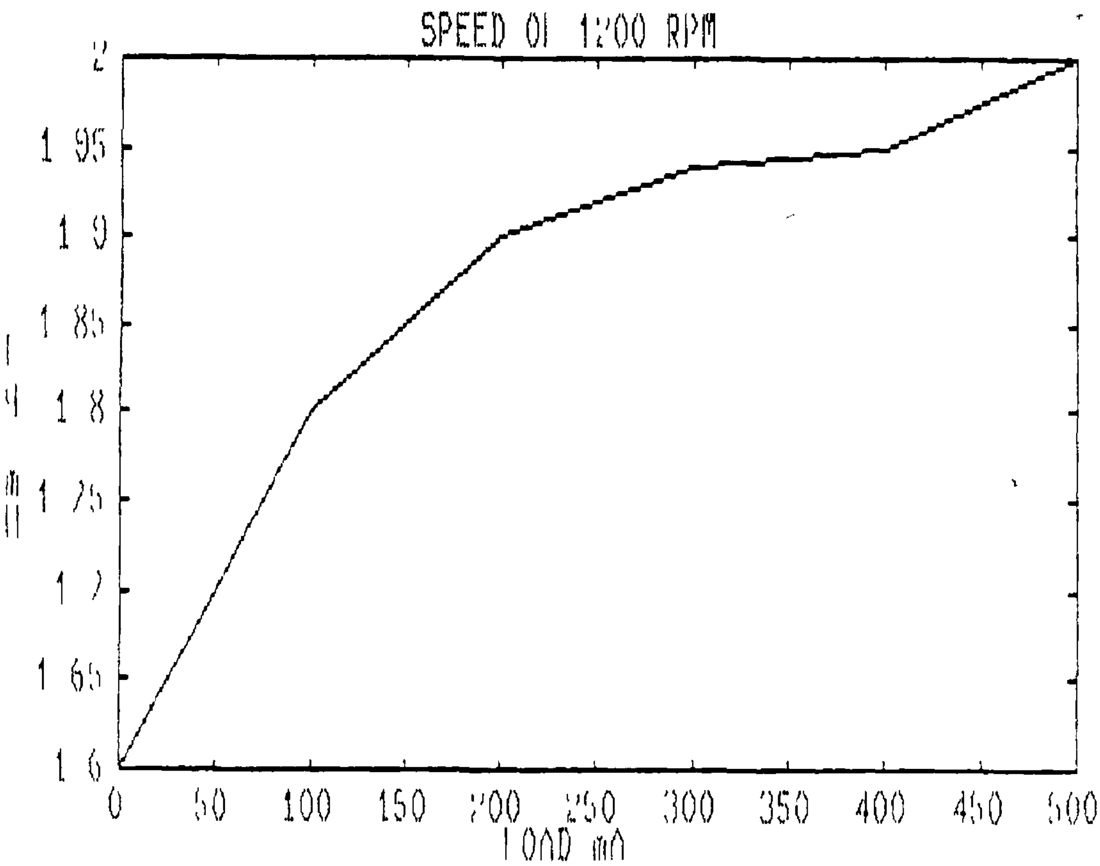

PLOT(4 6)

assuming 90^0 torque angle. Equation (2.32) can be written as:

$$T = K\lambda_m p/2 \ I_q \qquad \ldots\ldots\ldots\ldots \qquad (4.13)$$

using the same assumption as above. The Q axis coil is pseudostationary in nature [B2] so the back emf induced in it, on the basis of the transformation of section 2.4.3, is the same as that induced in an individual phase coil. Equation (4.13) becomes, combining the product of λ_m and p/2 to become a single back emf constant:

$$T = KK_E I_q \qquad \ldots\ldots\ldots\ldots \qquad (4.14)$$

since I_q equals I_A(peak), it can be concluded that the value K must assume to balance the equation is:

$$K = 3/2$$

4.3 The basis for the DC motor representation

4.3.1 The 90^0 torque angle condition has been referred to on quite a number of occasions in the course of this Chapter. It constitutes an important condition in synchronous motor control, as it means the machine can be represented by a linear DC equivalent motor. This ensures that classical linear analysis and control can be applied directly to the resultant linear system to effect velocity control.

4.3.2 To derive the $I_q(S)/U_q(S)$ transfer function for the linearized system, equations (2.23, 2.24, 2.30, 4.1) are used. If I_d is equal to zero the equations (2.23, 2.24, 2.30) reduce to:

$$U_d = -W_E L_q I_q \quad \ldots\ldots\ldots\ldots\ldots\ldots \quad (4.15)$$

$$U_q = L_q \frac{dI_q}{dt} + R_q I_q - W_E \lambda_m \quad \ldots\ldots\ldots\ldots \quad (4.16)$$

$$T = \frac{3}{2} \cdot \frac{p}{2} \lambda_m I_q \quad \ldots\ldots\ldots\ldots \quad (4.17)$$

substituting equation (4.17) into (4.1) results in:

$$\frac{3}{2}\frac{p}{2} \lambda_m I_q = J\frac{dw}{dt} + DW + T_L \quad \ldots\ldots\ldots\ldots\ldots (4.18)$$

taking the laplace transforms of equations (4.16, 4.18) yield,

$$U_q(S) = SL_q I_q(S) + R_q I_q(S) + W_E(S)\lambda_m \ \ldots\ldots \ (4.19)$$

and,

$$\frac{3}{2}\frac{p}{2} \lambda_m I_q(S) = SJ\, W_m(S) + DW_m(S) + T_L(S) \ \ldots \ . \ (4.20)$$

From equation (4.20),

$$W_m(S) = \frac{\frac{3}{2}\frac{p}{2}\lambda_m I_q(S)}{(JS+D)} - \frac{T_L}{(JS+D)} \qquad \ldots\ldots \; (4.21)$$

substituting into equation (4.19) and noting that
$6\,W_m(S) = W_E(S)$,

$$U_q(S)=I_q(S)\left[SL_q+R_q+\frac{\lambda^2{}_m \frac{3}{2}\frac{p}{2}6}{(JS+D)}\right] + \frac{\lambda_m T_L}{(JS+D)} \qquad \ldots\ldots \; (4.22)$$

Assuming a load torque of zero,

$$\frac{I_q(S)}{U_q(S)} = \frac{Js+D}{S^2L_qJ+(DL_q+R_1J)S+(R_qD+9\cdot p.\lambda^2{}_m)} \qquad \ldots\ldots \; (4.23)$$

Substitution of the values derived in the previous sections into this equation yields the transfer function:

$$\frac{I_q(S)}{U_q(S)} = \frac{500S + 4652.9}{S^2+484.28S+316608} \qquad (4\ 24)$$

Thus the motor model of figure (4.1) can be replaced by the linear block of figure (4.3). So the major criterion for current control in terms of the best servo performance can be defined to be a maintenance of the torque angle at 90^0 over the entire motor speed range, and for all conceivable load conditions.

5. Design of a Current Control System

5.1 3 Phase Controller Design

5.1.1 The essence of current control is to achieve as high a torque/amp ratio as possible. This requires maintaining the torque angle at 90^0. The problem with current control is the inherent nonlinearity of the 3 phase system [B14, P16]. Nonlinear systems generally require some sort of adaptive control technique to achieve reasonable performance [P17, P18]. But the nature of adaptive control requires a large amount of computer time to generate output signals. Thus a compromise is needed.

5.1.2 To perform a frequency response evaluation on the motor, in order to obtain the gain and phase characteristics, it is necessary to use an iterative procedure. This is because of the nonlinearity of the system. Using frequency response plots, it should be possible to design a suitable controller. The criterion for controller design is that at top speed a torque reduction of no less than 5%. This corresponds to a phase lag of less than 15^0. Figure (5.1) illustrates a single motor phase with its associated control hardware. The harmonic distortion radio (HDR) is included in the forward path. The electrical equation of the motor phase, written in phasor format is:

$$V = jW_E L\ I_a + R\ I_a + E \quad . \ ... \ ... \ (5.1)$$

If the back emf is assumed to have a phase angle of 0^0, IE, β is set to 0^0 and the angle between back emf and phase current is defined as σ, then

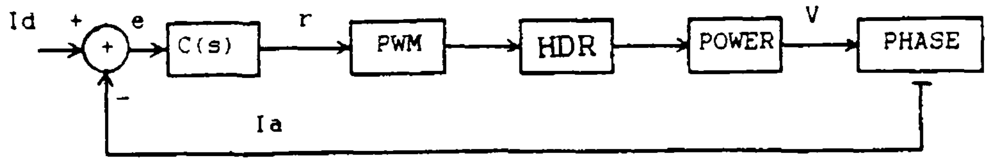

FIGURE(5 1)

A SINGLE MOTOR PHASE WITH CURRENT CONTROL

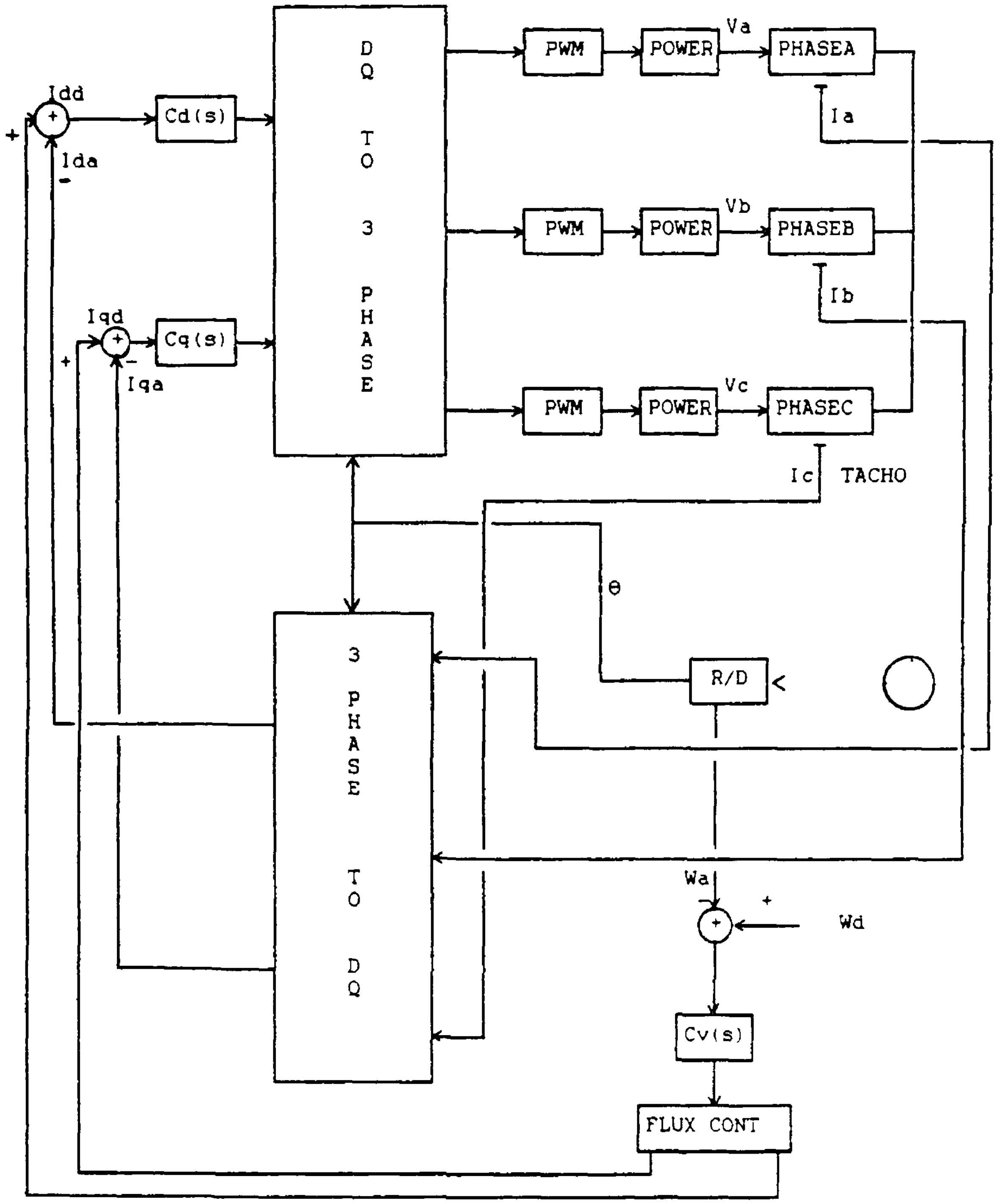

FIGURE(5 2)

COMPLETE DQ CONTROL SCHEME

$$V = E + I_a[R \cos\sigma - W_E L \sin\sigma] + jI_a[R \sin\sigma + W_E L \cos\sigma] \qquad \text{..........} \quad (5.2)$$

The transfer function of the motor winding, I_a/V, can be determined from equation (5.2) and expressed in magnitude and angle form. In particular,

$$\left|\frac{I_a}{V}\right| = \frac{1}{\sqrt{(E/I_a + R \cos\sigma - W_E L \sin\sigma)^2 + (R.\sin\sigma + W_E L \cos\sigma)^2}} \qquad \text{..........} \quad (5.3)$$

$$\angle I_a - \angle V = \Phi - \mathrm{TAN}^{-1}\left[\frac{(R \sin\sigma + W_E L \cos\sigma) I_a}{E + (R \cos\sigma - W_E L.\sin\sigma) I_a}\right] \qquad \text{..........} \quad (5.4)$$

Because of the balanced nature of the motor windings, the equations above relate to any Phase.

5.1.3 Assuming an under modulated signal the PWM stage of the system acts, in steady state velocity conditions, as a linear amplifier. The gain of the amplifier is expressed in equation (3.9). The modulation index, as defined in section 3.3.1, depends on the magnitude of both carrier and modulator. The carrier signal on the test motor controller has a peak to peak magnitude of 4 volts, while the phase voltage, at 100% modulation, assumes a peak to peak level of 320 volts. This means the gain of the PWM stage is 80 in the linear operating region. Although the gain falls off somewhat when over modulation occurs, the figure 80 will be used as an approximation in subsequent theory.

5.1.4 The harmonic distortion ratio affects the forward path gain as a function of modulation index. Plot (3.20), the plot of modulation index against harmonic distortion ratio, can be described by a set of piecewise linearised functions.

$$HDR(m_1)=\begin{cases} 0.7m_1 & 0 \le m_1 \le 0.41 \\ 2.33m_1-0.65 & 0.41 < m_1 \le 0.49 \\ 1.643m_1-0.315 & 0.49 < m_1 \le 0.63 \\ 0.756m_1+0.243 & 0.63 < m_1 \le 1 \\ 1 & m_1 > 1 \end{cases} \qquad \ldots\ldots\ldots\ (5.5)$$

Where m_1 is the modulation index. The harmonic distortion ratio at zero modulation is not a measurable quantity, but it is assumed to be 0 in the above equation, because of the downward trend of plot (3.20) towards zero modulation.

5.1.5 The controller stage of figure (5.1) can be represented by its transfer function. This is described as.

$$C(S) = \frac{K(1+S\tau_1)(1+S\tau_2)\ \ldots\ (1+S\tau_n)}{(1+S\tau_{n+1})(1+S\tau_{n+2})\ \ldots\ (1+S\tau_m)} \qquad \ldots\ldots\ldots\ (5.6)$$

equation (5.2) represented in magnitude and phase form becomes:

$$|C(S)| = \frac{K\sqrt{(1+(W_E\tau_1)^2)(1+(W_E\tau_2)^2)\ldots\ldots(1+(W_E\tau_n)^2)}}{\sqrt{(1+(W_E\tau_{n+1})^2)(1+(uW_E\tau_{n+2})^2\ldots\ldots(1+(W_E\tau_n)^2)}} \qquad \ldots\ldots\ldots\ (5.7)$$

$$\angle C(S) = TAN^{-1}(W_E\tau_1)+TAN^{-1}(W_E\tau_2)+\ldots TAN^{-1}(W_E\tau_m) - TAN^{-1}(W_E\tau_{n+1})-TAN^{-1}(W_E\tau_{n+2})\ldots -TAN^{-1}(W_E\tau_n) \qquad \ldots\ldots\ (5.8)$$

Referring to figure (5.1)

$$C(S) = R(S)/E(S) \qquad \ldots\ldots\ (5.9)$$

$$\Longrightarrow |E(S)| = |R(S)|/|C(S)| \qquad \ldots\ldots\ (5.10)$$

$$\Longrightarrow |E(S) = |R(S)|/|C(S) \qquad \ldots\ldots\ (5.11)$$

$$\text{and } \angle E(S) = \angle R(S) - \angle C(S) \qquad \ldots\ldots\ (5.12)$$

5.1.6 The system error, E(S), is defined as:

$$E(S) = I_d(S) - I_a(S) \qquad \text{..........} \quad (5.13)$$

$$\Longrightarrow \quad I_d(S) = E(S) + I_a(S)$$

if β is defined as the angle of E(S), then $I_d(S)$ can be evaluated as:

$$|Id(S)| = \sqrt{(|E(S)|\cos\beta + |I_a(S)|\cos\sigma)^2 + (|E(S)|\sin\beta + |I_a(S)|\sin\sigma)^2} \qquad \text{..........} \quad (5.14)$$

$$\angle I_d(S) = \mathrm{TAN}^{-1}\left[\frac{|E(S)|\sin\beta + |I_a(S)|\sin\sigma}{|E(S)|\cos\beta + |I_a(S)|\cos\sigma}\right] \qquad (5.15)$$

5.1.7 The equations developed thus far describe the closed loop system fully. They enable a simulation of both open and closed loop frequency responses to be performed, for any selected controller, C(S). The only prerequisites of simulation are:

1. The actual winding current, I_a, is set over the whole frequency range. In other words a value of I_a is chosen and all other values are worked out based on it. This allows the variation in frequency response with load be determined.

2. The demand current, I_d, is always in phase with the back emf. This prerequisite is fulfilled in the control structure of figure (3.7).

3. Friction and windage losses are ignored.

5.1.8 Plot (5 1) shows motor gain response I_a/v, with the winding current, I_a, assuming values described in the plot. The reason for such a sharp fall off in gain

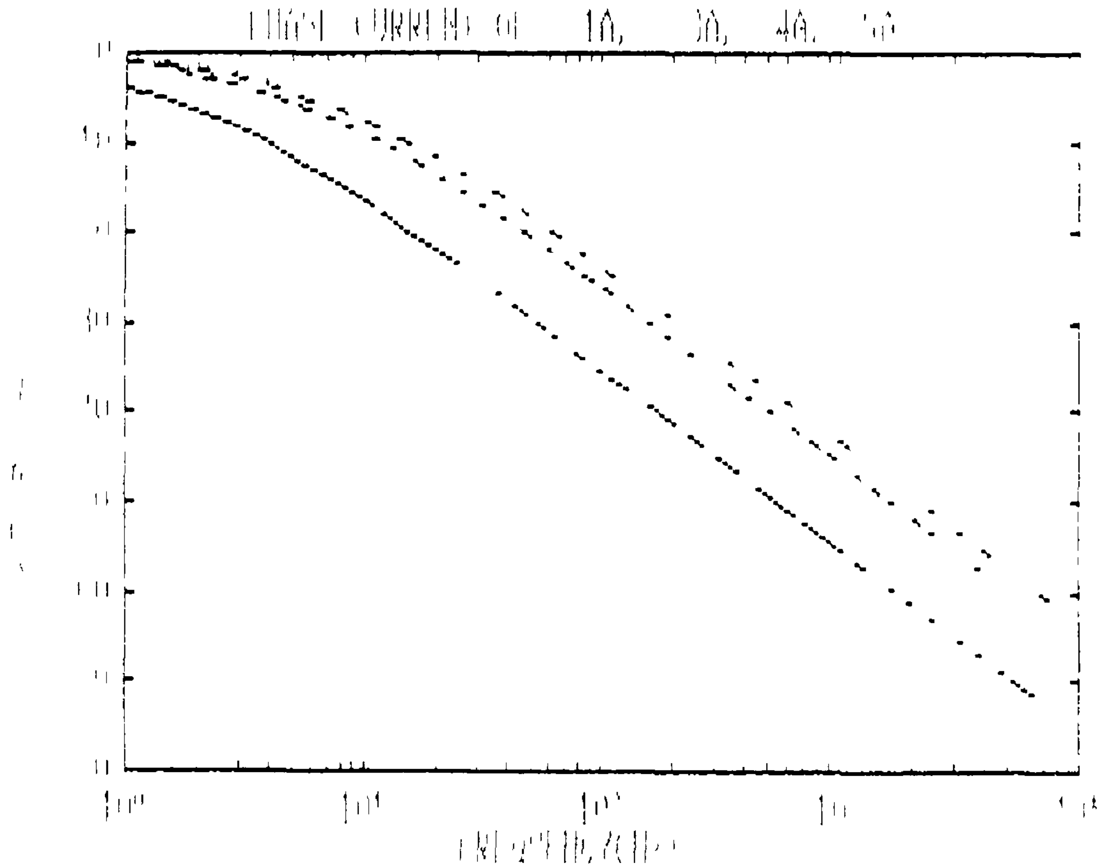

PLOT(5 1)

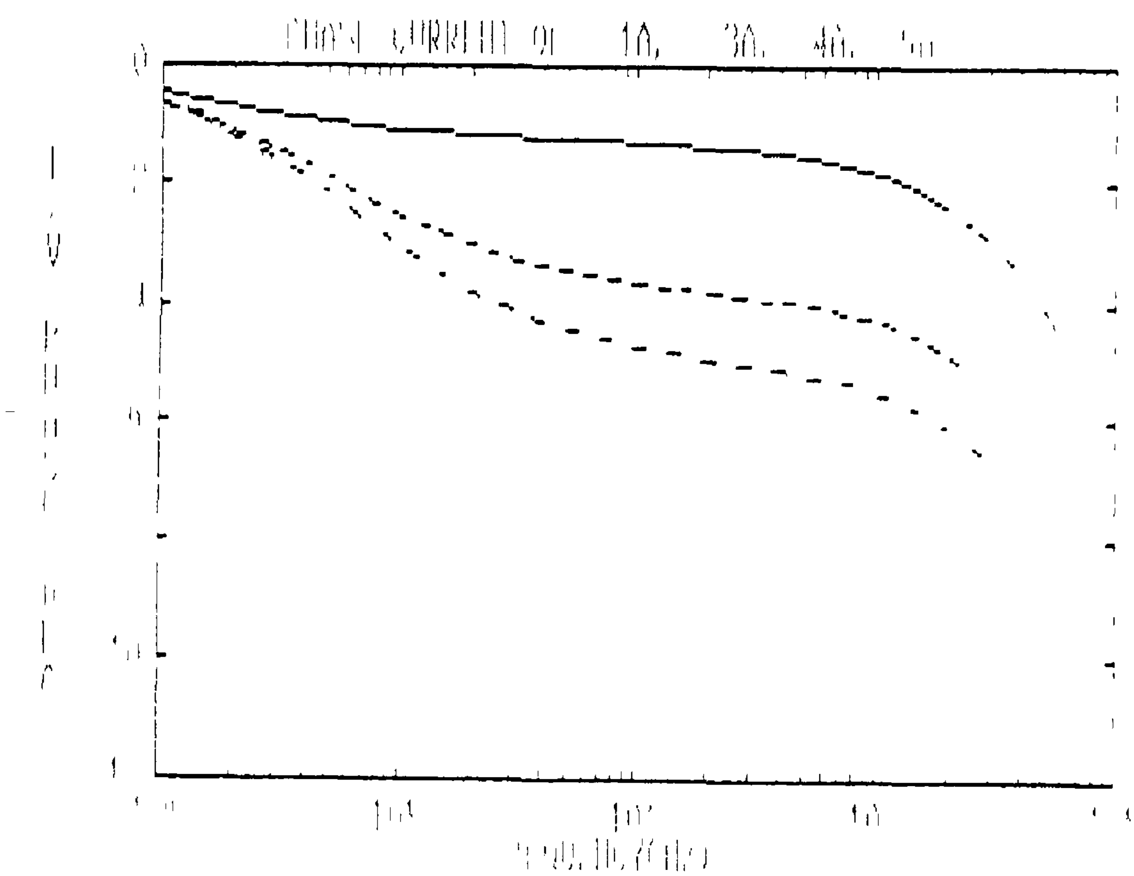

PLOT(5 2)

is the presence of the back emf. For a set value of I_a, speed increases require greater phase voltages to overcome the back emf. Plot (5.2) illustrates the curves of the variation in phase angle between I_a and V with the indicated values of I_a. As is evident, the phase current affects the phase and gain responses to a considerable extent. Using the principles of gain margin and phase margin [B10,B11,B12] as indications of stability, the motor is stable. It is only necessary to apply the criterion set down in section 5.12 as the basis for choosing C(S).

5.1.9 The presence of the harmonic distortion ratio dictates the type of controller used in the current loop. The ratio effectively reduces the gain at the lower frequency range, so it is necessary to counteract this reduction. A phase lag controller performs such a function [B10, B11, B12]. With correct design a phase lag controller increases the lower frequency gain without affecting the gain margin by a considerable amount. the transfer function of a lag controller can be described as:

$$C(S) = \frac{k(1+S\tau_1)}{(1+S\tau_2)} \qquad (5\ 16)$$

where $\tau_2 > \tau_1$. The breakpoints of the gain response are $1/\tau_2$ and $1/\tau_1$ respectively. The frequency at which the phase response reaches a minimum is:

$$f_{min} = \sqrt{\frac{1}{4\pi^2\tau_1\tau_2}} \qquad (5\ 17)$$

Using equation (5.17) and the theory of appendix (3) it is possible to design a controller to yield a desired open loop frequency response.

5.1.10 Plots (5.3, 5.4) show the magnitude and phase responses of the open loop system for a controller with the following specifications:

$$C_1 \longrightarrow \begin{cases} K = 16.6 \\ \tau_1 = 0.0013s \\ \tau_2 = 0.00462s \end{cases}$$

The harmonic distortion ratio is not included. The gain response has a flat section up to around 10 Hz and then it slopes off. The higher the phase current the higher the gain seems to be, and this trend is maintained over the whole frequency range. The open loop phase margin varies between 162^0 and 164^0 for currents of 1A and 5A respectively. The gain margin is very large, as is the phase crossover frequency. Plots (5.5, 5.6) illustrate the closed loop characteristics. The bandwidth defined in relation to the -3dB point varies between 600 Hz and 1 KHz depending on the phase current. The lower the current the lower the bandwidth. Closed loop phase exhibits a very slow fall off in the 0 Hz - 1 KHz range. This ensures that the torque angle is near to 90^0 over the whole speed range. The phase angle at 50 OHZ varies between -1^0 and -5^0 current dependent so the phase characteristics for I_a equal to 1A are in accordance with the design criterion of section 5 1.2.

5.1.11 With the harmonic distortion ratio taken into consideration a different set of plots result. Plots (5.7, 5.8) are plots of the open loop responses and plots (5.9, 5.10) show the closed loop characteristics. The lower end of the open loop gain has been reduced by a considerable amount, up to 45 dB in the case of a 1A phase current. The phase response of the open loop system is very much the same as plot (5.3). The

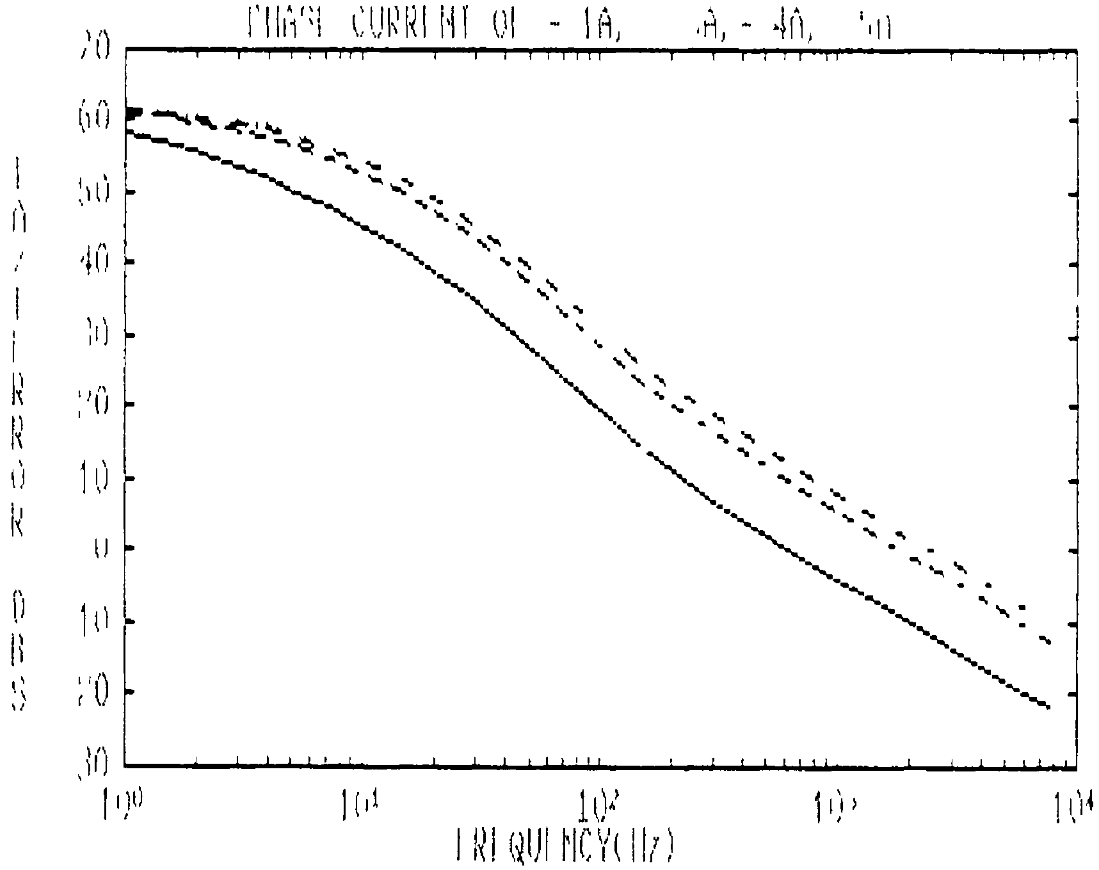

PLOT(5 3)

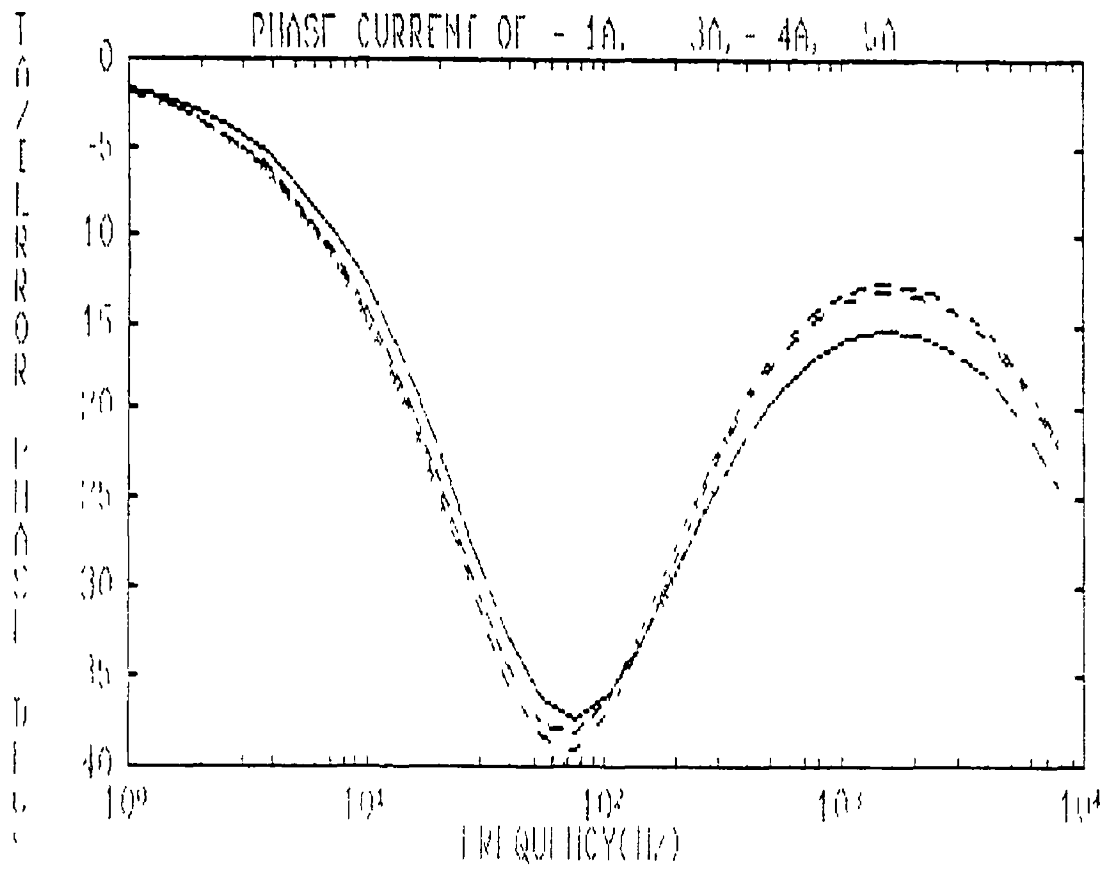

PLOT(5 4)

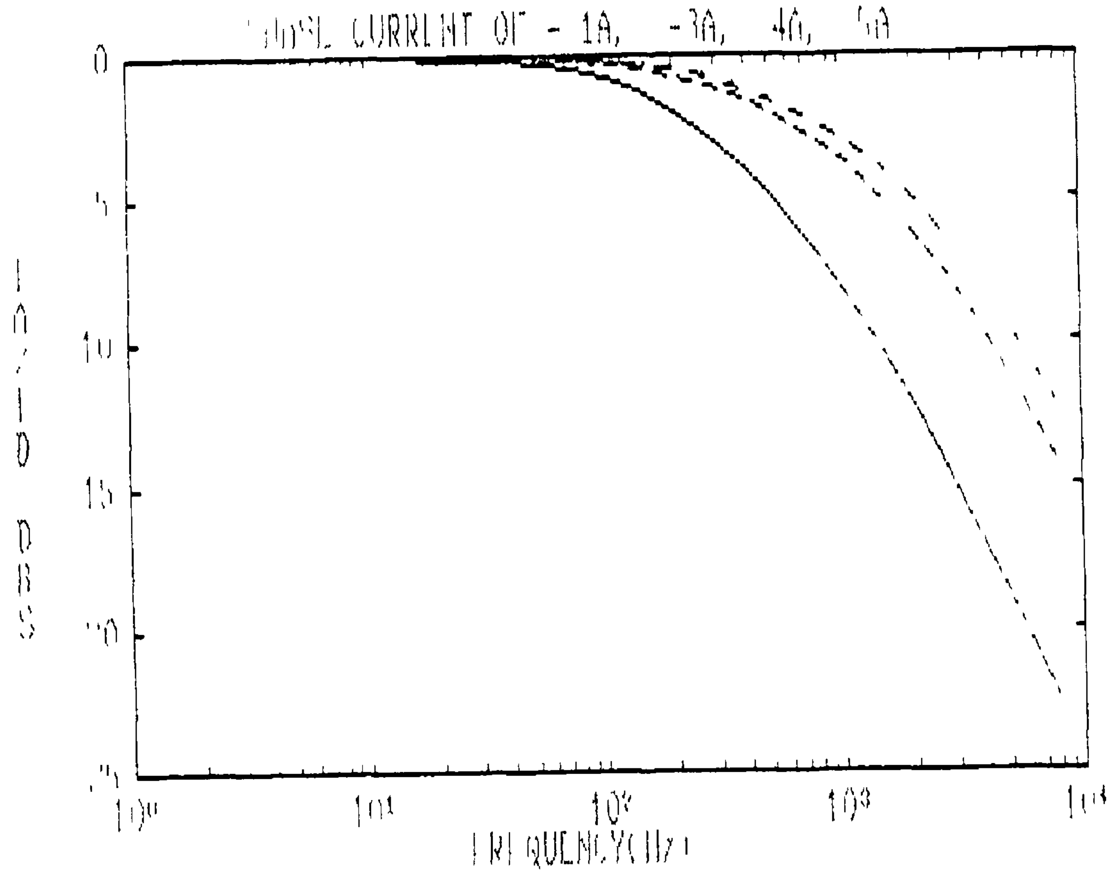

PLOT(5 5)

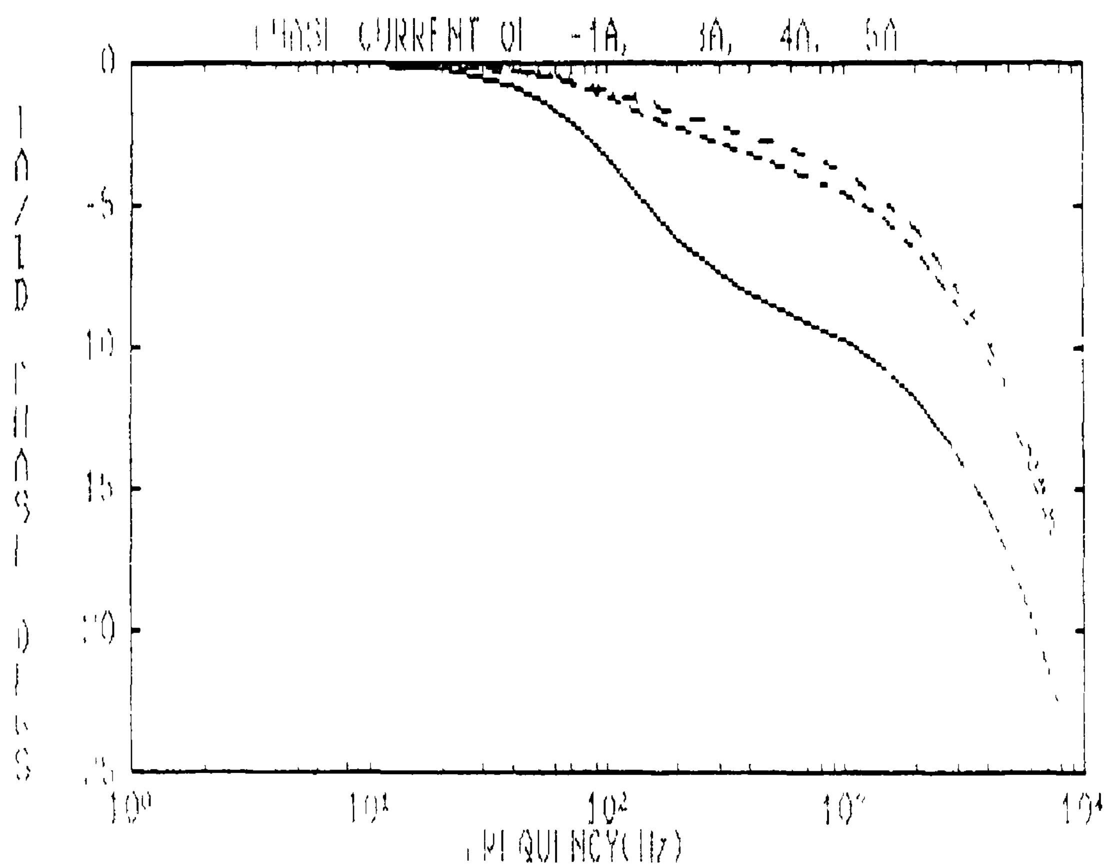

PLOT(5 6)

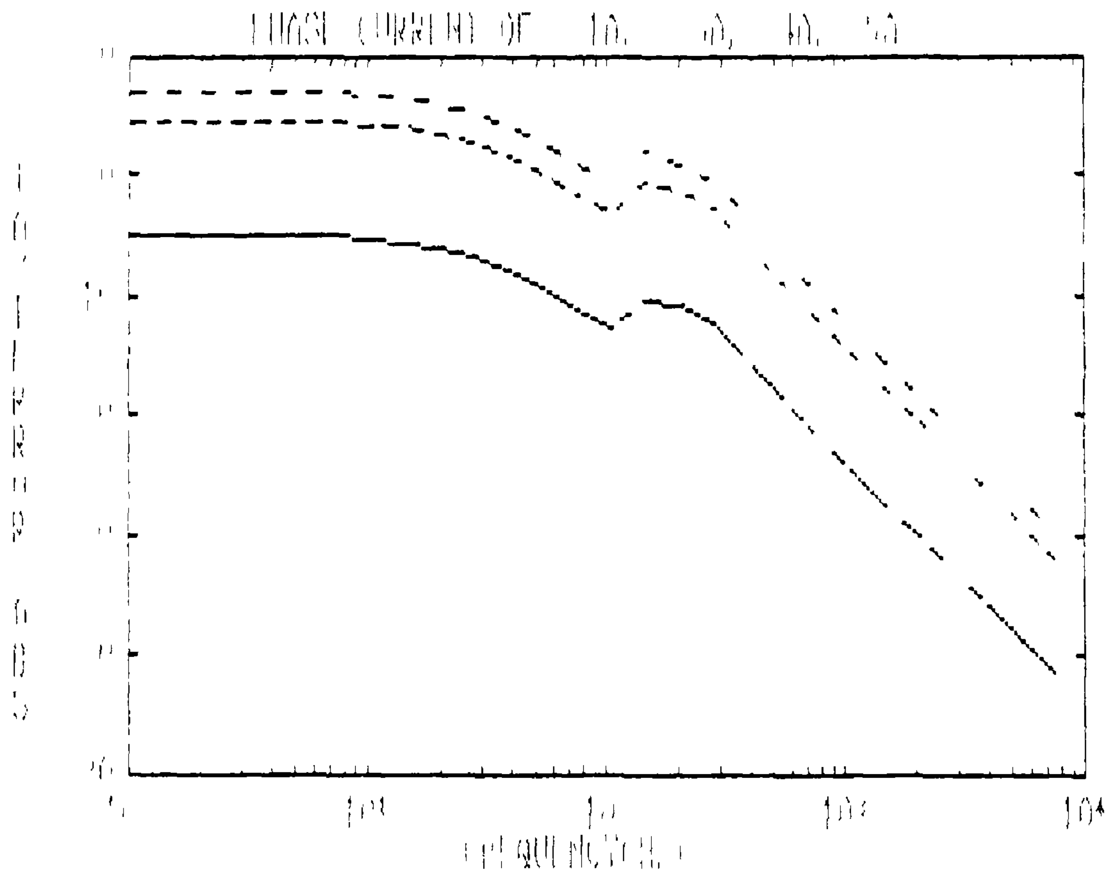

PLOT(5 7)

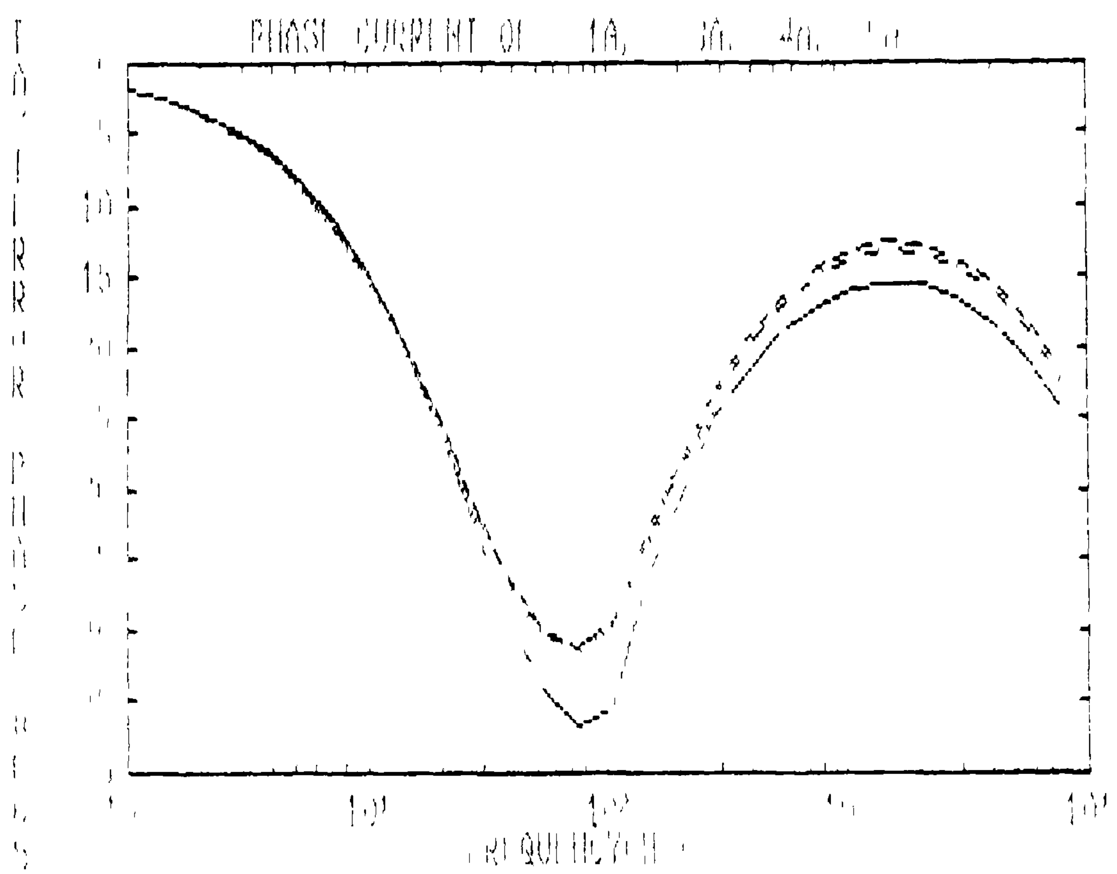

PLOT(5 8)

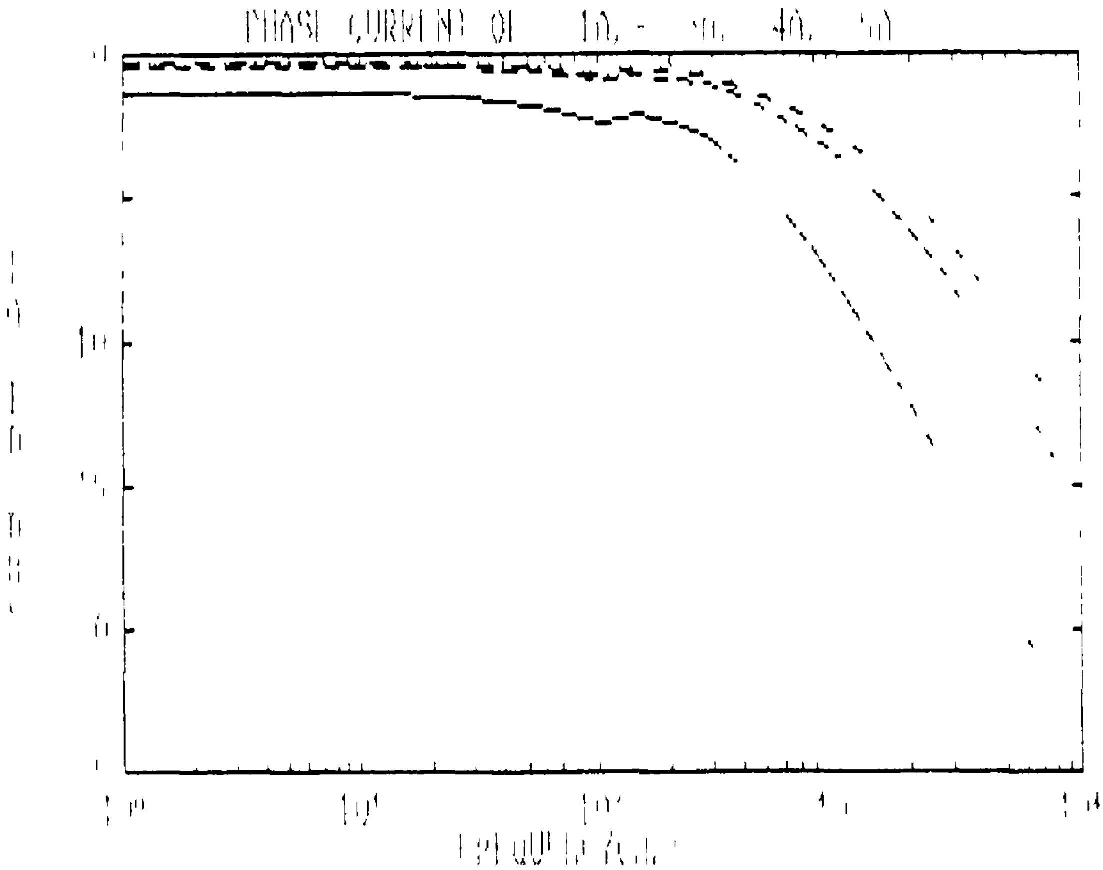

PLOT(5 9)

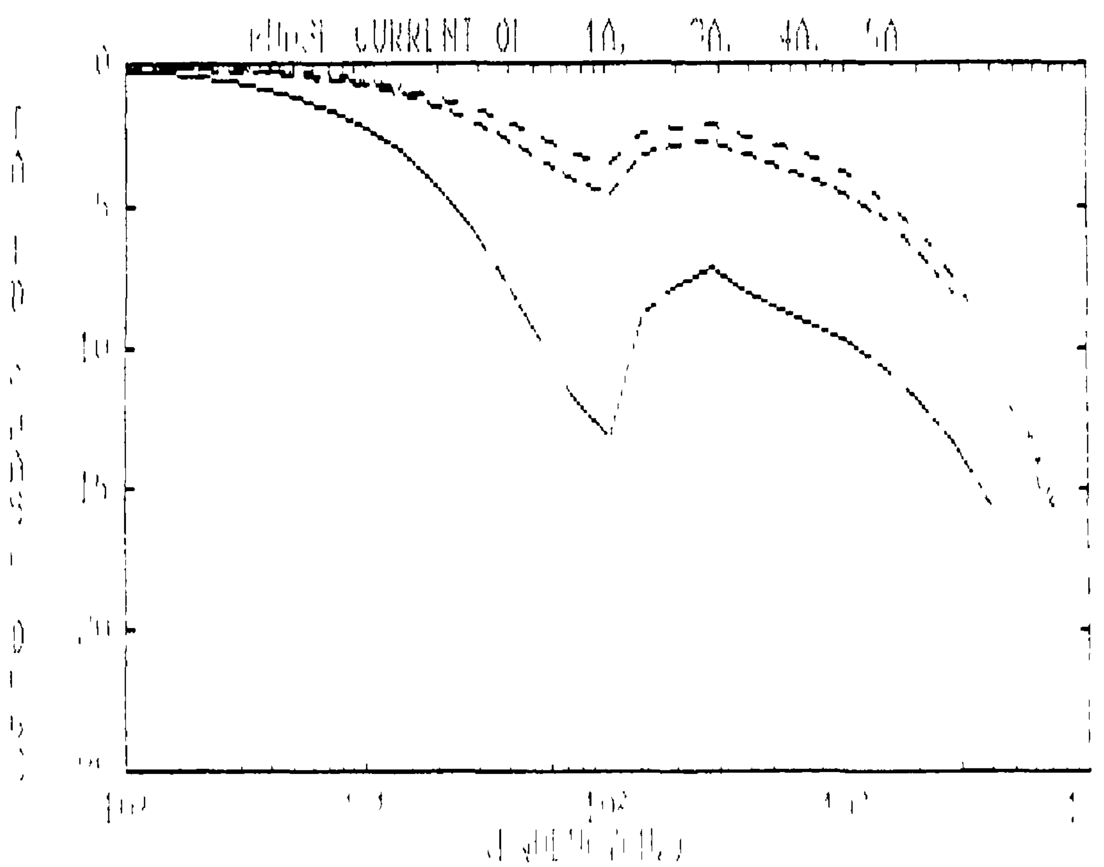

PLOT(5 10)

interesting result is that the gain and phase margins are practically the same as in the case where the harmonic distortion ratio is not considered. This is because the ratio assumes a value of 1 at high speeds due to the presence of the back emf. The closed loop bandwidth also remains static as illustrated in Plot (5.9). Plot (5.10) shows the closed loop phase which seems to trough at 100 Hz, down to -12^0 in the case of a current of 1A, but only down to -3.5^0 in the high current cases.

5.1.12 The controller described in section 5.1.10 would seem to fulfil the necessary requirements of control. It exhibits stability and exhibits characteristics in accordance with section 5.1.2. The only undesirable feature is the closed loop phase characteristics of plot (5.10). Consider a controller described by:

$$C_2 \longrightarrow \begin{cases} k & = 16.6 \\ \tau_1 & = 0\ 00026\text{S} \\ \tau_2 & = 0.00097\text{S} \end{cases}$$

Plots (5.11 ... 5.14) show the open and closed loop characteristics for gain and phase without the inclusion of harmonic distortion ratio. There has been a reduction in the phase margin. It now varies between 130^0 and 140^0 (I_a dependent). The gain margin still remains large, as does the phase crossover frequency. The closed loop bandwidth is the same, but the closed loop phase, for I_a of IA is around -15^0, which is of a magnitude larger than that with C_1 as the controller. This still ensures a very small reduction in torque at 500 Hz, in the order of 5%.

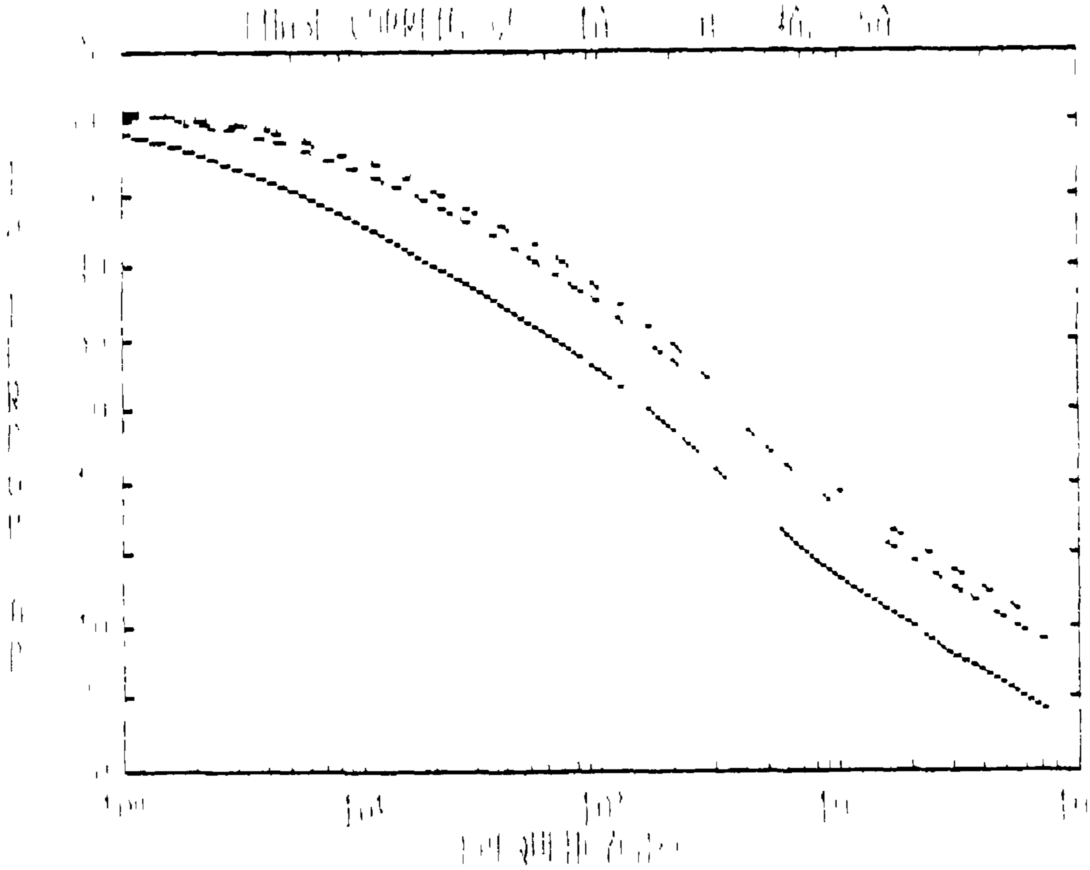

PLOT(5 11)

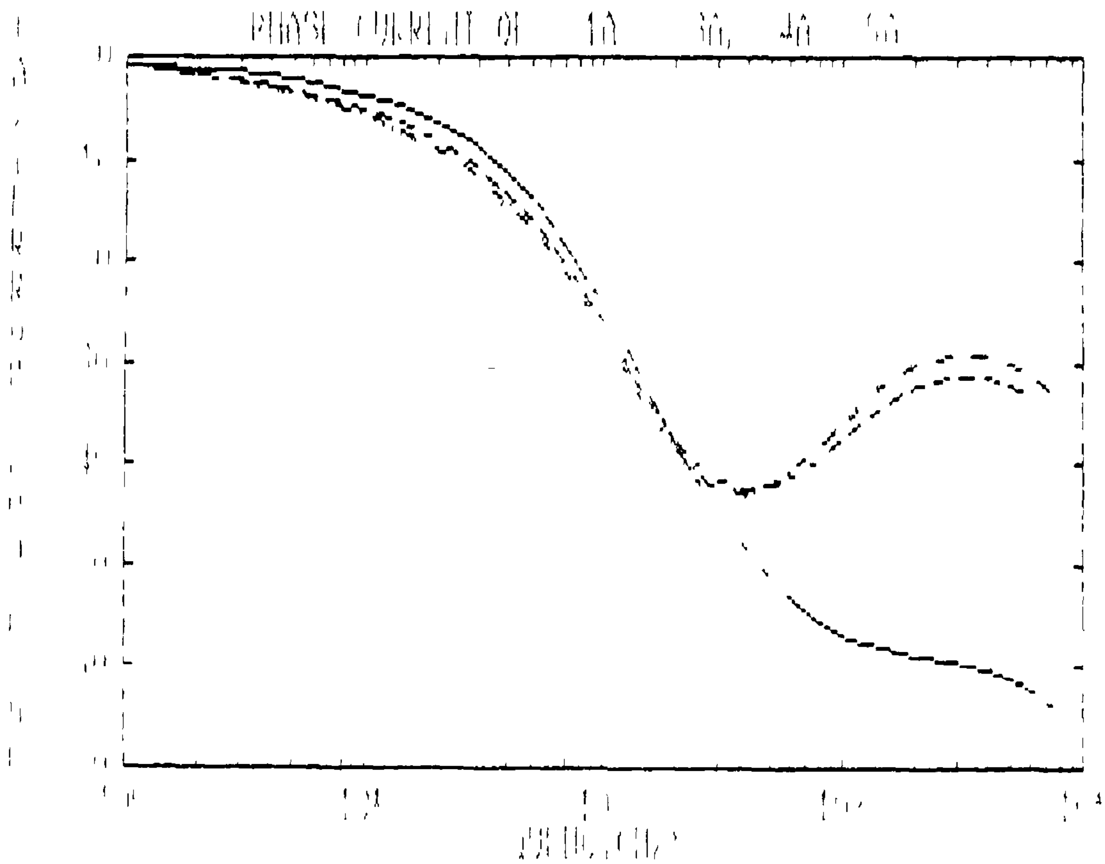

PLOT(5 12)

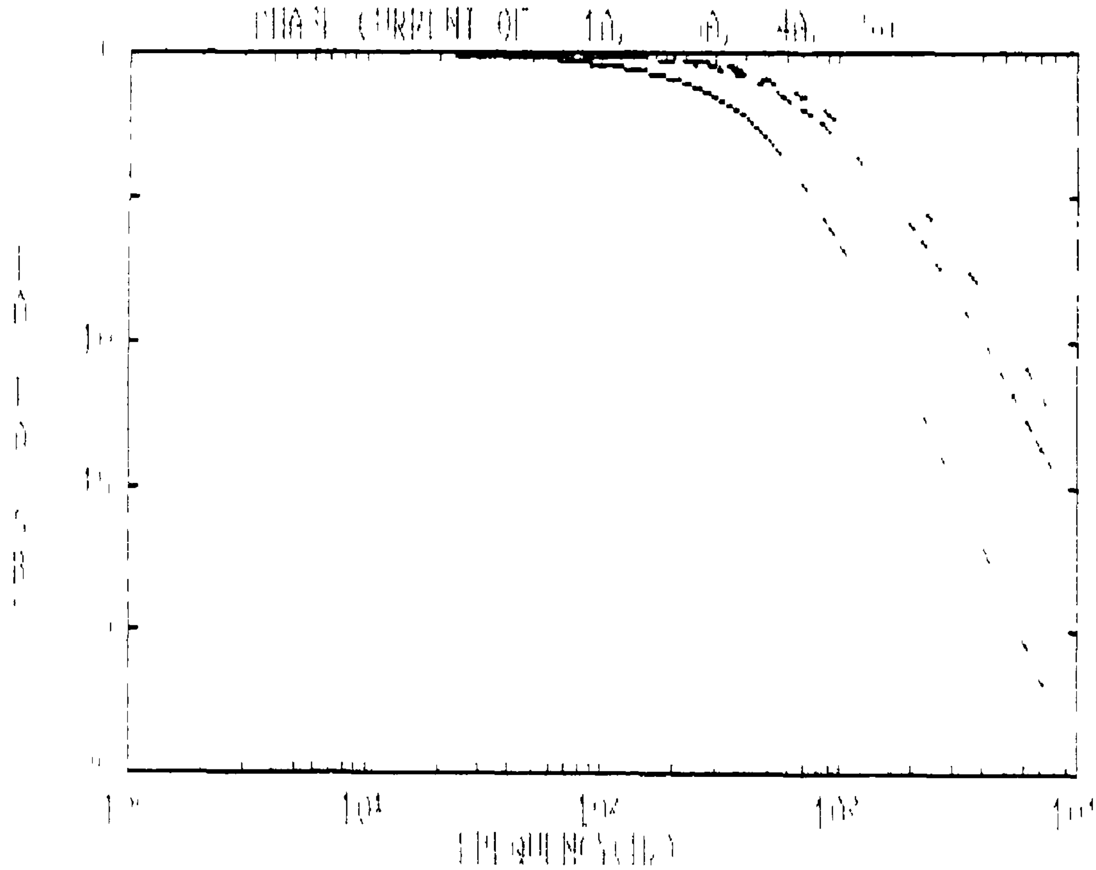

PLOT(5 13)

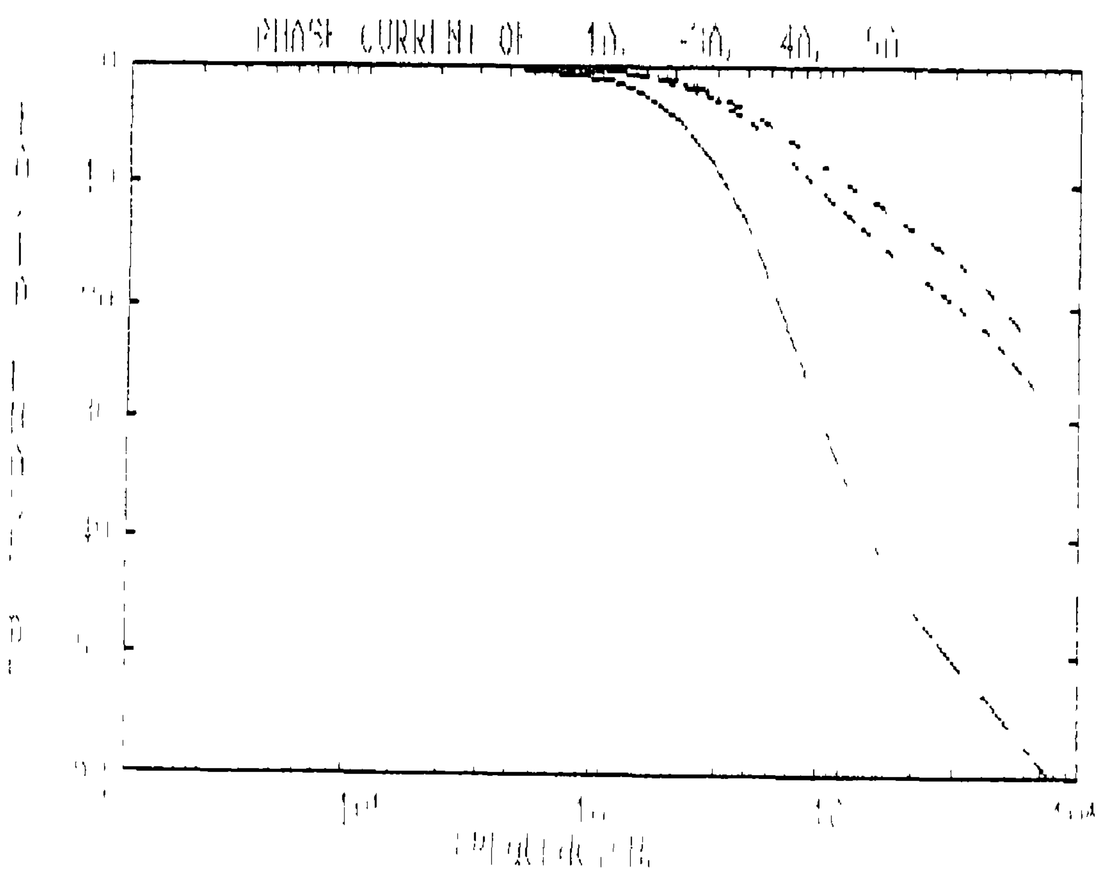

PLOT(5 14)

5.1.13 Plots (5.15 ... 5.18) illustrate the frequency response with the harmonic distortion ratio included. The gain margin, phase crossover frequency and closed loop bandwidth have not varied by any significant amount from plots (5.7 ... 5.10). The phase margin has been reduced, but is still large enough to ensure stability. The trough nature of the closed loop phase has almost been eliminated, although at the expense of a sharper phase falloff. This, however, only reduces the motor torque by 4% from its maximum value.

5.1.14 The reason for using phase lag control, ie because the harmonic distortion ratio tended to reduce the gain at the lower frequency range, is valid, except (as is evidenced from plots (5.3 ... 5.18)) the ratio does not overly affect the important open and closed loop characteristics. So is phase lag control really necessary? If a controller described by:

$$C_3 \longrightarrow \begin{cases} k & = & 16.6 \\ \tau_1 & = & 0 \\ \tau_2 & = & 0 \end{cases}$$

is implemented, plots (5.19 ... 5.26) show open and closed loop responses without and with the harmonic distortion ratio included. The phase margin varies between 168^0 and 178^0 over the range of phase currents, but the system is still stable. At the motor's maximum speed, 500 Hz, the phase response seems to be only -0.5^0. This is certainly acceptable in light of the controller selection criterion outlined in section 5.1.2.

5.1.15 The motor is inherently a non linear system, so it may be argued that the laws of linear systems theory cannot be applied to it in the case of controller

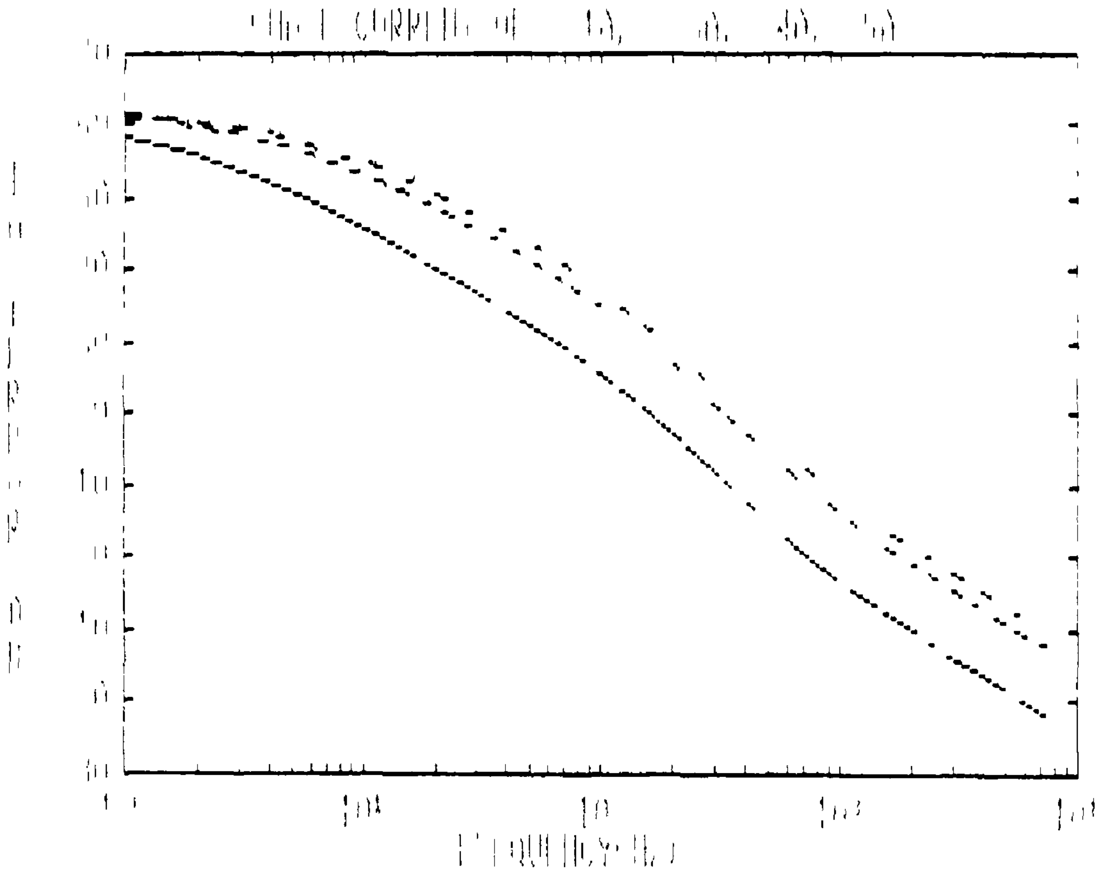

PLOT(5 15)

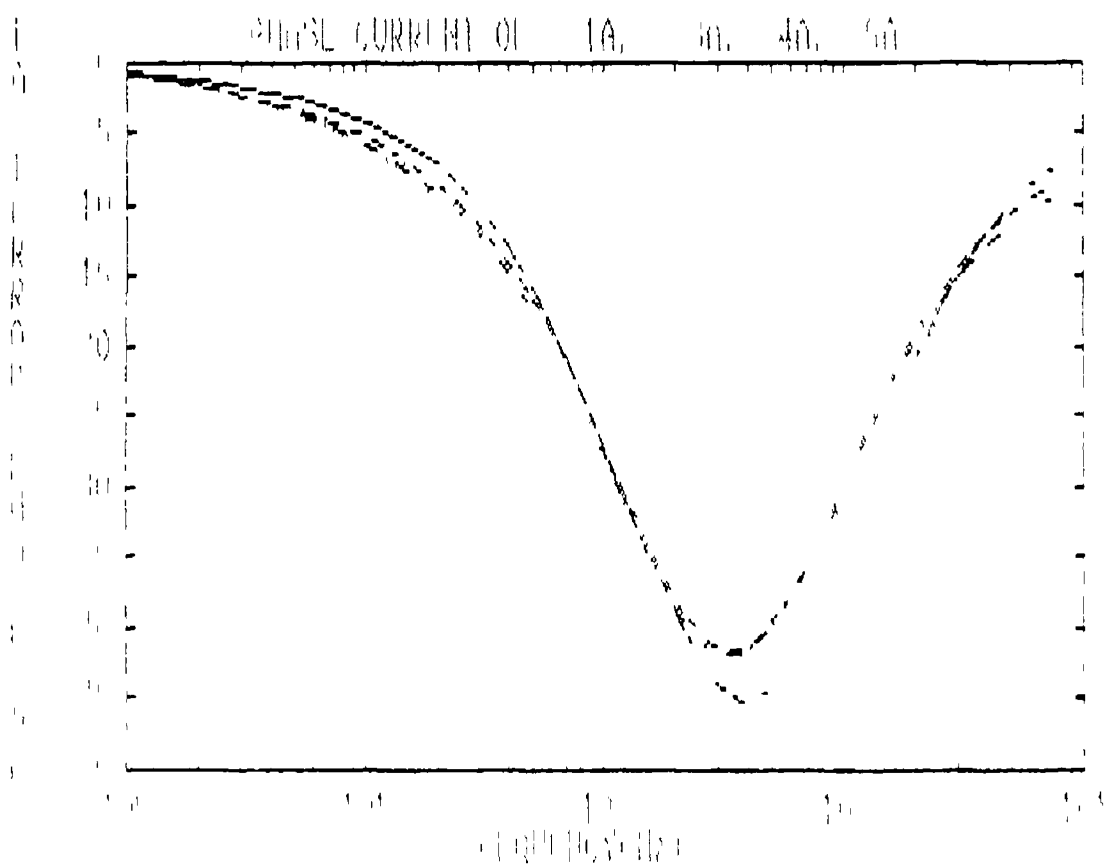

PLOT(5 16)

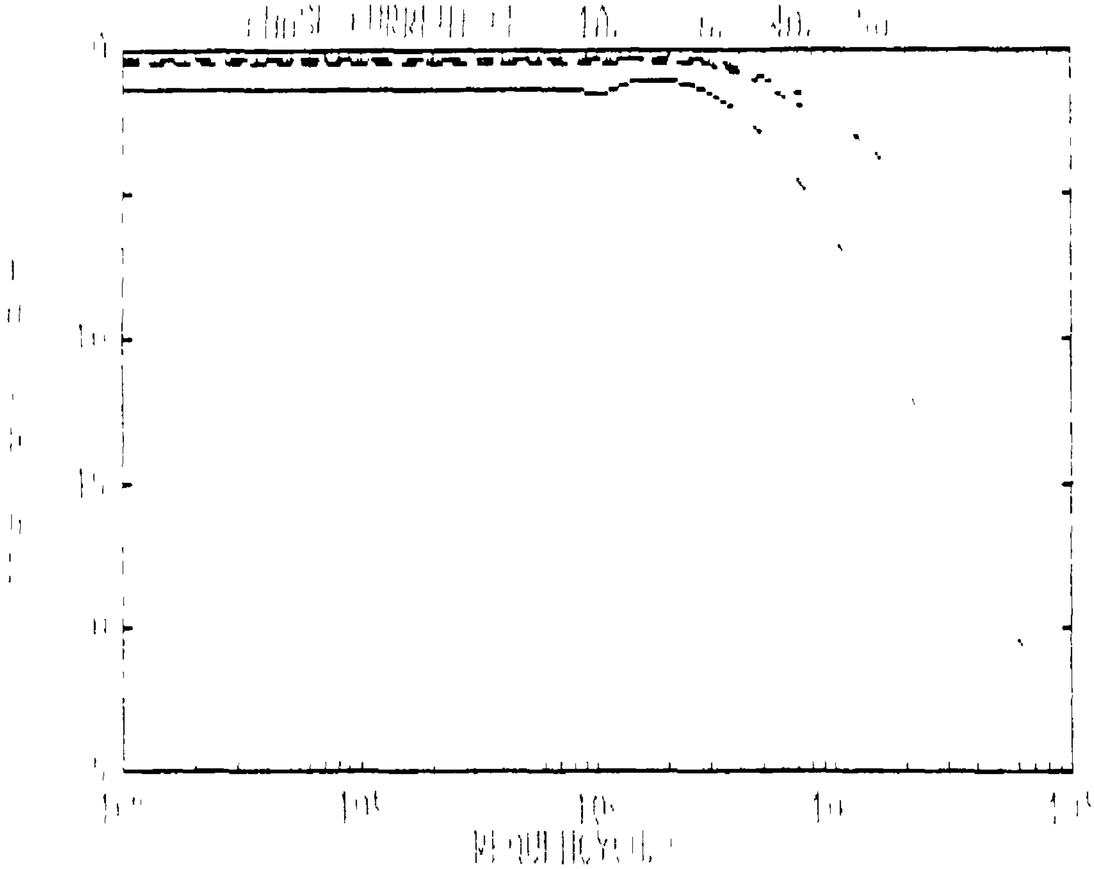

PLOT(5 17)

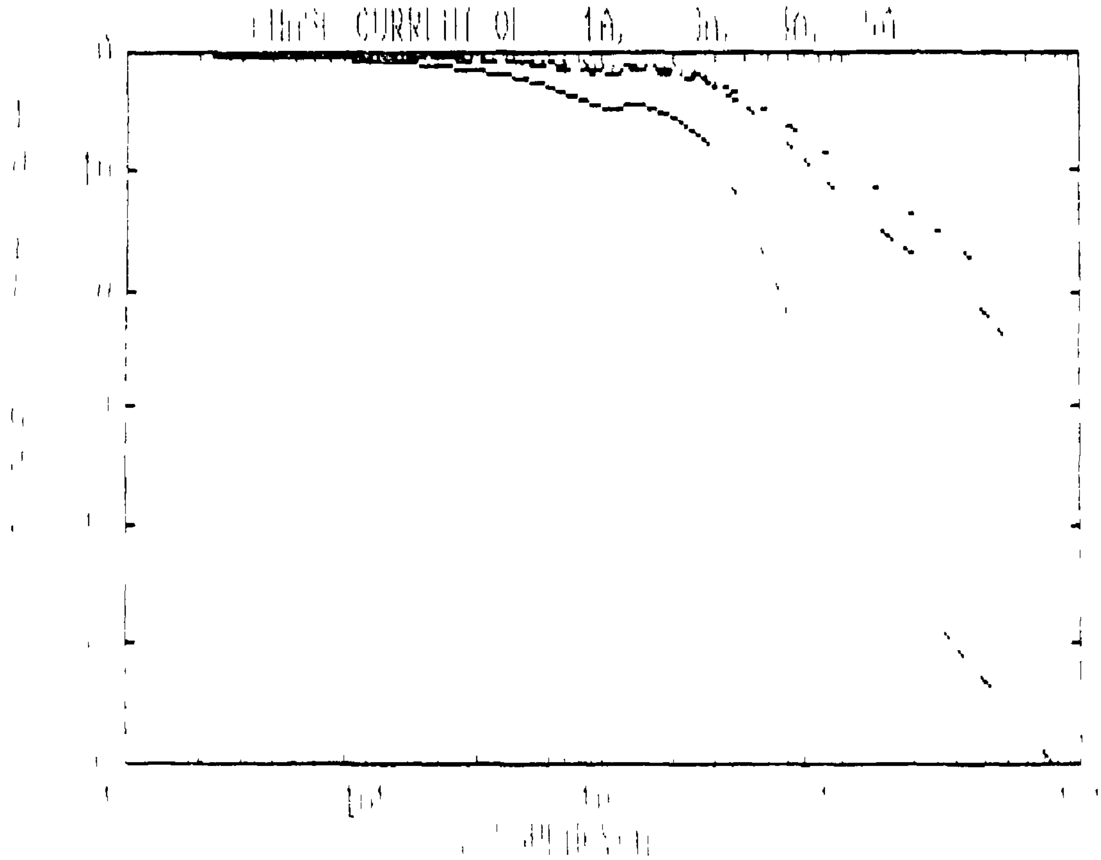

PLOT(5 18)

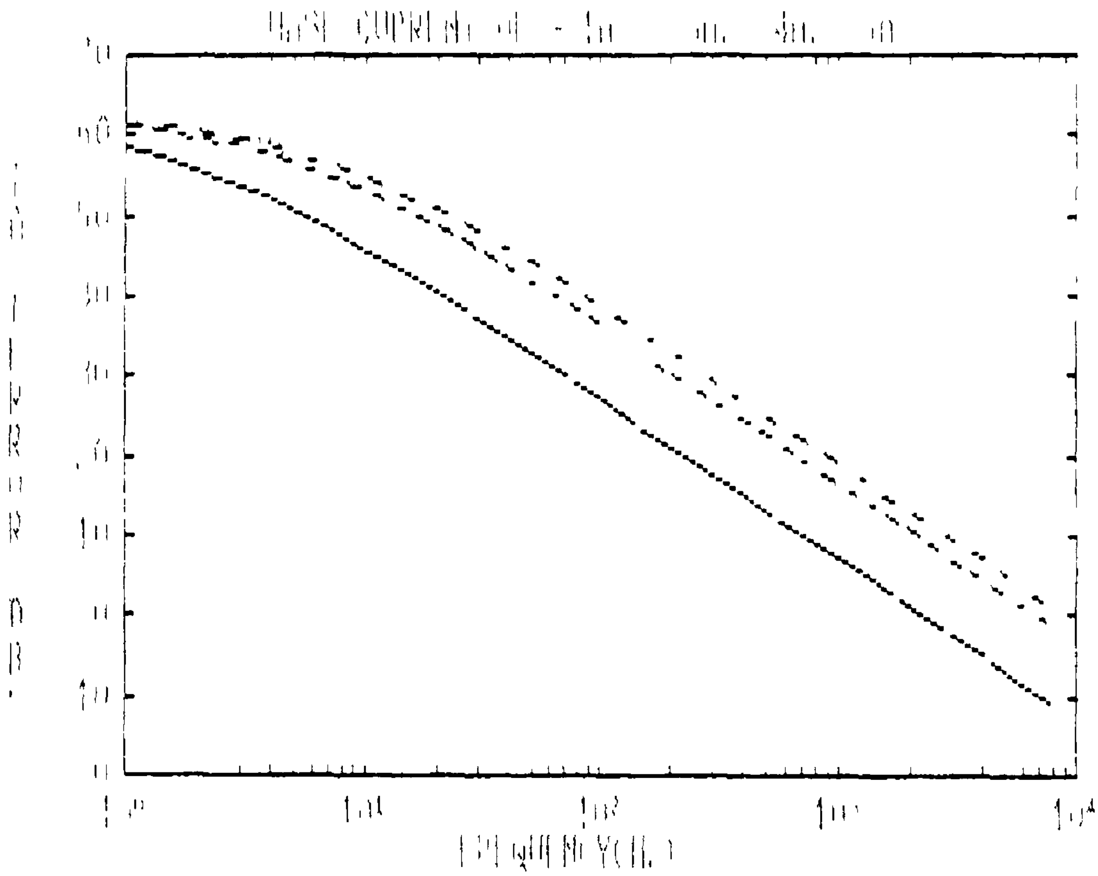

PLOT(5 19)

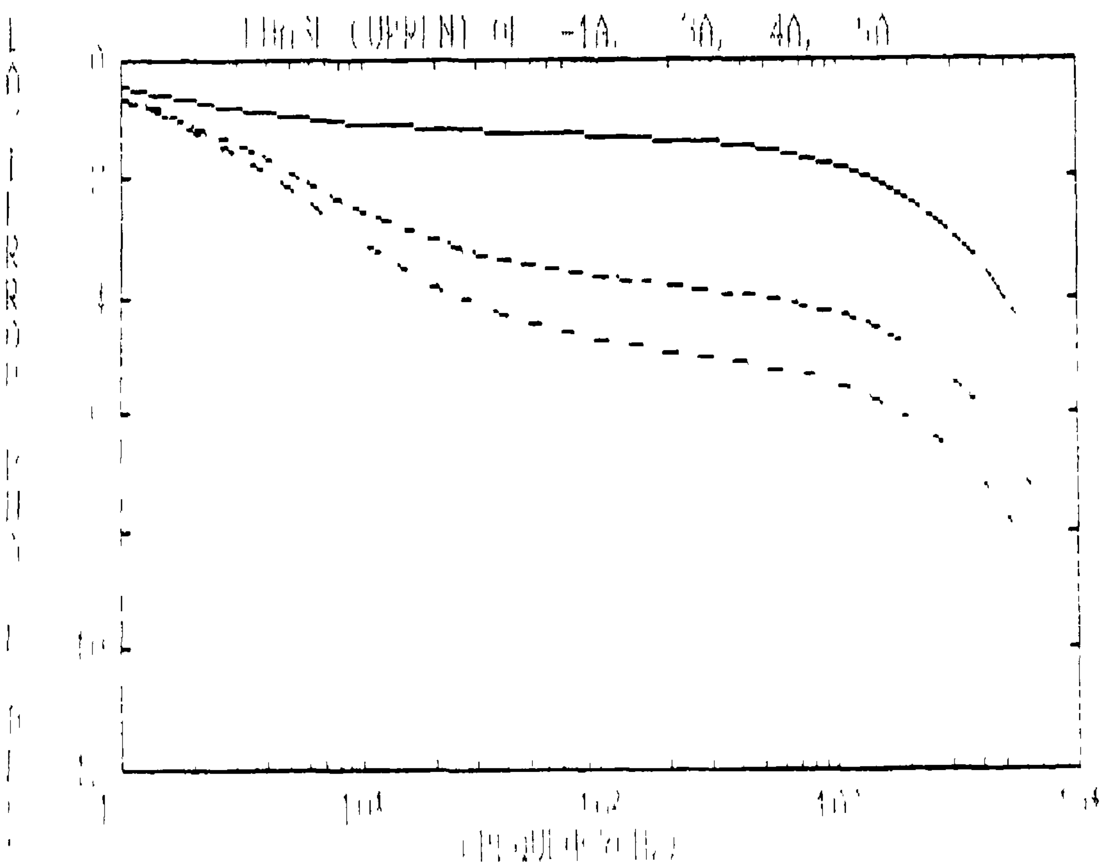

PLOT(5 20)

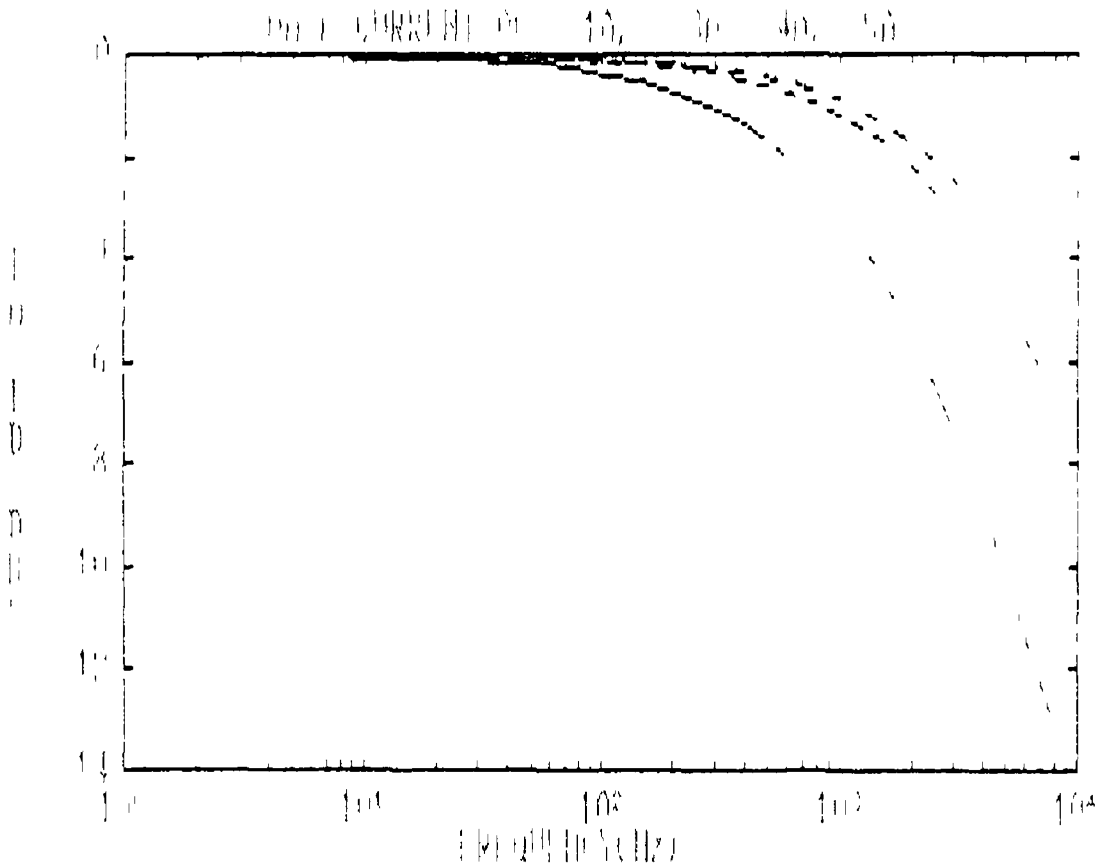

PLOT(5 21)

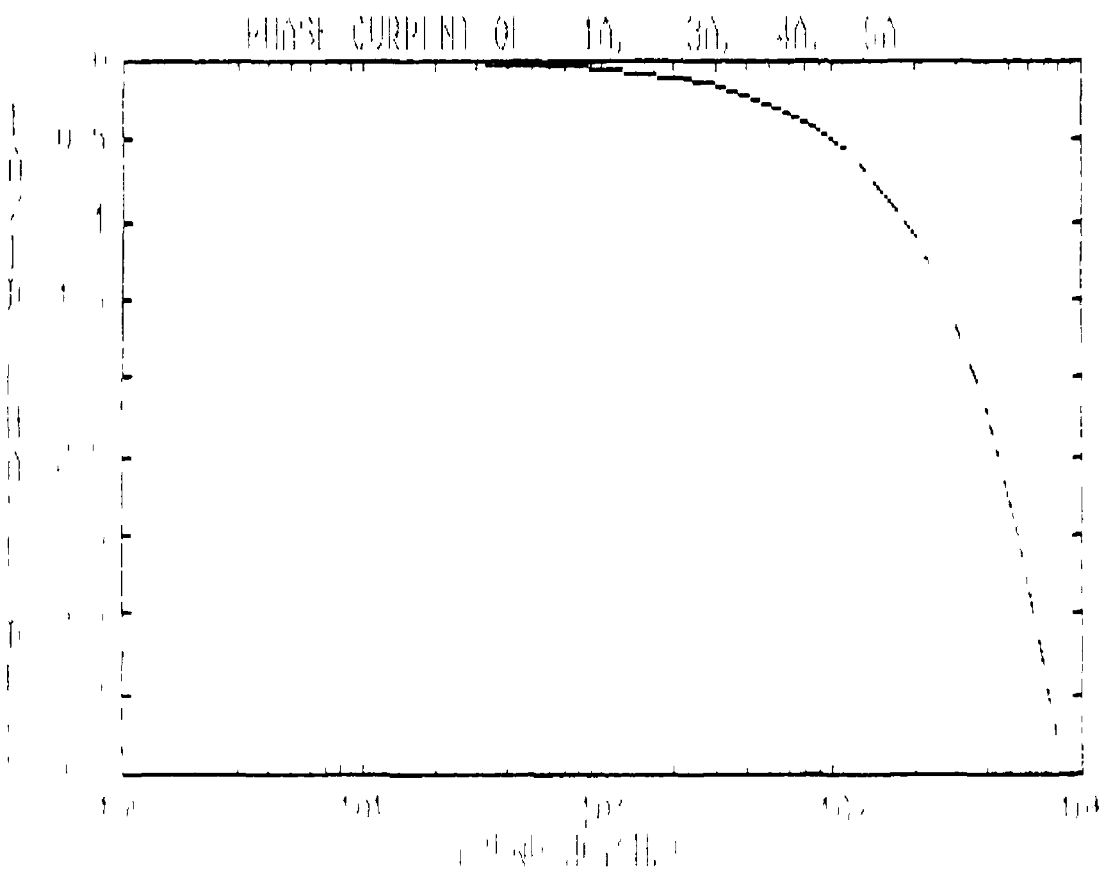

PLOT(5 22)

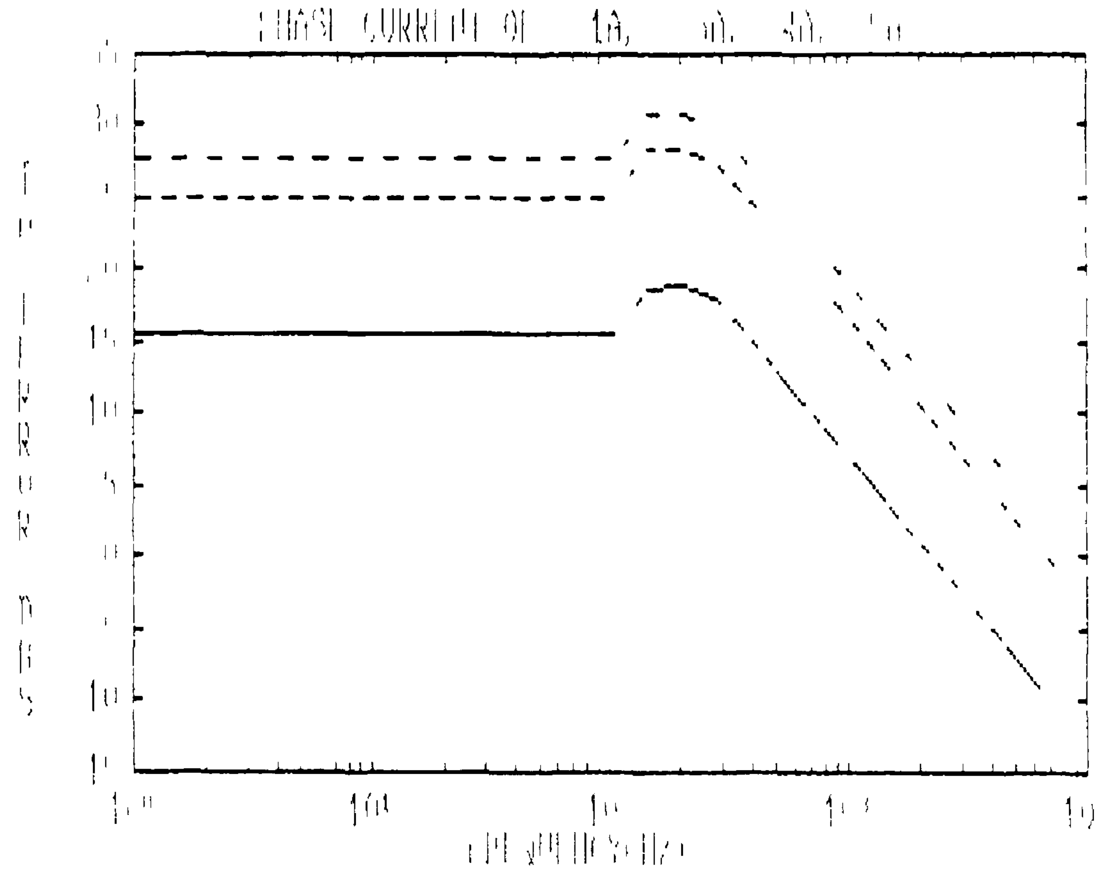

PLOT(5 23)

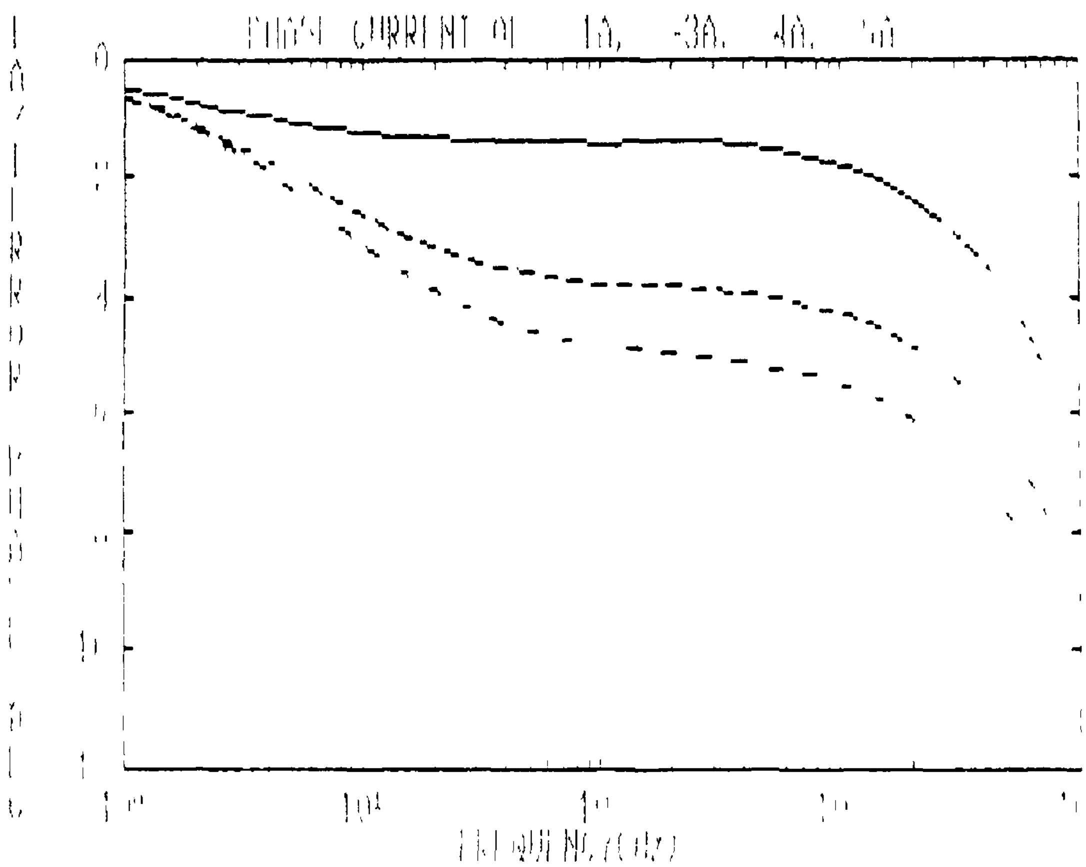

PLOT(5 24)

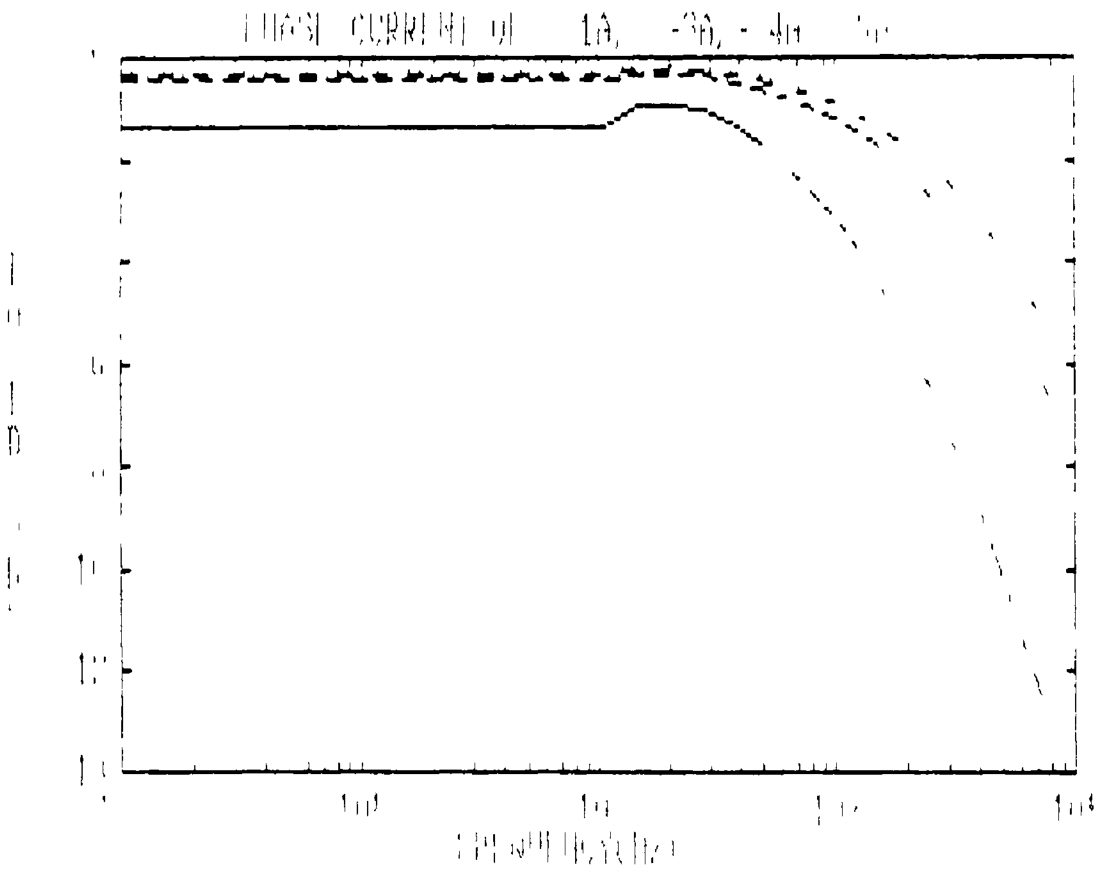

PLOT(5 25)

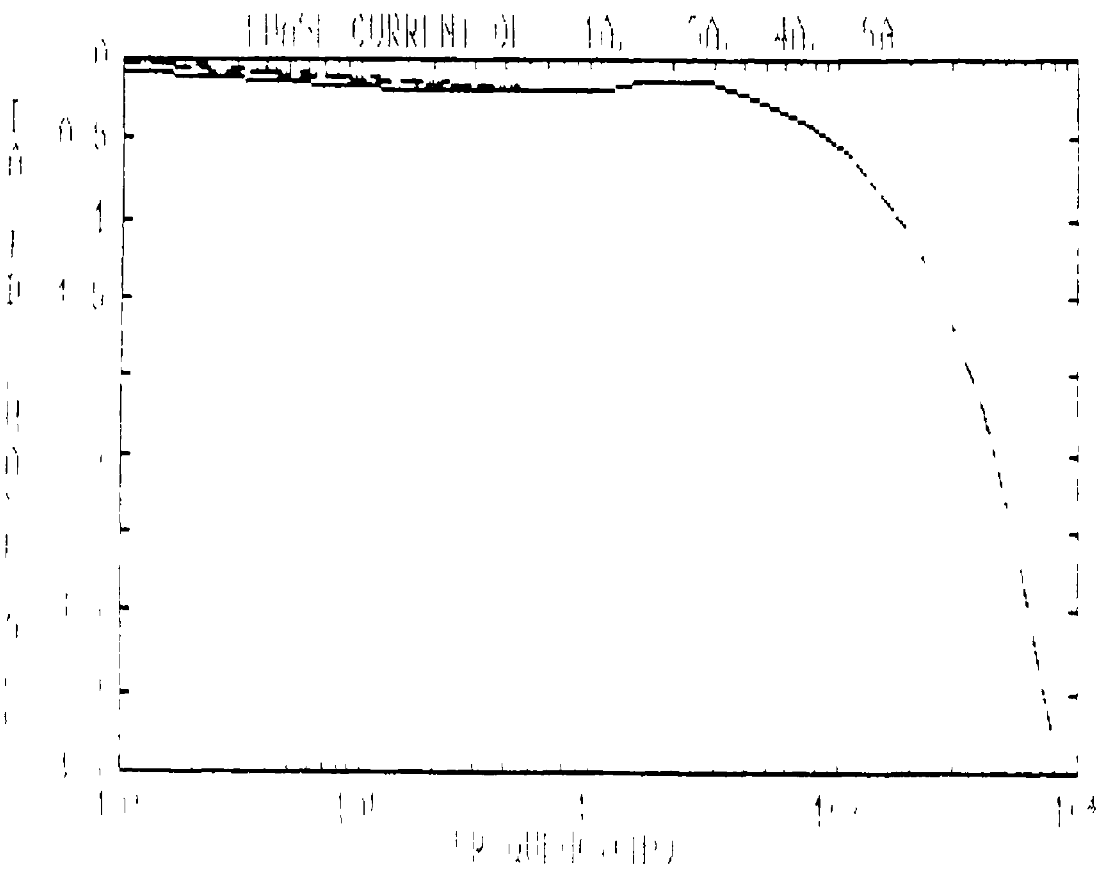

PLOT(5 26)

design. What can be said is that the frequency response plots presented are valid, and they exhibit the characteristics of stability, in that there is no possibility of sustained oscillation in the closed loop [B15]. So the basis for controller design would seem to be sound, at least in theory. It would seem, also, that because of the level of stability exhibited by the winding it is not necessary to use lag control at all. In fact, based on the frequency response plots it would seem that purely proportional control, with a high gain to limit steady state error, is on a par with, if not excels over, lag control.

5.2 DQ Controller design

5.2.1 The objective of DQ control, in the context of previously stated control objectives, is to regulate the direct axis current, I_d, around zero, and to servo control the quadrature axis current I_q. This ensures maximum torque output over the motors speed range. [P19]. This section presents a design procedure for a Q axis controller.

5.2.2 A block diagram representation of an entire DQ control system is shown in figure (5.2). The flux controller has the function of determining the motor torque angle. If 90^0 is desired then the output signals from the flux controller assume the values:

$$I_{qd} = I \quad \dots\dots\dots\dots\dots\dots \quad (5.18)$$

$$I_{dd} = 0 \quad \dots\dots\dots\dots\dots\dots \quad (5.19)$$

Where I is the output from the velocity controller. At all times the following relationship must hold [P13].

$$I = \sqrt{I_{qd}^2 + I_{dd}^2} \quad \dots\dots\dots\dots\dots \quad (5.20)$$

This relationship can be proven by reference to figure (5.3) and a simple application of the theorem of Pythagorus. The controllers $C_d(S)$, $C_q(S)$ have the function of controlling the D and Q axis currents respectively, and to ensure that this task is performed effectively, suitable control schemes have to be proposed.

5.2.3 The design method of root locus [B9,B10,B11] can be applied to equation (4.24) to produce a suitable control scheme for the Q axis. Figure (5.4) shows the

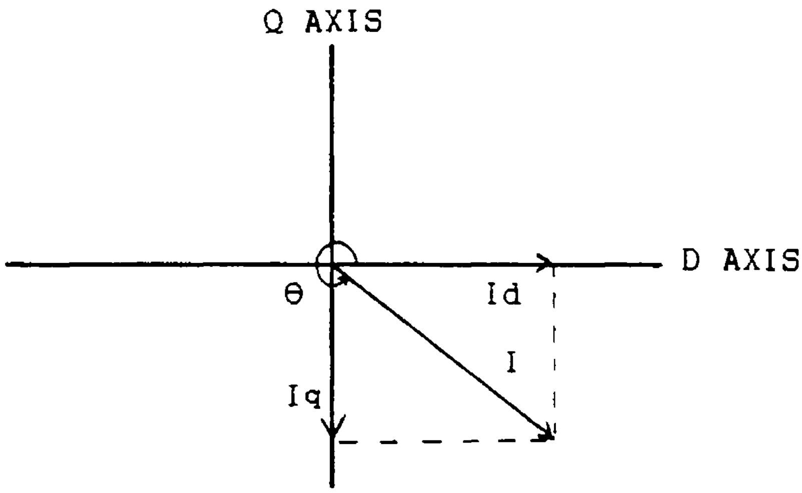

FIGURE(5 3)
D AND Q AXIS CURRENTS

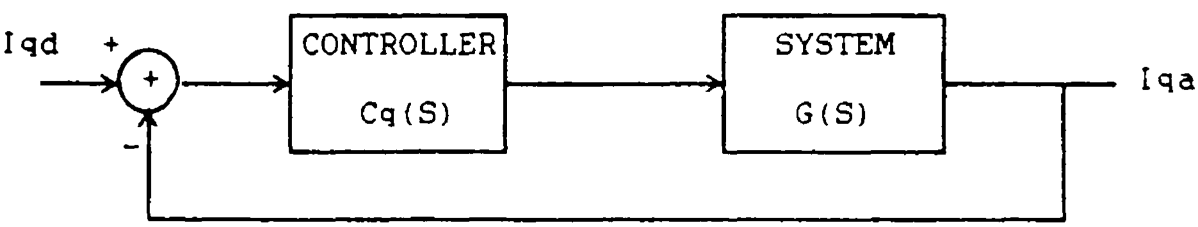

FIGURE(5 4)
Q AXIS CONTROLLER

motor Q axis in its linearised form, with the loop closed. The transfer function of the system is·

$$\frac{Iqa(S)}{I_{qd}(S)} = \frac{C_q(S)G(S)}{1+C_q(S)G(S)} \qquad (5\ 21)$$

where G(S) is the Q axis transfer function (equation 4.29)). If $C_q(S)$ is initially assumed to be proportional in nature, then equation (5.21) becomes:

$$\frac{I_{qa}(S)}{I_{qd}(S)} = \frac{K_pG(S)}{1+K_pG(S)} \qquad (5\ 22)$$

with

$$P(S) = 1+k_pG(S) \qquad \text{............} \ (5.23)$$

as the systems characteristic equation. Root locus maps the variation of the zero's of the characteristic equation (the poles of the system) with gain.

5.2.4 Plot (5.27) illustrates the root locus with k_p varying between 0 and 10. Plot (5.28) shows the same root locus, but with the gain assuming values between 0 and 3. A greater amount of information can be gleaned from the plots of the variation in the system poles with K_p. Plots (5.29, 5.30) indicate this variation. The real part of the pole, only, is plotted against k_p, but after critical damping has occurred (after k_p = 1.5) the pole is purely real. Plot 2 becomes dominant with large k_p and as such dictates system response. K_p has to be larger than 1.5, to avoid underdamping, and less than 6 to maintain the dominant time constant (that of pole 2) lower than 10 mS. In fact the lower the time constant the better the system response time.

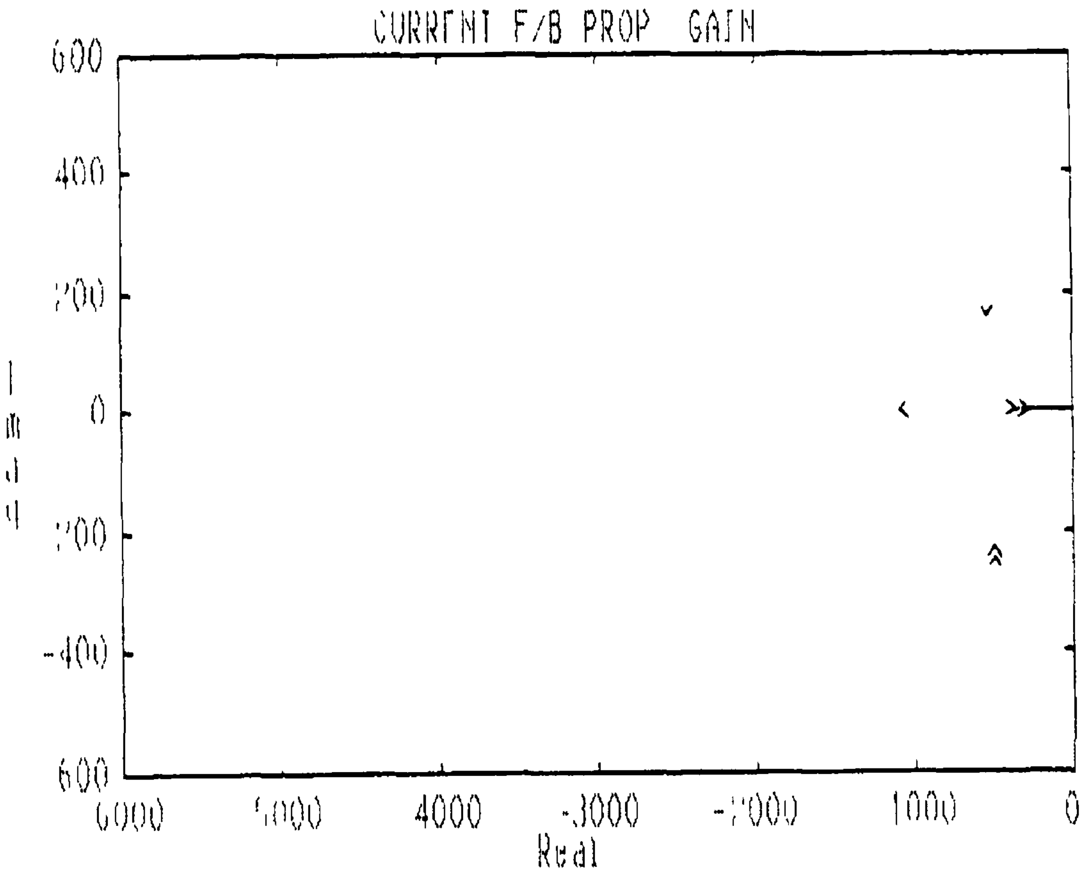

PLOT(5 27)

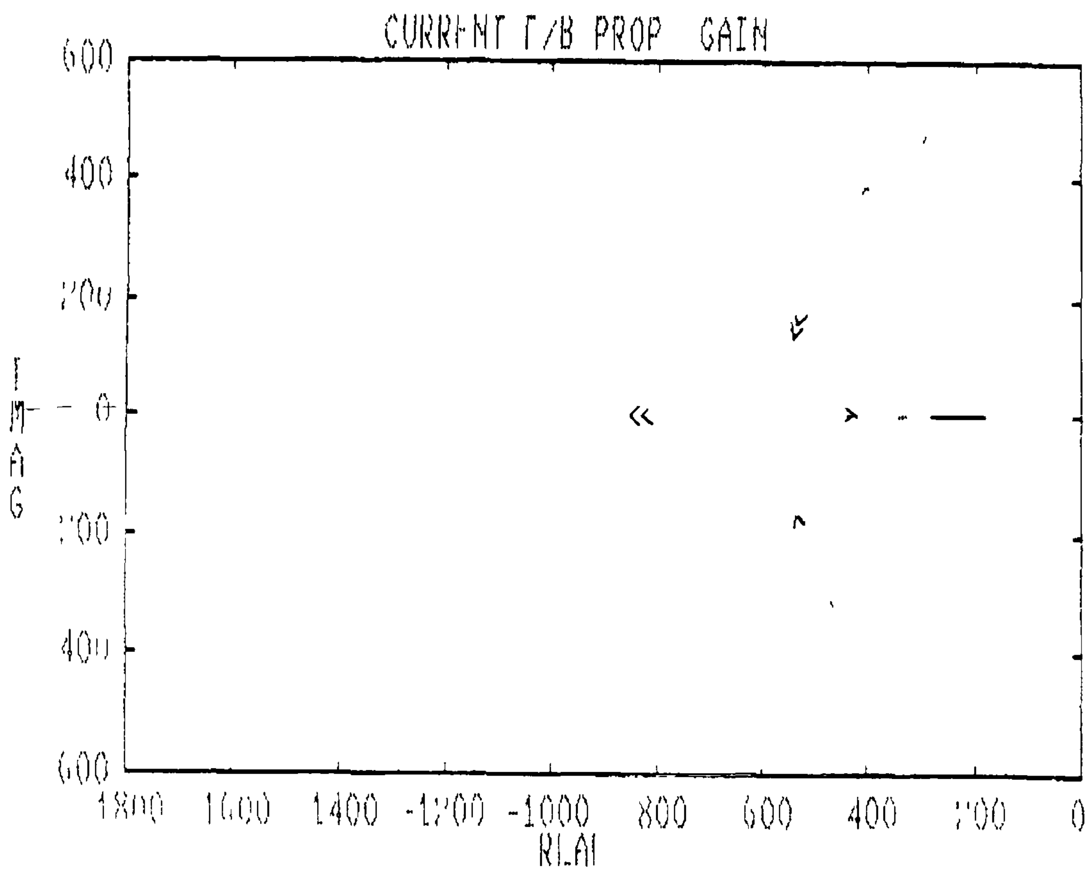

PLOT(5 28)

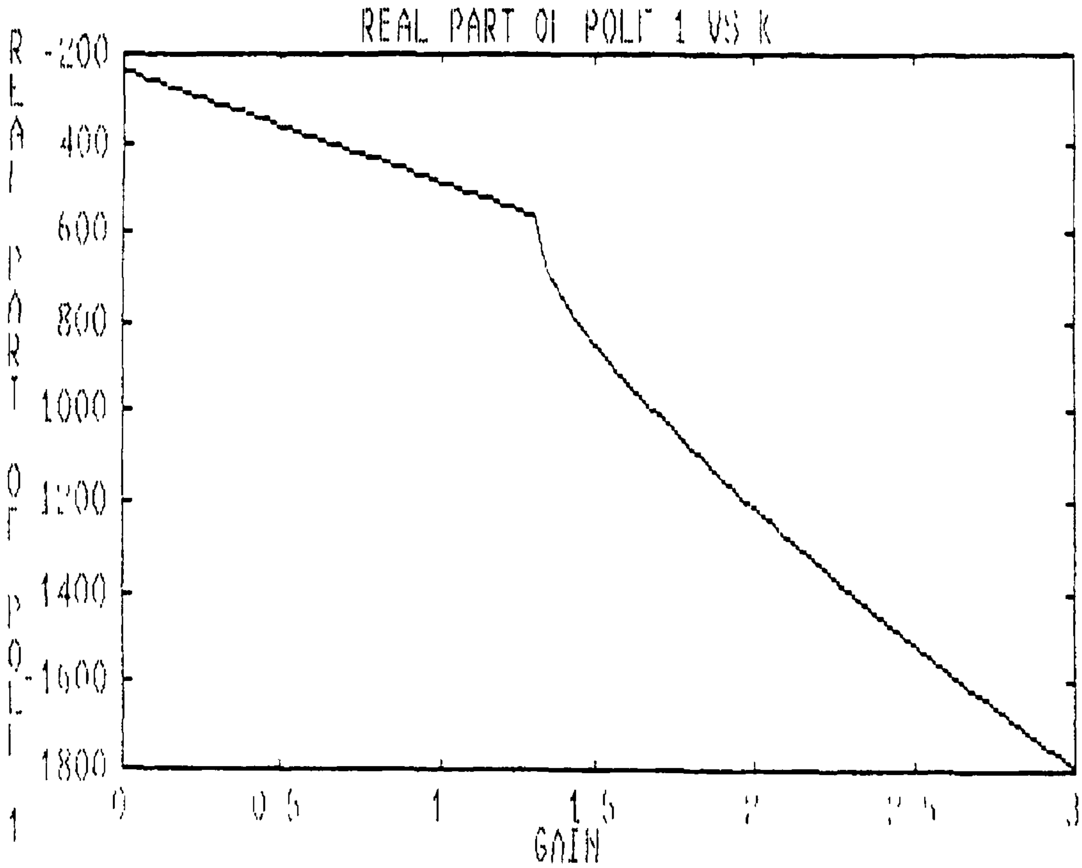

PLOT(5 29)

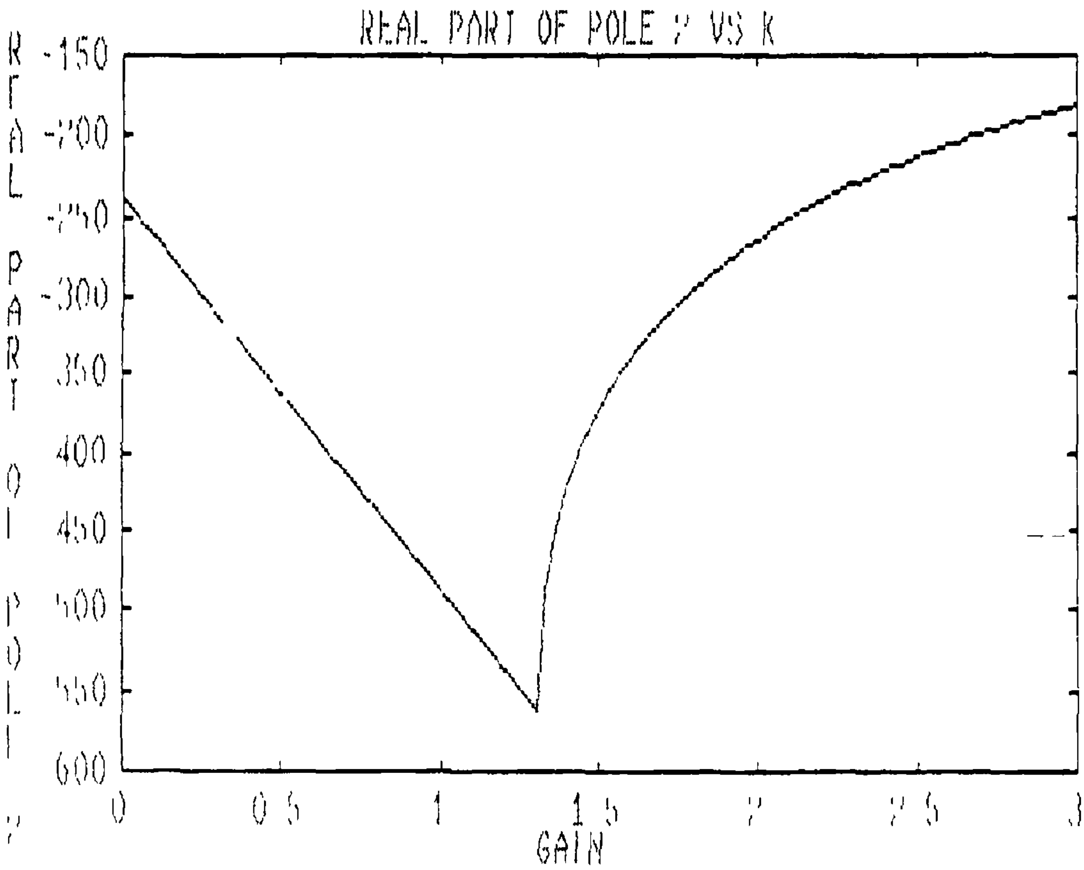

PLOT(5 30)

5.2.5 The major problem with proportional control is the presence of a steady state error. The addition of an integrator to the controller is necessary to eliminate the steady state error. A P+I controller assumes the form:

$$C_q(S) = Kp(1+1/(TiS)) \;............\; (5.24)$$

Since the root locus method allows only one parameter vary it is necessary to choose a value of T_i before applying the method. The system characteristic equation now looks like:

$$P(S) = \frac{1+K\ AS^2+(A/T_1+B)S+B}{S(S^2+CS+D)} \qquad (5\ 25)$$

where A = 500

B = 4642.85

C = 484.2

D = 310714.7

5.2.6 A value of 50 mS was chosen for T_i and the root locus method applied to the system. Plot (5.31) illustrates the obtained locus. Poles 1 and 2 have not varied by any considerable amount. This fact is shown in plots (5.32, 5.33). The presence of an integrator in the controller introduces an extra pole to the system. The variation of this pole with k_p is clearly seen in plot (5.34) This new pole assumes the role of dominance and it makes the overall system response very sluggish.

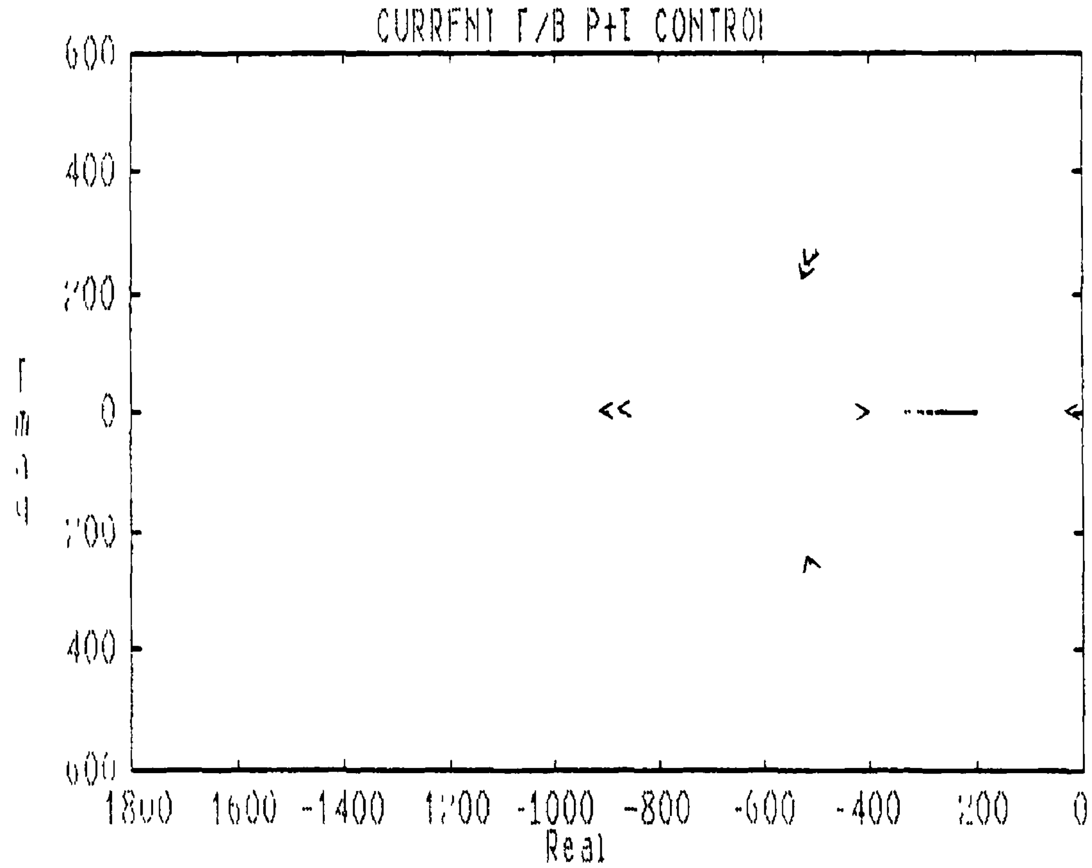

PLOT(5 31)

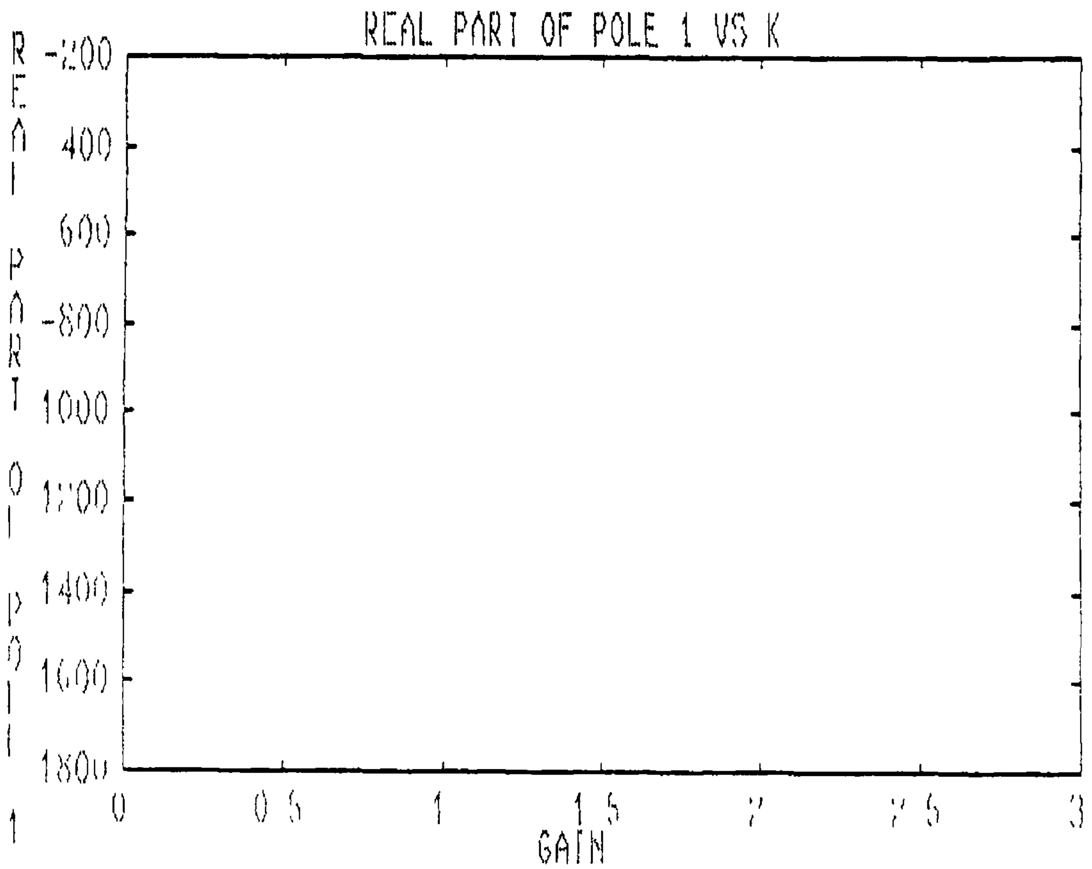

PLOT(5 32)

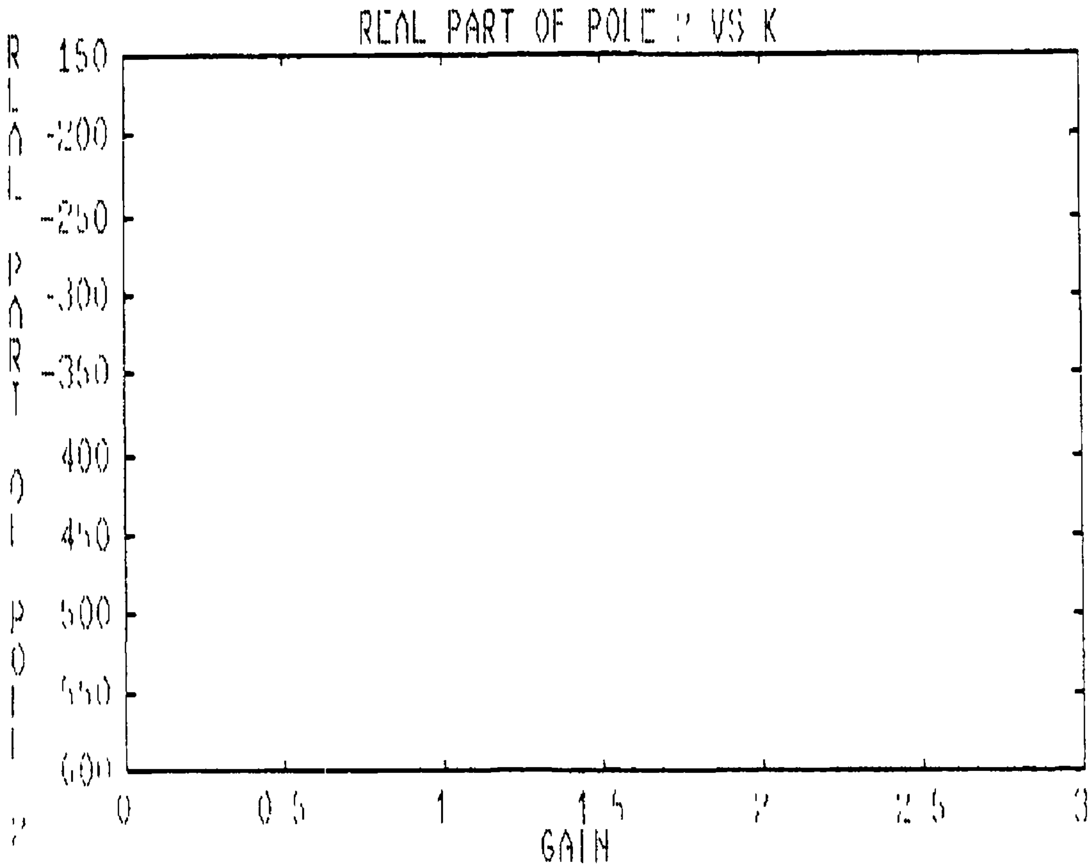

PLOT(5 33)

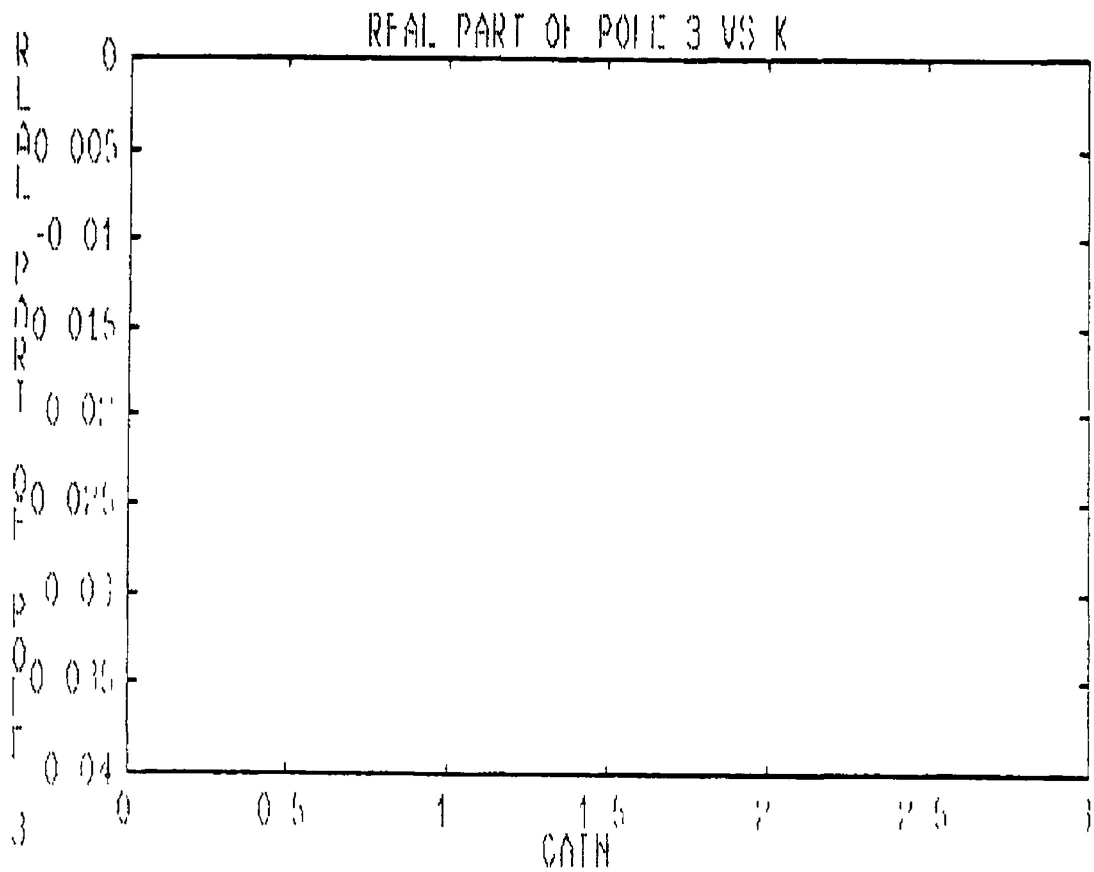

PLOT(5 34)

5.2.7 The presence of this new pole in the system can be explained by a consideration of the basics of root locus theory [B10,B11,B12]. The characteristic equation of equation (5.25) can be rewritten as:

$$S(S^2+CS+D)\ P(S) = S(S^2+CS+D)+k_p(AS^2+[A/T_1+B]S+B) \qquad \text{.................. (5.26)}$$

In solving the characteristic equation as root locus essentially does, the right hand side of 5.26 is equated with zero. Equation (5.26) can be rewritten as·

$$0 = M(S) + k_pN(S) \qquad \text{.................. (5.27)}$$

where

$$M(S) = S(S^2+CS+D) \qquad \text{.................. (5.28)}$$

$$N(S) = AS^2+(A/T_1+B)S+B \qquad \text{.................. (5.29)}$$

5.2.8 The roots of M(S), by convention, are called poles, and the roots of N(S) are called zeroes. The path a closed loop system pole traces out on the locus plot is called a branch. One of the fundamental rules of root locus is that a branch originates at a pole, and terminates at a zero (when $k_p = \infty$). So a branch originates at S=0, and terminates at a root of N(S). The roots of N(S) are dictated by the value of T_i. For T_1 assuming a value of 50 mS, as earlier chosen the roots of N(S) are:

$$Z_1 = -0.3205$$

$$Z_2 = -28.9$$

Thus the termination point of the branch originating from S=0, and as such the minimum value that system pole 3 can assume, is -0.3205. Plot (5.35) illustrates

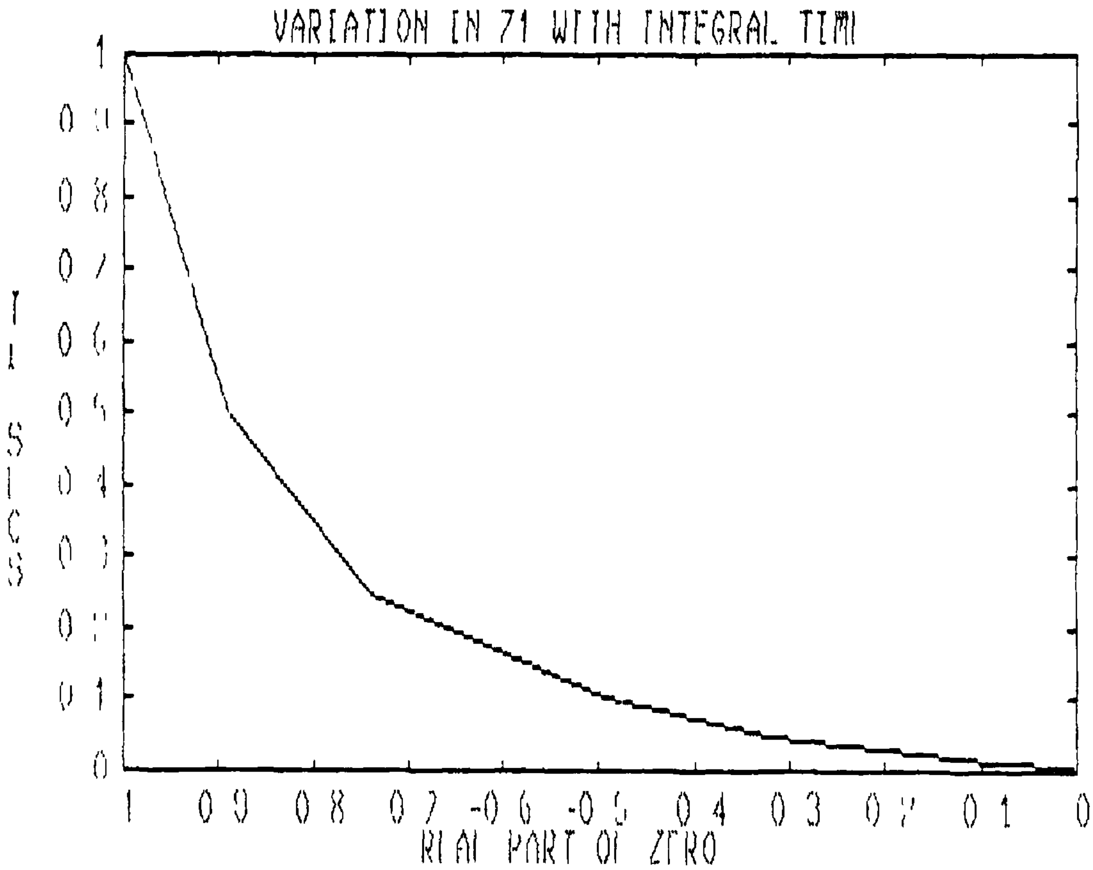

PLOT(5 35)

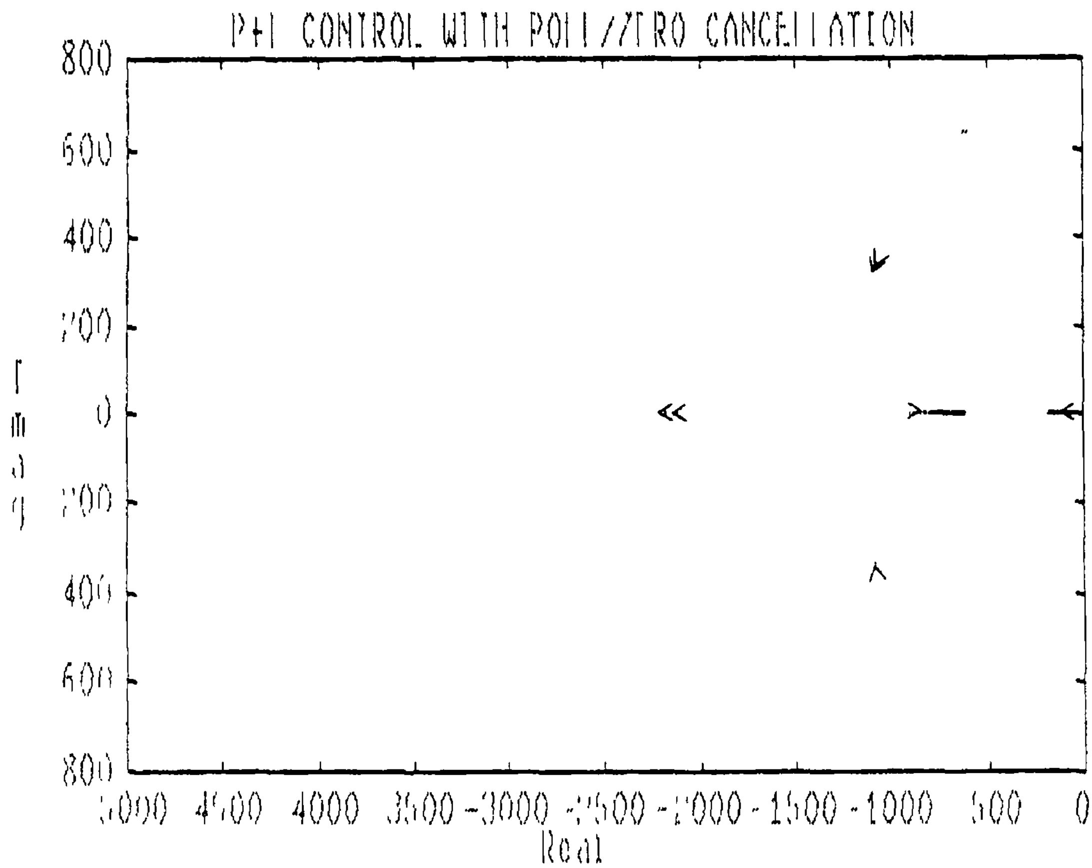

PLOT(5 36)

how Z_1 changes with T_i. The lower the value of T_i, the lower the magnitude of Z_1. It is not feasible to increase T_i in order to increase Z_1'S magnitude. The other zero, Z_2, is also affected by changes in T_i. If T_i is increased towards infinity the controller becomes more and more proportional in nature so the purpose of the inclusion of an integrating element is defeated. It would seem that some other control scheme is needed.

5.2.9 If the zero, Z_1, could someway be increased in magnitude then this would provide a solution to the problem. Pole/zero cancellation provides a means of achieving this aim [B11,B12]. If T_i is chosen to be 5 mS then the values assumed by Z_1 and Z_2 are:

$$Z_1 = -0.00443$$
$$Z_2 = -209$$

If $C_q(S)$ is amended to

$$C_q(S) = K_p(1+1/ST_i)([S+500]/[S+0.00443]) \qquad \text{............. (5.30)}$$

zero Z_1 is cancelled and replaced by a zero at S=-500. Plot (5.36) shows the root locus for this situation. Plots (5.37 ... 5.39) illustrate the real part of the poles plotted against k_p. The dominance of pole 3 has been reduced, and its magnitude at a gain of 10 is of the order that would enable a dominant pole time constant of about 6 mS. In fact a better response could be achieved with an even lower value of T_i, as this would increase the magnitude of Z_2. However the magnitude of Z_1 would be decreased and the cancellation of a zero of such a minute magnitude would

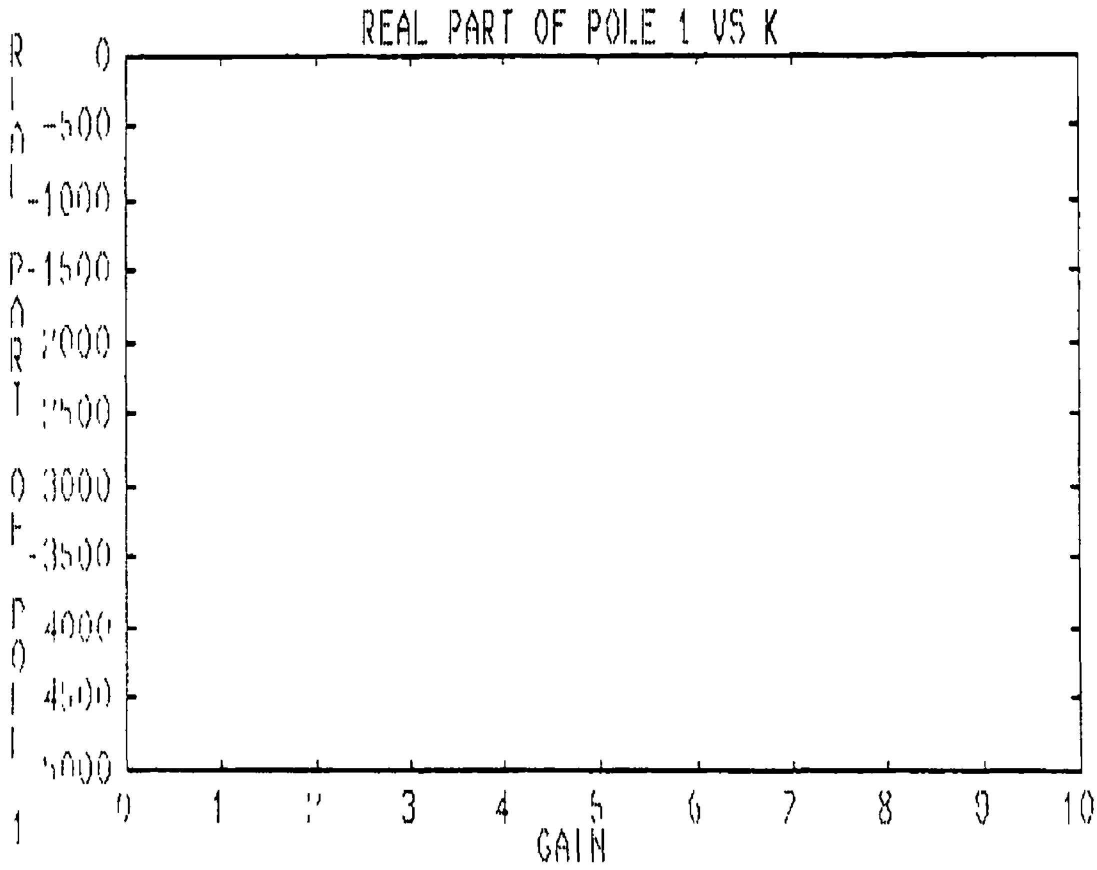

PLOT(5 37)

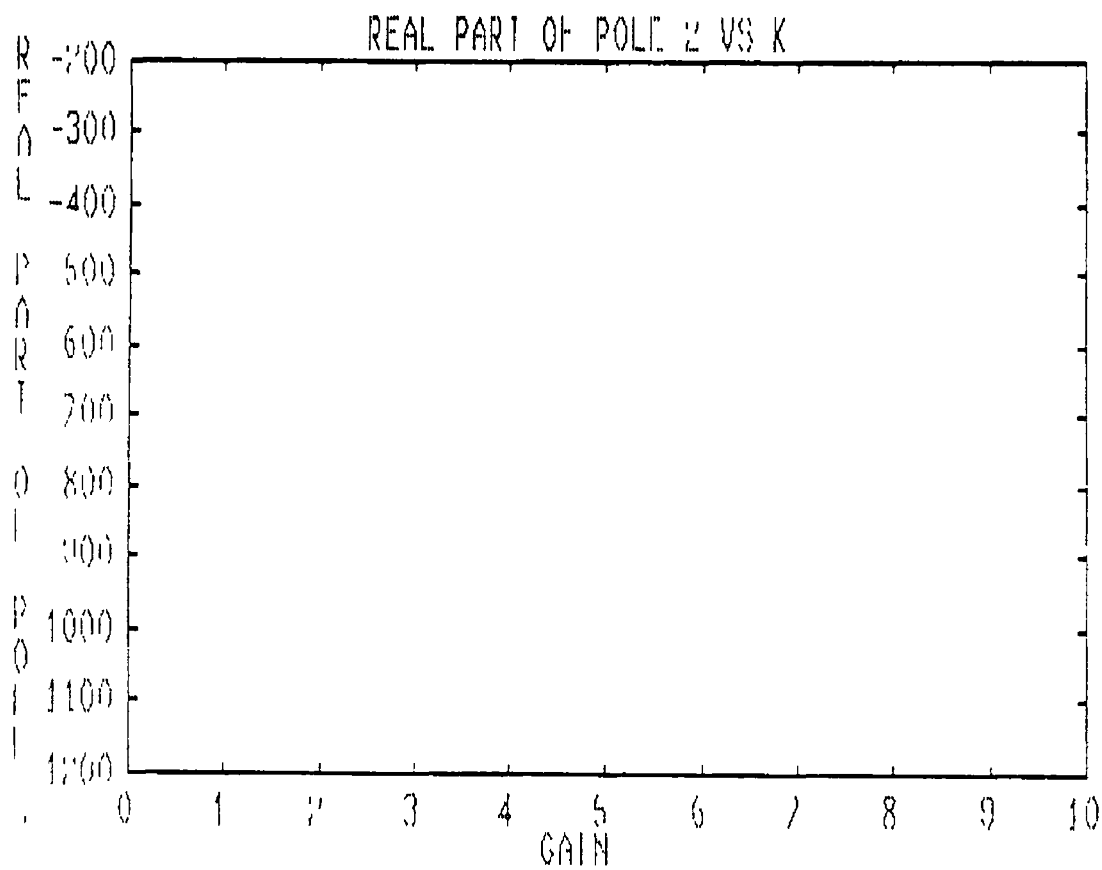

PLOT(5 38)

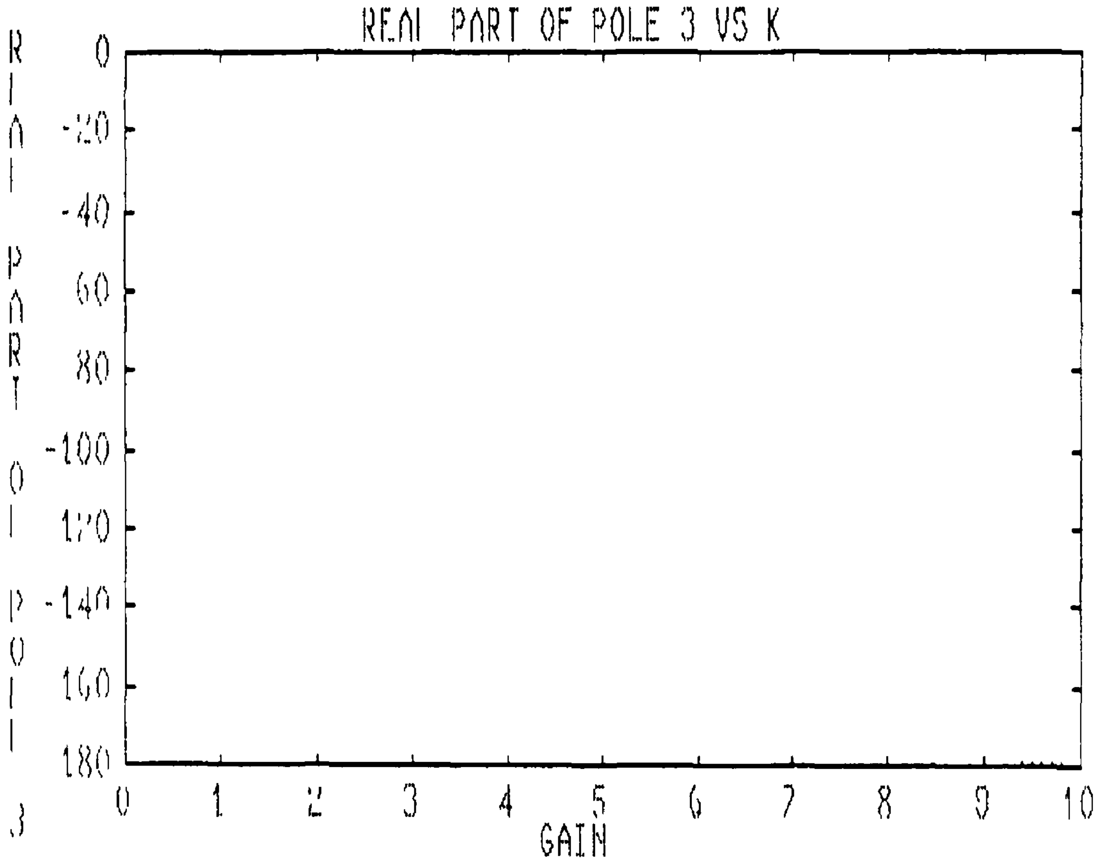

REAL PART OF POLE 3 VS K
REAL PART OF POLE 3
0
-20
-40
-60
-80
-100
-120
-140
-160
-180
0
1
2
3
4
5
6
7
8
9
10
GAIN

PLOT(5 39)

pose problems. If the reason for an integral element in the control structure is considered, this problem can be overcome. The integrator eliminates the steady state error, but it is not necessary, in order to achieve this objective, to have a control structure like that in equation (5.24). Consider a controller described by:

$$C_q(S) = \frac{k_p}{S} T(S) \qquad \ldots\ldots\ldots\ldots\ldots \quad (5.31)$$

The root of the numerator of equation (4.24) is located at S = -9.3. If T(S) had the format·

$$T(S) = \frac{(S+\beta)(S+\alpha)}{(S+9.3)} \qquad (5.32)$$

suitable choice of β and α could shape the root locus of Plot (5.35) as desired, and place the closed loop system poles where required. The necessity of having to cancel a zero of the order of -0.00443 would be eliminated.

5 2.10 The gain, k_p, used in the construction of the root loci corresponds to the total forward path gain. As such it includes the PWM amp gain. Since the dynamics of the harmonic distortion ratio are not fully understood yet it is hard to guage how it affects the loci. But since the system is stable as k_p tends toward infinity, fluctuations in gain generated by the loss ratio should not affect stability. The gain values obtained from the loci, although they include the PWM gain, will be those actually implemented. In effect a gain value erring on the side of caution.

6. Dynamic simulation of an AC machine.

6.1 The 3 Phase representation

6.1.1 System simulation is a useful exercise in that it allows dynamic response tests be performed without the necessity of test rigs, once the simulation has been verified. It also allows access to system variables that may not be physically accessible in the actual system. The most useful facet of simulation in the context of control is the ability to test control algorithms without the risk of overdriving the system or damaging components. An evaluation of the actual controllers can also be performed, using the simulation. To this end the simulation presented here was initially designed.

6.1.2 Simulation necessitates the discretization of the system equations. There are various methods of discretization ranging from forwards rectangular to pole mapping [B12,B13] each displaying its merits and demerits. The method eventually chosen was backwards rectangular with a continuous to discrete transformation of:

$$S \longrightarrow (1-Z^{-1})/T_S \quad \ldots\ldots\ldots\ldots\ldots\ldots \quad (6.1)$$

where S is the laplace transform operator, Z is the z transform operator and T_S is the sampling time. Backwards rectangular was chosen due to the relatively simple discrete equations that result from such an approximation. This is helpful in the context of digital controller design as the comparatively small computation time needed allows a smaller sampling time be achieved. The actual discrete equation of the backwards rectangular approximation takes the form:

$$\frac{df(t)}{dt} \approx [F(k) - F(k-1)] \,/\, T_s \;\ldots\ldots\ldots\ldots \quad (6.2)$$

where T_s is small. The limit of the right hand side goes to the derivative, as T_s goes to zero. So if backwards rectangular is used to approximate the whole of the closed loop system, the sampling time of that part comprising the motor and all physically continuous system components can be chosen to be as small as is necessary to ensure an accurate representation. The controller, which will be discrete in nature can have as its sampling rate, a time that can be reasonably achieved by a microprocessor based system. The only criterion is that the slower sampling rate in this case the microprocessor, is an integral number of the faster rate. [B14]

6.1.3 Appendix (4) describes the full set of equations of the 3 phase motor and control system is discrete form. Although the motor is not represented in the format of equations (2.17 ... 2.22) the DQ representation is dynamically equivalent and is simplier to simulate.

6.1.4 To determine the effectiveness of the simulation a comparison was made in terms of dynamic velocity response and steady state current phase angle. The current controller used was C_1, which is actually implemented in the test motor system. The velocity loop was closed with a gain of 1. Plot (6 1) shows the actual system response to a velocity step of 1000 RPM. The initial velocity was 0 RPM. Plot (6.2) illustrates the simulated response under the same conditions. The steady state error is due to the low velocity loop gain, so the actual velocity is only 660 RPM. Although the plots are not identical, the difference is small.

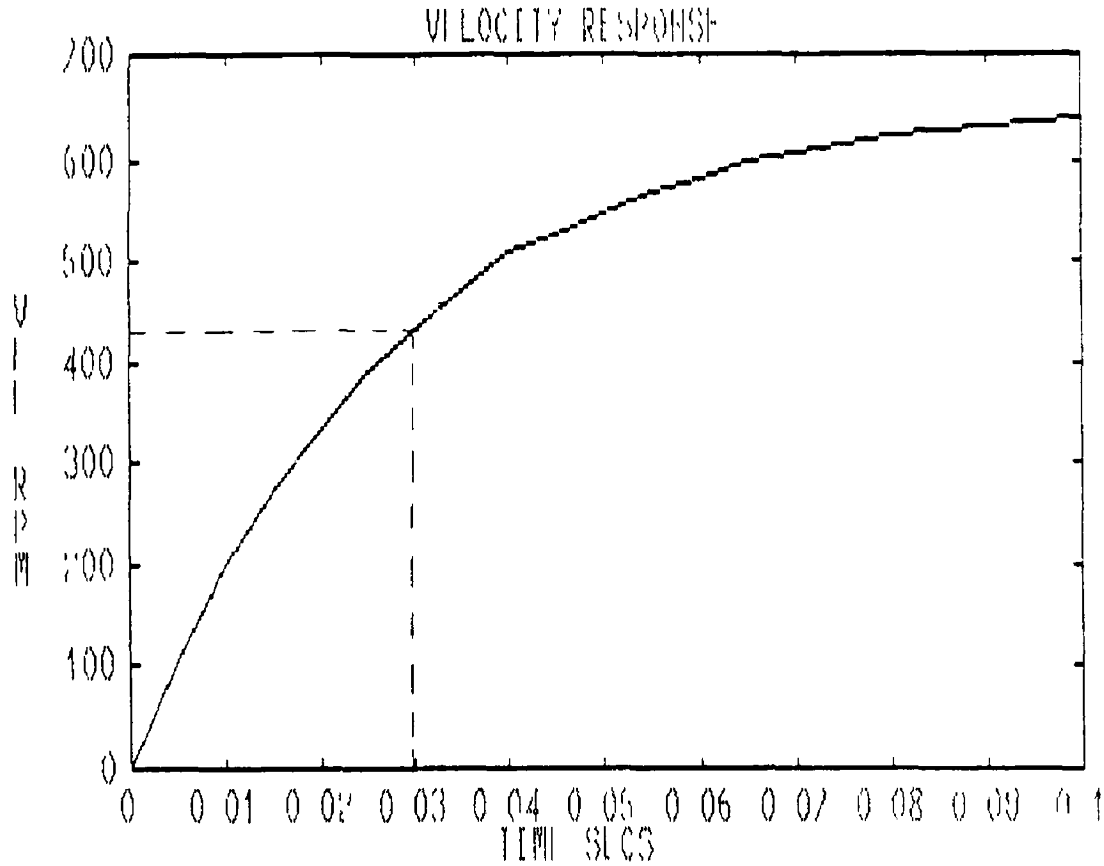

PLOT(6 1)

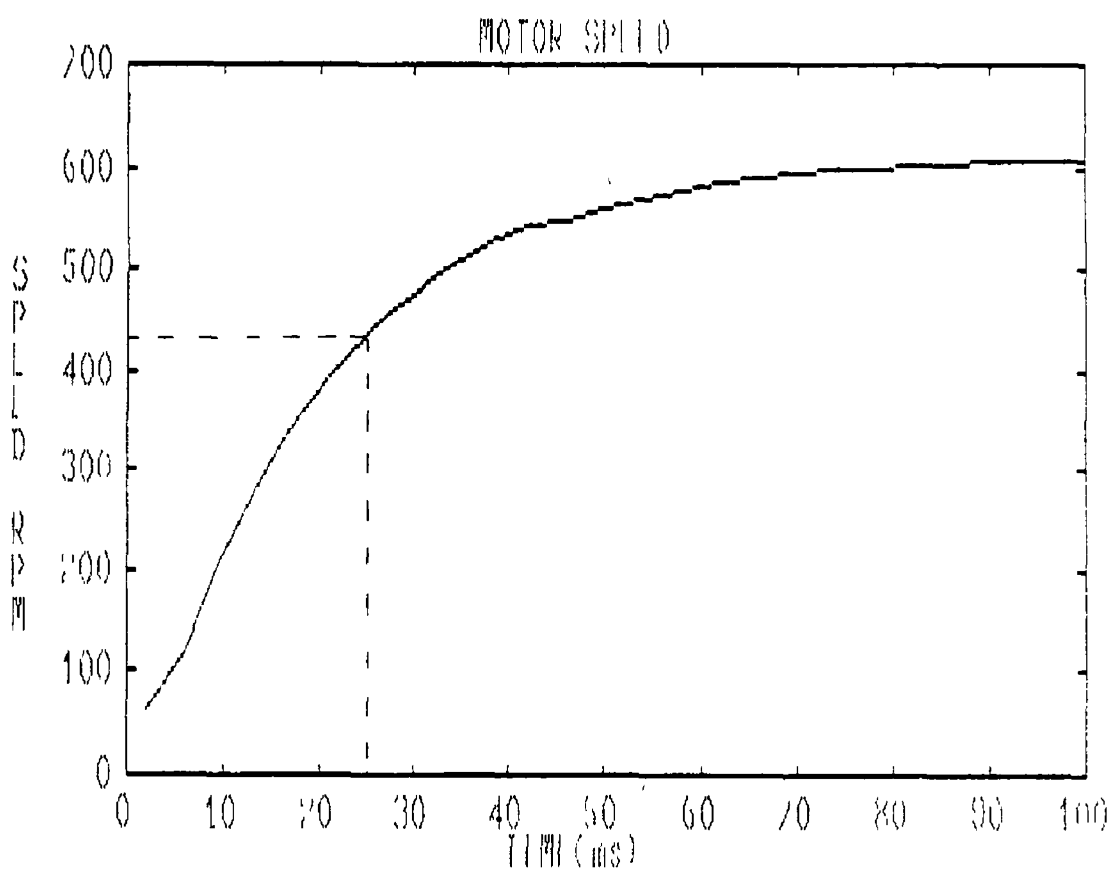

PLOT(6 2)

The time constant of Plot (6.1) is 29 mS, while the simulation has a time constant of 25 mS, a difference of 14%. Plot (6.3) illustrates the actual and simulated gain responses for the current loop, while plot (6.4) shows the phase responses for the actual and simulated. At 100 Hz, as indicated in the plot, the phase of the simulated differs by 23% from the actual. This percentage difference decreases as the frequency goes up, being only 9% at 300 Hz. The correspondence between the simulated and actual gain responses is also quite close. Thus it can be concluded that the simulation is a resonable representation of the motor.

6.1.5 The confirmed accuracy of the frequency response plots ensures that the current control system, incorporating either C_1, C_2, C_3 will display the simulated steady state attributes. So the predicted stability is well founded. The validation of the dynamic simulation allows a dynamic performance assessment of the system with either C_1, C_2, C_3 in place. This enables the best controller in terms of dynamic performance and stability be chosen. A controller sampling time of 0.4 ms was chosen, and this value is used in all subsequent simulations. The choice of 0.4 ms is justified in Chapter 7.

6.1.6 Plot (6.5) shows the 3 phase currents against time with a velocity step of 0 - 1000 RPM. The controller in place is C_1. The magnitude of the phase currents initially rises to provide the torque necessary for acceleration. The frequency also rises with speed at the extreme right of the plot the currents settle to a level sufficient to overcome friction and windage losses This is the situation when the machine has reached the steady state velocity

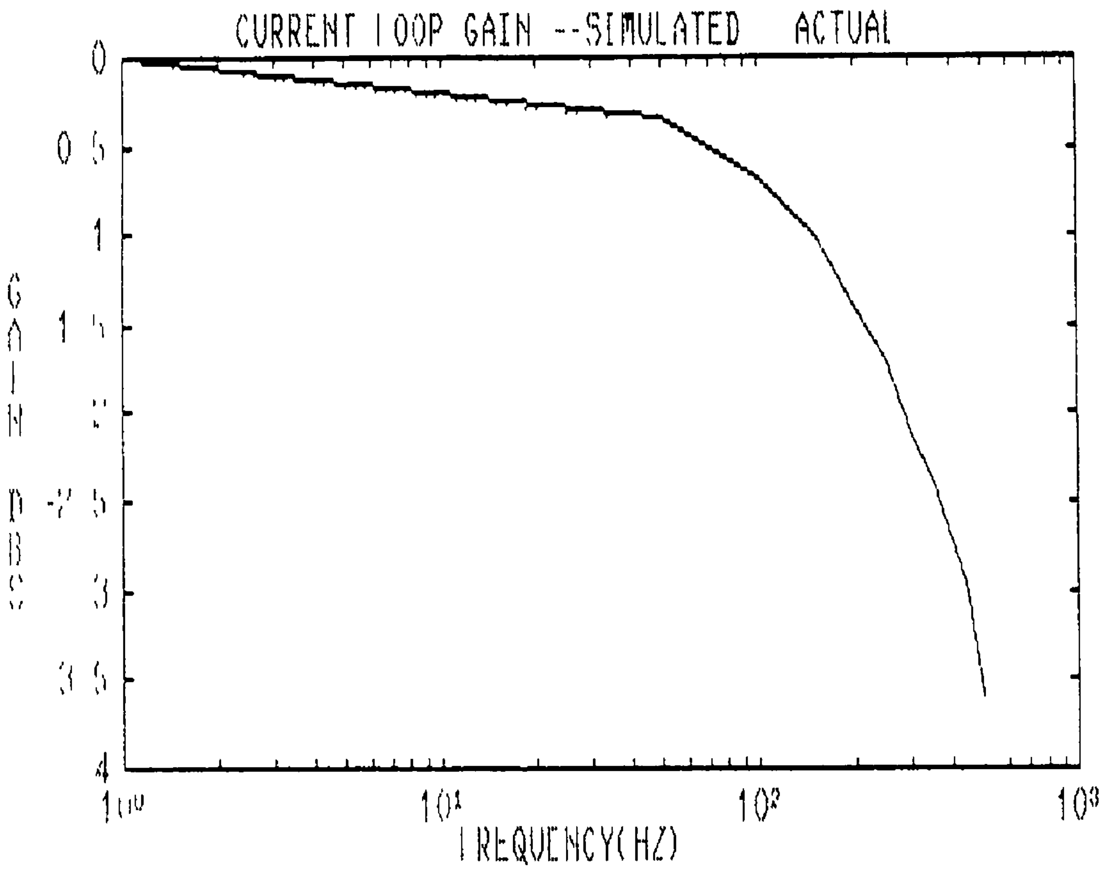

PLOT(6 3)

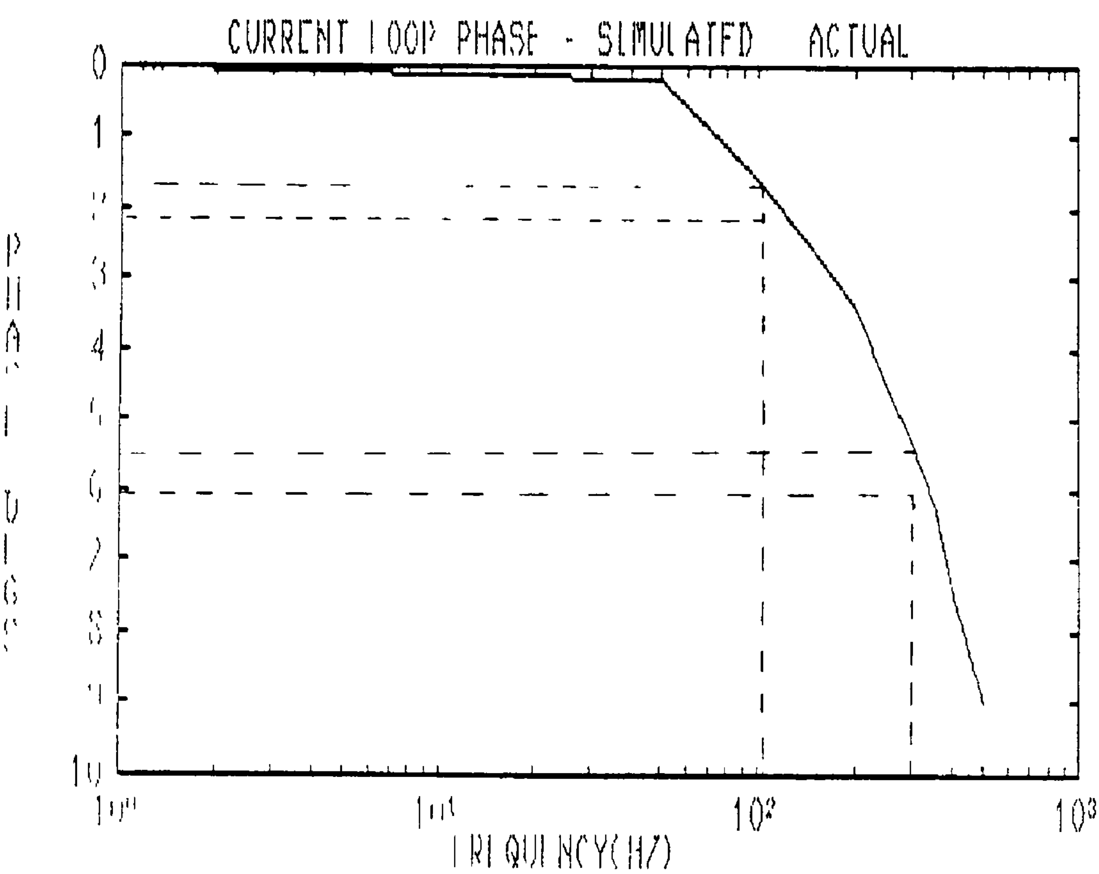

PLOT(6 4)

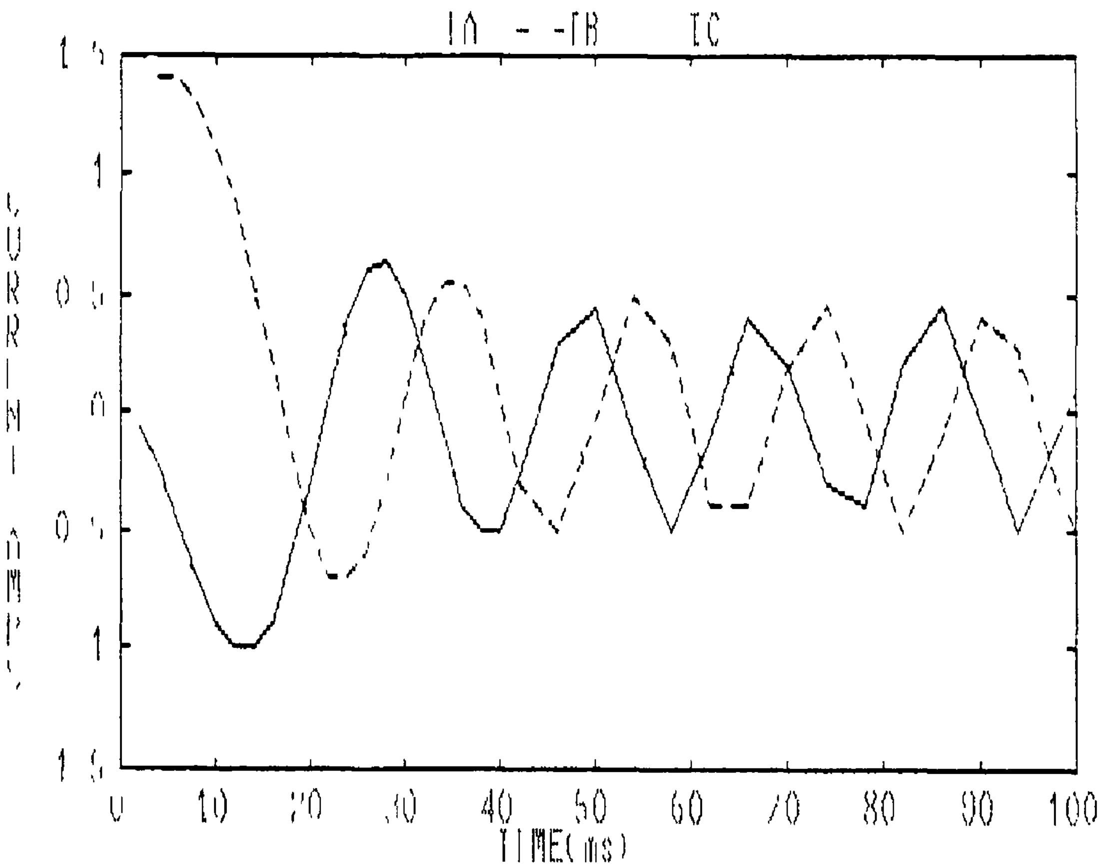

PLOT(6 5)

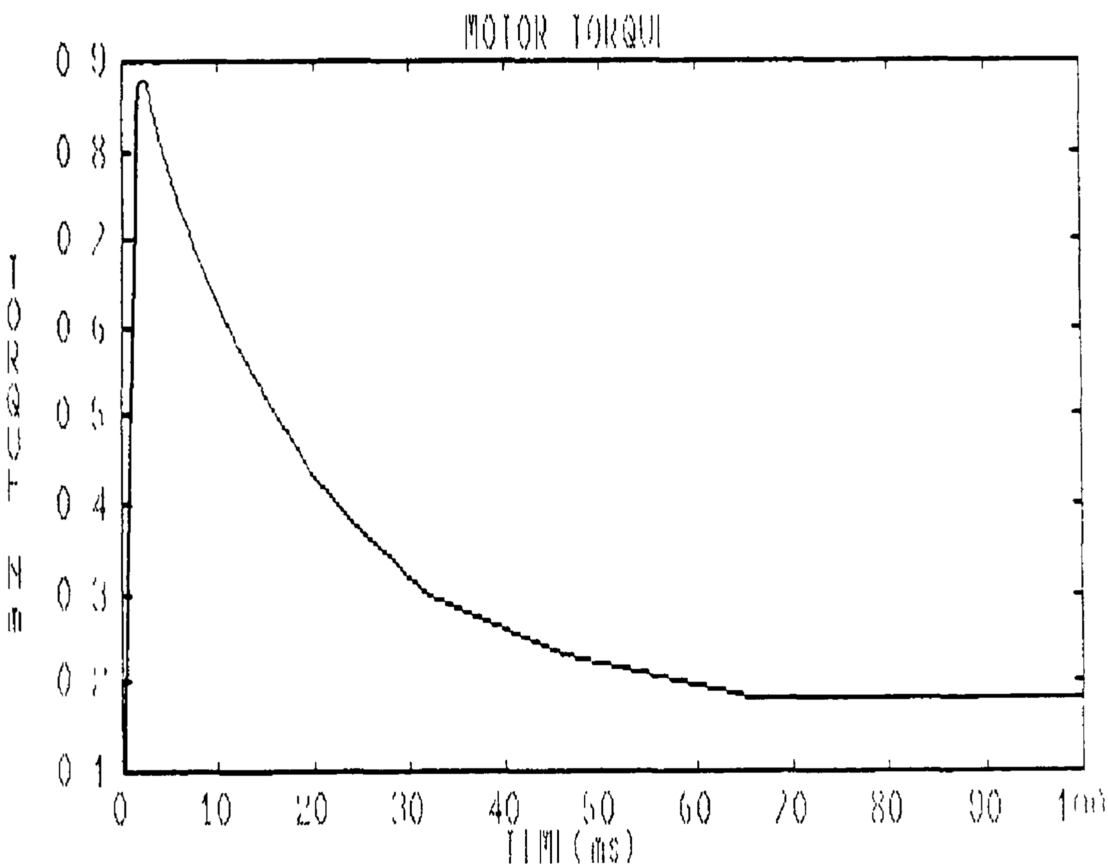

PLOT(6 6)

level. Plot (6.6) illustrates the torque response over the range. Plot (6.7), shows the direct and quadrature axis currents, I_d and I_q.

6.1.7 The same simulations were performed with compensator C_2 in place. Plots (6.8 ... 6.11) show velocity, 3 phase current, torque and direct and quadrature currents respectively. From plot (6.8) the velocity time constant is found to be 26.5 ms, and the torque angle is found to be 87^0.

6.1.8 Controller C_3 produces the plots (6.12 ... 6.15) of velocity, 3 phase current, torque and I_d, I_q. The velocity time constant is found, from plot (6.12), to be 7 ms. Plot (6.15) yields a steady state torque angle of 93^0.

6.1.9 The difference in velocity time constants between continuous C_1 and C_2 is not much being only 6%. The time constant of the response with compensator C_3 implemented is however substantially smaller than the time constants of C_1 and C_2, being only 28% of either. Also, the phase angle at 660 RPM with C_3 implemented is positive, due to the negative value of I_d, indicating that the actual current leads the demand. There will be a certain amount of error in the simulation by virtue of the fact that it is a discrete time system representing a continuous time system. So the positive nature of the phase angle could be due to the level of error. But the extra torque produced in the simulation, by the incorrect sign of I_d may have affected the velocity time constant by an unacceptable amount.

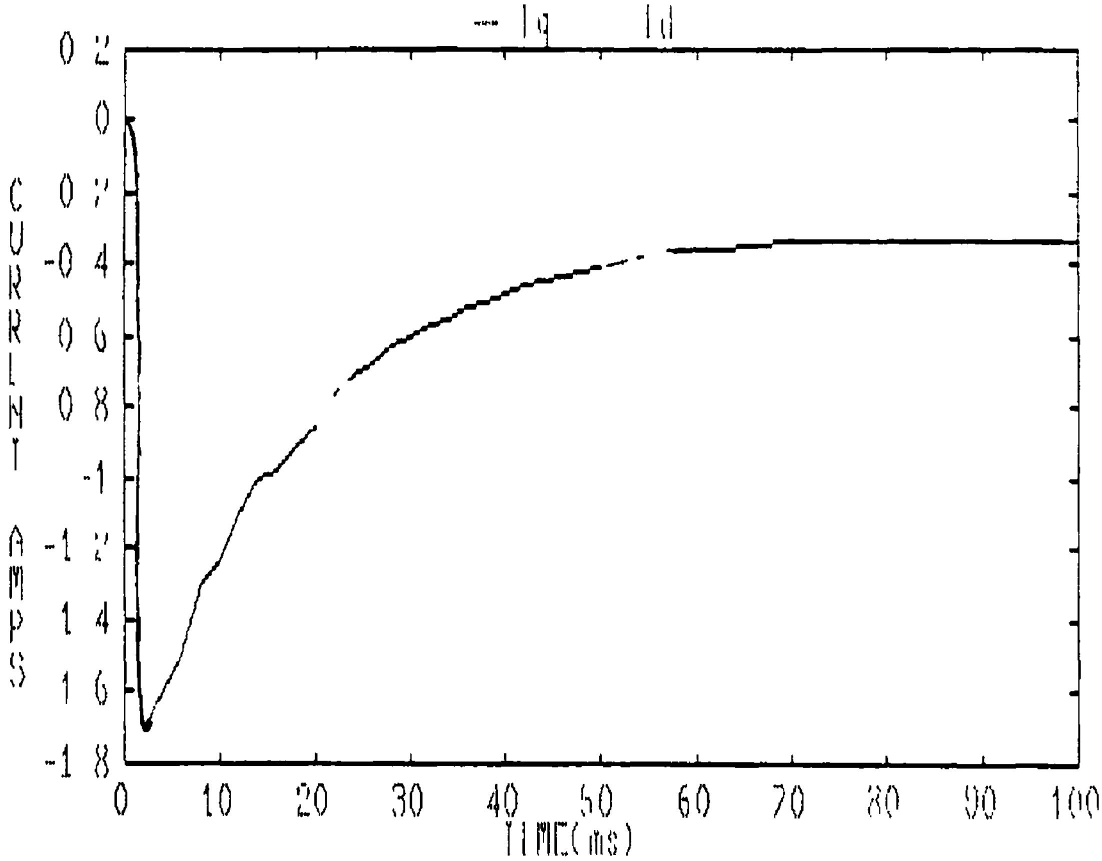

PLOT(6 7)

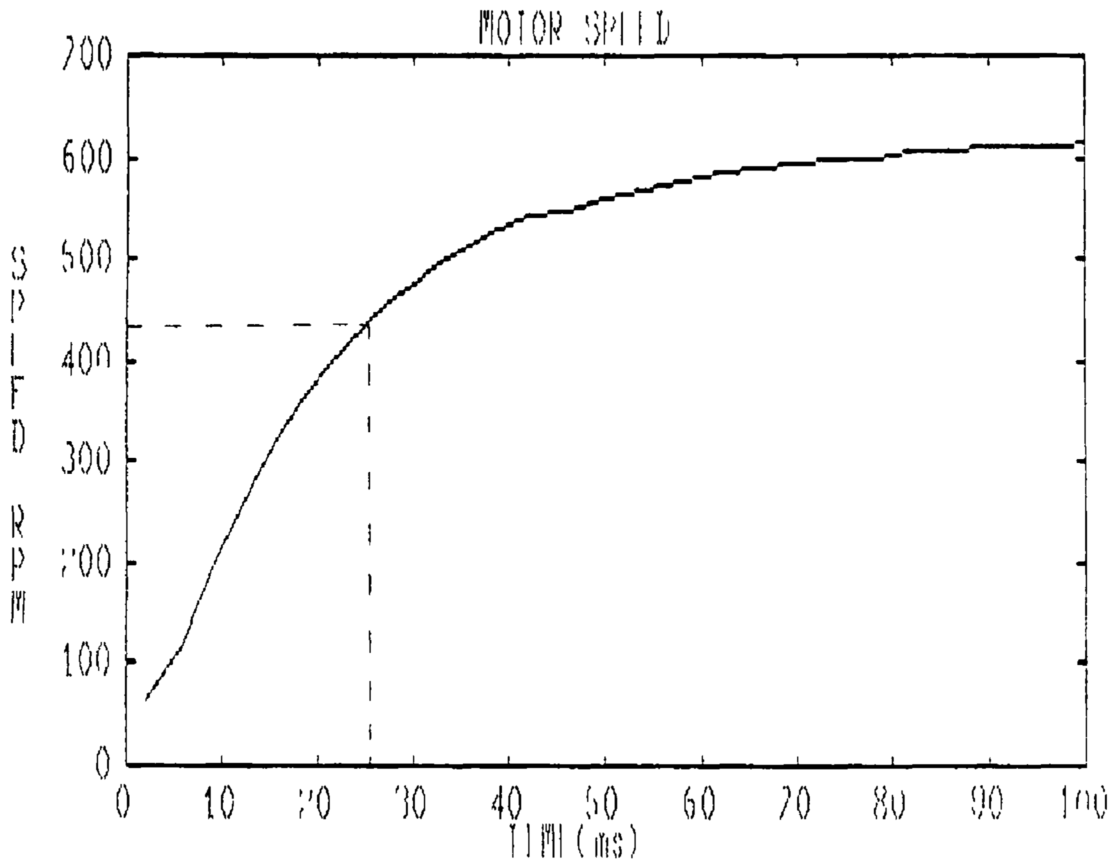

PLOT(6 8)

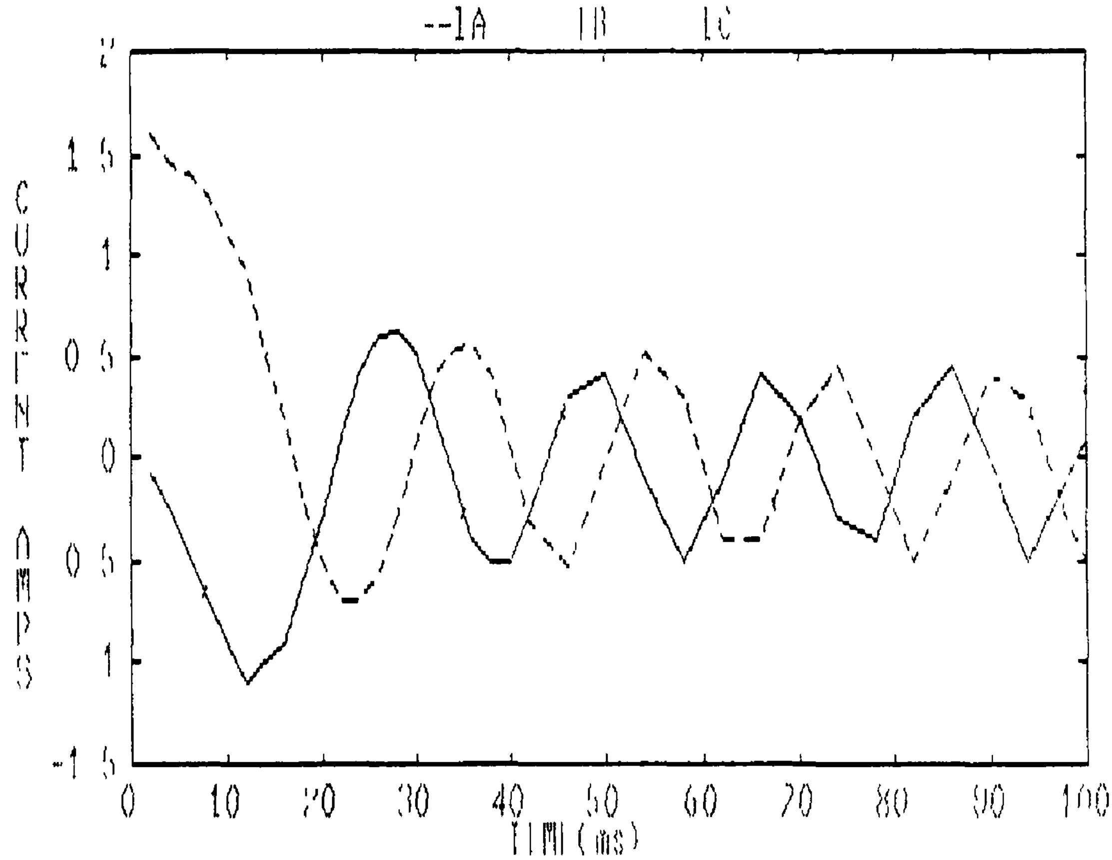

PLOT(6 9)

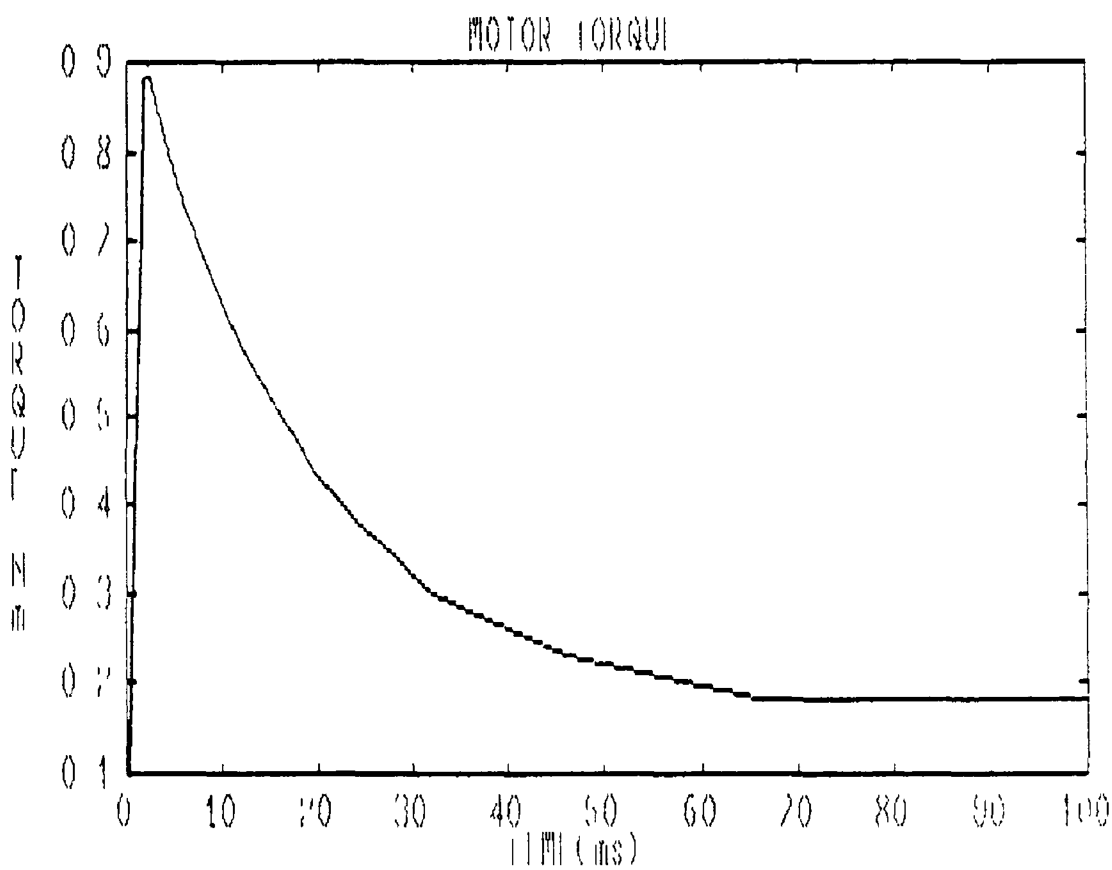

PLOT(6 10)

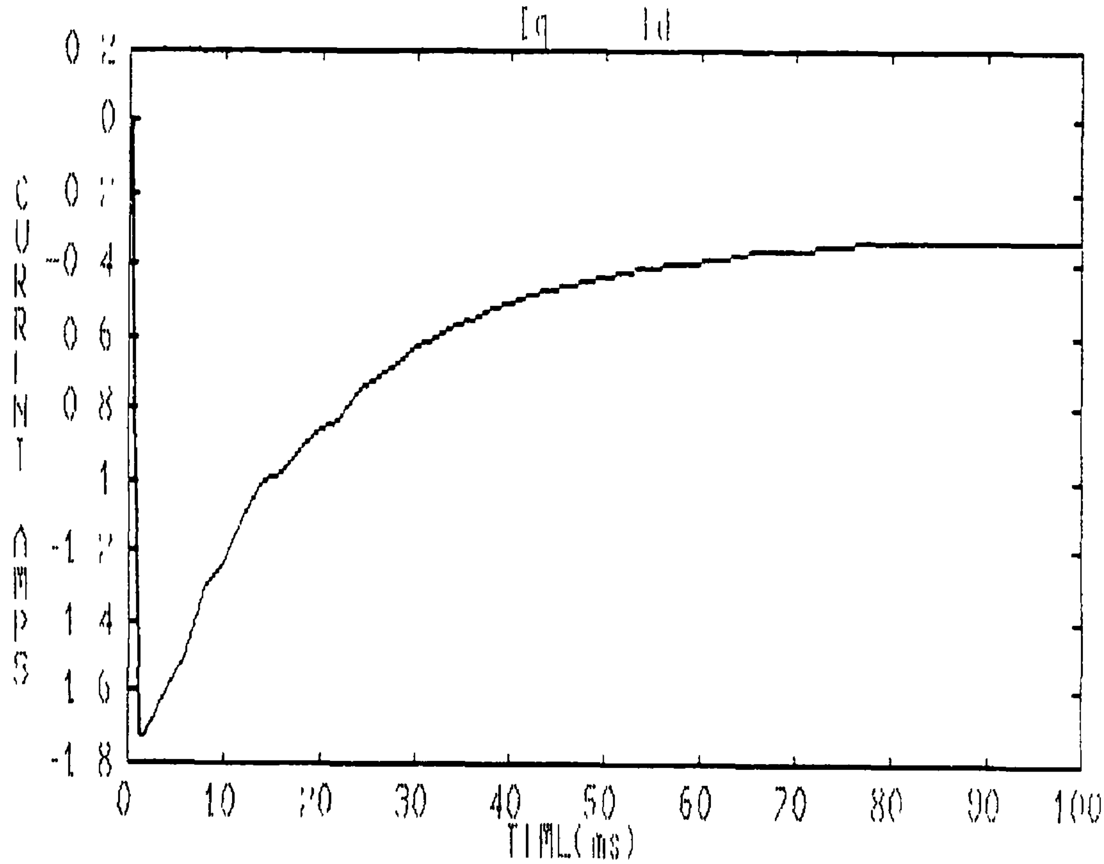

PLOT(6 11)

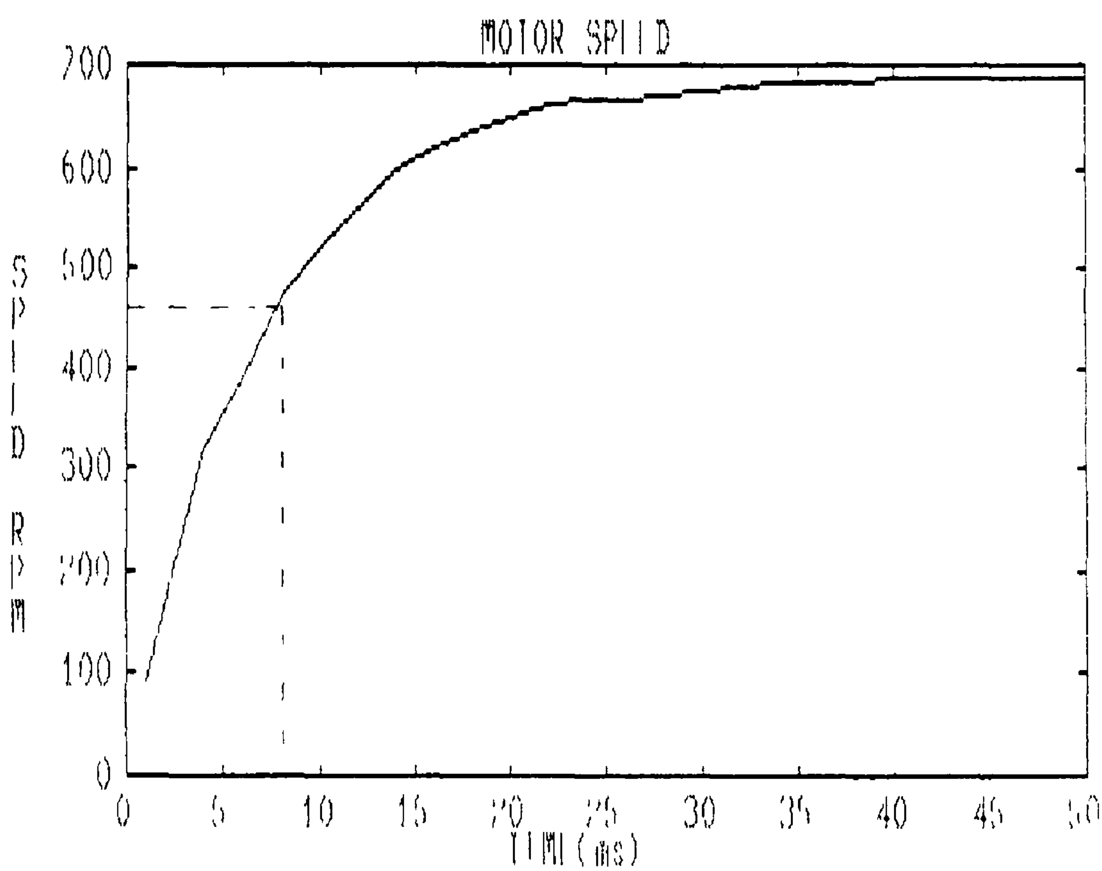

PLOT(6 12)

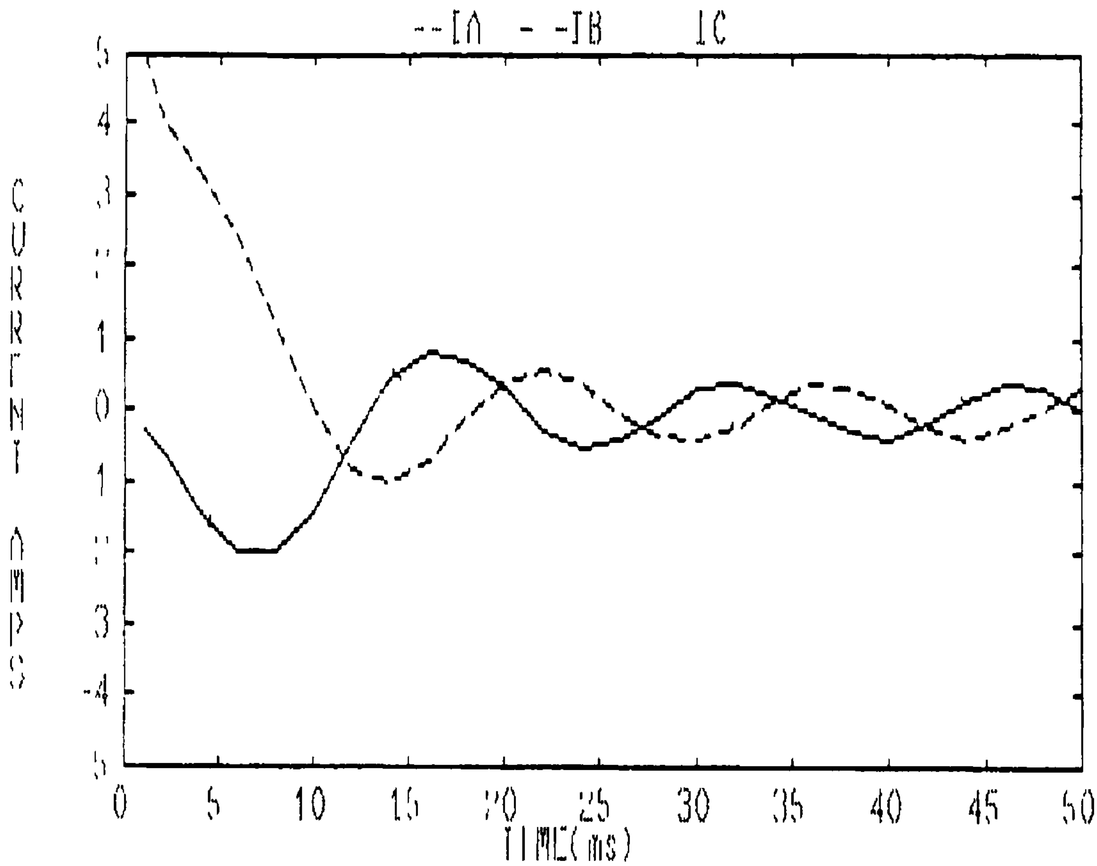

PLOT(6 13)

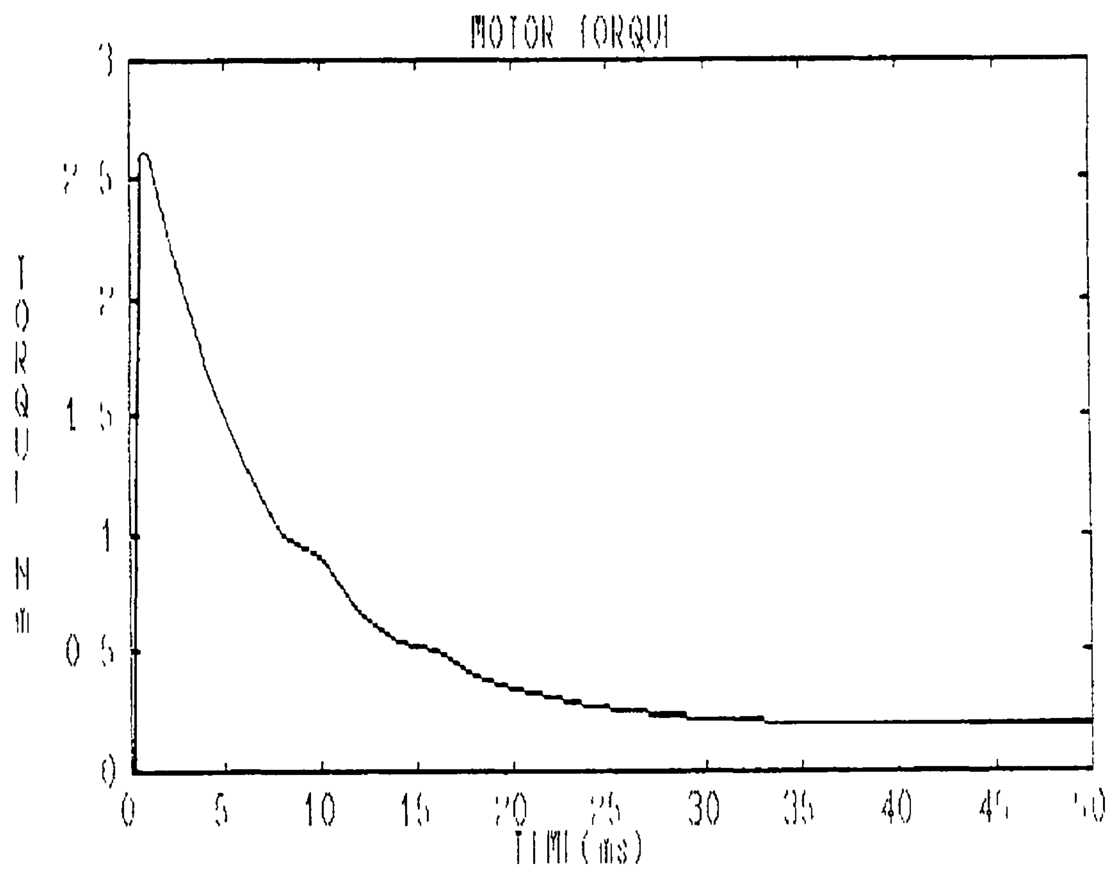

PLOT(6 14)

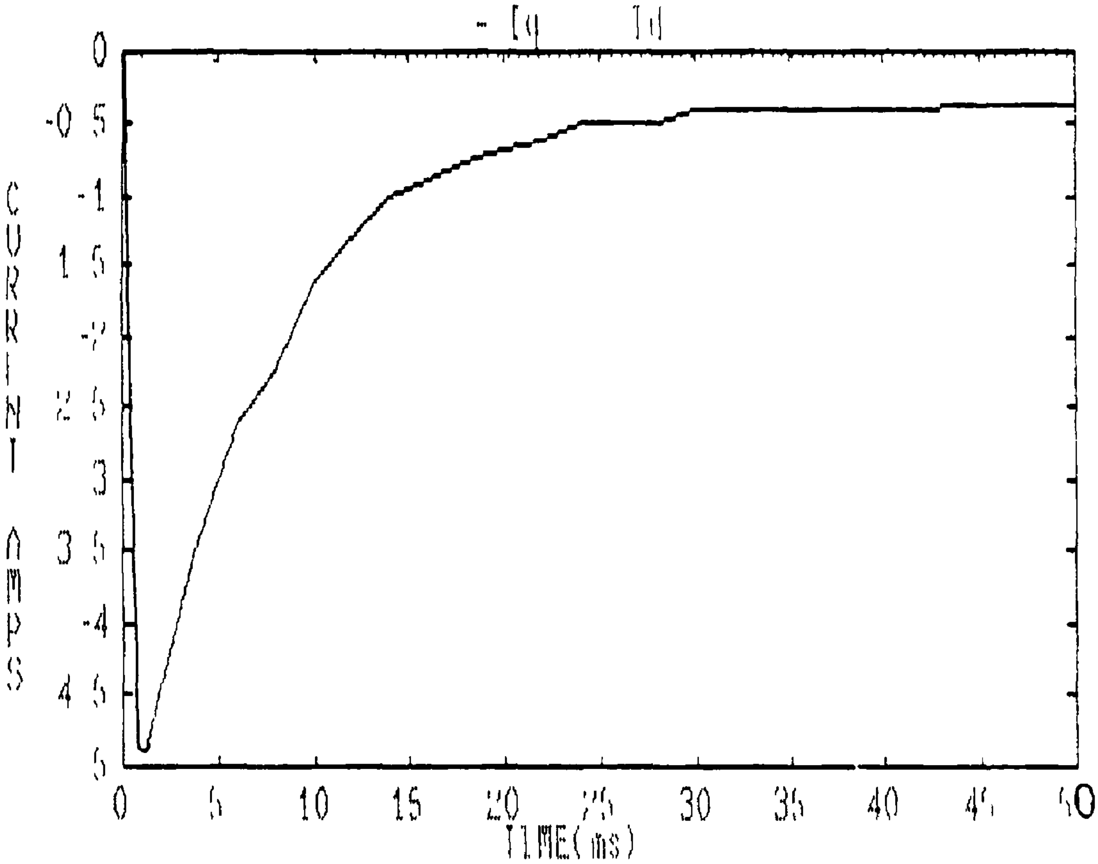

PLOT(6 15)

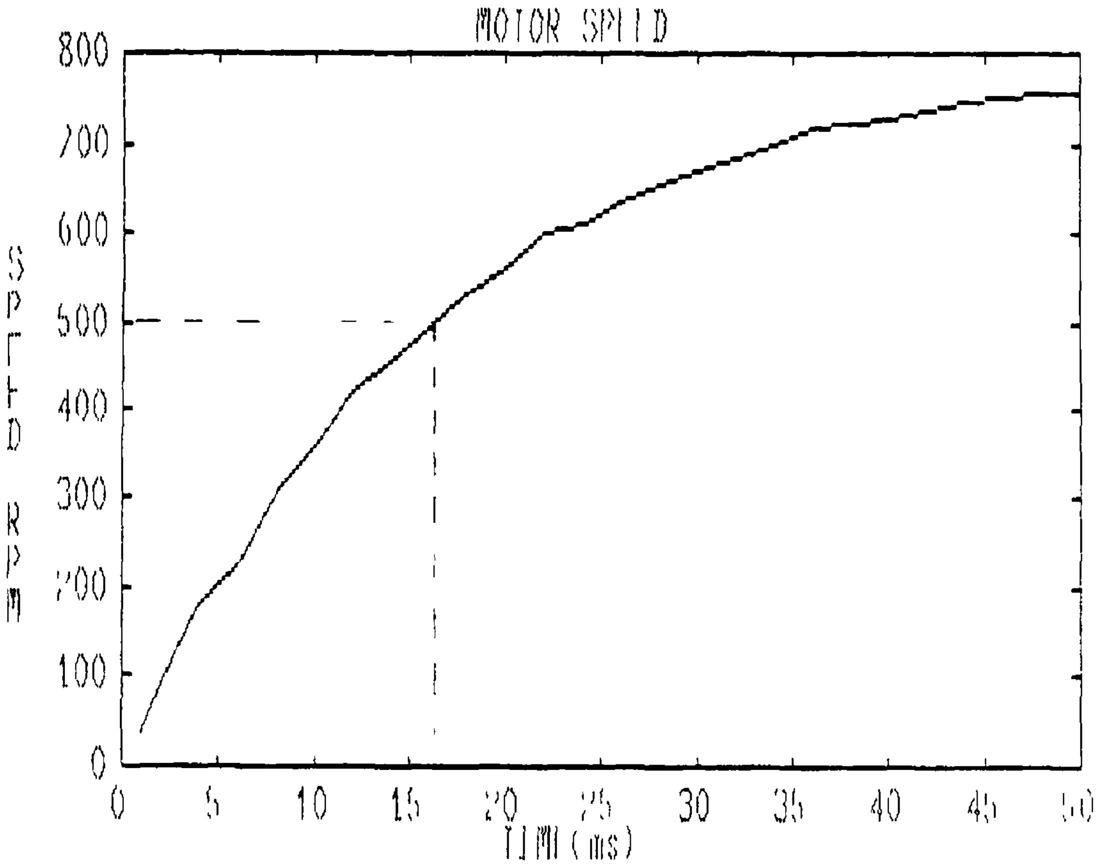

PLOT(6 16)

6.2 The Q Axis Representation

6.2.1 The mechanism for simulation of the Q axis system remains the same as that used for the 3 phase system, in that the backwards rectangular approximation to S is used. The reasons for choosing backwards rectangular over other forms of discretization are those outlined in section 6.1.3. The simulation equations are presented in appendix (5). Figure (6.1) shows the Q axis representation in block diagram form. The simulation assumes the D axis current is regulated about zero.

6.2.2 In plot (6.16) the motor speed response is shown to a step in speed of 0 - 1000 RPM. The simulation time was 0.1 mS. The controller implemented in the current loop was proportional in nature. The gain of the controller was not, as indicated in section 5.2.3, between 1.5 and 6. The reason for not choosing a value between 1.5 and 6 is because of the existence of the PWM amplifier. The analysis performed in section 5.2 assumed that k_p represented the total forward path gain, including the PWM amp. The amp itself has a gain in the linear region of 80, so to have a total forward path gain of 6 would mean a controller gain of 0.075. This is unrealistic in an actual system. The stability indicated by the locus plots of section 5.2 at high gain allows a realistic choice of controller gain. The value chosen for the simulation was unity, and a total forward path gain of 80. The time constant of the motor velocity response is 16 mS. Plot (6.17) illustrates the response of the Q axis current with time. The level of steady state error is quite large as evidenced by plot (6 18), settling at 0 53.

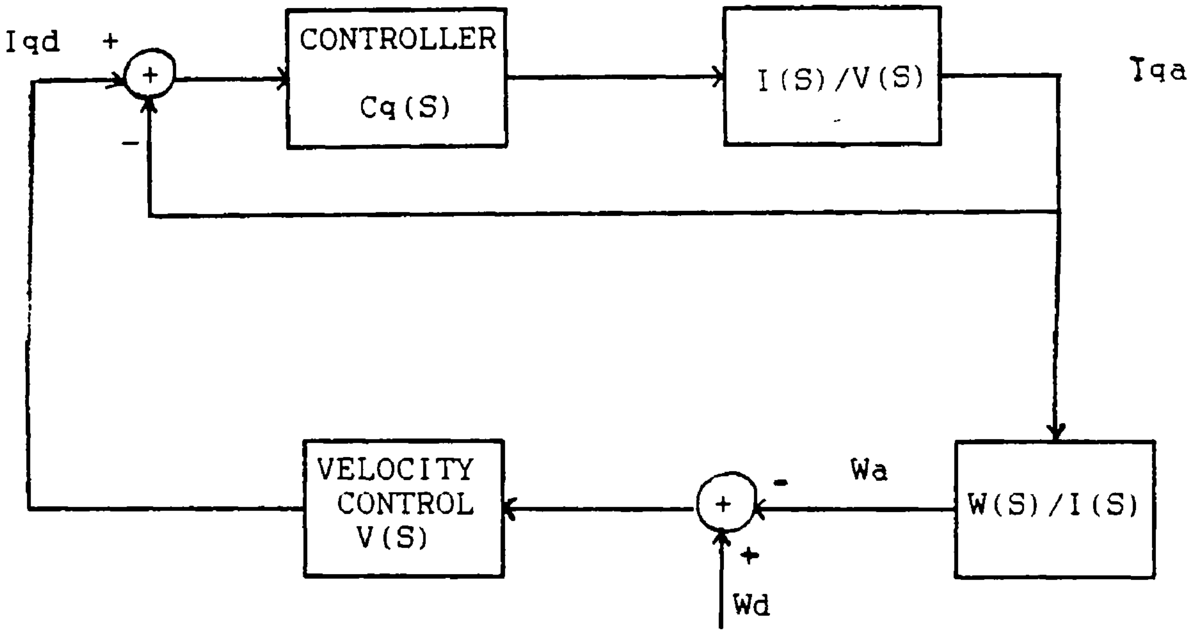

FIGURE(6 1)
BLOCK DIAGRAM OF Q AXIS CONTROLLER SIMULATION

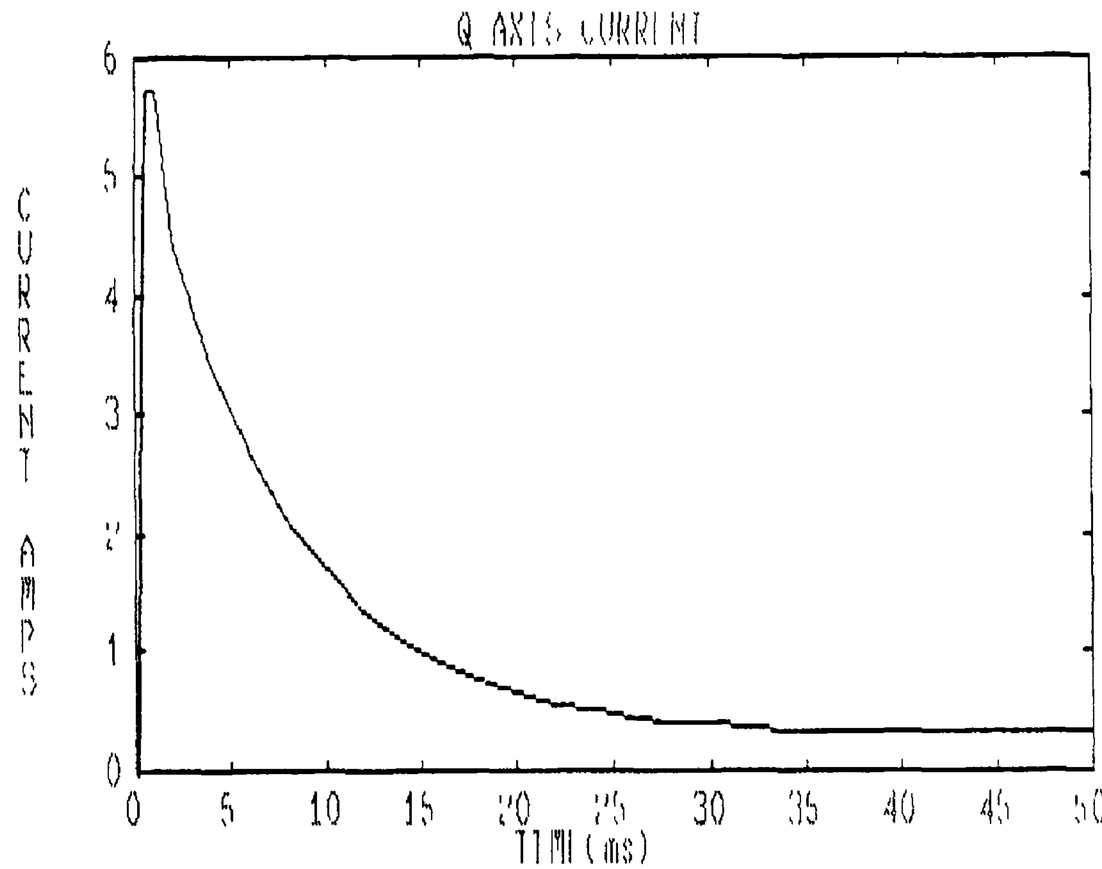

PLOT(6 17)

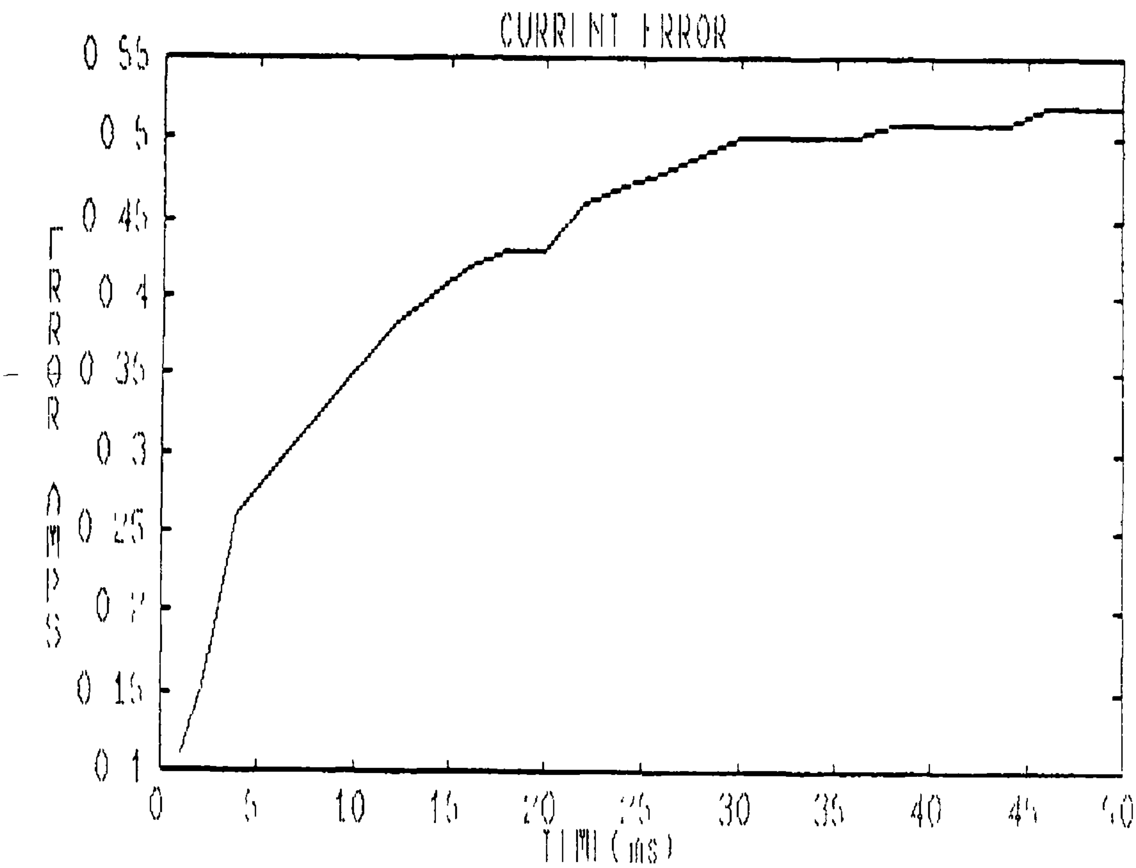

PLOT(6 18)

6.2.3 When the P+I controller designed in section 5.2 is implemented in simulation, plots (6.19 ... 6.21) result. The controller gain was 1 and the integral time was 30 mS. The step in velocity was 0 - 1000 RPM and the sampling time was 0.1 mS. The response is certainly more sluggish, as was suggested in section 5.2, the velocity time constant being 25 mS. Plot (6.20) illustrates the response of the motor current with time. Plot (6.21) indicates that the steady state error of the current controller is approaching zero with time. However even after 100 mS it still has not settled at zero.

6.2.4 To eliminate the sluggishness evidenced in the response plots of the previous section, a pole/zero compensation method was proposed (in section 5.2). But when implemented, with α = 500 β = 209, and a gain of 1, the simulation exhibited stability problems, at a sampling time of 0.1 mS. Even when the sampling time was reduced, the stability problems still existed. Pole/zero compensation requires almost perfect cancellation of the pole or zero, to work effectively. This is possible mathematically and the root locus plots of section 5.2 assume perfect cancellation. But when a continuous time compensator is discretised its nature changes. This would seem to be the basis for the instability of the simulation. A proper pole/zero compensator for a digital application should cancel the appropriate discrete pole or zero This should be the basis for design.

6.2.5 The response plots of the Q axis controller with both P and P+I compensation implemented indicate that Q axis control does provide velocity response on a par with 3 phase control, in the case of a P+I

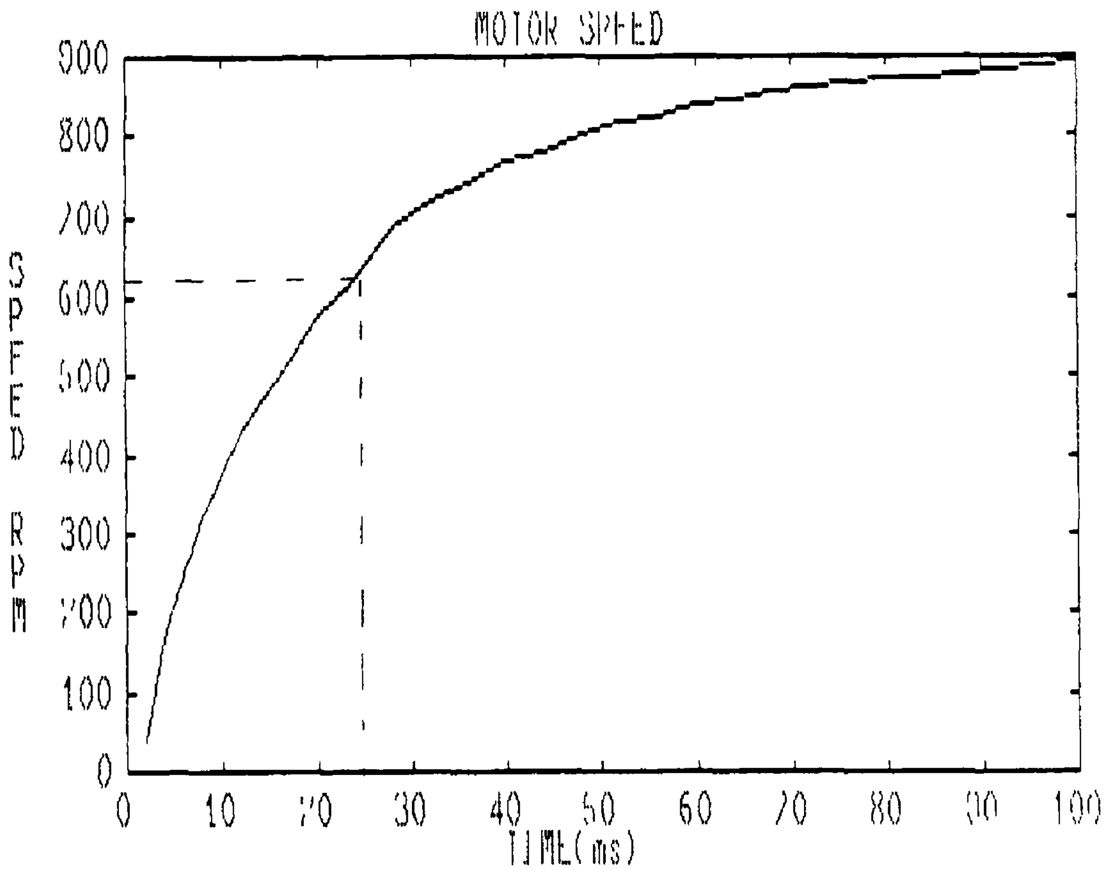

PLOT(6 19)

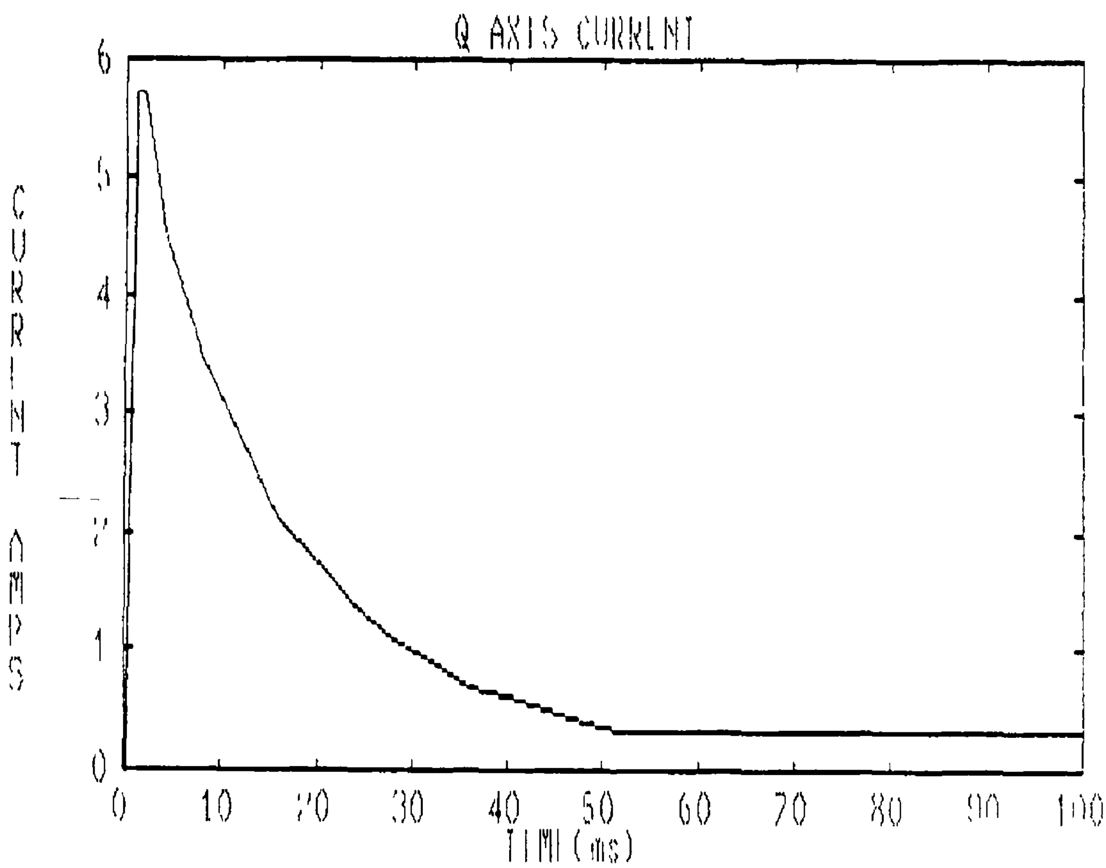

PLOT(6 20)

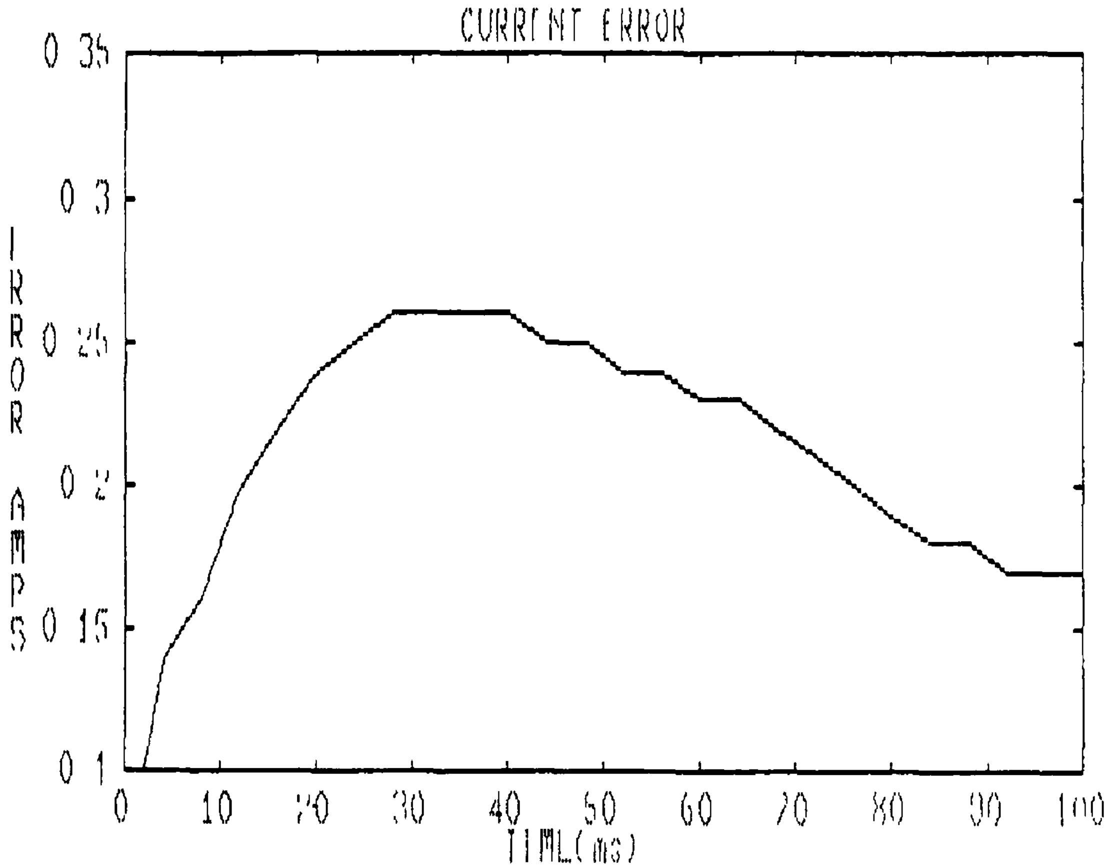
CURRENT ERROR
0 35
0 3
0 25
0 2
0 15
0 1
ERROR AMPS
0
10
20
30
40
50
60
70
80
90
100
TIME(ms)

PLOT(6 21)

implementation, and better than 3 phase control in the case of P control. If the initial criterion of control is considered, this being a maintenance of the phase lag in the current loop at greater than -15^0, then Q axis control is superior. This is because, with the D axis current regulated about zero, the overall phase lag in the current loop is 0^0. But Q axis control assumes the D axis current is zero, so for it to work efficiently this must be the case.

7. Hardware design and controller realisation

In the preceding chapters 3 phase and DQ motor theory have been developed in parallel. Both structures have been modelled, simulated and suitable control schemes have been proposed for each. This chapter includes a proposed implementation of only one control system, this being the 3 phase scheme.

7.1 Microprocessor Selection

7.1.1 The selection of the microprocessor is an important part of system design given that the microprocessor is the heart of the system. It was decided to concentrate on 16 bit processors as it was envisaged that sufficient processing power for the particular application could be supplied by them. The wide availability of development systems for 16 bit processors and the comparatively low cost of 16 bit processors in relation to 32 bit systems were also of primary consideration in this decision. It was further decided to opt for a minimum system configuration, in other words to use the processing power of the processor alone, and not to include floating point accelerators and other associated peripherals.

7.1.2 The two leading 16 bit processors were thus chosen for evaluation, those being the Motorola M68000, and the intel 80186. Both run at a clock speed of 8 MHz and both have 16 bit external data buses (The 68000 differs from the 80186 in that its internal data bus is 32 bits wide).

7 1.3 Figure (7.1) illustrates, in flow diagram form, the processing requirements in one sample period. The motor is a 3 phase system, so 3 separate currents loops

TAKE IN A AND B PHASE ERROR VALUES

ea(k) AND eb(k)

DETERMINE C PHASE ERROR VALUE

$ec(k)=-(ea(k)+eb(k))$

UPDATE CONTROLLER OUTPUT VALUES

$ca(k)=\alpha ca(k-1)+\beta ea(k)+\mu ea(k-1)$

$cb(k)=\alpha cb(k-1)+\beta eb(k)+\mu eb(k-1)$

$cc(k)=\alpha cc(k-1)+\beta ec(k)+\mu ec(k-1)$

UPDATE ALL VARIABLES

$ca(k-1)=ca(k)$

$ea(k-1)=ea(k)$

$cb(k-1)=cb(k)$

$eb(k-1)=eb(k)$

$cc(k-1)=cc(k)$

$ec(k-1)=ec(k)$

OUTPUT ALL CONTROLLER VALUES

FIGURE(7 1)

FLOWCHART SHOWING SEQUENCE OF CONTROLLER INSTRUCTIONS need to be controlled. The controller structure was taken to be a first order approximation to a lag compensator. The basis for comparison rested on which processor could execute the instructions in the quickest time. The instructions of figure (7.1) were written in the assembly language of each processor, and using the execution time tables of each processor the sample period for each was obtained. [B17,B18]

M68000 - 0.45 mS
80186 - 0.4 mS

7.1.4 Although the 80186 proved to be the faster processor in executing the instructions of one sample period, this is not basis enough for its selection. Other factors have to be considered. The M68000 comes in a dil package which is 8 cm long and 2.2 cm wide. The surface area of the 80186, which comes in a pin grid array package is much smaller, its dimensions being 2.9 cm long by 2.9 cm wide. Also the 80186 contains on board peripheral devices, such as a direct memory access controller, an interrupt controller and a waveform generation unit, while to provide the same facilities on an M68000 system, peripheral devices would have to be externally interfaced to the system. This is cost prohibitive, and also takes up printed circuit board area.

7.1.5 All arguments tend to indicate that the 80186 is the most suitable processor for the application. The most important factor in terms of performance would have to be the size of sample time. However the factors of cost and board area also deserve full consideration. These factors are industrial in nature, in that they are usually considered in volume production. However to make a system design worthwhile it has not only to be technically feasible, but also cost effective in an industrial sense. This is why cost and printed circuit board area were considered in the processor choice. In the light of these considerations the 80186 was chosen for the implementation.

7.2 Approaches to PWM Generation

7.2.1 The theoretical PWM spectrum evaluated and presented in Chapter 3 constitutes the ideal situation, one that is impossible to emulate in practice. Firstly the modulating wave is assumed to have a perfectly sinusoidal structure, and the carrier wave is assumed to be perfectly triangular. This is never the case. Secondly the two signals are assumed to be synchronised. The practical PWM generator of figure (3.6) involves no synchronisation, so the carrier and modulating waves drift in time. This causes subharmonics to be generated, which can cause problems at low speeds. It is therefore desirable to use a PWM generator scheme that minimises or eliminates both problems and generates a PWM signal that most closely resembles the theoretical.

7.2.2 There are two major methods of generating a PWM signal, these being analog or a microprocessor based digital method. The analog method uses an analog carrier and modulator and tends to exhibit the problem of drift, due to lack of synchronisation. The digital method simply involves the evaluation of the signal by computer, whatever the actual computation method. It tends to exhibit the problem of imperfect wave structure, due to the digital nature of the signals.

But as PWM is a digital signal it would seem to lend itself to a digital generation method.

7.2.3 Two different methods of digital generation will be considered here. These are

1. numerical comparison
2. Look of table

These methods will be explained and compared to each other in the following paragraphs.

7.2.4 The numerical comparison method of PWM generation is perhaps the simplest to implement. Its concept comes directly from the explanation given in section 3.2.2 as to how a PWM signal is generated from a modulating wave and carrier in that if the value of the modulating wave register exceeds the value of the carrier register then PWM is high. PWM is low if the reverse occurs. The carrier signal is obtained by allowing a register to ramp up to a maximum and then ramp down to a minimum, at the carrier frequency. Figure (7.2) illustrates the digital carrier assuming n discrete values. The size of increment, inc and the periodic time, T, are related, due to the finite computation time of microprocessors. If β is the computation time required by a microprocessor to increment the carrier register by one step then:

$$inc = \frac{\beta(max-min)}{T} \quad \ldots\ldots \quad \ldots\ldots\ldots \quad (7.1)$$

where max is the maximum magnitude of the carrier, min is the minimum magnitude, and T is the carrier period.

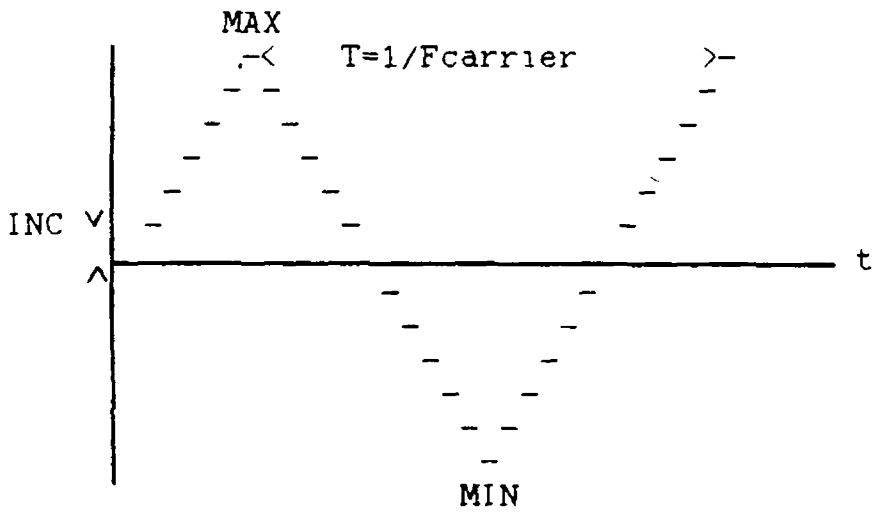

FIGURE(7 2)
A DISCRETISED CARRIER WAVE

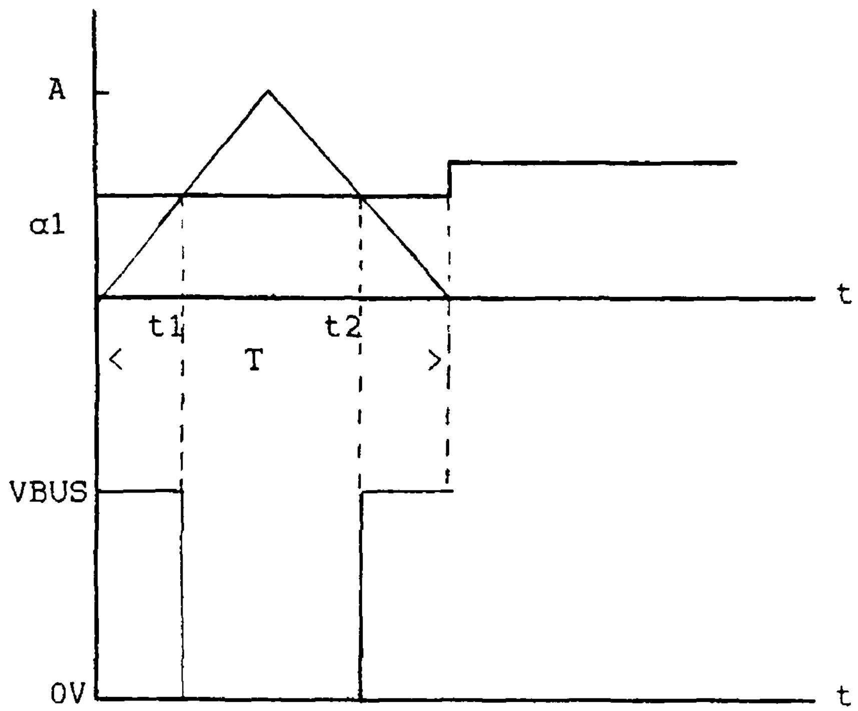

FIGURE(7 3)
PWM GENERATION USING THE LOOK UP TABLE METHOD

For set values of max, min and β the higher the carrier frequency desired the lower the resolution obtainable. Lowering the values of max and min will not provide a solution due to the limited resolution obtainable from microprocessor registers themselves.

7.2.5 The problem is compounded when the relationship between the carrier and the modulating signal is considered. In the process of PWM the modulator intersects the carrier twice every carrier period. Consider the mechanism of numerical comparison PWM. The modulating signal is updated once every Ts seconds where Ts is the sampling rate of the microprocessor system. At this instant it is compared to the value of the carrier register and the PWM signal is switched high or low as appropriate and remains at this level for Ts seconds. If the condition of

$$Ts > T/2$$

is fulfilled then the resulting PWM will not have the desired 2 intersection points per cycle. If for example the condition

$$T_s = T$$

were fulfilled then the PWM signal would switch only half the number of times required. Thus it can be concluded that numerical comparison PWM has the prerequisite that the condition of

$$T_s \leq 2T$$

is met before proper implementation can take place. Based on the sampling time obtained in section 7.1.3, the maximum carrier frequency obtainable is 1.25 kHz, which is much lower than the 5 kHz currently implemented in the analog test controller. It is desirable to have as high a carrier frequency as technically possible (this is constrained by the switching times of the VSI power transistors) in order to reduce the effects of the harmonics located at the carrier frequency and multiples thereof. This being the case, the 1.25 kHz realisable with the sample and compare method of PWM generation would seem to be inadequate in comparison to the 5 kHz implemented in the analog test controller.

7.2.6 The 'Look up table' method of PWM generation uses a look up table to produce the PWM signal. The look up table is referenced, simply, by the value of the modulating signal at each sampling instant. Figure (7.3) illustrates an implementation of this method of generation. Consider the equation of the carrier wave over one period.

$$F_C(t) = \begin{cases} \frac{2At}{T} & 0 \le t < t_C \\ 2A - \frac{2At}{T} & t_C \le t < T \end{cases} \quad \ldots\ldots\ldots\ldots\ldots\ldots \quad (7.2)$$

If the sampling rate T_C is equal to T, and if the carrier and modulator are synchronised as indicated in the figure, then the switching points t_1 and t_2 can be related to α_1, the level of the modulating signal by:

$$t_1 = \frac{\alpha_1 T}{2A} \quad \ldots\ldots\ldots\ldots\ldots\ldots \quad (7.3)$$

$$t_2 = T(1-\alpha_1/2A) \quad \ldots\ldots\ldots\ldots\ldots\ldots \quad (7.4)$$

Since the carrier is periodic, the equations (7.3, 7.4) hold at every sample instant. A look up table can be constructed based on all possible values of α_1. The values t_1 and t_2 simply refer to time durations from the moment of modulating signal update. The look up table method is not constrained to one carrier period per sample interval. It is possible to have n carrier periods per sample. The look up table would then include the 2n switching points necessary.

7.2.7 The look up table method is better than numerical comparison in that the carrier frequency, 1/T, can be multiples of the sampling frequency, $1/T_S$. In effect, the achievable frequency based on the results of section 7.1.3 is at least double that of numerical comparison, being 2.5 kHz, and certainly a carrier frequency of 5 kHz and higher is achievable. So it would seem that the look up table of PWM generation is viable.

7.3 Hardware design

7.3.1 To make the hardware as flexible as possible a structure like that of figure (7.4) was chosen. The analog to digital converters or A/D's in the figure convert the current error signals for the A and B phases to a digital format. The current error for the C phase is not required. The reason for this is that in a balanced 3 phase system, which the test motor is, the C phase current error can be constructed from the A and B phase signals. The resolution of the A/D converters is 8 bit.

7.3.2 The structure of figure (7.4) is flexible in that the output signals are generated by digital to analog converters, in this case 8 bit, so the output signal can assume 256 discrete levels. Although for the look up table method of PWM generation the output stages only need to assume 2 discrete levels, the D/A structure allows the modulating wave in its analog form be output to an analog PWM generator as well. So this allows 2 possible alternatives of PWM generation.

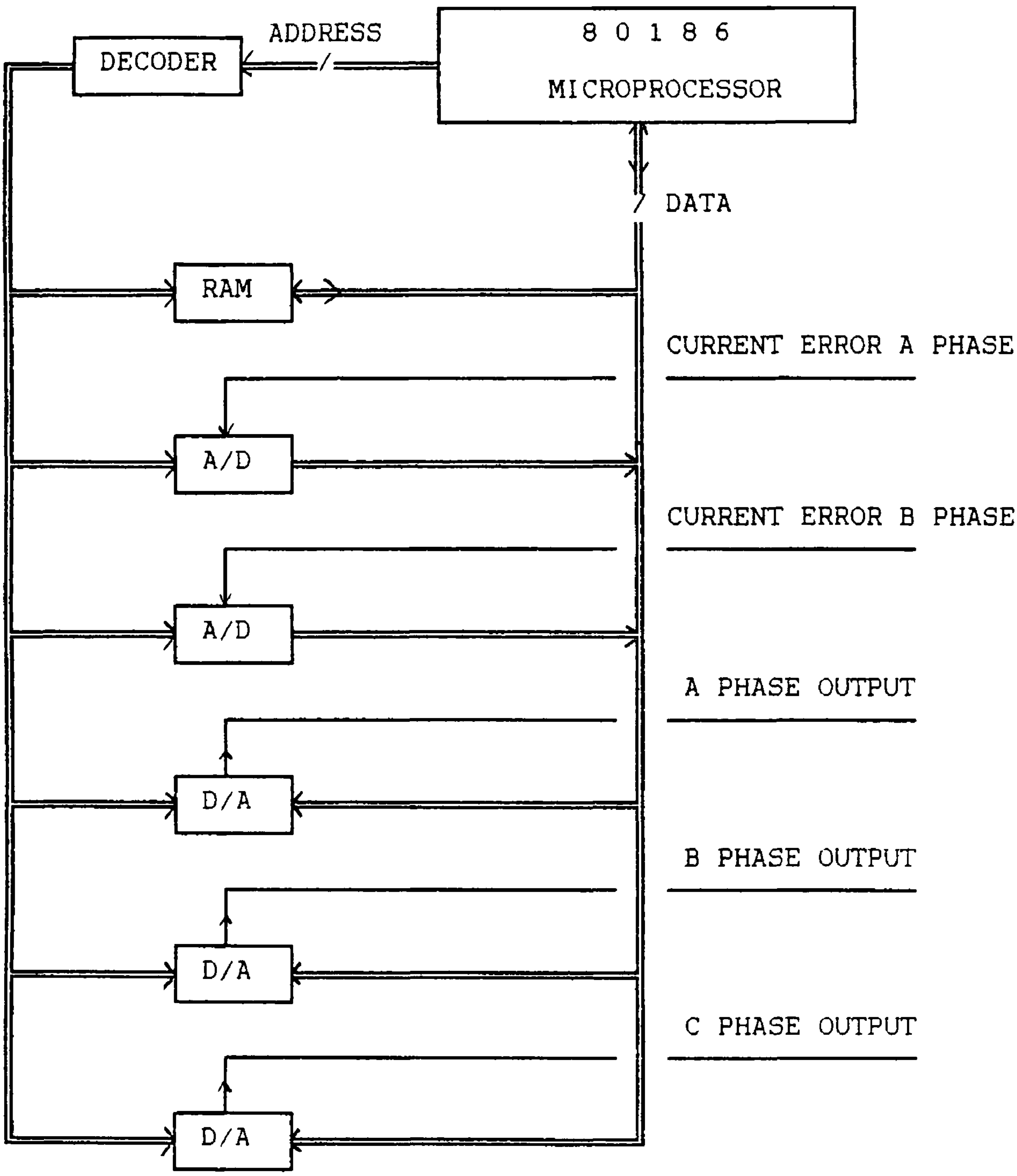

FIGURE(7 4)
DIGITAL COMPENSATOR SYSTEM STRUCTURE

7.4 Algorithm and software structure

7.4.1 The implemented software structure is that outlined in figure (7.1). The control algorithms are flexible in nature in that they represent first order discrete approximations to either lag, lead, P or P+I compensation schemes. The actual compensation scheme only depends on the values selected for coefficients α, β and μ. The actual order of approximation could be extended to second order, or even higher orders. The disadvantage is that at higher order approximations the discrete equations tend to have a large number of elements. This would require more computation time and hence would reduce the sampling time.

7.4.2 The most important part of the software is the method of number representation. The input to the system is an 8 bit sign and magnitude number, as is the output. However to adequately represent the compensator algorithms of figure (7.1) sign and magnitude form is not suitable. A more accurate number system is required. A floating point system can provide the desired accuracy, and in particular a system with one bit sign, eight bit mantissa and eight bit exponent is deemed adequate. This representation has a resolution of 0.004. The mechanism of conversion from 8 bit sign and magnitude to floating point format, and vice versa, is through the use of a look up table, which is quick and efficient. The only disadvantage of the 8 bit mantissa is that it does have limited resolution, and therefore quantisation error can occur. However an increase in resolution would necessitate an increase in processing time. This would reduce the sampling frequency. The question can be posed as to how much resolution is necessary? Since the output is only 8 bit it would be reasonable to assume that the 8 bit mantissa is adequate.

7.5 Further experiment

7.5.1 Both the hardware and software designed in this chapter are very flexible in structure. The hardware is flexible in that it allows different PWM generation methods be implemented. The software exhibits flexibility in that the compensator algorithms can be changed very easily to implement a wide range of compensation schemes. The assumption that the schemes designed in chapter 5 would work seems to be well founded in the light of the simulated results of chapter 6. The structure for designing other compensators has been fully developed, based on the frequency response method outlined in chapter 5. The structure for evaluation of the compensators also exists in the simulation developed in chapter 6. So implementation is the next logical step, and this forms the basis for further experiment.

8. Discussion and Conclusions

8.1 Discussion

8.1.1 The effect of harmonic distortion is fully quantified in chapter 3, by the harmonic distortion ratio. This ratio refers only to a steady state situation, when the motor is turning at constant speed, and the torque load is fixed. The frequency response plots of chapter 5, showing the closed current loop gain and phase characteristics seem to indicate that the harmonic distortion does not affect the steady state attributes by a considerable amount. In particular the phase and gain characteristics with the phase current assuming higher values (4A, 5A) are almost identical, with and without the distortion ratio included in the simulation. The problem with harmonic distortion arises when dynamic characteristics are considered. It is necessary in order to fully consider the effect, that harmonic distortion be fully quantified in mathematical terms, and not just by empirical means, although this has been useful in unearthing the issue. This would allow proper controller design to take place based on a fully quantified dynamic system.

8.1.2 The linearised motor model developed in chapter 4 allows linear systems theory be applied in the design of a Q axis control system. The model, however, assumes that the D axis current is regulated about zero. The basis for the design of a Q axis controller is well founded, assuming that Id is effectively regulated. There is however no equivalent linear method of design when it comes to producing a D axis regulator. Thus to effectively implement the control structure of figure (5.2) it may be the case that the D axis regulator would have to be tuned on a trial and error basis There is one criterion that the regulator would need to fulfil. This is that it must produce no steady state error. This would suggest a P+I compensator format.

8.1.3 The simulations implemented in chapter 6 do not include the effects of harmonic distortion, so as such there is a certain amount of error in the dynamic characteristics produced by them. This cannot be avoided without a fuller understanding of the distortion.

8.1.4 The hardware designed in chapter 7 has the processing capabilities to implement the DQ control structure of figure (5.2). The actual algorithms could be programmed, ie the 3 phase to DQ transformation, compensator algorithms, and DQ to 3 phase transformation, but the sampling time may not be of a level sufficient to provide adequate control over the entire motor speed range. However the hardware flexibility allows a solution to this problem. The 80186 can be implemented in a multiprocessing environment. This means that another processor working in conjunction with the 80186 (maybe another 80186) could perform the axes transformations, and using the DMA channel (direct memory access) could communicate the results of the transformation to the 80186, leaving it with only compensator algorithms to process.

8.2 Conclusions

8.2.1 There is a need to mathematically quantify the harmonic distortion effect and to assess its effect on the dynamic characteristics of the closed current loop. This would require analysis of both phase current and voltage at the instances when both transistors in the VSI inverter leg are turned off. The distortion effect should be less evident in faster switching transistors, as the hysteresis delay time, Δt, could be reduced. So with improved power transistor technology, resulting in faster switching times, the effect of harmonic distortion in VSI fed machines should be reduced.

8.2.2 The linear representation of the brushless dc machines requires that the D axis current be zero. This necessitates the design of an effective D axis regulator with zero steady state error. Since there is no equivalent linear basis for such a design (equivalent to the Q axis controller design), it would have to be designed using a nonlinear design method.

8.2.3 The simulations implemented in chapter 6 appear to yield satisfactory results. However, as they do not take harmonic distortion into consideration they do not truly represent the entire system. An improvement on the simulations would include the dynamic effects of the distortion.

8.2.4 Digital compensation would seem to be a viable alternative to analog compensation, in the current loop, in that it offers the same level of control performance. It proves superior, however, when flexibility and adaptability are considered, as it allows easy implementation of a wide range of compensation schemes, precise representation of compensation coefficients, and zero drift of these coefficients. In this light digital compensation would seem to be more desirable than analog compensation.

APPENDIX (1)

The six step approximation is an odd function so A_n is zero. W(x) is the six step function.

$$bn = \frac{1}{\pi}\int_0^{\pi} W(X)\ \mathrm{Sinnxdx}$$

$$= \frac{2V}{\pi}\left[\int_0^{\pi/3} \frac{1}{3}\ \mathrm{Sinnxdx} + \int_{\pi/3}^{2\pi/3} \frac{2}{3}\ \mathrm{Sinnxdx} + \int_{2\pi/3}^{\pi} \frac{1}{3}\ \mathrm{Sinnxdx}\right]$$

$$= \frac{2V}{\pi}\left[-\frac{1}{3n}\ \mathrm{Cosnx}\Big|_{o}^{\pi/3} - \frac{2}{3n}\ \mathrm{Cosnx}\Big|_{\pi/3}^{2\pi/3} - \frac{1}{3n}\ \mathrm{Cosnxdx}\Big|_{2\pi/3}^{\pi}\right]$$

$$= \frac{2V}{\pi}\left[-\frac{1}{3n}(\mathrm{Cosn}\pi/3-1) - \frac{2}{3n}(\mathrm{Cos}2\pi n/3 - \mathrm{Cos}\pi n/3) - \frac{1}{3n}(\mathrm{Cos}\ n\pi - \mathrm{Cos}\ 2\pi n/3)\right]$$

$$= \frac{2V}{\pi}\left[\frac{1}{3n}(1-\mathrm{Cosn}\pi/3) + \frac{2}{3n}(\mathrm{Cos}\pi n/3 - \mathrm{Cos}2\pi/3) + \frac{1}{3n}(\mathrm{Cos}2\pi n/3-\mathrm{Cosn}\pi)\right]$$

APPENDIX (2)

A consideration of the PWM wave of figure (3.5) allows an evaluation of the fourier coefficients. The voltage level of the wave swings from V_{BUS} to OV or from OV to V_{BUS}. To make an evaluation of the fourier coefficients easier it will be assumed that the two voltage levels are $V_{BUS}/2$ and $-V_{BUS}/2$. This in effect means that the DC level of the wave will be assumed to be zero. This can be considered as DC voltages of the same level applied to a 3 phase balanced system have no effect. It will also be assumed that there are k switching instances over one cycle, and one cycle corresponds to a cycle of the modulating wave. U_b corresponds to V_{BUS}, and α_i is the ith angle in radians.

$$a_n = \frac{1}{\pi}\int_{-\pi}^{\pi} PWM(x)Cos(nx)dx$$

$$= \frac{2}{2\pi}\left[\int_{o}^{\alpha 1} ubCosnxdx - \int_{\alpha 1}^{\alpha 2} ubCosnxdx\right.$$

$$\left. + \int_{\alpha 2}^{\alpha 3} ubCosnxdx + \ldots \pm \int_{\alpha k}^{2\pi} ubCosnxdx\right]$$

$$= \frac{u_b}{2k\pi}\left[Sinnx\Big|_{o}^{\alpha 1} - Sinnx\Big|_{\alpha 1}^{\alpha 2} + \ldots \pm Sinnx\Big|_{\alpha k}^{2\pi}\right]$$

$$= \frac{u_b}{2k\pi}\left[2\ Sinn\alpha 1 - 2\ Sinn\alpha 2 + \ldots \pm 2Sinn\alpha k\right]$$

$$\Longrightarrow a_n = \frac{U_b}{k\pi}\sum_{i=1}^{k}(-1)^{i-1}\ Sinn\alpha r \qquad \ldots\ldots \quad (A2.1)$$

b_n can be evaluated similarly

$$b_n = \frac{U_b}{\pi n} (1+(-1)^i + \sum_{i=1}^{k} (-1)^i \ \mathrm{Cos} n\alpha_i) \qquad \text{..... (A2.2)}$$

The magnitude of the n^{th} harmonic is therefore:

$$M_n = \sqrt{a_n^2+b_n^2} \qquad \text{...... (A2.3)}$$

and the phase angle is

$$\Phi_n = \mathrm{TAN}^{-1}\left[\frac{a_n}{b_n}\right] \qquad \text{... .. (A2.4)}$$

assuming line voltages to a 3 phase system of:

$$U_A = |V| \ \mathrm{Cos}(W_E t) \qquad \text{...... (A2.5)}$$

$$U_B = |V|.\ \mathrm{Cos}(W_E t-2\pi/3) \qquad \text{(A2.6)}$$

$$U_C = |V|.\ \mathrm{Cos}(W_E t-4\pi/3) \qquad \text{...... (A2.7)}$$

The resultant phase voltages for a 3 phase system are:

$$U_{AO} = 1/3 \quad (2U_A-U_B-U_C) \qquad \text{...... (A2.8)}$$

$$U_{BO} = 1/3 \quad (2U_B-U_C-U_A) \qquad \text{...... (A2.9)}$$

$$U_{CO} = 1/3 \quad (2U_C-U_B-U_A) \qquad \text{..... (A2.10)}$$

The first current harmonic per phase is generated as a result of the applied first voltage harmonic and the back emf.

If it is assumed that the phase of the back emf is 0 then the current per phase due to the back emf alone is

$$I_b = \frac{K_E W_m}{\sqrt{R^2+W_E{}^2L^2}} \quad \exp(-j\theta) \qquad \ldots\ldots (A2.11)$$

$$\text{where } \theta = TAN^{-1}\left[\frac{W_E L}{R}\right] \qquad (A2.12)$$

The current due to the first voltage harmonic is

$$I_h = \frac{|M_1|}{\sqrt{R^2+W_E{}^2L^2}} \quad \exp(j[\alpha-\theta]) \qquad \ldots\ldots (A2.13)$$

where α is defined as the angle between the first voltage harmonic and the back emf.

If the assumption is made that the current controller maintains the angle between the resultant current and back emf at 180^0 (this depends on the back emf convention used) then the sum of Ib and I_h should be real and negative.

$$Ib = |Ib| \ Cos(-\theta)+j|Ib| \ Sin(-\theta) \qquad \ldots\ldots (A2.14)$$

$$I_h = |I_h| \ Cos(\alpha-\theta)+j|I_h| \ Sin(\alpha-\theta) \qquad \ldots\ldots (A2.15)$$

$$Ib + I_h = |Ib| \ Cos(-\theta)+|Ih| \ Sin(\alpha-\theta) \\ +j[|Ih|Sin(\alpha-\theta)+|Ib|Sin(-\theta)] \ \ldots \ (A2.16)$$

$$\Longrightarrow \quad \frac{|Ih|}{|Ib|} \ Sin(\alpha-\theta) - Sin(\theta) = 0 \qquad (A2.17)$$

solve for α and substitute into (A2.16) to solve for Ib+Ih.

The kth current harmonic

$$I_k = \frac{|M_k|}{\sqrt{R^2+(kW_E)^2L^2}} \qquad (A2.18)$$

APPENDIX (3)

The controller described by:

$$C(S) = \frac{k(1+S\tau_1)}{(1+S\tau_2)} \qquad \text{........... (A3.1)}$$

has a phase function

$$P(f) = TAN^{-1}(2\pi f\tau_1) - TAN^{-1}(2\pi f\tau_2) \qquad \text{.... (A3.2)}$$

The function reaches a minimum at the point when the derivative is zero

$$\frac{dP(f)}{df} = \frac{\alpha}{\alpha^2+f^2} - \frac{\beta}{\beta^2+f^2} \qquad \text{.......... (A3.3)}$$

with $\frac{dp(f)}{df} = 0$

$$\Longrightarrow \quad \frac{\alpha}{\alpha^2+f^2} = \frac{\beta}{\beta^2+f^2} \qquad \text{...... (A3.4)}$$

where

$$\alpha = \frac{1}{2\pi\tau_1} \qquad \text{........... (A3.5)}$$

$$\beta = \frac{1}{2\pi\tau_2} \qquad \text{... ...... (A3.6)}$$

Solving for F yields

$$f_{min} = \sqrt{\alpha\beta} \qquad \text{..... .... (A3.7)}$$

If equation (A3.2) is equated with the desired minimum angle, R, then

$$R = TAN^{-1}(f/a) - TAN^{-1}(f/\beta) \quad .... \text{(A3.8)}$$

$$\Longrightarrow \quad TAN(R) = TAN(TAN^{-1}(f/\alpha) - TAN^{-1}(f/\beta)) .. \quad \text{(A3.9)}$$

$$\Longrightarrow \quad TAN(R) = \frac{f/\alpha - f/\beta}{1+f^2/\alpha\beta} \quad .\text{(A3.10)}$$

Choosing a minimum frequency and phase angle and solving between (A3.7) and (A3.10) yields values for α and β and hence for τ_1 and τ_2.

APPENDIX (4)

The equations listed in this appendix are derived from figures (3.7, 4.1), where figure (3.7) shows the 3 phase control structure, and figure (4.1) the DQ motor representation.

1. Velocity control

$$e_v(k) = W_d(k) - W_a(k) \qquad \text{..........} \quad \text{(A4.1)}$$

using P+I control

$$V(k)=V(k-1)+K_{pv}e_v(k)-K_{pv}(1-Ts/Tiv)ev(k-1) \qquad \text{..........} \quad \text{(A4.2)}$$

where T_{iv} is the compensator integral time.

2. Current control

Current error A phase

$$e_{IA}(k)=V(k)Sin(6\theta(k))-I_{Aa}(k)) \qquad \text{..........} \quad \text{(A4.3)}$$

Current error B phase

$$e_{IB}(k)=V(k)Sin(6\theta(k)-2\pi/3)-I_{Ba}(k)) \qquad \text{..........} \quad \text{(A4.4)}$$

Current error C phase

$$e_{IC}(k)=V(k)Sin(6\theta(k)-4\pi/3)-I_{ca}(k)) \qquad \text{.....} \quad \text{(A4.5)}$$

Current control for either A, B or C phases, using a lag compensator.

$$C(k)=\frac{T_{1p}}{(T_s+T_{1p})}C(k-1)+Kp_1\frac{(T_s+T_{1z})}{(T_s+T_{1p})}e_I(k)-\frac{(k_{p1}T_{1z})}{(T_s+T_{1p})}e_I(k-1) \qquad \text{(A4.6)}$$

Where T_s is the sample time, T_{1z} is the zero time, T_{1p} is the pole time, and k_{p1} is the compensator gain.

3. Pulse width modulation and line voltages

The linear amplifier approximation is made to the modulated wave. The loss ratio is not considered.

$$U_{AX}(k) = C_A(k)PWM \qquad \text{(A4.7)}$$

$$U_{BX}(k) = C_B(k)PWM \qquad \text{(A4.8)}$$

$$U_{CX}(k) = C_c(k)PWM \qquad \text{(A4.9)}$$

$PWM = 80$

4. Line to neutral voltages

$$U_{AO}(k) = 1/3\ (2U_{AX}(k) - U_{BX}(k) - U_{CX}(k)) \qquad \text{(A4.10)}$$

$$U_{BO}(k) = 1/3\ (2U_{BX}(k) - U_{AX}(k) - U_{CX}(k)) \qquad \text{(A4.11)}$$

$$U_{CO}(k) = 1/3\ (2U_{CX}(k) - U_{AX}(k) - U_{BX}(k)) \qquad \text{(A4.12)}$$

5. The DQ voltages

$$Ud(k) = 2/3\ [\cos(6\theta(k))U_{AO}(k)+\cos(6\theta(k)-2\pi/3)U_{BO}(k)+\cos(6\theta(k)-4\pi/3)U_{CO}(k)] \qquad \text{(A4.13)}$$

$$U_q(k) = 2/3\ [\sin(6\theta(k))U_{AO}(k)+\sin(6\theta(k)-2\pi/3)U_{BO}(k)+\sin(6\theta(k)-4\pi/3)U_{co}(k)] \qquad \text{(A4.14)}$$

APPENDIX 5

1. Velocity control

as equations (A4.1, A4.2)

2. Current Control

$$e_{Iq}(k) = I_{qd}(k) - I_{qa}(k) \qquad \text{....... (A5.1)}$$

P Control

$$C_{Iq}(k) = Kpe_{Iq}(k) \qquad \text{.......... (A5 2)}$$

P+I Control

$$C_{Iq}(k) = C_{Iq}(k-1)+kpe_{Iq}(k)-kp(1-T_s/To)e_{sq}(k-1) \qquad \text{.......... (A5.3)}$$

Pole/zero cancellation

From equation (5.31)

$$C_{Iq}(k)=AC_{Iq}(k-1)+BC_{Iq}(k-2)+Ce_{Iq}(k)+De_{Iq}(k-1)+Ee_{Iq}(k-2) \qquad \text{.......... (A5.4)}$$

where $A = \dfrac{2+9.3Ts}{1+9.3T_s}$ $B = \dfrac{-1}{1+9.3T_s}$ $C = \dfrac{kp(1+(\alpha+\beta)T_s)}{1+9.3T_s}$

$D = \dfrac{-kp(2+(\alpha+\beta)T_s}{1+9.3T_s}$ $E = \dfrac{kp}{1+9.3T_s}$

6. The DQ currents

$$I_d(k) = \frac{L_d}{(L_d+T_sR_d)} I_d(k-1) - \frac{6W_a(k)L_qT_sI_q(k)}{(L_d+T_sR_d)} + \frac{T_sU_d(k)}{(L_d+T_sR_d)} \quad \ldots\ldots\ldots\ldots \text{(A4.15)}$$

$$I_q(k) = \frac{L_q}{(L_q+T_sR_q)} I_q(k-1) - \frac{6W_a(k)L_dT_sI_d(k)}{(L_q+T_sR_q)} + \frac{T_sU_q(k)}{(L_q+T_sR_q)} + \frac{6Wa(k)T_s\lambda_m}{(L_q+T_sR_q)} \quad \ldots\ldots\ldots\ldots \text{(A4.16)}$$

7. The machine torque

$$T(k) = 3/2.p/2\ [-L_qI_q(k).I_d(k)+L_dI_d(k)\ I_q(k)+\lambda_mI_q(k)] \quad \ldots\ldots\ldots\ldots \text{(A4.17)}$$

8. The mechanical speed

$$W_a(k) = \frac{J}{(J+T_sD)} .W_a(k-1) + \frac{T_s}{(J+T_sD)} T(k) \quad \ldots\ldots\ldots\ldots \text{(A4.18)}$$

9. The rotor angle

$$\theta(k) = \theta(k-1) + T_sW_a(k) \quad \ldots\ldots\ldots\ldots \text{(A4.19)}$$

10. The 3 Phase Currents

$$I_{Aa}(k) = I_d(k)\mathrm{Cos}(6\theta(k)) + I_q(k)\ \mathrm{Sin}(6\theta(k)) \quad \ldots \text{(A4.20)}$$

$$I_{Ba}(k)=I_d(k)\mathrm{Cos}(6\theta(k)-2\pi/3)+I_q(k)\mathrm{Sin}(6\theta(k)-2\pi/3) \quad \ldots\ldots\ldots\ldots \text{(A4.21)}$$

$$I_{Ca}(k)=I_d(k)\mathrm{Cos}(6\theta(k)-4\pi/3)+I_q(k)\mathrm{Sin}(6\theta(k)-4\pi/3) \quad \ldots\ldots\ldots \text{(A4.22)}$$

3. Pulse width modulation and DQ voltages

$$U_q(k) = C_{Iq}(k)\ PWM \qquad \text{.........} \quad (A5.5)$$

4. The machine torque

   as equation (A4.17)

5. The mechanical speed

   as equation (A4.18)

Definition of symbols

$Wd(k)$	-	Demand velocity at sample k
$Wa(k)$	-	Actual velocity at sample k
$e_V(k)$	-	Velocity error at sample k
$e_V(k-1)$	-	Velocity error at sample k-1
$V(k)$	-	Velocity controller o/p at sample k
$V(k-1)$	-	Velocity controller o/p at sample k-1
$e_{IA}(k)$	-	Current error A Phase at sample k
$e_{IA}(k-1)$	-	Current error A Phase at sample k-1
$e_{IB}(k)$	-	Current error B Phase at sample k
$e_{IB}(k-1)$	-	Current error B Phase at sample k-1
$e_{IC}(k)$	-	Current error C Phase at sample k
$e_{IC}(k-1)$	-	Current error C Phase at sample k-1
$C_A(k)$	-	Current controller o/p A Phase at sample k
$C_A(k-1)$	-	Current controller o/p A Phase at sample k-1
$C_B(k)$	-	Current controller o/p B Phase at sample k
$C_B(k-1)$	-	Current controller o/p B Phase at sample k-1
$C_C(k)$	-	Current controller o/p C Phase at sample k
$C_C(k-1)$	-	Current controller o/p C Phase at sample k-1
PWM	-	Linear gain of PWM amplifier
$U_{AX}(k)$	-	Line voltage A Phase at sample k
$U_{BX}(k)$	-	Line voltage B Phase at sample k
$U_{CX}(k)$	-	Line voltage C Phase at sample k
$U_{AO}(k)$	-	Line to neutral voltage A Phase at sample k
$U_{BO}(k)$	-	Line to neutral voltage B Phase at sample k
$U_{CO}(k)$	-	Line to neutral voltage C Phase at sample k
$Ud(k)$	-	Direct axis voltage at sample k
$U_q(k)$	-	Quadrature axis voltage at sample k
$Id(k)$	-	Direct axis current at sample k
$Id(k-1)$	-	Direct axis current at sample k-1
$Iq(k)$	-	Quadrature axis current at sample k
$Iq(k-1)$	-	Quadrature axis current at sample k-1
$T(k)$	-	Machine torque at sample k
$\theta(k)$	-	Rotor angle at sample k

$\theta(k-1)$ - Rotor angle at sample k-1

$I_{Aa}(k)$ - A Phase Current at sample k

$I_{Ba}(k)$ - B Phase Current at sample k

$I_{Ca}(k)$ - C Phase Current at sample k

k_{pv} - Velocity controller proportional gain

T_{iv} - Velocity controller integral time

T_{ip} - Current controller pole time

T_{iz} - Current Controller zero time

k_{pi} - Current Controller proportional gain

T_s - sample time.

APPENDIX (6)

MOOG 304-8 MOTOR

LINE-LINE INDUCTANCE	-	4 mH
LINE-LINE RESISTANCE	-	1 8 Ω
BACK EMF CONSTANT	-	.3175 V/RAD/S
TORQUE CONSTANT	-	0.476 A/Nm
PHASE CURRENT CONTINUOUS	-	9 9A PEAK
PHASE CURRENT MAX	-	30A PEAK
RATED TORQUE CONTINUOUS	-	4.7 Nm
RATED SPEED	-	5000 RPM
BUS VOLTAGE	-	320V

REFERENCES

B1 'Electric Mahines'

GR. SLEMON, A STRAUGHEN
ADDISON-WESLEY

B2 'The general theory of Alternating Current Machines'

B Adkins, R G Harley
CHAPMAN AND HALL

B3 'Electrical machines and their Applications'

J HINDMARSH
PERGAMON

B4 'Control of Electrical Drives'

W LEONHARD
SPRINGER-VERLAG

B5 'DC Motors, Speed Controls, Servo Systems'

ELECTRO-CRAFT CORPORATION

B6 'Adjustable Speed AC Drive Systems'

Edited by B K Bose
IEEE PRESS

B7 'Alternating Current Machines'

M G Say
PITMAN 1983

B8 'Advanced engineering mathematics'

C R Wylie, L C Barratt
McGRAW HILL 1982

B9 Modulation theory

H S Black
VAN NOSTRAND 1953

B10 'Introduction to dynamics + Control'

H M Power, R J Simpson
McGRAW HILL 1978

B11 'Control and Dynamic Systems'

Takahashi, Rabins, Auslander
ADDISON-WESLEY 1972

B12 'Control Systems Engineering'

J Nagrath, M Gopal
WILEY 1982

B13 'Applied Digital Control

J R Leigh
PRENTICE HALL INTERNATIONAL 1985

B14 'Digital Control Systems'

B C Kud
HRN 1980

B15 'Essentials of non linear control'

J R Leigh
PETER PEREGRUNUS LTD

B16 'Modelling analysis and control of dynamic systems'

W J Palm III
Wiley 1983

B17 Motorola M68000

Application notes

B18 Intel IAPx186

Application notes

E1 Encylopaedia Brittanica
Vol 11

E2 Encylopaedia Americana
Vol 16

P1 'A loss minimised sinusoidal PWM inverter'

J T Boys, S J Walton
IEE PROCEEDINGS
Vol 132, Pt.B, No 5 September 1985

P2 'A comparison of PWM strategies for inverter fed induction motors'

J M D Murphy, M G Egan
IEEE IAS
Vol IA-19, No 3, May/June 1983

P3 'Torque voltage and current harmonics of synchronous machines'

E D Goodman
IEEE IAS Vol IA-20 No 1 Jan/Feb 1984

P4 'New Sinusoidal Pulsewidth-modulated inverter'

SR Bowes
IEE PROCEEDINGS
Vol 122, No 11, November 1975

P5 'Novel approach to the analysis and synthesis of modulation processes in power converters'

PROCEEDINGS IEE, Vol 122, No 5 May 1975.

P6 'Harmonic effects in PWM inverter induction motor drives'

G B Kliman
IEEE IAS ANNUAL MEETING
PP 783-790, 1972

P7 'A new high quality PWM AC drive'

D A Grant
IEEE IAS Vol IA-19 No 2 March/April 1983

P8 'Dynamic modelling of brushless DC motors for aerospace applications'

N A Demerdash T W Nehl
IEEE AES
Vol AES-16 No 6, November 1980

P9 'A Brushless system for position control'

A Vagati, F Villata
IFAC CONTROL IN POWER ELECTRONICS AND ELECTRICAL DRIVES, LAUSANNE, SWITZERLAND, 1985.

P10 'Brushless servo system with expanded torque - speed operating range'

E K Persson, S Meshkat
MOTORCON PROCEEDINGS, APRIL, 1985

P11 PWM control of Brushless DC motors for Robotic Applications'

P F Muir, C P Newman
IEEE, IE Vol 1E-32, No 3 AUGUST 1985

P12 'Estimation of torque pulsation due to the behaviour of a converter and an inverter in a Brushless DC-drive system'

S Funabiki, T Himei
IEE PROCEEDINGS VOL 132, Pt.B, No 4, July 1985

P13 'Current Control of Voltage source inverters for fast four-quadrant drive performance'

C D Schauder, R Caddy
IEEE IAS VOL IA-18 No 2 MARCH/APRIL, 1982.

P14 'Derivation of synchronous machine parameters from text'

F P Demillo J R Ribeiro
IEEE PAS, VOL PAS -96, NO 4, JULY/AUGUST 1977

P15 'Methods for testing permanent magnet polyphase AC motors'

TJE Miller
CONFERENCE RECORD OF THE IAS 1981 ANNUAL MEETING, PHIL, PA, 5-9 OCTOBER

P16 'Non linear adaptive control of a synchronous machine'

R E Betz
R J Evans

IEEE AES VOL AES-21, NO 5, SEPTEMBER 1985

P17 'Non linear controller allowing for an upper bound on the system internal variables'

C Celertano, P Marino

IFAS CONTROL IN POWER ELECTRONICS AND ELECTRICAL DRIVES.
Luasanne, Switzerland, 1983

P18 'Microprocessor based adaptive control for electrical drives'

IFAC CONTROL IN POWER ELECTRONICS AND ELECTRICAL DRIVES, Lausanne, Switzerland, 1983.

P19 Theory of Power-electronic AC motor control for modelling estimation and control and/or analysis'

Yasuaki Kuroe Hiromasa Haneda
PROCEEDINGS OF 25th CONFERENCE ON DECISION AND CONTROL, ATHENS, GREECE.
December 1986. PP 54-61.